

TALLINN UNIVERSITY OF TECHNOLOGY
DOCTORAL THESIS
67/2018

**Functional Analysis of Ice-Binding
Proteins and Practical Application
in Ice Cream**

ALEKSEI KALEDA



TALLINN UNIVERSITY OF TECHNOLOGY

School of Engineering

Department of Materials and Environmental Technology

This dissertation was accepted for the defense of the degree 15/10/2018

Supervisor:

Associate Professor Katrin Laos
School of Science
Tallinn University of Technology
Tallinn, Estonia

Co-supervisor:

Associate Professor Ido Braslavsky
The Robert H Smith Faculty of Agriculture, Food and
Environment
The Hebrew University of Jerusalem
Rehovot, Israel

Opponents:

Dr Peter Dekker
DSM Food Specialties

Dr Maddalena Bayer-Giraldi
Glaciology; Polar Biological Oceanography
Alfred Wegener Institute Helmholtz Centre for Polar
and Marine Research

Defense of the thesis: 13/12/2018, Tallinn

Declaration:

Hereby I declare that this doctoral thesis, my original investigation, and achievement, submitted for the doctoral degree at Tallinn University of Technology has not been submitted for doctoral or equivalent academic degree.

Aleksei Kaleda



European Union
European Regional
Development Fund



Investing
in your future

signature

Copyright: Aleksei Kaleda, 2018

ISSN 2585-6898 (publication)

ISBN 978-9949-83-347-4 (publication)

ISSN 2585-6901 (PDF)

ISBN 978-9949-83-348-1 (PDF)

TALLINNA TEHNIKAÜLIKOOL
DOKTORITÖÖ
67/2018

**Jääga seonduvate valkude
funktsionaalne analüüs ja kasutamine
jäätises**

ALEKSEI KALEDA

Contents

List of Publications	7
Author's Contribution to the Publications	8
Introduction	9
Abbreviations	11
1 Literature review	12
1.1 What are ice-binding proteins?.....	12
1.2 Adsorption to ice	14
1.3 Mechanism of thermal hysteresis	16
1.4 Crystal shapes and ice plane affinity	18
1.5 Ice recrystallization inhibition	20
1.6 Kinetics of adsorption	21
1.7 Practical applications	22
2 The aims of this dissertation	23
3 Materials and methods	24
3.1 Materials	24
3.2 Thermal hysteresis	24
3.3 Ice recrystallization inhibition	25
3.3.1 Full method	25
3.3.2 Accelerated method.....	26
3.4 Ice crystal morphology	27
3.5 Fluorescence-based ice planes affinity	27
3.6 Kinetics of accumulation	28
3.7 Ice cream production	28
3.8 Ice cream analysis	29
3.8.1 Ice crystal visualization	29
3.8.2 Hardness	29
3.8.3 Melting	29
3.8.4 Sensory analysis	29
3.9 Statistical analysis	29
4 Results and discussion.....	31
4.1 <i>EfcIBP</i>	31
4.2 <i>EfcIBP</i> thermal hysteresis and ice recrystallization inhibition activity	31
4.3 Ice crystals in <i>EfcIBP</i> solution	34
4.4 <i>EfcIBP</i> ice plane affinity	36
4.5 <i>EfcIBP</i> adsorption kinetics	37
4.6 <i>EfcIBP</i> mutants	38
4.7 IBP ice cream.....	43
4.7.1 Ice recrystallization inhibition	43
4.7.2 Ice cream microstructure	44
4.7.3 Ice cream texture and melting behavior	45
5 Conclusions	48
References	49
Acknowledgments.....	59

Abstract.....	60
Lühikokkuvõte.....	62
Appendix 1	65
Appendix 2	83
Appendix 3	99
Appendix 4	119
Curriculum vitae.....	129
Elulookirjeldus.....	130

List of Publications

These publications form the basis of the thesis and are reproduced in the appendix with permission from the publishers:

- I Mangiagalli, M., Bar-Dolev, M., Tedesco, P., Natalello, A., **Kaleda, A.**, Brocca, S., Pascale, D., Pucciarelli, S., Miceli, C., Braslavsky, I., Lotti, M. (2017), Cryo-protective effect of an ice-binding protein derived from Antarctic bacteria. *FEBS J*, 284: 163-177. doi:10.1111/febs.13965
- II Mangiagalli, M., Sarusi, G., **Kaleda, A.**, Bar Dolev, M., Nardone, V., Vena, V. F., Braslavsky, I., Lotti, M., Nardini, M. (2018), Structure of a bacterial ice binding protein with two faces of interaction with ice. *FEBS J*, 285: 1653-1666. doi:10.1111/febs.14434
- III **Kaleda, A.**, Haleva, L., Sarusi, G., Pinsky, T., Mangiagalli, M., Bar-Dolev, M., Lotti, M., Nardini, M., Braslavsky, I. (2018), Saturn-shaped ice burst pattern and fast basal binding of an ice-binding protein from an Antarctic bacterial consortium. *Langmuir*. doi:10.1021/acs.langmuir.8b01914
- IV **Kaleda, A.**, Tsanev, R., Klesment, T., Vilu, R., Laos, K. (2018). Ice cream structure modification by ice-binding proteins. *Food Chemistry*, 246, 164–171. doi:10.1016/j.foodchem.2017.10.152

Author's Contribution to the Publications

Contribution to the papers in this thesis are:

- I The author performed ice recrystallization experiments, analyzed the results, made Figures 5 and 6 and wrote the methods section about ice recrystallization inhibition assay.
- II The author performed ice recrystallization experiments, some thermal hysteresis measurements, analyzed the results, made Figures 8 and 9, wrote the methods section about ice recrystallization inhibition assay.
- III The author performed ice crystal morphology and fluorescence-based ice plane affinity (FIPA) assay experiments; analyzed results of ice morphology, FIPA and accumulation kinetics experiments; made Figures 1-6, and S1-3, S6-7; and wrote major part of the manuscript.
- IV The author prepared winter rye extract, made ice creams, measured ice recrystallization inhibition, ice crystal size, hardness, melting; analyzed all results; made all figures and wrote the manuscript.

Introduction

Large areas of Earth are in permanently cold conditions. Low temperature can be considered extremal for life as it significantly affects cellular function: biochemical reactions and physical processes are slowed down, the fluidity of cell membranes is decreased (De Maayer, Anderson, Cary, & Cowan, 2014). Even more dangerous is water crystallization. Ice crystals can physically rupture cells or cause cell dehydration by pulling water out (Bredow, Tomalty, Smith, & Walker, 2018).

Water crystallization process consists of several steps. The first step is nucleation — formation of new ice crystal nuclei. The second step is nuclei growth. Recrystallization (changes in size and shape of the crystals) can be delineated as the third step. Nucleation can be significantly accelerated by the presence of solid particles or other ice crystals that can catalyze the formation of new ice nuclei on their surface (Kiani & Sun, 2011).

The so-called psychrophilic organisms have adapted to cold environments by employing different strategies, for example by changing the cell membranes composition, and by synthesizing cold-shock proteins and cold-active enzymes (D'Amico, Collins, Marx, Feller, & Gerday, 2006). Another strategy that is especially important for organisms living in freezing conditions is the production of ice-binding proteins (IBPs). These unique biomolecules, as their name suggests, are able to bind to ice crystals and stop their growth.

IBPs were first found in Antarctic fish living at -1.87°C (DeVries & Wohlschlag, 1969). Since then many other IBPs were discovered in a wide variety of organisms: fish, plants, insects, snow fleas, copepods, diatoms, fungi, bacteria, and yeasts (Bar Dolev, Braslavsky, & Davies, 2016).

IBPs exhibit three principal properties: thermal hysteresis (TH), ice recrystallization inhibition (IRI), and ice crystal shape modification. TH is the gap between freezing and melting points that appears in an IBP solution. IRI is the ability of IBPs to keep ice crystal population stable and prevent their growth and recrystallization. Different proteins have different TH, IRI and shaping activities. Moreover, TH and IRI activities are uncorrelated (Capicciotti, Poisson, Boddy, & Ben, 2015; Luuk L C Olijve et al., 2016). Plant IBPs can have low TH, but be very effective at inhibiting recrystallization (Capicciotti et al., 2015; Sidebottom et al., 2000).

Ice growth and recrystallization control by IBPs can potentially be used in practical applications.

Cryopreservation at very low temperature is used to store all kinds of biological samples not only for research applications, but also in medicine. However, cells often do not survive freezing and thawing process due to ice formation and recrystallization that physically damage the cells. Cryoprotectants, such as dimethyl sulfoxide and glycerol, are usually added to the cells to reduce cryoinjury; however, high concentrations are needed and some cryoprotectants are toxic. IBPs use as cryoprotectants can increase cell survival by preventing ice growth and recrystallization. In addition, IBPs can potentially avoid any toxic effects as IBPs are active at low concentrations (H. J. Kim et al., 2017; Nishijima et al., 2014).

In opposite to cryopreservation, some IBPs that form sharp ice crystals can be used to cause physical damage to cancer cells during cryosurgeries (Koushafar & Rubinsky, 1997).

Ice formation on freezers, roads or aircraft is a major problem. Spraying IBPs or even chemically immobilizing them on surfaces can be an effective anti-icing strategy (Gwak et al., 2015).

Introduction of IBP genes into cultivated plants or fishes, such as tomato or salmon, that are normally susceptible to freezing damage can increase their tolerance to low temperatures by producing endogenic IBPs (Bredow, Vanderbeld, & Walker, 2017; R. Wang, Zhang, Gong, & Hew, 1995).

IBPs can also be used in frozen foods. Ice growth and recrystallization, accelerated by temperature fluctuations during storage and transport, result in deterioration of frozen food texture or damage cellular structure in meat and vegetables. Development of food grade IBPs can potentially be very lucrative (Venketesh & Dayananda, 2008).

Some IBP commercialization has already been achieved, but on the whole, practical application of IBPs is still limited for the reason that IBP production is expensive and commercial sources remain highly restricted. One of the ways of increasing IBP use in commercial products is finding new proteins that have higher activity, thus would require a lower amount of expensive material to achieve the same effect.

A bacterial ice-binding protein was discovered in the metagenome of Antarctic ciliate *Euplotes focardii* consortium and recombinantly produced. It was found that this protein, *Efcl*BP, possesses high ice recrystallization inhibition activity at a very low concentration while having moderate TH. In addition, the *Efcl*BP produced highly unusual ice crystal shapes. The basis of these properties was not understood.

An international collaborative project was undertaken to better understand the underlying reasons for this peculiar IBP behavior. The *Efcl*BP structure was resolved and ice-binding sites were confirmed by computer modeling and mutagenesis. TH, IRI, and shaping activities were assessed in the wild-type *Efcl*BP and its mutants; crystallographic planes that the *Efcl*BP binds to were determined, and accumulation kinetics were measured. The experimental findings deepened our understanding of how IBPs bind to ice and clarified the importance of ice plane affinity and accumulation speed for the IBP activity.

To better assess possibilities for practical use of IBPs, ice creams containing IBPs from different sources were produced. The study of IBP ice cream properties, such as microstructure and sensory properties, established that the application of IBPs in ice creams is not straightforward. The difficulties that a commercial ice cream producer would encounter by incorporating IBPs are demonstrated in this thesis.

Abbreviations

AFGP	antifreeze glycoprotein
AFP	antifreeze protein
Afp4	antifreeze protein from <i>Glaciozyma antarctica</i> PI12 (Antarctic yeast)
ColAFP	<i>Colwellia</i> sp. SLW05 antifreeze protein (Antarctic bacterium)
EfcIBP	<i>Euplotes focardii</i> consortium ice-binding protein (Antarctic bacterium)
FfIBP	<i>Flavobacterium frigoris</i> PS1 ice-binding protein (Antarctic bacterium)
FIPA	fluorescence-based ice plane affinity
GFP	green fluorescent protein
IBP	ice-binding protein
IBS	ice-binding site
INP	ice-nucleating protein
IRI	ice recrystallization inhibition
LeIBP	<i>Leucosporidium</i> sp. AY30 ice-binding protein (yeast)
LpIBP	<i>Lolium perenne</i> ice-binding protein (perennial ryegrass)
MpAFP	<i>Marinomonas primoryensis</i> antifreeze protein (Antarctic bacterium)
NagIBP	<i>Navicula glaciei</i> ice-binding protein (Antarctic diatom)
RiAFP	<i>Rhagium inquisitor</i> antifreeze protein (beetle)
sbwAFP	spruce budworm antifreeze protein (<i>Choristoneura fumiferana</i>)
sfAFP	snow flea antifreeze protein (<i>Hypogastrura harveyi</i>)
SfIBP	<i>Shewanella frigidimarina</i> ice-binding protein (Antarctic bacterium)
TH	thermal hysteresis
TisAFP	<i>Typhula ishikariensis</i> antifreeze protein (snow mold)
TmAFP	<i>Tenebrio molitor</i> antifreeze protein (mealworm)
wt	wild type

1 Literature review

1.1 What are ice-binding proteins?

Ice-binding proteins (IBPs) are naturally occurring proteins that bind to ice. Their primary role is to help organisms coexist with ice by inhibiting ice crystal growth and recrystallization (Bar Dolev et al., 2016).

Pure water can remain liquid without ice formation in the range $-40\text{ }^{\circ}\text{C}$... $0\text{ }^{\circ}\text{C}$. Spontaneous formation of ice crystals in the absence of nucleation centers is classified as primary nucleation. However, in case of pre-existing ice crystals water can freeze at temperatures just below $0\text{ }^{\circ}\text{C}$ (Hobbs, 2010) due to secondary nucleation and existing crystals growth (Chow, Blindt, Chivers, & Povey, 2005). IBPs attach to ice crystals, stop their growth, and prevent secondary nucleation, thus depressing the solution freezing point below the equilibrium melting point. This results in freezing hysteresis (Bar Dolev et al., 2016). In addition, IBPs prevent ice melting, causing a slightly elevated melting point (Celik et al., 2010). Thermal hysteresis is the difference between the nonequilibrium melting and freezing points (Bar Dolev et al., 2016).

The average size of ice crystals present in a solution grows with time i.e. the large crystals grow larger at the expense of smaller ones, which disappear (Venketesh & Dayananda, 2008). This phenomenon is termed recrystallization and is attributed to the differences in surface curvature (Gibbs-Thomson effect) (Zachariassen & Kristiansen, 2000). Recrystallization takes place most rapidly at temperatures just below equilibrium freezing point and is accelerated when environmental temperatures fluctuate within the sub-zero range (Donhowe & Hartel, 1996; Griffith & Ewart, 1995). Growing ice crystals are likely to cause mechanical damage to tissues and cells, for example in snow-covered overwintering plants. Low concentrations ($\ll 1\text{ }\mu\text{M}$) of IBPs are effective in inhibiting recrystallization and protecting frozen tissues from damage. In contrast, the thermal hysteresis effect is observable at much higher concentrations ($> 1\text{ }\mu\text{M}$) (Kristiansen & Zachariassen, 2005; S. O. Yu et al., 2010). The exact mechanism of effective IRI activity at such low concentration is poorly understood (Capicciotti et al., 2015).

One of the first indications of the presence of an IBP even at a very low concentration is its modification of ice crystal shape (Bar Dolev et al., 2016; C A Knight, DeVries, & Oolman, 1984). Ice crystals have many crystal planes (Figure 1) and IBPs bind to at least one. Ice crystals grown in pure water have a round disk-like shape (Bredow et al., 2018). IBPs bound to specific ice planes prevent growth or melting in that direction, thus creating facets with hexagonal symmetry (Bar-Dolev, Celik, Wettlaufer, Davies, & Braslavsky, 2012; Strom, Liu, & Jia, 2005). Crystal shape modification can be used for example by bacteria or algae that live in Antarctica ice waters. Excreted IBPs modify ice growth in a way that stable brine pockets and channels are formed in the sea ice and these brine pockets are colonized by the microorganisms (J A Raymond, Janech, & Fritsen, 2009; James A Raymond, Fritsen, & Shen, 2007).

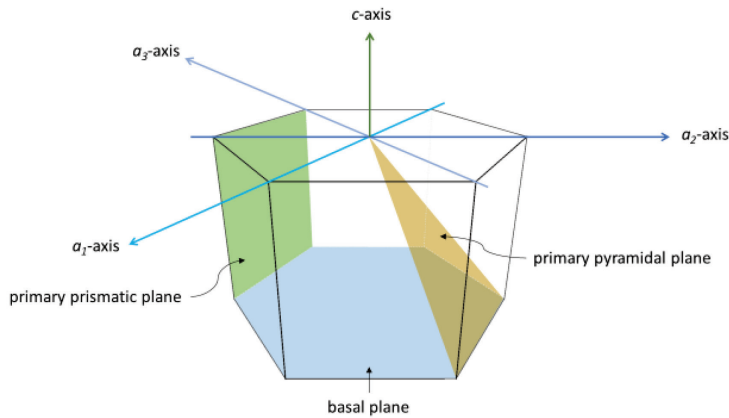


Figure 1. The hexagonal unit cell of an ice crystal showing the direction of axes and the primary prismatic, the primary pyramidal and the basal planes (Oude Vrielink, Aloï, Olijve, & Voets, 2016).

Remarkably, it was demonstrated that some bacteria can use IBPs also as ice adhesins. For example, a marine bacteria *Marinomonas primoryensis* has an ice-binding domain at the end of a long (0.6 μm) 1.5 MDa protein that it uses to attach to ice crystals and float closer to the water surface, where nutrients and oxygen are more readily available (Guo et al., 2013; Guo, Garnham, Whitney, Graham, & Davies, 2012; Vance et al., 2014).

According to the primary function of the protein, IBPs are also called antifreeze proteins (AFPs) or thermal hysteresis proteins, ice recrystallization inhibition proteins and ice structuring proteins (Bar Dolev et al., 2016; Bredow et al., 2017; Clarke, Buckley, & Lindner, 2002; Venketesh & Dayananda, 2008). AFPs in freeze-avoidant organisms act as antifreeze by lowering freezing temperature (Bar Dolev et al., 2016). Ice recrystallization inhibition proteins are employed by freeze-tolerant organisms to stop ice recrystallization that can cause damage during freezing (Charles A. Knight & Duman, 1986). However, regardless of the primary function, most IBPs exhibit some level of all three principal activities (Bar Dolev et al., 2016).

Typically, IBPs are excreted outside the cells, where ice crystal formation begins in the event of freezing. In fish, IBPs are concentrated in blood (H. J. Kim et al., 2017) and in plants are located in the apoplast, the space outside the plasma membrane (Bredow & Walker, 2017).

Closely related to IBPs are ice-nucleating proteins (INPs) that increase freezing point and thus trigger ice nucleation at higher temperatures. These proteins are found for example in bacteria that live on plants, such as *Pseudomonas syringae*. This bacteria has ice-nucleating proteins anchored outside the cell and by promoting ice nucleation and subsequent freeze damage of a plant surface this bacteria gets access to nutrients from the plant tissues (Zachariassen & Kristiansen, 2000).

Given the diversity of organisms, it is not surprising that IBPs demonstrate a diversity of protein structures. At least 10 different structures have been described. Those include single α -helices, single β -solenoids, four-helix bundles, polyproline type II helix bundles, and small globular proteins. This leads to the conclusion that these proteins evolved independently to achieve the same functionality — bind to ice (Bar Dolev et al., 2016).

Fish antifreeze proteins have been classified into five groups. Those are antifreeze glycoproteins (AFGPs) and antifreeze proteins types I, II, III, and IV. AFGPs consist of a peptide backbone (repeating alanine-alanine-threonine) with a disaccharide residue connected to the threonine and are 2.6–33 kDa in size. Type I are typically small (3.3–4.5 kDa) alanine-rich α -helices. Type II are 11–24 kDa cysteine-rich globular proteins. Type III are 6.5–14 kDa globular proteins with β -sandwich in secondary structure. Type IV are 12 kDa glutamine and glutamate-rich four-helix bundles (Barrett, 2001).

Ice-binding properties have been found in other non-protein molecules, such as safranin O, poly(vinyl alcohol), zirconium acetate, xylomannan (Drori et al., 2016; Inada & Lu, 2003; Mizrahy, Bar-Dolev, Guy, & Braslavsky, 2013; Walters, Serianni, Sformo, Barnes, & Duman, 2009), and also synthetic molecules have been designed (Carsten Budke & Koop, 2006; Huang et al., 2012; Mitchell et al., 2017; Sproncken, Surís-Valls, Cingil, Detrembleur, & Voets, 2018).

1.2 Adsorption to ice

As mentioned before, ice-binding protein structures are diverse, however, they do share some common features. Site-specific mutagenesis shows that IBPs bind through ice-binding sites that are generally flat, extensive and rather hydrophobic (Bar Dolev et al., 2016). Some variety to this general rule exists, one such notable IBP is type I AFP isoform called Maxi (Sun, Lin, Campbell, Allingham, & Davies, 2014).

The ice-binding site (IBS) is usually formed by flat arrays of threonine-x-threonine amino acid motifs and to a smaller extent consists of other amino acids such as valine, glycine, and alanine (Schauperl et al., 2017). Typically, ice-binding sites form a regular pattern of grooves (*Figure 2*) and amino acid side chains on the IBS have a spacing similar to water molecules in the ice lattice that is 7.35 Å along the *c*-axis and 4.52 Å along the *a*-axis on prism plane, or 7.83 Å and 4.52 Å on the basal plane (Hakim et al., 2013; Petrenko & Whitworth, 2002).

Mutagenesis studies of fish AFPs demonstrated that hydrophobic residues on the IBS are important and that threonine hydroxyl groups are not the main mechanism for binding as it was previously believed (J Baardsnes et al., 1999; Sönnichsen, DeLuca, Davies, & Sykes, 1996).

It was proposed that IBS orders solvation waters into an ice-like quasi-liquid layer, called anchored clathrate layer (Hudait, Odendahl, Qiu, Paesani, & Molinero, 2018; Smolin & Daggett, 2008). These waters form cages around hydrophobic groups and are in turn connected to the protein through hydrophilic groups (Hudait et al., 2018; Kondo et al., 2012). The ordered waters then merge with the ice-water interface and the protein freezes on the ice surface (Nutt & Smith, 2008). The hydration pattern on an IBS resembles the basal and the primary prism planes of ice and consists of several layers (up to 15 Å) of ordered water molecules (Midya & Bandyopadhyay, 2014). Formation of polypentagonal and hexagonal water networks that fit different ice lattice structures facilitates binding of one IBS to multiple ice planes (Mahatabuddin et al., 2018; C. Wang, Pakhomova, Newcomer, Christner, & Luo, 2017).

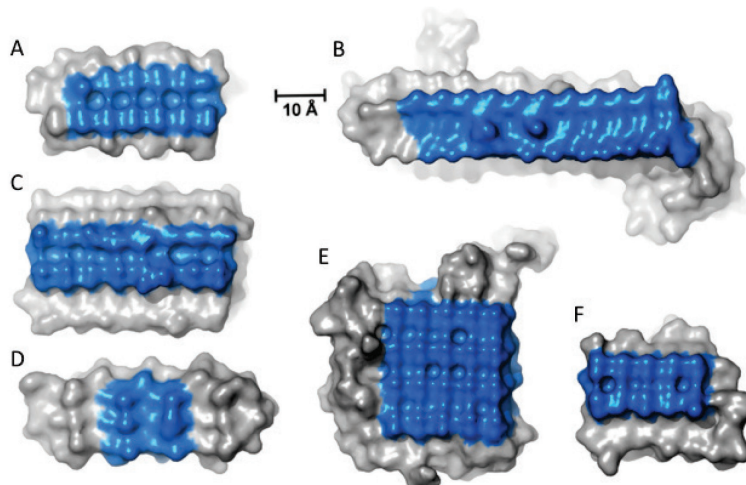


Figure 2. Ice-binding surfaces colored in blue of A) mealworm *Tenebrio molitor*, TmAFP, B) marine bacteria *Marinomonas primoryensis*, MpAFP, C) perennial ryegrass *Lolium perenne*, LpAFP, D) snow flea *Hypogastrura harveyi*, sfAFP, E) beetle *Rhagium inquisitor*, RiAFP, F) eastern spruce budworm *Choristoneura fumiferana*, CfAFP. This figure was originally published in the *Journal of Biological Chemistry* (Hakim et al., 2013) © the American Society for Biochemistry and Molecular Biology.

An extreme case of water ordering is the Maxi protein. Maxi consists of a bundle of four α -helices that expose the IBS inside a cavity that forms between the bundles. The internal IBS organizes more than 400 water molecules that form a network of ordered waters that extend to the outside surface and participate in ice binding (Sun et al., 2014).

As mentioned previously, ice-nucleating proteins are similar to IBPs. The mechanism of ice nucleation is much less studied; however, limited research shows that INPs act in the same way as IBPs, organizing anchored clathrate waters on an ice-binding site (Hudait et al., 2018; Pandey et al., 2016). The key difference is that ice-binding sites of INPs are larger and can be extended even further by protein aggregation. Large area acts as a nucleation center, organizing and stabilizing significant amount of waters, thus allowing easier formation of initial ice nucleus from which a crystal can grow (Gurian-Sherman & Lindow, 1993).

For ice binding to occur several properties of the IBS must be in a specific range. The residues need to be positioned at a certain distance that fits the ice lattice. Water molecules have to form an ice-like anchored clathrate layer. For the water ordering, the residues need to be moderately hydrophobic. Too hydrophilic surfaces induce strong ordering of the waters, but hinder ice binding, while too hydrophobic surfaces are not able to order the waters into ice-like structures (Cox, Kathmann, Slater, & Michaelides, 2015; Schauperl et al., 2017; Schauperl, Podewitz, Waldner, & Liedl, 2016).

The research into the binding mechanics is still ongoing, and some studies indicate that anchored clathrate motif is not a universal requirement for ice binding (Hudait et al., 2018). For example, AFGP8 binding occurs through the adsorption of methyl groups to the ice surface (Mochizuki & Molinero, 2018); and the ice-like waters were not found on an IBP from beetle *Dendroides canadensis*, suggesting that it binds directly through the ordered array of threonine residues (Meister et al., 2015).

1.3 Mechanism of thermal hysteresis

Colligative freezing point depression is a thermodynamic phenomenon and it is proportional to the molal concentration of the solute molecule regardless of the solute species. This also lowers the melting point, therefore, in this case, there is no difference between the freezing and melting points. However, IBPs lower the freezing temperature at much lower concentration, thus IBPs act non-colligatively (Y. Yeh & Feeney, 1996). For example, mealworm *Tenebrio molitor* IBP (*TmAFP*) lowers the freezing point by 2 °C at 1 mg mL⁻¹, while salt at the same concentration lowers the freezing point only by 0.03 °C (Bar, Celik, Fass, & Braslavsky, 2008).

Surface tension energy at the ice-water interface also changes the equilibrium freezing/melting temperature. Smaller solid particles have a lower equilibrium melting point compared to larger ones, this is known as the Gibbs-Thomson effect (Johari, 1997). The Gibbs-Thomson equation relates the curvature of a surface to the equilibrium phase transition temperature (Bar Dolev et al., 2016).

The adsorption-inhibition mechanism based on the Gibbs-Thomson effect was suggested as the explanation for the IBP activity. IBP molecules adsorb to the surface of growing ice. This forces the ice to grow only between the adsorbed molecules, forming curved surfaces. The convex ice shapes continue to grow until they reach a critical curvature where further attachment of water molecules becomes energetically unfavorable due to the Gibbs-Thomson effect. Here, ice crystal growth stops and continues only when the temperature drops more, and the curvature of the ice cannot increase further and circumvent the decrease in temperature. This causes the decrease in the freezing point below the equilibrium melting point of flat ice. The temperature at which IBP action fails and rapid ice growth (burst) starts is called the hysteresis freezing point or the nonequilibrium freezing point (Bar Dolev et al., 2016; C A Knight, 2000).

Adsorption of IBPs also inhibits ice melting by the same Gibbs-Thomson mechanism, except the ice between the bound molecules melts into a concave shape (Celik et al., 2010; C A Knight & Devries, 1989; Naullage, Qiu, & Molinero, 2018). This raises the nonequilibrium melting point above the melting point. It was shown that this melting hysteresis can be up to 0.44 °C for some IBPs and the superheated crystals are stable for hours. However, melting hysteresis is always smaller than freezing hysteresis (Celik et al., 2010).

The difference between the nonequilibrium freezing and nonequilibrium melting points is the thermal hysteresis (TH) (Bar Dolev et al., 2016).

According to TH activity, IBPs are classified into moderate and hyperactive (Scotter et al., 2006). Moderate IBPs typically have TH up to 1 °C at millimolar concentrations, while hyperactive are an order of magnitude more active at micromolar concentrations than moderate and can even go as high as 6 °C at millimolar concentrations (Celik et al., 2010).

A recent study established what limits the degree of thermal hysteresis (Naullage et al., 2018). The maximum curvature that the ice can attain depends on the distance between pinned molecules. By itself, the curvature at a given distance in case of superheating or supercooling is a thermodynamic property that does not depend on the nature of the molecules. However, the distribution of IBP distances on the ice surface does depend on the IBP concentration and the binding free energy. The study showed that the irreversible ice growth starts with the formation of an ice bridge over the pinned molecule that joins convex ice fronts around it. The molecule is then overgrown and remains in the ice (if it is a strong binder). In the same manner, irreversible melting occurs when liquid channels form underneath the pinned molecule. The molecule then

detaches and ice melts. The size of the IBP (height and width) is the property that determines the freezing hysteresis. The larger the molecule, the more difficult for the ice to form a bridge over it, and the larger freezing hysteresis is (Naullage et al., 2018). This is confirmed by other studies of large synthetic IBP constructs (Jason Baardsnes, Kuiper, & Davies, 2003; DeLuca, Comley, & Davies, 1998; Leinala et al., 2002; Phippen et al., 2016). Melting hysteresis depends mostly on the molecule width, as the molecule does not protrude into the ice and stays flat on the surface. This is the reason why melting hysteresis is smaller than freezing hysteresis. The energy barrier for nucleation of a liquid bridge under flat part of the IBP is much smaller than the one for nucleation of an ice bridge over the bulky IBP part. The same study also pointed out that the experimental TH is much lower than achieved in simulations because of a distribution of distances between IBPs on the ice surface. The ice bridging starts in the region of lower protein density with higher ice curvature, this leads to overgrowth of proteins by ice, creating even larger distances between surface IBPs, and a cascade of such events leads to fast ice growth. To conclude, the degree of thermal hysteresis depends on the IBP size, its binding energy and the longest distances in the protein distribution at the ice surface (Naullage et al., 2018).

A fluorescent microscopy study demonstrated that the average distance between hyperactive GFP-*Tm*AFP (*Tenebrio molitor* IBP fused with green fluorescent protein, GFP) on ice surface was 7-35 nm and that TH linearly increased (from 0.2 °C to 0.6 °C) as the distance decreased. The same study showed that there is no such correlation for moderate GFP-AFP type III (fish type III IBP fused with green fluorescent protein) because moderate IBPs do not protect the crystal from all sides, thus the TH is limited by the unprotected crystal side (Drori, Davies, & Braslavsky, 2015a). The significance of affinity to different ice planes is discussed further in more detail.

Reversibility or irreversibility of IBP binding is still a point of research. The Gibbs-Thomson mechanism implies that the binding is irreversible. This is experimentally confirmed for GFP-AFP type III and GFP-*Tm*AFP. Part of an ice crystal with adsorbed GFP-AFP type III was bleached, and the crystal was kept for 20 h. The bleached part remained the same for the whole duration of the experiment, confirming that there is no dynamic exchange with the solution (Pertaya et al., 2007). Hyperactive GFP-*Tm*AFP maintained TH even after the IBP solution around the crystal was exchanged for water (Celik et al., 2013). However, when the solution exchange experiment was performed with moderate GFP-AFP type III, TH was diminished. This reiterates that moderate IBPs do not protect the ice from all directions and in the case of continuing ice growth rely on additional binding of remaining IBPs in solution (Drori, Davies, & Braslavsky, 2015b). This irreversible binding is exploited by several IBP isolation methods called ice affinity purification (Adar, Sirotinskaya, Bar Dolev, Friehmann, & Braslavsky, 2018; Kuiper, Lankin, Gauthier, Walker, & Davies, 2003; Marshall, Basu, & Davies, 2016). Still, other studies show that AFGPs bind to ice reversibly and are not incorporated into the ice (Mochizuki & Molinero, 2018; Zepeda, Yokoyama, Uda, Katagiri, & Furukawa, 2008). Reversible binding was also demonstrated in ice etching experiments (described further in more details) where random lysine/alanine copolymers adsorbed to ice in specific orientations and formed transient patterns on the ice crystal, but were not incorporated into the growing ice (Charles A. Knight, Wierzbicki, Laursen, & Zhang, 2001).

On the whole, the exact mechanism of IBP adsorption to ice and thermal hysteresis is still not entirely clear. Experimental and computational research shows that different IBPs can bind reversibly or irreversibly, and the binding mechanism can proceed through

clathrate waters or direct adsorption of amino acid residues. However, given the multitude of IBP structures and roles the proteins fulfill in nature, this variability is not surprising.

1.4 Crystal shapes and ice plane affinity

There are several polymorphic forms of ice, however, under normal conditions, only hexagonal ice (Ih) is formed (Buckley & Lillford, 2009). The basic crystal unit takes on the form of a hexameric box (Figure 1). There are three crystallographic a -axes and one c -axis that form a crystal unit with c dimension 7.35 Å and a dimension 4.52 Å (Röttger, Endriss, Ihringer, Doyle, & Kuhs, 1994). According to the Miller-Bravais indices system, the crystallographic planes are defined numerically by the reciprocals of plane intersection points with these axes. An ice crystal has many planes, but the most important ones are the basal plane, the primary prismatic plane, the primary pyramidal plane, the secondary prismatic, and the secondary pyramidal planes. Water molecule organization on these planes is different, as shown in Figure 3. During ice growth, water molecules attach to these planes at a different rate. In pure water growth is faster in the direction of the prismatic planes than in the basal plane direction (Buckley & Lillford, 2009), this makes ice crystals grow in a disc-like manner with flat basal planes (Bredow et al., 2018).

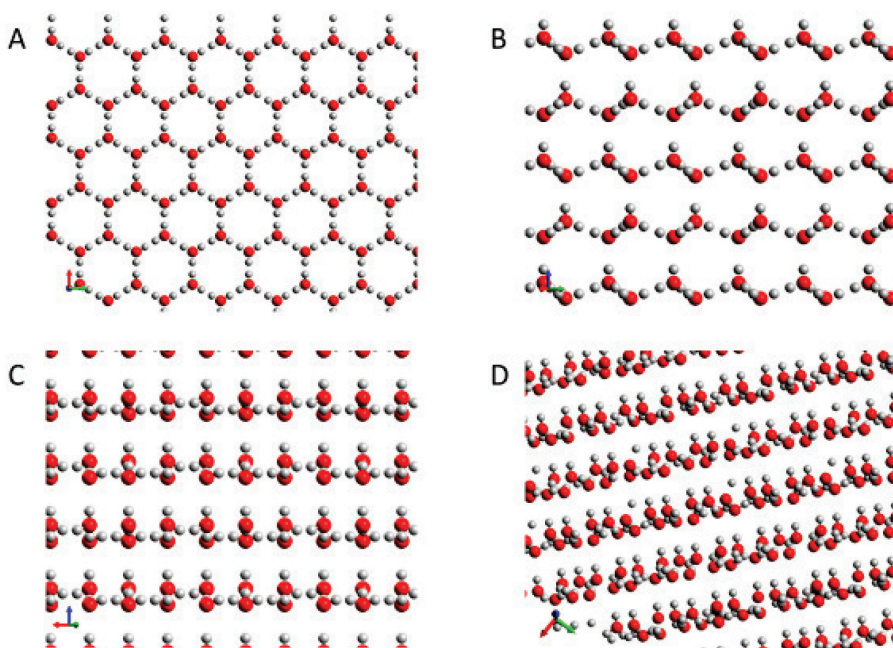


Figure 3. The position of water molecules on different ice crystal planes. Red indicates oxygen, gray hydrogen atoms. Arrows indicate axes. Blue arrow shows direction of the c -axis, while red and green define a -axes plane. A) Basal plane, B) primary prismatic plane, C) secondary prismatic plane, D) primary pyramidal plane. Figure generated in Avogadro 1.2 (Hanwell et al., 2012).

IBP adsorption to a crystal causes modification of its habit. Ice crystals in IBP solutions typically develop hexagonal shapes with sharp edges and clear facets. This effect is

apparent at very low IBP concentrations, even when TH is not observed. IBPs inhibit ice crystal growth by adsorbing to specific (one or more) ice crystal planes. IBPs slow down growth in their vicinity providing more of the target plane for IBP binding, thus the protected planes during crystal growth increase in area, developing a facet, while unprotected eventually vanish. At the end of this process, growth is arrested on the whole crystal. Fully developed crystals stay stable in the TH gap, but when the temperature is lowered below the hysteresis freezing point, a sudden burst-like growth occurs (Bar Dolev et al., 2016; Bar-Dolev et al., 2012).

Adsorption to specific planes results in ice crystal shapes that are characteristic to the IBP. For example, moderate fish AFPs of type I, II, and III produce hexagonal bipyramidal shapes that are elongated along the *c*-axis (Chao, DeLuca, & Davies, 1995); while hyperactive *Tm*AFP produces lemon-like shape (Graham, Liou, Walker, & Davies, 1997). Furthermore, hyperactive IBPs form shapes during melting, which is the result of localized melting inhibition caused by adsorbed IBPs. Burst behavior below hysteresis freezing temperature also varies. Bipyramidal crystals of moderate IBPs burst in the direction of the *c*-axis (through the basal plane) and hyperactive burst in *a* direction. All this behavior of ice crystals is the result of IBPs binding to specific ice planes (Bar-Dolev et al., 2012).

Growth and burst in the *c*-axis direction in moderate IBPs suggest that the basal planes of ice are left unprotected. Indeed, direct fluorescence microscopy experiments confirmed accumulation of moderate IBPs fused with green fluorescent protein on prismatic and/or pyramidal planes of single ice crystals. Differently from moderate IBPs, hyperactive were shown to accumulate on the basal planes in addition to pyramidal and prismatic (Pertaya, Marshall, Celik, Davies, & Braslavsky, 2008). Protection of an ice crystal from all sides was proposed to be the main reason why hyperactive IBPs have much higher TH activity, thus the basal plane affinity was previously suggested to be the basis for hyperactive/moderate classification (Pertaya et al., 2008; Scotter et al., 2006).

Ice-binding planes can be visualized in more details using an ice etching technique. This method involves the production of a large (few cm in diameter) axis-oriented single ice crystal hemisphere and incubation of the crystal in an IBP solution. Then the crystal is let to sublime in a freezer and opaque surface patterns consisting of bound protein appear on the otherwise transparent hemisphere. As the orientation of crystal axes is known, the pattern can then be mapped to specific ice planes that the protein prefers to bind to (C A Knight, Cheng, & DeVries, 1991). The technique was improved further by using fluorescently labeled IBPs and was named fluorescence-based ice plane affinity (FIPA). This increased sensitivity and allowed to see the differences in the amount of accumulated protein (Basu et al., 2014). Basu *et al.* article discusses in detail the FIPA method and interpretation of the results.

Some IBPs on the ice hemisphere form tilted elongated spots. This has been attributed to the physical orientation of molecules on the ice surface. Elongated molecules of type I helical fish AFPs would adsorb to the surface with their longer axis perpendicular to the longer axis of the spot (C A Knight et al., 1991). Furthermore, the binding to the ice planes is stereospecific. This makes sense, as Figure 3 shows that ice crystal planes, except the basal, are not left-right symmetric. An elegant experiment demonstrated that a synthetic D-isomer of a type I AFP — the mirror image of the natural L-isomer — also produces a mirror-image pattern on the ice hemisphere (Laursen, Wen, & Knight, 1994). Such binding orientation dependence reiterates that there exists a structural match between the ice-binding site and the ice crystal lattice. For example, α -helical type I fish AFP from

winter flounder has threonine residue repeats at a distance of 16.5 Å along its helix and this spacing closely matches the 16.7 Å lattice repeats on the pyramidal ice plane this protein binds to (C A Knight et al., 1991).

Another interesting phenomenon can be noticed in many ice crystals shaped by different types of IBPs. The ice crystals can appear asymmetric along the *c*-axis (Garnham, Nishimiya, Tsuda, & Davies, 2012; M. Kim, Gwak, Jung, & Jin, 2017; J. K. Lee et al., 2010). In other words, pyramids of a bipyramidal crystal are rotated by some degree with respect to each other around the *c*-axis and one side of the bipyramid is not a mirror image of the other. These crystals can appear with sharp pointy ends or wide and truncated. The geometrical name of these shapes is trapezohedron (Zhang & Laursen, 1999). Such crystal morphology can be directly linked to the ice adsorption plane of the IBP (Wierzbicki et al., 2000). In (Garnham et al., 2012) several mutants of a type III AFP were analyzed for their ice crystal shape and ice-binding planes using FIPA analysis. The degree of twisting asymmetry of the crystal roughly followed the binding pattern visualized by FIPA, which was also asymmetrically rotated around the *c*-axis (Garnham et al., 2012).

1.5 Ice recrystallization inhibition

Initial ice crystals that form in a solution are not at equilibrium. There is a dynamic driving force for all the crystals to become one single mass with a perfect structure (Buckley & Lillford, 2009). This results in a process where large crystals grow at the expense of smaller ones, called recrystallization. This spontaneous thermodynamic process results in a decrease of total crystal surface area per volume, thus lowering the free energy of the system (Oude Vrielink et al., 2016).

The most common three types of recrystallization are isomass, migratory and accretive. Isomass recrystallization is rounding off of irregularly shaped crystals into smoother ones. Sharp points of the crystal are less stable due to the surface curvature (Gibbs-Thomson effect) and easily melt, thus creating a more compact structure with a lower surface to volume ratio. Migratory recrystallization is the growth of large crystals while smaller melt and disappear. Smaller crystals have higher curvature, thus according to the Gibbs-Thomson effect, they melt more rapidly than bigger crystals with lower curvature. The water from the liquid phase then deposits onto bigger crystals. When this process happens at a constant temperature it is called Ostwald ripening; when the temperature fluctuates in can be described as melt-refreeze recrystallization. Accretive recrystallization is a fusion of contacting crystals through surface diffusion. This type of recrystallization takes place at high crystal phase volume where crystals are likely to be close to each other. After crystals fuse isomass recrystallization rounds them off. All these mechanisms are a part of the whole recrystallization process and happen at the same time. The outcome is an increase in average crystals size and a decline in the total number of crystals (Buckley & Lillford, 2009; Hassas-Roudsari & Goff, 2012).

Ice-binding proteins are very effective at ice recrystallization inhibition (IRI), stopping the process at a very low concentration (S. O. Yu et al., 2010). As it was described before, IBP molecules adsorb to the ice surface and create ripples between the molecules. If the temperature is lower than the equilibrium melting point of the ice crystal, convex shapes appear. Likewise, in the case of superheating the shapes are concave. At a given temperature in a population of crystals due to their curvature some smaller crystals are overheated, while larger are overcooled (the Gibbs-Thomson effect). IBPs thus can change the surface curvature of the ice crystals to compensate for the differences in their

size. This results in a metastable state where bigger crystals stay supercooled without growing and smaller ones are superheated without melting in a wide temperature range and recrystallization process is halted (Naullage et al., 2018).

It was suggested that strong binding to ice is not necessary for IRI activity, unlike for TH. Reversibly binding AFGPs are known to have moderate TH but are one of the best recrystallization inhibitors (Mochizuki & Molinero, 2018; Luuk L C Olijve et al., 2016). This can be possibly explained by the fact that recrystallization driving forces of tiny crystals are very small and weak binding is enough to counteract them (Naullage et al., 2018).

A quantitative method for ice recrystallization inhibition activity assessment was developed (C Budke, Heggemann, Koch, Sewald, & Koop, 2009). In this method, a thin wafer of polycrystalline ice is held at a constant temperature for two hours and the average crystal size is monitored. A 45% sucrose solution is used to establish a population of separate ice crystals with a low total volume. At these experimental conditions Ostwald ripening is the prevailing type of recrystallization. In this work, it was demonstrated that the cubic mean radius of ice crystals increases linearly in time. Measurement of crystal growth speed at different IBP concentrations can then be used to determine the concentration at which IBP is inhibiting ice recrystallization by 50% (C Budke et al., 2009).

1.6 Kinetics of adsorption

In a typical thermal hysteresis measurement, there is an incubation period, where a single ice crystal is held for a certain time at a temperature just below its melting point. This is to allow IBPs to accumulate on the crystal (Braslavsky & Drori, 2013). The accumulation time is important because it was found that IBP thermal hysteresis activity can significantly increase over incubation time (Kubota, 2011; Takamichi, Nishimiya, Miura, & Tsuda, 2007; Xiao et al., 2014). For example, TH of fish type I AFP from winter flounder increased by a factor of five and reached a plateau in 1–2 h of incubation (Chapsky & Rubinsky, 1997). Measurements of optical changes of ice-water interfaces using ellipsometry techniques showed that AFGPs also accumulate over time and a plateau is reached in approximately 1 h (Wilson, Beaglehole, & Devries, 1993).

A recent study compared TH dependence on incubation time of hyperactive *TmAFP* from mealworm *Tenebrio molitor*, hyperactive sbwAFP from spruce budworm, hyperactive *MpAFP* from marine bacteria *Marinomonas primoryensis*, and moderate fish type III AFP. It revealed that TH of *TmAFP* increased 3 to 10 times (at 40 μM or 1 μM respectively) over 12 h and did not reach a plateau. At 8 μM sbwAFP did not have TH activity at few seconds exposure time, however, after 2 min incubation it rose to 0.3 $^{\circ}\text{C}$ and after 12 h TH increased to 2.5 $^{\circ}\text{C}$, not showing a plateau. Differently from other two hyperactive IBPs, *MpAFP* TH increased over time only at a lower concentration (2.4 μM) with a plateau after 4 min. At a higher concentration (8 μM) there was no observed time dependence. Thermal hysteresis of moderate AFP type III at 40 μM had only very small dependence on incubation time. This work showed that different IBPs have different adsorption kinetics characteristic to the protein and that moderate type III AFP accumulates very fast, *MpAFP* and *TmAFP* are slow, and sbwAFP is extremely slow. The binding speed was thus suggested as another property that is different between moderate and hyperactive IBPs (Drori, Celik, Davies, & Braslavsky, 2014).

A direct visualization of IBP accumulation in time can be performed using fluorescence microscopy. Accumulation measurements were performed for GFP-tagged AFP type III and *TmAFP*. GFP-AFP type III, indeed, accumulated very fast, reaching a plateau in a few

minutes, while the accumulation of GFP-*TmAFP* continued for hours. An equation relating fluorescence intensity to the adsorption constant (Equation 1) was fitted to the results of GFP-*AFP* type III.

$$I = I_{max}(1 - e^{-tK_{on}C}) \quad (1)$$

Here I — measured intensity, I_{max} — maximum measured intensity (plateau), t — time [s], K_{on} — adsorption constant [$\mu\text{M}^{-1}\text{s}^{-1}$], C — IBP concentration [μM]. For the GFP-*TmAFP*, however, single exponent did not work, and a triple exponent was used. This suggests that many processes with different timescales happen during accumulation (Drori et al., 2014).

1.7 Practical applications

The results of the practical application of IBPs in cell cryopreservation are mixed. While some studies report that addition of IBPs improves cell, tissue or organ survival, other studies demonstrate that there is no benefit or even a harmful effect instead (Bang et al., 2013; Brockbank, Campbell, Greene, Brockbank, & Duman, 2011).

Nevertheless, some level of commercial application of IBPs has been achieved in the frozen food industry. Ice growth and recrystallization due to freezing, thawing, and temperature fluctuations during storage and transportation reduce food quality. IBPs can help protect cellular structure of frozen meat or fish and prevent drip loss (Payne, Sandford, Harris, & Young, 1994; C.-M. Yeh, Kao, & Peng, 2009), or preserve the smooth texture of ice cream (A Regand & Goff, 2006).

Unilever has already commercially produced some fat-free ice creams and ice popsicles containing recombinant fish type III AFP. However, at the moment of writing, Unilever does not use IBPs in its products. Kaneka Corporation in collaboration with Kansai University, Ichiei Company, and Fuji Hightech Company commercially produced IBP-containing extract from daikon radish sprouts and extract from mushroom *Flammulina velutipes* containing xylomannan — an ice-binding glycolipid. These novel products have found use in over 100 frozen Japanese foodstuffs such as sushi, udon noodles, steamed fish paste, rolled eggs, gyoza, hamburgers and deep-fried chicken (Kaneka Group, 2016; Kansai University, 2014). Nevertheless, the extracts remain locked to the Japanese market and very little information is available.

Overall, literature about IBP application in ice creams is scarce and contradictive. Recrystallization inhibition effect was proven in ice cream mixes and ice creams (A Regand & Goff, 2006). However, it was noted that addition of IBPs induces accretion of ice crystals and IBP ice creams have higher hardness and iciness (Byass et al., 2004; Daniel, Hoddle, Jones, Oldroyd, & Singleton, 2004; A Regand & Goff, 2006). It was hypothesized that iciness appears from ice crystal shape modification that is caused by IBPs and that this effect can be avoided by adding IBPs after the bulk of ice crystals have already been formed. However, this method requires modification of ice cream production method and expensive redesign of equipment (Darling & Hoddle, 2001).

To summarize, the practical application of IBPs for cryopreservation or in foods is not straightforward and requires extensive research.

2 The aims of this dissertation

The first aim of this dissertation is to perform a functional analysis of the *Euplotes focardii* consortium ice-binding protein (*EfcIBP*) and clarify the basis of its unusual properties. For this purpose, the thesis:

- assesses thermal hysteresis, ice recrystallization inhibition, and ice shaping activities of *EfcIBP*.
- confirms ice-binding sites using point mutagenesis and reevaluates contribution of the ice-binding sites to the TH, IRI and shaping.
- implements a fluorescence-based ice plane affinity method to visualize *EfcIBP* adsorption to the ice crystal planes and reassesses adsorption planes of *EfcIBP* mutants.
- measures protein ice adsorption kinetics using fluorescence microscopy.

Furthermore, the second aim of the thesis is to evaluate the potential application of IBPs in ice cream and study the textural and structural properties of IBP-containing ice creams.

3 Materials and methods

Detailed descriptions are available in the publications in the appendix. The following sections are provided to make the materials and methods more accessible to the reader.

3.1 Materials

Efc1BP, GFP-*Efc1BP*, and their mutants were produced by Marco Mangiagalli as described in Publications I, II, and III.

Cold acclimated winter rye extract and recombinant fish type III AFP that were used in ice cream experiments were produced as described in the Publication IV (2.1–2.3).

Ice cream components are listed in the Publication IV (2.1).

3.2 Thermal hysteresis

Thermal hysteresis measurements were performed using a LabVIEW-operated (National Instruments Corp., USA) custom-made nanoliter osmometer described previously in detail (Braslavsky & Drori, 2013). Lyophilized protein samples were dissolved in 20 mM ammonium bicarbonate buffer (pH 8.5) and diluted to the desired concentration in the same buffer. Samples of approximately 10 nL were injected into oil on the microscope cold stage. The samples were cooled as presented in *Figure 4*.

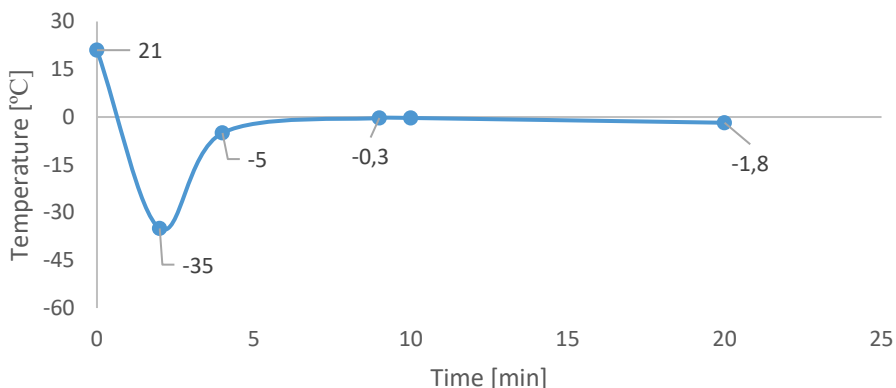


Figure 4. A simplified example of a temperature profile of the thermal hysteresis measurement experiment.

Samples were cooled until freezing (around -35 °C) and then warmed until a single ice crystal of ~10 μm diameter remained. The melting temperature of the crystal was recorded and then the crystal was held for 1 min slightly below the melting point. After incubation, the temperature was lowered by 0.0025 °C per second. The temperature at which burst-like growth commenced was determined as the hysteresis freezing point. The difference between the melting point and the hysteresis freezing points is the TH value. Each measurement was repeated at least three independent times.

3.3 Ice recrystallization inhibition

Ice recrystallization inhibition activity was measured by two methods. The principal difference between the methods is that the full method implements constant temperature for recrystallization, while the second uses temperature fluctuation to accelerate the recrystallization process. The full method was used for IRI measurements of the *EfcIBP* and its mutants, while the accelerated method was used in ice cream mixes.

3.3.1 Full method

Publications I and II used different equipment for ice recrystallization inhibition assessment, thus there are slight differences in the procedure described in the articles, however, the principle is identical.

IRI was assessed using a sucrose-sandwich assay (Alejandra Regand & Goff, 2006) with modifications (C Budke et al., 2009). Samples contained 45% sucrose, 50 mM NaCl, 10 mM Tris (pH 8.0) and up to 1 μ M of protein. Samples of 1.4 μ L were placed on a sapphire sample holder and covered with a 13-mm diameter circular glass coverslip. The sapphire was used to reduce temperature gradients. The sample was sealed with immersion oil to avoid evaporation and mounted on the stage of a Motorized Cryobiology System (model MDBC196, Linkam Scientific, UK). A copper plate with a 2.5-mm diameter slit was placed on top of the sample to further reduce temperature gradients. Immersion oil was used between the sample, the stage, and the slit to improve thermal contact. The Linkam stage was placed on a light microscope (BX41, Olympus America Inc., USA) and operated using a custom-built LabVIEW interface. The temperature profile of the experiment is presented in Figure 5. The system was cooled from room temperature to -50 $^{\circ}$ C at a rate of 130 $^{\circ}$ C min^{-1} and sustained at -50 $^{\circ}$ C for 1 min. The temperature was then elevated to -20 $^{\circ}$ C at a warming rate of 130 $^{\circ}$ C min^{-1} and then warming continued to -10 $^{\circ}$ C at a rate of 10 $^{\circ}$ C min^{-1} . The final stage of heating up to the annealing temperature of -7.4 $^{\circ}$ C was conducted at a slow rate of 1 $^{\circ}$ C min^{-1} to avoid overheating. The sample was maintained at this temperature for 60 min. During this period, recrystallization was recorded using an EXi Aqua Bio-Imaging camera (QImaging, Canada) every 1 min. The experiment was carried out with different concentrations of protein and repeated at least three times for each concentration.

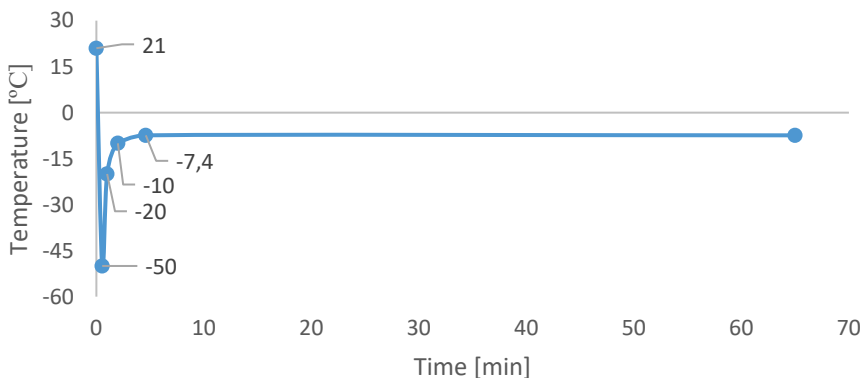


Figure 5. The temperature profile of the full ice recrystallization inhibition assessment experiment.

The IRI was calculated following the mathematical description derived by Budke *et al.* (C Budke *et al.*, 2009). The images were processed using Fiji (Schindelin *et al.*, 2012) to calculate the mean radius of the crystals and the total crystal volume. The cube of the mean crystal radius was calculated for all images and plotted against time. The slope of the curve obtained from time points 30–60 min (where total crystal volume Q is stable) was taken as the recrystallization rate constant (K_d). In all experiments, Q was below 10% (in high volume fraction the theory for IRI calculation is not legitimate).

In the Publication I a sigmoidal curve was fitted to the K_d against concentration plot. The inflection point of the curve, termed the C_i value, represents the 50% inhibition concentration (C Budke *et al.*, 2009). The rate constant in the absence of protein was determined by measuring the recrystallization rate of buffer without protein.

In the Publication II to correct the effect of different ice volume fractions between experiments, K_d values were extrapolated to zero volume fraction ($Q = 0$) as described in (C Budke *et al.*, 2009) and marked as K_{d0} .

3.3.2 Accelerated method

IRI in ice cream mixes was determined by a modified sucrose sandwich assay (A Regand & Goff, 2006). A 3 μ L drop of ice cream mix (35% dry solids) containing different concentrations of IBPs was placed between a microscope slide and 18 mm square coverslip and sealed with silicone oil to prevent evaporation.

The sample was flash frozen in liquid nitrogen and placed onto a cold stage (Linkam PE120, UK) mounted on a microscope (Nikon Eclipse E200-LED, Japan). A drop of cold ethanol was placed on top of the sample to prevent condensation. Cold stage temperature at the beginning of the experiment was $\sim 1^\circ\text{C}$ and it was programmed to change the temperature in six steps, as presented in *Figure 6*.

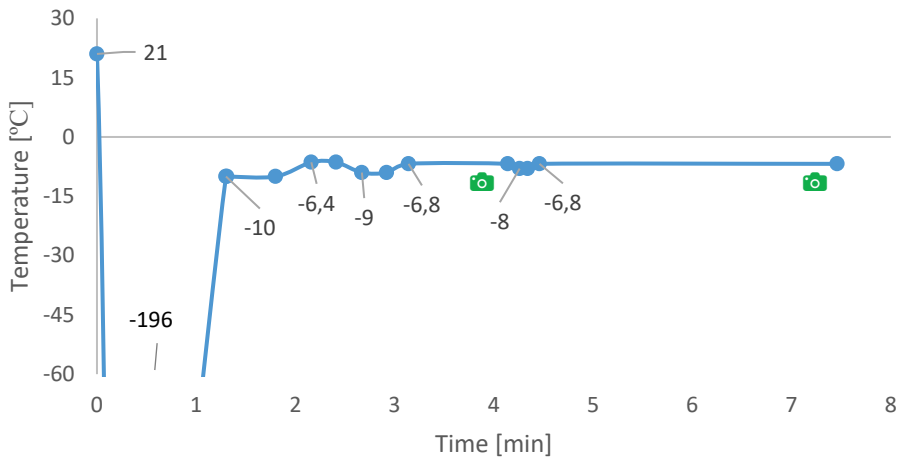


Figure 6. The temperature profile of the accelerated ice recrystallization inhibition assessment experiment. Green camera symbols indicate the time when photos were made.

Two photos were made at the end of steps 4 and 6, with 200 s total time in between the photos (indicated by camera symbols in *Figure 6*). Photos were automatically analyzed with a macro written for Fiji (Schindelin *et al.*, 2012) and the mean radius of ice crystals was calculated. At least 8000 crystals were measured in each photo.

IRI activity was calculated as described in (C Budke et al., 2009). The mean cubic radius of ice crystals was plotted against time and the slope of the line was taken as recrystallization rate constant K_d . Recrystallization rates against concentration were plotted and a sigmoidal curve was fitted. The inflection point of the curve (C_i) represents the 50% recrystallization inhibition concentration.

3.4 Ice crystal morphology

Ice crystals were observed in the nanoliter osmometer. Crystals were produced as described above in the thermal hysteresis method. Samples contained 3.3–50 μM of protein in 20 mM ammonium bicarbonate buffer (pH 8.5). Single crystals of typically 30 μm diameter were obtained slightly below their melting temperature. Then the temperature was slowly dropped, and the crystal shapes were observed during initial growth and burst. Each experiment was repeated to observe growth from different *c*-axis orientations.

3.5 Fluorescence-based ice planes affinity

Fluorescence-based ice plane affinity (FIPA) was used to determine IBP ice plane binding preference. A modified method of (Basu et al., 2014) was used. Ice monocrystals were grown as described by (C A Knight et al., 1991). Plastic or glass beakers were insulated from the sides and filled with 2.5 L of degassed double distilled water. A weighted 50 mL tube with a small hole in the cap was placed on the bottom of each beaker to reduce pressure buildup and avoid bubble nucleation. The beakers were then left in a freezer at $-1\text{ }^\circ\text{C}$ for three days, and a slab of ice approximately 6 cm thick grew on top of the water. The ice was then examined through crossed polarizers, and large single crystals were cut out by melting the ice with hot metal plates. The orientation of the *c*-axis was established by careful observation of the birefringence color pattern that appears when looking through crossed polarizers (Basu et al., 2014; Petrenko & Whitworth, 2002).

A small oriented single ice crystal block was mounted on a brass cold finger as described by (C A Knight et al., 1991). A hemispherical glass cup (diameter 60 mm) was filled with cold double distilled water, and the crystal was submerged in the water. The cup and cold finger were enclosed within an isolated Styrofoam box. The crystal was then allowed to grow into a ~ 40 mm in diameter hemisphere; then the water was replaced by 50 mL of 0.01–0.07 mg mL^{-1} protein solution in cold 10 mM Tris buffer. The hemisphere was then allowed to grow at a constant temperature $-4.5\text{ }^\circ\text{C}$ for 3.5 h until it reached 46 mm in diameter, thus adding a layer of 3 mm of ice to the hemisphere. Cold finger with the hemisphere was then rotated upside down, and the flat part of the sphere was evened out by a warm metal plate. The temperature of the cold finger was then set to $+1\text{ }^\circ\text{C}$, and the hemisphere was carefully wiped by a paper tissue to remove non-specifically bound protein (Hanada, Nishimiya, Miura, Tsuda, & Kondo, 2014) and was put into a $-18\text{ }^\circ\text{C}$ freezer as soon as it detached from the cold finger. The hemisphere was etched at least overnight and then was imaged inside the $-18\text{ }^\circ\text{C}$ freezer in fluorescent light and then observed visually.

The orientation of ice crystal *a*-axes was determined by pit etching. Hemisphere was covered with plastic wrap, and a small hole was made with a needle in the center of the basal plane. The hemisphere was then put into a lyophilizer for 15–30 min until a clearly visible hexagonal hole appeared. Sides of the hexagonal pit coincide with the primary prism planes of the ice crystal lattice (Brumberg et al., 2017).

3.6 Kinetics of accumulation

The fluorescence experiment between two coverslips was performed on a custom-built LabVIEW controlled cold stage mounted on a fluorescence microscope (Ti Eclipse, Nikon, Japan) with sCMOS camera (Neo 5.5 sCMOS, Andor, UK), described in more detail in (Celik et al., 2013; Haleva et al., 2016). The experiment followed the method of (Celik et al., 2013).

A sample of 1.6 μL containing GFP-*Efc*IBP or GFP-sbwAFP (in 10 mM Tris-HCl pH 8.0, 20 mM NaCl) in different concentrations was placed on a sapphire slide and covered with a 16-mm diameter circular glass coverslip. The gap between the sapphire and the coverslip was sealed by immersion oil to prevent drying of the sample. The sapphire was placed on a copper slab with a 2-mm diameter hole to observe the fluorescence. The combination of sapphire and a small hole was designed to minimize temperature gradients in the sample. Oil was placed between the copper stage and the sapphire to improve the thermal contact. The stage temperature was then lowered until the solution froze at around $-25\text{ }^{\circ}\text{C}$. The temperature was then raised past the melting point until only a few crystals remained. The temperature of the stage was then slowly lowered until crystal burst. The protein-bound ice was observed for 15 minutes in fluorescent light at a constant temperature. Image analysis was performed using NIS Elements AR software (Nikon, Japan). Fluorescent measurements represent the difference between the fluorescence at a given time and the fluorescence at the time of initial crystal burst.

Basal plane fluorescence intensity profiles of GFP-*Efc*IBP and GFP-sbwAFP were analyzed over time. The binding kinetics of the IBPs were then calculated by fitting measured fluorescence intensity to the Equation 1. The accumulation rate value (K_{on}) of each protein can then be calculated as the concentration is known.

3.7 Ice cream production

A low-fat dairy ice cream was used in the experiments. The recipe was adapted from (Bramley, Gray, Turan, Spors, & Frisch, 2011). The ice cream consisted of 0.5% milk fat, 11.5% milk solids-non-fat, 29.4% carbohydrates, 0.15% emulsifier and 0.2% stabilizer. Dry components were measured together and carefully mixed to homogeneity with a small amount of water to avoid clumps. Remaining liquid components were added after that. The ice cream mix was heated to $65\text{ }^{\circ}\text{C}$ and homogenized with a two-stage homogenizer (Gea Niro Soavi, Italy) at the homogenization pressure of 12 MPa on the first stage and 28 MPa on the second stage according to a local ice cream manufacturer instruction. After that, the mix was pasteurized at $85\text{ }^{\circ}\text{C}$ and left to cool and ripen overnight at $4\text{ }^{\circ}\text{C}$. IBPs were added into the mix before freezing: *E. coli* extract containing type III AFP up to concentration 35 mg L^{-1} of AFP, and 65 mg L^{-1} of winter rye extract total protein (400 mg L^{-1} lyophilized extract dry weight). The ice cream mixes were frozen using a scraped surface barrel freezer (Armfield FT-25-BA, UK) at a set draw temperature $-5\text{ }^{\circ}\text{C}$ and packed into 300 mL containers. The ice cream was hardened at $-40\text{ }^{\circ}\text{C}$ for 24 h and afterward stored at $-18\text{ }^{\circ}\text{C}$. Ice cream without IBP was marked as control ice cream.

3.8 Ice cream analysis

3.8.1 Ice crystal visualization

Ice crystal aggregates were visualized using polarized light microscopy (Nikon Eclipse E200-LED, Japan). The method was elaborated from the one used by (Ndoye & Alvarez, 2015). Sample preparation and microscopy were performed entirely in a cold chamber at temperature $-18\text{ }^{\circ}\text{C}$ to avoid temperature fluctuations and crystal melting. Tiny ice cream piece was resuspended in $100\text{ }\mu\text{L}$ of silicone oil ($-18\text{ }^{\circ}\text{C}$) in a test tube and vortexed for 10 s. A drop of suspension was pressed between a microscope slide and a coverslip. The sample was then placed on a microscope cold stage holding the temperature at $-18\text{ }^{\circ}\text{C}$ and a drop of ethanol was placed on top of the coverslip to prevent condensation. Photos were analyzed with Fiji software (Schindelin et al., 2012) and aggregate ice crystal area was measured.

3.8.2 Hardness

Type III AFP ice cream hardness was determined by a penetration test with a TA.XT2i texture analyzer (Stable Micro Systems, United Kingdom). The procedure was elaborated from (Varela, Pintor, & Fiszman, 2014). Each sample container ($4\times 6\times 10\text{ cm}$) was taken out of the freezer ($-18\text{ }^{\circ}\text{C}$) and tested at room temperature ($21\text{ }^{\circ}\text{C}$) exactly after 10 min. The samples were penetrated to a depth of 15 mm with a 3-mm diameter cylindrical probe at a speed of 2 mm s^{-1} . The maximum applied force (N) was used as a measure of hardness.

3.8.3 Melting

Control and type III AFP (3 mg L^{-1}) ice creams were cut into blocks of equal weight and immediately transferred onto metal sieves with 1 mm opening. Generic webcams were placed in front of the samples and photos were made at regular intervals. The experiment was performed at room temperature ($21\text{ }^{\circ}\text{C}$) and samples were held for 2.5 h to ensure complete melting. Photos were processed in Fiji software (Schindelin et al., 2012) and the relative sample height was calculated.

3.8.4 Sensory analysis

A trained panel of seven ice cream assessors evaluated ice cream samples containing extract from winter rye (65 mg L^{-1} of total protein) comparing it to the same ice cream without rye extract. Sensory analysis was based on the (Bodyfelt, Tobias, & Trout, 1988; Guinard et al., 1997) methods. Samples were divided as separate portions into 30 mL plastic cups and were assessed in duplicate. The samples were coded, and their order randomized. Ice cream samples were prepared and stored at $-18\text{ }^{\circ}\text{C}$, before evaluation the samples were let at room temperature for 5 min. The experts were asked to assess the ice cream sweetness, roughness, and friability on a scale from 0 to 15, with score fifteen for very sweet, friable or rough ice cream.

3.9 Statistical analysis

In the IRI experiment in the Publication I, a sigmoidal curve was fitted to the K_d vs concentration data using non-linear regression with brute force in R 3.2.4 (R Foundation for Statistical Computing, Austria) package “nls2” 0.2. A profile likelihood 95% confidence interval for the C_i point was calculated using the “nlstools” 1.0-2 R package. IRI measurement for each concentration point was repeated at least five times and the averaged K_d value was used for curve fitting.

In the Publication II, the IRI experiment was repeated at least five times for each concentration. Statistical analysis and plotting were performed using R 3.4.3. The mean K_d values and 95% confidence intervals at 0.02 μM and 0.1 μM protein concentration were calculated by a nonparametric bootstrapping method from R package “Hmisc” 4.0-3 using 1000 resamples.

In the Publication IV, average recrystallization rates of at least two replicates per point were plotted against concentration and a sigmoidal curve was fitted. Curve fitting was performed by non-linear regression with brute force in R 3.4.0 with “nls2” 0.2 package and 95% profile likelihood confidence interval for the C_i point was calculated using the “nlstools” 1.0-2 R package. Mean K_d value of 5 replicates of ice cream mix without IBP was used in curve fitting as a growth limiting rate constant for vanishing protein concentration.

Thermal hysteresis measurements in the Publication II were repeated at least three independent times and average TH was reported.

Fluorescence-based ice plane affinity experiments in the Publication III were performed at least twice for each crystal orientation.

In the Publication III, the ice crystal shape experiments in the nanoliter osmometer were repeated many times (>10) until the crystal was observed from all sides and its shape could be undoubtedly interpreted.

In the Publication III, an equation provided by (Drori et al., 2014) was fitted for each IBP adsorption experiment using Microsoft Excel Solver add-in. The average adsorption constant K_{on} was calculated from at least three replicates.

In the Publication IV, crystal aggregate size measurement was performed in four replicates. For each ice cream sample 40 pictures were made, from which at least 450 crystal aggregates were analyzed to determine the median Feret (maximum caliper) diameter of the aggregates.

In the Publication IV, the ice cream hardness test was performed eight times in different areas of the same ice cream sample and mean hardness was calculated.

In the Publication IV, the ice cream melting experiment was performed in two replicates.

In the Publication IV, sensory analysis mean values and 95% confidence intervals were calculated by a nonparametric bootstrapping method from R 3.4.0 package “Hmisc” 4.0-2 using 1000 resamples.

4 Results and discussion

A summary of the findings of the Publications I–IV is presented in this section. More detailed discussions are available in the papers.

4.1 *Efc*IBP

The wild-type (wt) *Efc*IBP, a 24 kDa bacterial ice-binding protein from ciliate *Euplotes focardii* consortium, was recombinantly produced in *Escherichia coli*. According to computational homology modeling and protein crystallization results, *Efc*IBP is a so-called IBP-1 fold type (Figure 7) that is common among other bacterial IBPs such as *Col*AFP from *Colwellia* sp. SLW05 (Hanada et al., 2014), *Tis*AFP (isoforms 6, 8) from *Typhula ishikariensis* (Cheng, Hanada, Miura, Tsuda, & Kondo, 2016; Kondo et al., 2012), and *Le*IBP from *Leucosporidium* sp. AY30 (J. H. Lee et al., 2012).

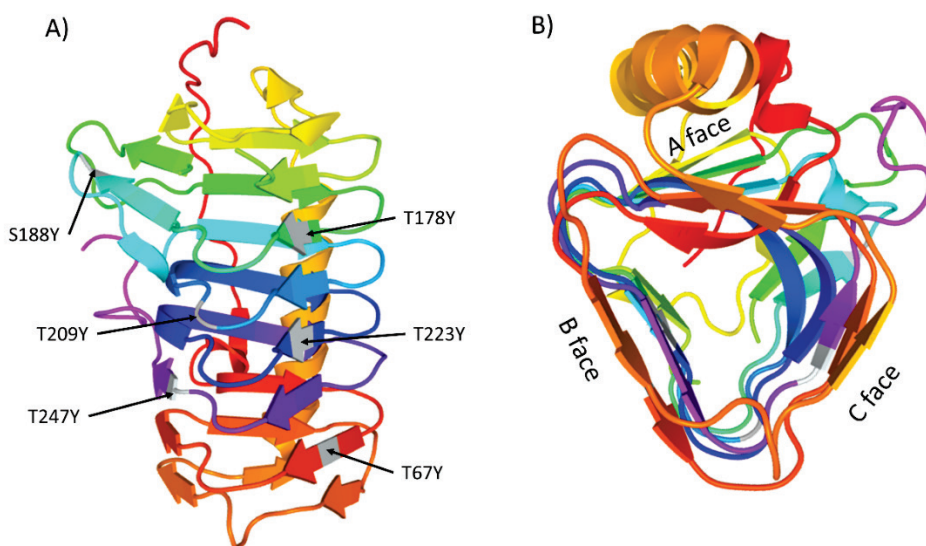


Figure 7. The 3D structure of *Efc*IBP, Protein Data Bank accession code 6EIO. A) The location of amino acid mutations is shown with arrows (discussed further in the text). B) The three distinct faces are shown. Figure generated with Web3DMol (Shi, Gao, & Zhang, 2017).

More specifically, *Efc*IBP is folded into a right-handed β -helix with a triangular cross-section (Figure 7). The three sides are formed by parallel β -sheets named A, B, and C faces. A single α -helix is aligned along the A face, thus screening it from the solvent. The B face is flat and regular, while C face has two regions. The first region forms a flat surface, but the second markedly diverges away from the protein core. Both B and C faces are fully exposed to the solvent.

4.2 *Efc*IBP thermal hysteresis and ice recrystallization inhibition activity

Thermal hysteresis activity of the wt *Efc*IBP is 0.46 $^{\circ}\text{C}$ at 40 μM as shown in Figure 8. This value is in the range of moderate fish AFPs (Celik et al., 2010; Davies, 2014). As can be seen in the plot, the activity at 50 μM is still rising and this means that at higher

concentrations TH may be higher as well. However, in practice, TH measurements at such high concentration are very hard to perform due to the fast melting of superheated crystals. In other words, it is impossible to form a tiny single ice crystal that is used in TH measurement. For comparison, moderate AFP type III produces the same TH at 300 μM (DeLuca et al., 1998; Takamichi, Nishimiya, Miura, & Tsuda, 2009) and hyperactive *TmAFP* at 40 μM with 8 min incubation time yields 1.1 $^{\circ}\text{C}$ (Drori et al., 2014). Other IBP-1 fold proteins were reported to have a variety of TH activities: *ColAFP* 1.6 $^{\circ}\text{C}$ at 50 μM (Hanada et al., 2014), *LeIBP* 0.2 $^{\circ}\text{C}$ at 50 μM (J. H. Lee et al., 2012), *TisAFP8* 1.3 $^{\circ}\text{C}$ at 50 μM (Xiao et al., 2010), *Afp4* from *Glaciozyma antarctica* 0.08 $^{\circ}\text{C}$ at 200 μM (Hashim et al., 2014), and *NagIBP* from *Navicula glaciei* 3.2 $^{\circ}\text{C}$ at 1.6 mM (Xiao et al., 2014).

No differences in TH were detected between 1 min and 10 min incubation time, indicating that *EfcIBP* binds to ice quickly within 1 min, like other moderate AFPs (Drori et al., 2014).

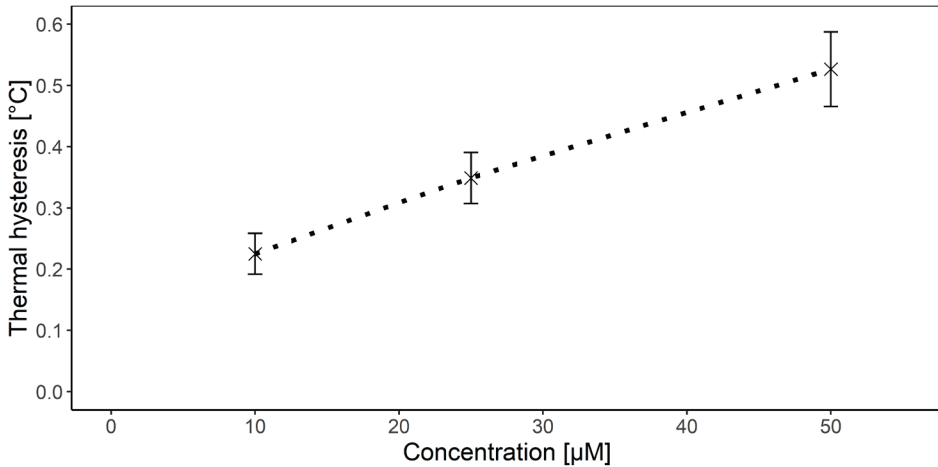


Figure 8. Thermal hysteresis of the wild-type *EfcIBP*. Vertical bars are standard deviations ($n=3$).

EfcIBP is a strong ice recrystallization inhibitor, as can be seen in Figure 9A. Addition of as little as 0.1 μM is very effective in slowing recrystallization and only some crystals grow and develop clear facets that are typical for IBPs. At higher concentration of 1 μM crystals are totally stable and no changes are observed.

Quantification of the IRI activity of *EfcIBP* is shown in Figure 9B and compared to moderate AFP type III and hyperactive *TmAFP* (Figure 9C).

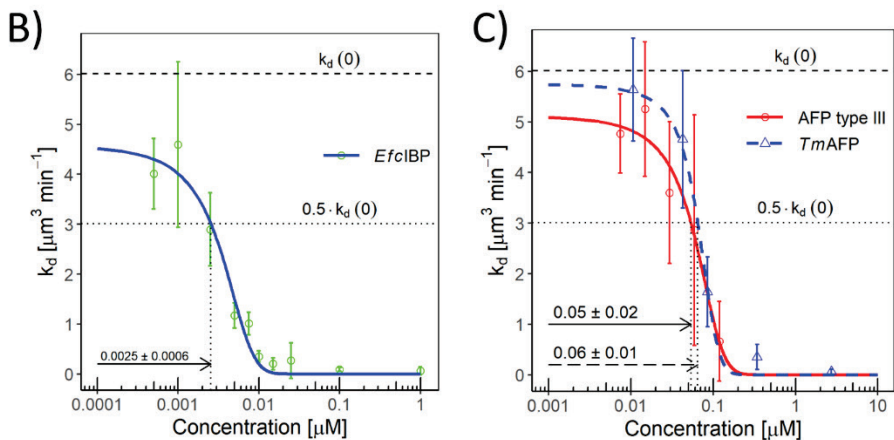
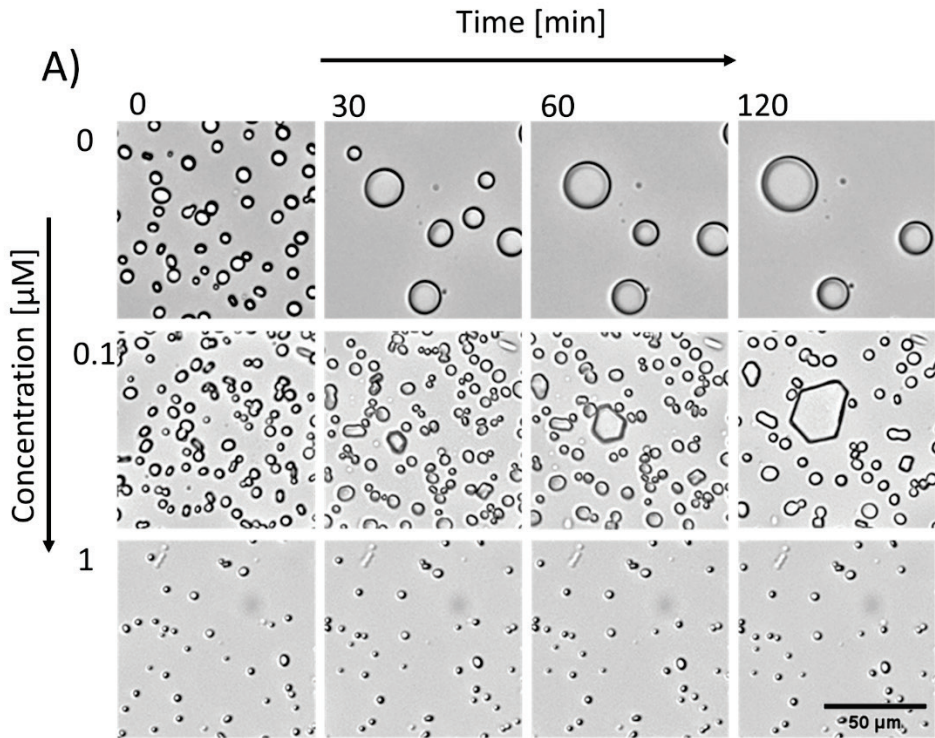


Figure 9. A) Ice crystal size during recrystallization experiment at different *EfcIBP* concentrations. B, C) Quantitative measurement of recrystallization inhibition activity of B) *EfcIBP* and for comparison C) fish type III AFP and *TmAFP*. The concentration that inhibits recrystallization by 50% (C_i) is shown for every protein by arrows. The vertical axis represents recrystallization speed.

The C_i or concentration that inhibits recrystallization by 50% is the inflection point of the curve and is used for comparison between proteins. Below this concentration recrystallization inhibition is ineffective. As can be seen in Figure 9 B, C the C_i point of *EfcIBP* is $0.0025 \pm 0.0006 \mu\text{M}$ ($2.5 \pm 0.6 \text{ nM}$) and it is an order of magnitude lower than

type III AFP and *Tm*AFP that have $0.05 \pm 0.02 \mu\text{M}$ and $0.06 \pm 0.01 \mu\text{M}$ respectively. In other words, *Efc*IBP is an order of magnitude stronger ice recrystallization inhibitor than type III AFP and *Tm*AFP. It is also very high compared to other proteins and C_i values in the nanomolar range (1 nM) were previously reported only for AFGPs (Carsten Budke et al., 2014; Luuk L C Olijve et al., 2016).

4.3 Ice crystals in *Efc*IBP solution

The ice crystal shape of the wt *Efc*IBP at the beginning of crystal growth during cooling appears as a wide hexagonal truncated trapezohedron (Figure 10A). A simplified model for this shape is shown in Figure 10B. At a constant temperature the crystal is stable, but when the temperature is gradually lowered, the growth happens in small sharp steps in *a*-axis direction, in other words, crystal grows, then stops, then grows again. This continues until a smooth biconvex or obtuse-angled bipyramidal crystal is formed (Figure 10A rightmost frame). Unlike sharp-pointed crystals that are commonly produced by moderate fish AFPs, this crystal is shorter in the *c*-axis and longer in *a*-axis with the *c*:*a* ratio 1:4.5. In other words, *Efc*IBP ice crystal grows in *a*-axis direction until prism planes are eliminated, while fish AFPs grow in the *c*-axis direction until basal planes are minimized. It should be noted, that the initial truncated trapezohedron has facets at a different angle than fully grown biconvex crystal. The significance of this fact is explained further in connection to the FIPA results.

The stepwise growth changes depending on the protein concentration. At a higher concentration, the number of growth steps can be as little as one, while at a lower concentration the number of steps is larger, and the growth becomes more continuous. A similar stepwise growth behavior was observed in *Lpl*IBP from *Lolium perenne* (Bar-Dolev et al., 2012). In comparison, ice crystals of hyperactive IBPs remain stable during cooling until burst at the freezing hysteresis temperature.

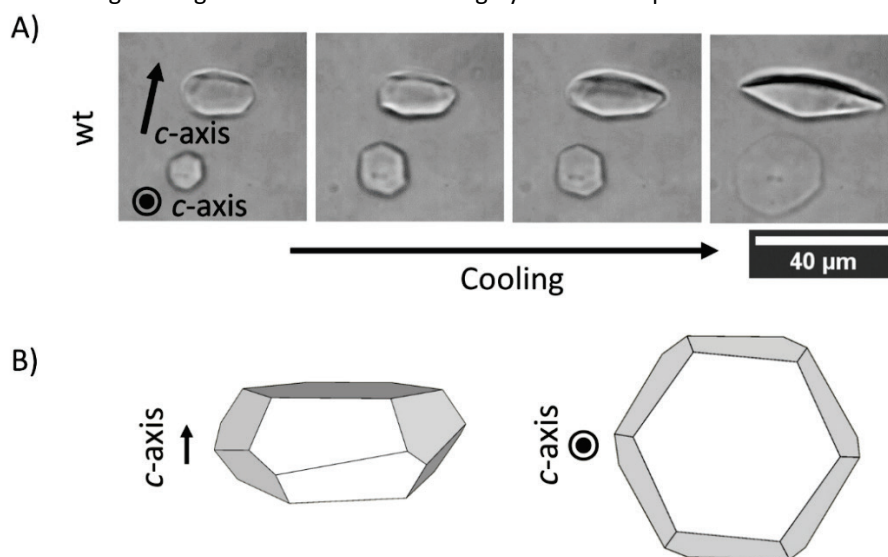


Figure 10. A) Growth pattern of ice crystals in 5 μM *Efc*IBP solution during gradual cooling. B) A simplified model of the ice crystals visible in the leftmost frame of (A). The direction of the *c*-axis is shown.

*Efc*IBP ice crystals also have a unique burst pattern that is shown in *Figure 11*. When the biconvex crystal is fully formed, and the cooling is continued, the crystal bursts in *a*-axis direction as a thin disc protruding around the circular edge of the crystal. When observed from the side, the burst crystal resembles Saturn. This is most visible in *Figure 11* G-H (side view) and O-P (top view). Bursting in *a*-axis direction is typical for hyperactive proteins, including *Efc*IBP hyperactive homolog proteins such as *Sfl*BP from *Shewanella frigidimarina* (Vance, Graham, & Davies, 2018), *Ffl*BP from *Flavobacterium frigidis* PS1 (Do, Kim, Kim, & Lee, 2014), and *Co*/AFP that all burst dendritically. The non-dendritic bursting of the wt *Efc*IBP can be explained by the low degree of supercooling that is achieved before burst (low TH), thus the ice does not grow dendritically.

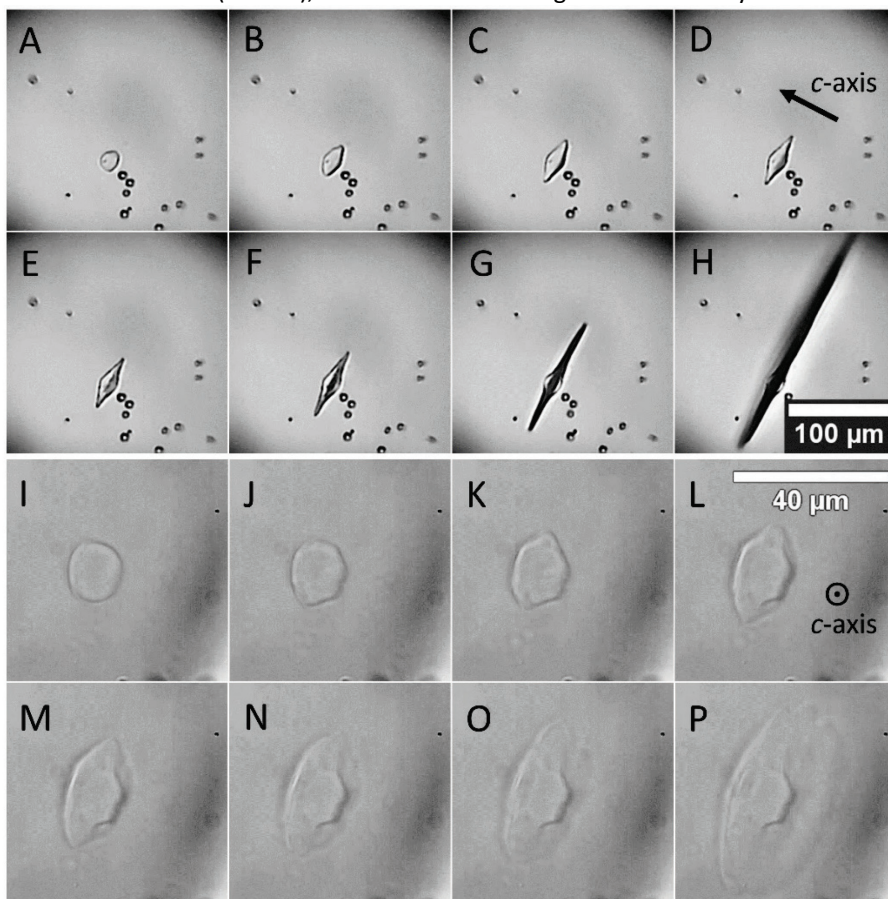


Figure 11. The growth and burst pattern of ice crystals in EfcIBP solution. A-H) 5 μM EfcIBP solution with the c-axis in the image plane. I-P) 25 μM solution of GFP-EfcIBP with the c-axis normal to the image plane.

The shape and bursting behavior of ice crystals provided some clues for the binding plane affinity of *Efc*IBP. To investigate its affinity further the *Efc*IBP was fused with the green fluorescent protein (GFP) and fluorescence-based ice plane affinity (FIPA) assay and other fluorescent microscopy methods were used. Fusion with GFP did not change ice crystal shape and burst behavior (*Figure 11* I-P). *Figure 11*

4.4 *Efc1BP* ice plane affinity

FIPA assay of GFP-*Efc1BP* showed a surprisingly intricate binding pattern (Figure 12). The protein shows an asymmetrical roughly triangular pattern with distinctive bright spots of higher affinity. The protein covers most of the ice hemisphere, except for the curved stripes in the direction of the *c*-axis and also the equatorial belt. This indicates that *Efc1BP* binds to most pyramidal planes with different angles and does not bind to the prismatic plane. Two sets of spots of higher affinity are located on different pyramidal planes. This is confirmed by the fact that these spots have 12-fold symmetry on the whole sphere, which is a feature of pyramidal planes (Basu et al., 2014). The first set of spots is located at a very small angle to the basal plane and forms a small ring around the *c*-axis. This pyramidal plane will be further named as near-basal. Such a close angle to the basal plane has not been reported before. The second set of spots is much further away from the basal plane and are located close to the secondary pyramidal plane, but not exactly on it, as the spots are asymmetric and shifted with respect to each other around the *c*-axis. A darker spot on the tip of the hemisphere surrounded by the near-basal ring suggests that the binding directly to the basal plane is weak, however, it is difficult to make sure as the bright spots are too close.

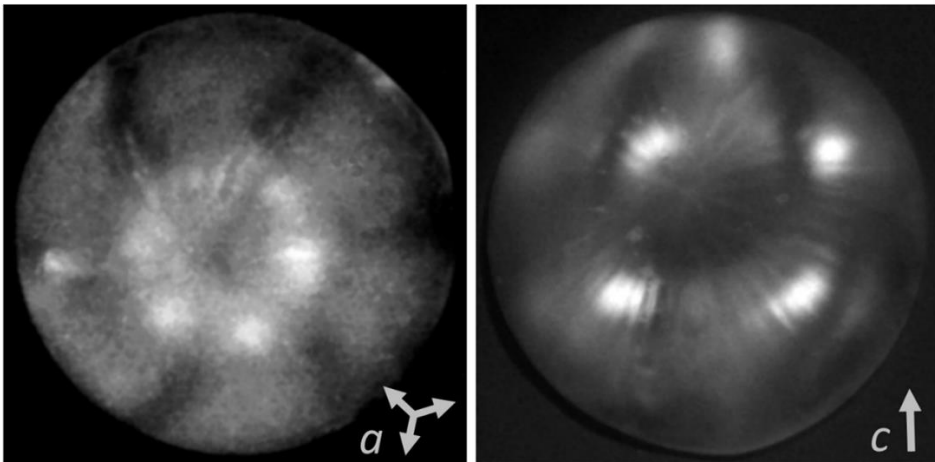


Figure 12. Fluorescent GFP-*Efc1BP* adsorbed to the ice hemisphere. Arrows indicate the orientation of crystal axes.

Overall, the *Efc1BP* ice plane adsorption pattern observed by FIPA is consistent with the ice crystal growth and burst behavior. The near-basal (and basal) binding prevents growth in the *c*-axis direction, consequently, the ice crystal grows and bursts through the unprotected prismatic plane in *a*-axis direction.

As was mentioned before, the wild-type *Efc1BP* ice crystal during initial growth has pyramidal crystal faces at a different angle than at the end of the growth. The angle at the beginning corresponds to the position of the second set of asymmetric higher affinity spots. In other words, the restriction of crystal growth in these spots direction, plus in the basal direction due to the basal and near-basal binding, is the reason why the truncated trapezohedron shape is formed. In the absence of the basal and near-basal affinity, this pattern would have produced a bipyramidal crystal with acute-angled apices in the *c*-axis direction that is very typical to fish AFPs. Ice grows faster in *a* direction than in *c*, therefore, when cooling is continued the *Efc1BP* trapezohedron ice crystal bursts in

a -axis direction even though it is partially protected from that side by adsorption to pyramidal angles. However, *EfcIBP* continues to bind to the near-basal pyramidal plane that is at a small angle to the basal plane, forcing the growing parts of the crystal to shrink in thickness. In the end, this creates a typical wide biconvex shape (or bipyramid with obtuse-angled tips) with a sharp circular edge. The growth stops when the crystal has only the near-basal planes and the prismatic and other pyramidal planes are eliminated.

4.5 *EfcIBP* adsorption kinetics

Adsorption kinetics of GFP-*EfcIBP* were assessed using fluorescent microscopy and compared to hyperactive GFP-sbwAFP that binds to the basal plane (Pertaya et al., 2008). When *EfcIBP* ice crystals are grown between two coverslips, the ice is forced into a thin layer of 10 μM . This creates truncated crystals with long spicules that are actually ice sheets seen in profile (Figure 13). The sheets expose large basal planes that in this experiment show strong accumulation of GFP-*EfcIBP*, which is different from FIPA, where the preferred plane is near-basal and direct basal accumulation is weaker. Fluorescence intensity measurements show that GFP-*EfcIBP* accumulates on the ice crystal in approximately one minute and then the intensity remains constant. This is compared to GFP-sbwAFP that accumulates on the basal plane much slower, as is common in hyperactive AFPs (Drori et al., 2014).

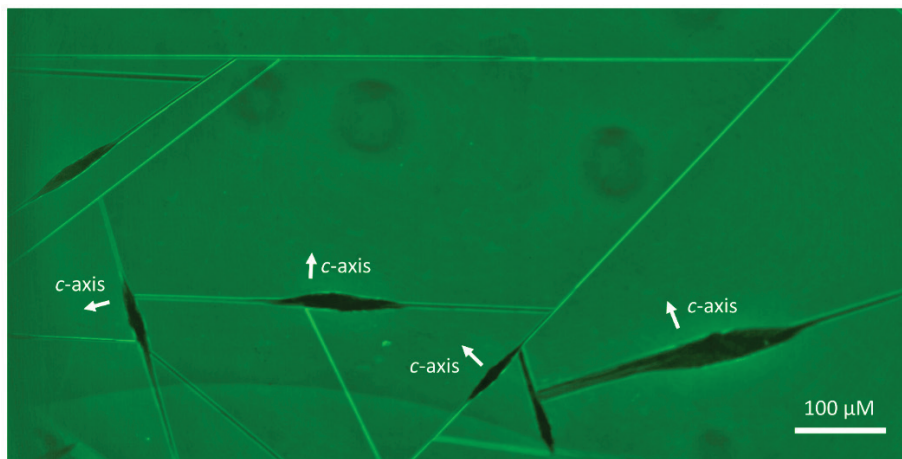


Figure 13. Burst ice crystals in 10 μM GFP-*EfcIBP* visualized by fluorescent light. Arrows indicate the direction of c -axis.

Quantitative accumulation measurements of GFP-*EfcIBP* (on the basal and on pyramidal plane) and GFP-sbwAFP (on the basal plane) are presented in Figure 14. Equation 1 was fitted to the fluorescence intensity vs time data and the adsorption constants K_{on} were calculated. The *EfcIBP* K_{on} value for the basal plane is $4 \pm 1 \text{ mM}^{-1} \text{ s}^{-1}$ and on a pyramidal plane (crystal side) $2 \pm 1 \text{ mM}^{-1} \text{ s}^{-1}$. Therefore, the pyramidal binding is approximately as fast as basal, however, the fluorescence intensity is lower. The GFP-*EfcIBP* adsorption constant is close to the value reported for type III AFP with $K_{\text{on}} = 8 \pm 1 \text{ mM}^{-1} \text{ s}^{-1}$ (Drori et al., 2014), but the difference is that AFP type III binds this fast to the prism plane. In comparison, the basal plane adsorption constant of GFP-sbwAFP is an order of

magnitude lower with $K_{on} = 0.3 \pm 0.1 \text{ mM}^{-1} \text{ s}^{-1}$, but the fluorescence intensity that it achieves is much higher.

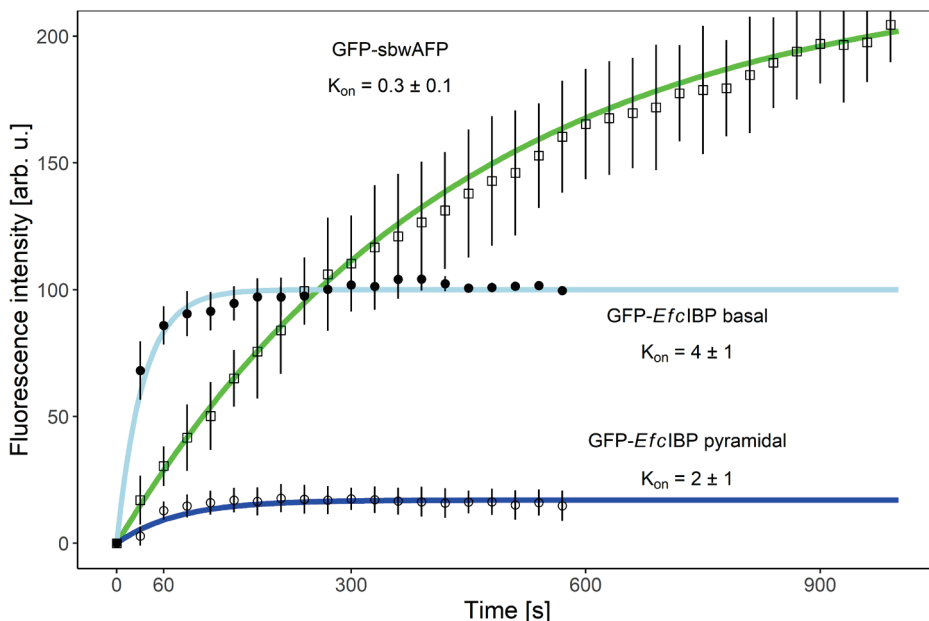


Figure 14. Adsorption kinetics of $10 \mu\text{M}$ GFP-EfcIBP on the basal plane (sheet) and pyramidal plane (crystal side) and $7.6 \mu\text{M}$ GFP-sbwAFP on the basal plane. The adsorption constants K_{on} are shown [$\text{mM}^{-1} \text{ s}^{-1}$]. Vertical bars represent standard deviation ($n=3$).

Previously it was reported that hyperactive IBPs accumulate slowly on the basal and prism planes and that accumulation on the basal plane can take hours, while moderately active IBPs bind fast to the prism plane and cannot bind to the basal plane (Drori et al., 2014, 2015b). Affinity to the basal plane was therefore proposed to be the feature that delineated hyperactive IBP class with high TH (Pertaya et al., 2008). However, EfcIBP is a fast basal plane binder reaching saturation in 60 s and yet has moderate TH. This indicates that basal plane affinity alone is not sufficient to achieve hyperactivity and that prismatic binding is important as well.

4.6 EfcIBP mutants

Protein docking studies to the basal plane and the prism plane revealed that both B and C faces of EfcIBP participate in ice adsorption. Therefore, these faces were considered for further study through point amino acid mutations. Six mutants were produced. The locations of the mutations are shown in Figure 7A. The B face mutations are T178Y, T223Y, and T67Y; the C face mutations are S188Y, T209Y, and T247Y. The code means that threonine (T) or serine (S) at a certain position on the protein backbone is replaced by tyrosine (Y). As was mentioned before, threonine is often found on ice-binding sites in T-X-T motif, including the EfcIBP, as threonine plays an important role in anchored clathrate waters organization.

Thermal hysteresis activities of the mutants are shown in Figure 15. At $40 \mu\text{M}$ the B face mutants T178Y, T223Y, and T67Y have TH $0.12 \text{ }^\circ\text{C}$, $0.06 \text{ }^\circ\text{C}$, and $0.04 \text{ }^\circ\text{C}$ respectively. At the same concentration TH of the C face mutants S188Y, T209Y, and T247Y is $0.22 \text{ }^\circ\text{C}$,

0.1 °C, and 0.02 °C. Reduced TH activities of all mutants indicate that both B and C faces participate in binding and no clear distinction of which face is more important for TH can be made.

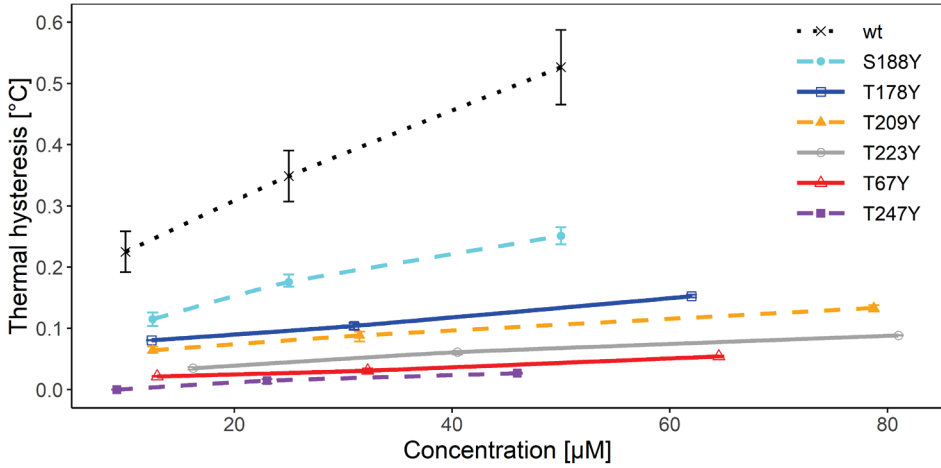


Figure 15. Thermal hysteresis activity of the *EfcIBP* B face (solid lines, empty markers) and C face (dashed lines, filled markers) mutants compared to the wild type. Vertical lines represent standard deviation ($n=3$).

Ice recrystallization inhibition was also measured to complement TH data and gain more insight into the effect of mutations on binding and *EfcIBP* activity. The measurements were performed at two concentration points and are presented in Figure 16. At lower concentration of 0.02 µM, all mutants clearly show significantly reduced (or none in case of T247Y) IRI activity, while the wt is still able to completely arrest recrystallization process. The activity of the mutants is more pronounced at higher concentration of 0.1 µM, where even the T247Y shows some weak recrystallization inhibition. These results support the conclusion that both B and C protein faces are important for ice adsorption.

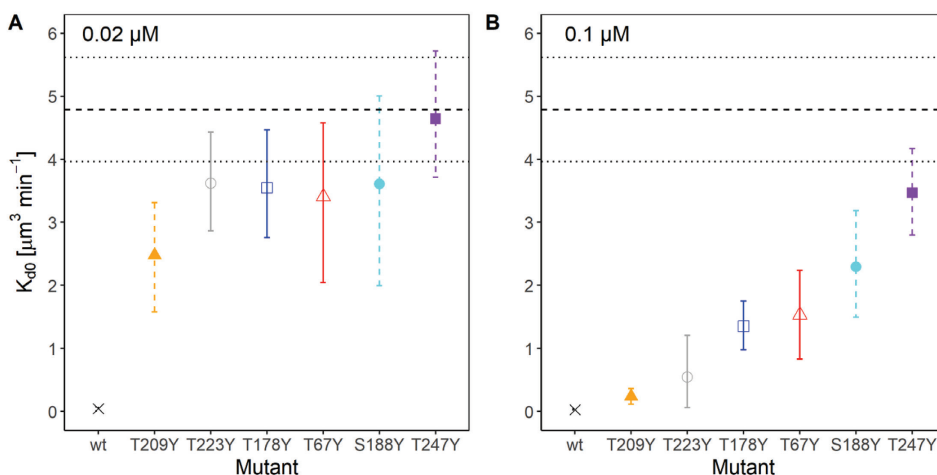


Figure 16. Ice recrystallization inhibition of the EfcIBP mutants compared to the wild type. The vertical axis represents recrystallization speed recalculated to zero ice volume. A) Measured at 0.02 μM and B) at 0.1 μM protein concentration. Vertical lines show 95% confidence intervals ($n=5$). Horizontal dashed and dotted lines represent mean and 95% confidence interval for the buffer without IBP. Colors and shape codes are the same as in Figure 15.

Comparison of TH and IRI data reveals (Figure 15 and Figure 16) that there is no obvious correlation between the activities. For example, the S188Y mutant has the highest TH activity of all the mutants, but it shows marginally higher IRI activity than the T247Y. This is made more obvious by Figure 17, where TH and IRI relative efficacy is compared. Since both TH and IRI activities stem from IBPs binding to ice, one would expect that reduction of TH activity would lead to an identical reduction in IRI activity, thus creating a series of horizontal lines on the relative activity plot. However, this is not what is observed in Figure 17. Therefore, it is possible that TH and IRI activities depend on different features of the binding sites or some other factors are important.

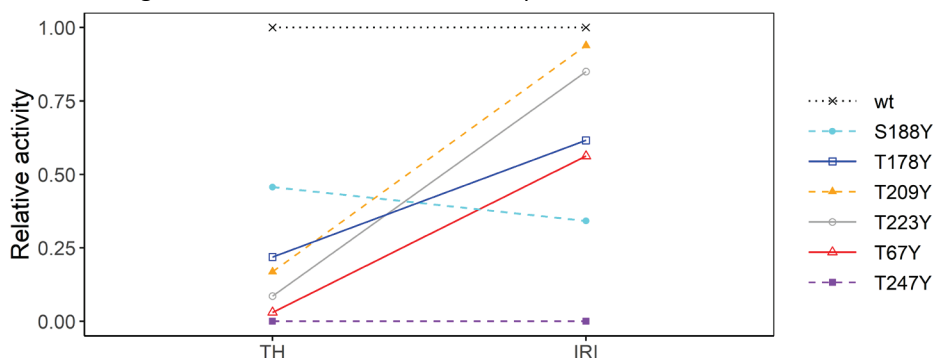


Figure 17. Comparison of relative TH at 40 μM and IRI efficacy at 0.1 μM of the wt EfcIBP and its mutants. Here 0 is minimum observed TH and IRI efficacy and 1 is maximum. Colors and shape codes are the same as in Figure 15.

To further investigate the effect the mutations had on *EfcIBP*, ice crystal shape analysis, FIPA, and kinetics experiments were performed.

As seen in *Figure 18*, all the mutants have a similar to the wt ice crystal shape with a different degree of twisting asymmetry. All mutants grow and burst as thin discs in *a*-axis direction. During cooling mutants T178Y, S188Y, and T209Y also grow in steps, like the wt. In other mutants (T223Y, T67Y, and T247Y), however, ice crystal growth is gradual with no steps observed. This is correlated with their TH activity, as these mutants are the weakest.

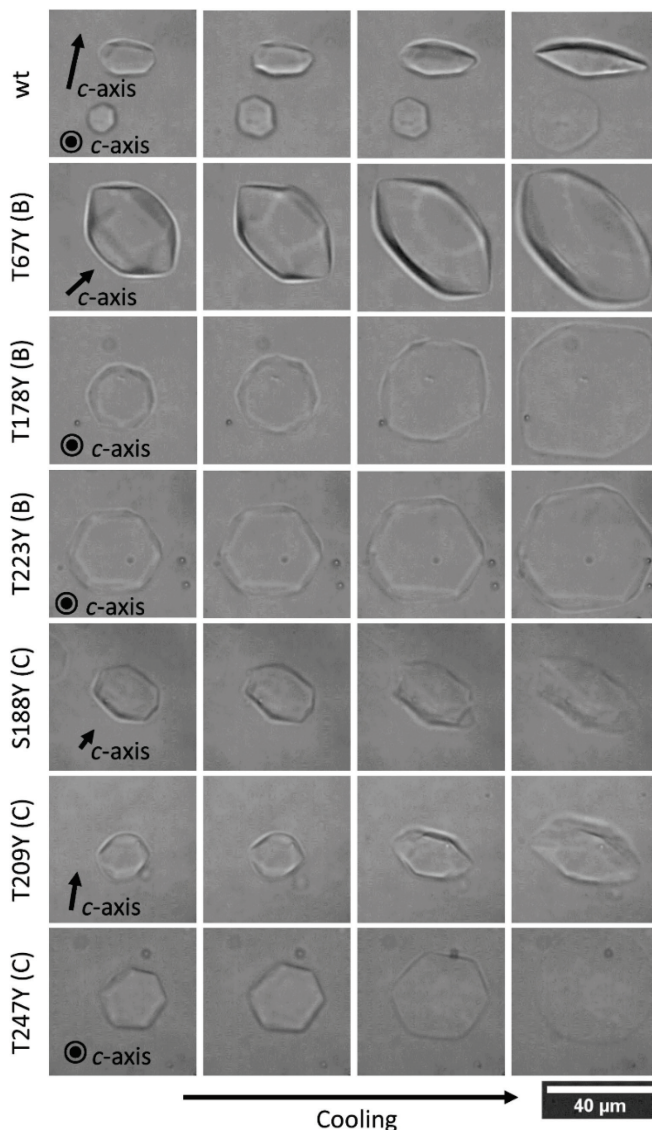


Figure 18. Ice crystal shapes formed by the wt EfcIBP and its mutants during cooling. WT figure is repeated here for easier comparison. The letter in parenthesis indicates the protein face that was mutated. Concentration of T67Y, T178Y, T223Y, T209Y mutants is 10 μM; S188Y 3.3 μM; T247Y 50 μM; and wt EfcIBP 5 μM.

The binding patterns of some weakest in TH mutants are presented in *Figure 19*. The mutants produce significantly dissimilar from the wt patterns with affinity spots that are different in shape and location. This suggests that the mutations did not completely disable the ice-binding sites, but rather modified their affinity by rearranging anchored clathrate water networks that are formed on the ice-binding sites.

The most striking fact is that the pattern of GFP-T67Y is completely symmetrical. This feature is reflected in the ice crystal shape, that is a well-defined hexagonal bifrustum (not trapezohedron) with no twisting asymmetry (*Figure 18*).

As can be seen in *Figure 19*, the mutants retain some basal or near-basal affinity with generally weak affinity to other pyramidal planes. The GFP-T223Y has no near-basal spots with only a small spot directly on the basal plane. This suggests that the central part of the B face is responsible for the near-basal binding (*Figure 7*).

Even though these mutants all have basal affinity with some generally weak pyramidal binding, their TH activity is low. This reinforces the conclusion that basal affinity alone is not sufficient to achieve hyperactivity when pyramidal or prism affinity is low. Therefore, affinity strength to specific ice planes, in addition to accumulation speed, are the factors that determine IBP activity.

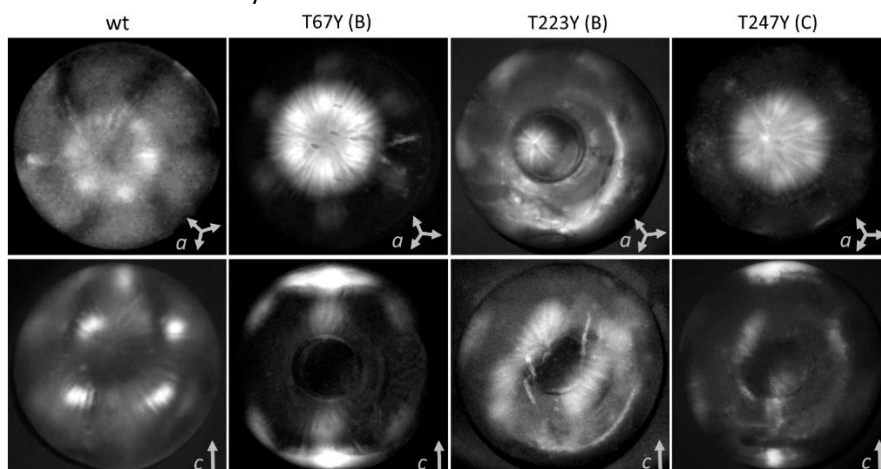


Figure 19. Ice plane affinity of the wt GFP-EfcIBP and some of its mutants. Letters in parenthesis indicate the mutated protein face. Crystal axis directions are shown by arrows. WT figure is repeated here for easier comparison.

Attempts to investigate the binding kinetics of the GFP-EfcIBP mutants T67Y, T223Y, and T247Y were unsuccessful. These mutants did not completely block ice growth and there was no visible accumulation of fluorescent signal. The ice crystal shapes produced between coverslips were generally similar to the wt (*Figure 13*), but with some differences. GFP-T223Y made crystals to grow in rod-like shapes with parallel basal planes. This shape corresponds well to the absence of near-basal binding. Recrystallization was observed in GFP-T247Y solution, where burst crystals were rounded off.

To summarize, EfcIBP has TH in the range of moderate IBPs and is a fast binder like moderate IBPs, but its basal plane affinity and *a*-axis ice crystal burst direction classifies EfcIBP as hyperactive. FIPA analysis demonstrated that strong prismatic and pyramidal binding are necessary for hyperactivity, in addition to basal. Thus, a new class of

moderate IBPs can be defined, which binds strongly to the basal plane, but weakly to the prismatic or pyramidal.

EfcIBP high ice recrystallization inhibition and its unusual shaping activity can be beneficial for the whole *Euplotes focardii* consortium. Antarctic waters are always at risk of freezing and *EfcIBP* can prevent ice growth, acting at a very low concentration diluted in the sea. Moreover, the planar crystal growth habit prevents complete freezing and can create pockets of water between the crystal plates, thus maintaining the liquid environment where the entire bacterial-ciliate community can survive.

4.7 IBP ice cream

Ice cream is a sensitive product that needs to be preserved under controlled conditions. Ice crystal growth and recrystallization that are promoted by temperature fluctuations reduce ice cream texture quality as bigger ice crystals cause a rough or crystalline mouthfeel. Ice-binding proteins have the potential of reducing the crystal size, therefore improving the mouthfeel, and increasing shelf life by preventing recrystallization. This work was undertaken to assess the potential of IBPs as a novel ingredient in ice cream. Two different sources of IBPs were used. Fish type III AFP was recombinantly produced in *Escherichia coli* and a winter rye extract was prepared from cold-acclimated plants. The IBPs were added to the ice cream mix just before the ice cream freezing process.

4.7.1 Ice recrystallization inhibition

Different from the *EfcIBP* recrystallization inhibition activity measurements, the ice cream mixes were analyzed using an accelerated method. *Figure 20* shows IRI activity of AFP type III and winter rye extract. The winter rye extract activity is recalculated to the total protein content, as the extract contains several IBPs (X. M. Yu, Griffith, & Wiseman, 2001) and their exact amount is unknown. The 50% recrystallization inhibition point (C_i) of the winter rye extract is $0.17 \pm 0.06 \text{ mg mL}^{-1}$ and of AFP type III $0.10 \pm 0.06 \mu\text{g mL}^{-1}$ (or $0.013 \pm 0.008 \mu\text{M}$). The difference between the C_i value of AFP type III measured in an ice cream mix and the value measured in sucrose solution ($0.05 \pm 0.02 \mu\text{M}$) (*Figure 9C*) can be explained by the fact that the ice cream mix contains stabilizers (locust bean gum and guar gum). The increase of IRI activity by a synergistic effect between IBPs and stabilizers was noted before (A Regand & Goff, 2006). However, a puzzling fact is that AFP type III IRI activity was reported to be two orders of magnitude lower with $C_i 4 \pm 2 \mu\text{M}$ (Luuk L. C. Olijve, Oude Vrielink, & Voets, 2016) or $5.9 \mu\text{M}$ (Luuk L C Olijve et al., 2016). No explanation for this discrepancy can be offered at the moment.

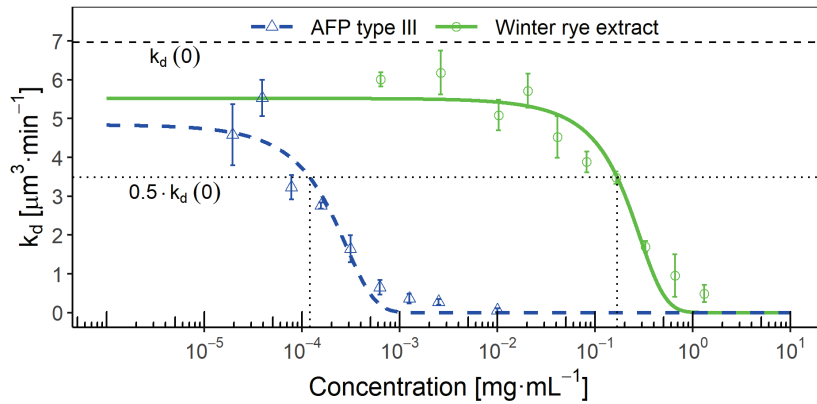


Figure 20. Ice recrystallization inhibition efficacy of AFP type III and winter rye extract (shown as total protein) in the ice cream mix. Vertical lines represent standard deviation ($n=2$). Dotted lines show C_i points.

For ice cream production the concentration range of AFP type III was chosen according to Unilever patents that recommend using 5–50 mg L^{-1} (Daniel, Hoddle, Jones, Oldroyd, & Singleton, 2004; Darling & Hoddle, 2001). According to Figure 20, this concentration falls into the range of maximum IRI activity. The concentration of winter rye extract was chosen to be 65 mg L^{-1} of total extract protein, which is below the 50% recrystallization inhibition point, in other words, ice recrystallization inhibition at this concentration is ineffective.

4.7.2 Ice cream microstructure

Ice creams containing different concentrations of AFP type III were produced and the microstructure of these ice creams was studied to reveal the impact IBPs have on ice cream. Figure 21 shows polarized light pictures from the control ice cream and the ice cream containing 35 mg L^{-1} of AFP type III. Under polarized light crystals appear white on a dark background, making them easier to see. In the control ice cream, the ice crystals are large and are separate from each other due to the disruptive sample preparation method. In the AFP type III ice cream, however, the crystals are tiny but are all joined together into strong aggregates that cannot be completely broken by the sample preparation. These agglomerates are smaller pieces of a big network-like continuous structure consisting of joined ice crystals that trap ice cream matrix in channels between the crystals. Increased ice crystal accretion was observed before also in sucrose solutions containing winter wheat IBPs (A Regand & Goff, 2006).

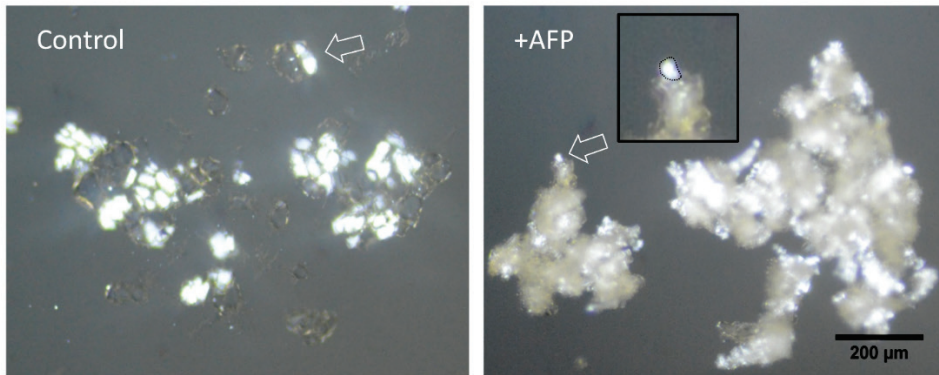


Figure 21. Representative polarized light photos of ice crystals from control ice cream and ice cream containing 35 mg L^{-1} of AFP type III. The arrows point to singular ice crystals.

Formation of strong ice crystal networks can be explained by the way IBPs modify ice crystals. Adsorption of IBPs forces the ice to grow between the bound molecules creating convex surfaces. Due to increased curvature, these ripples are unstable and easily melt. When such rippled surfaces of two crystals come into contact, these convex shapes due to accretion recrystallization fuse together and thus reduce the curvature and stabilize the system. Many crystals that come into contact fuse into large randomly organized three-dimensional networks that consequently have a striking effect on the overall ice cream texture.

4.7.3 Ice cream texture and melting behavior

The hardness of ice creams containing $0\text{--}25 \text{ mg L}^{-1}$ of fish AFP type III was evaluated using a texture analyzer. Figure 22A demonstrates that aggregation of crystals has a significant effect on overall ice cream hardness. While the control ice cream hardness is 5N, the addition of only 3 mg L^{-1} of AFP type III increases it fivefold. The hardness effect is remarkably dependent on AFP concentration and shows some saturation at concentrations higher than 10 mg L^{-1} .

To investigate the effect IBPs have on ice cream sensory properties, ice cream containing winter rye extract was assessed for roughness, friability, and sweetness. Figure 22B shows that assessors could clearly differentiate between the control and the IBP ice cream. The ice creams were graded on the scale 0 to 15, where 15 is very rough, friable or sweet. The IBP ice cream has the same sweetness, but significantly higher grades for roughness and friability. This means that the ice crystal aggregates are large enough to produce a rough or crystalline feeling in the mouth and their networks are extensive leading to ice cream breaking into pieces when bitten or scooped. The results of sensory analysis of winter rye IBP ice cream are consistent with the hardness analysis of AFP type III ice cream and support the microscopy evidence of ice crystal aggregation.

Other ice creams (including full fat and sorbet recipes) containing winter wheat extract, fish AFP type I, II, and AFGPs were produced in the lab with the same result of increased hardness and perceived crystallinity, indicating that the ice crystal aggregation effect might be a general property of many if not all IBPs. Moreover, increased hardness of ice cream was observed during freezing (the machine behaved differently as well), meaning that the aggregation process starts immediately inside the freezer and not later

during storage. Even though *Efc1BP* was not tested in ice cream, it is expected to behave in the same manner.

To complete the investigation into IBP ice cream its melting behavior was studied. Ice cream with the lowest AFP type III concentration (3 mg L^{-1}) was selected for this test. Figure 22C compares two equal weight pieces of the control ice cream and the AFP ice cream after 90 min of melting at room temperature. While the control ice cream is almost completely melted, the AFP ice cream still retains some shape, indicating that the rigid crystal network provides inner support, prevents the flow of melted ice cream and thus increases overall melting time. The better shape retention effect of AFP ice cream is clearly seen in Figure 22D that compares the relative height of control and AFP ice cream pieces during the melting experiment.

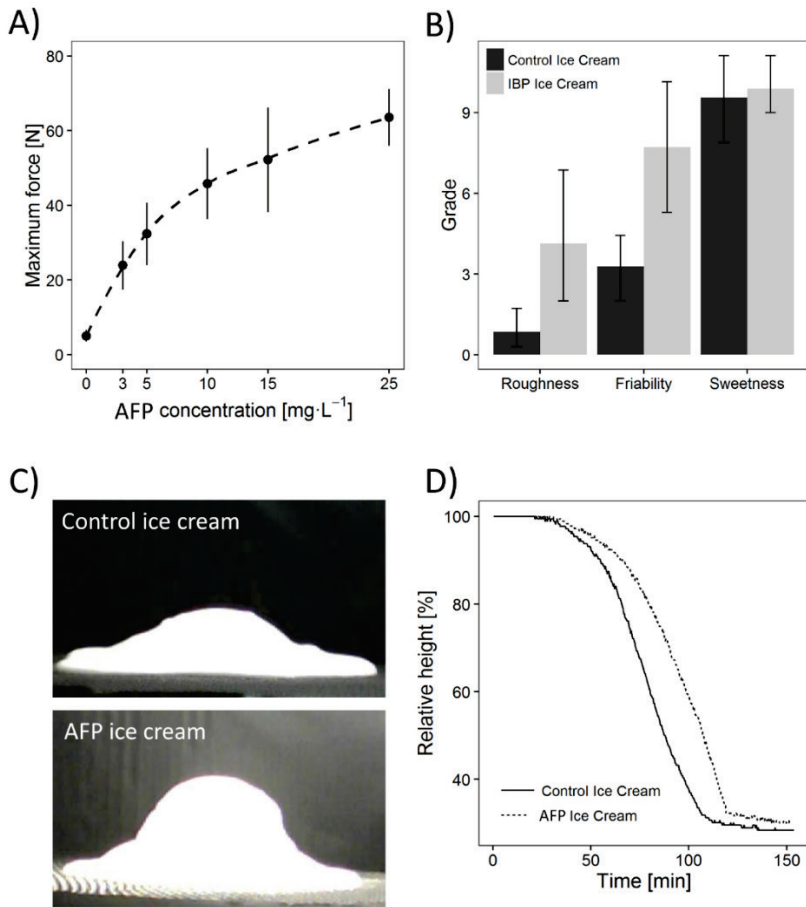


Figure 22. A) Hardness of ice creams containing AFP type III. Vertical bars represent standard deviation ($n=8$). B) Sensory analysis of control ice cream and ice cream containing 65 mg L^{-1} of winter rye extract total protein. The vertical axis represents mean grades given by assessors, where 15 means the strongest feeling. Vertical bars are 95% confidence intervals. C) Control ice cream and ice cream with 3 mg L^{-1} of AFP type III after 90 min of melting at room temperature. D) Relative height of ice cream pieces from (C) during melting experiment.

To conclude, the addition of IBPs to ice creams decreases the ice crystal size but also causes an undesired effect of crystal aggregation into strong network-like structures that significantly affect ice cream properties even at low concentrations. The resulting ice cream texture is very hard and brittle, and when eaten the ice cream is perceived as rough and crystalline. On the other hand, AFP ice cream has an enhanced shape-preserving property that can be used together with the hardening effect to produce novel frozen desserts with elaborate shape, unusual texture and longer consumption time.

It appears that crystal aggregation caused by IBPs is a general effect. If the suggested mechanism of aggregation due to fusion of ice ripples between adsorbed IBPs is correct, this effect would be observed in case of all IBPs, as the convex growth is the underlying basis for IBP activity. It is unclear if ice aggregation also has any biological significance. Perhaps rigid crystal structures are beneficial for maintaining stable brine pockets where sea bacteria can live or prevent mechanical damage of frozen plant tissues due to ice crystal movement. However, it might also be an entirely unwanted side-effect that cannot be avoided.

It has been suggested that the increased ice cream hardness can be circumvented by a better selection of stabilizers. Indeed, in-lab tests of IBP ice creams with different stabilizers demonstrated increased softness and lower ice crystal aggregation degree, however, the aggregation effect was still present, and the IBP ice cream was noticeably harder than the control ice cream without IBPs. This is corroborated by a recent Unilever patent that demonstrated decreased hardness of water ice confectionary containing type II AFP and defibrillated primary plant cell wall material compared to the confectionary only with the AFP, nevertheless, the hardness was still twofold higher compared to the confectionary with the stabilizer only (Farr et al., 2017).

The major implication of this study is that the simple addition of ice-binding proteins to ice creams does not immediately provide an improvement in smoothness, which is typically a most desired ice cream property. It is possible that further research into ice cream formulation and processing conditions will overcome the ice aggregation effect and create an ice cream with a soft texture, long shelf life, and slow melting. But at the moment it seems the use of IBPs is probably more advantageous in other frozen products that are melted before consumption, following the commercial applications of Kaneka Corporation's IBP products in Japan.

5 Conclusions

In this work, a bacterial ice-binding protein from *Euplotes focardii* consortium (*EfcIBP*) was functionally analyzed. In addition, the suitability of IBPs (on the example of fish AFP type III and winter rye extract) for application in ice creams was assessed.

The *EfcIBP* has moderate thermal hysteresis (0.46 °C at 40 μM), but exceptionally high ice recrystallization inhibition (50% inhibition at 2.5 nM).

Fluorescence-based ice planes affinity assay demonstrated that *EfcIBP* has a unique asymmetric binding pattern, covering relatively weakly basal and most of pyramidal crystal planes with increased affinity on pyramidal near-basal planes and close to the secondary pyramidal planes.

EfcIBP accumulates fast on the basal plane. The K_{on} value for the basal plane of GFP-*EfcIBP* was found to be $4 \pm 1 \text{ mM}^{-1} \text{ s}^{-1}$. This is comparable to the rapid binding of moderate fish AFP type III, previously determined to be $8 \pm 1 \text{ mM}^{-1} \text{ s}^{-1}$, and is an order of magnitude higher than the basal plane accumulation of hyperactive GFP-sbwAFP ($0.3 \pm 0.1 \text{ mM}^{-1} \text{ s}^{-1}$).

The basal and near-basal affinity and fast accumulation kinetics explain the unique Saturn-like ice crystal shape produced by *EfcIBP*.

The *EfcIBP* tertiary structure consists of a right-handed β-helix with three faces (A, B, and C), which conforms to the IBP-1 fold found in other bacterial IBPs. Mutational studies indicate that singular amino acid changes on the B and C faces heavily affect thermal hysteresis and ice recrystallization inhibition activities of *EfcIBP*, indicating that both faces participate in binding. In addition, TH and IRI activities appear to be uncoupled. Fluorescence-based ice planes affinity analysis of the mutants showed that the mutations did not destroy the binding sites, but rather modified them, which resulted in changes in the ice crystal plane binding specificity.

EfcIBP has low thermal hysteresis and fast binding dynamics like moderate IBPs, but it has a basal plane affinity, not attributed before to this class of IBPs. Here, a new moderate IBP subclass is defined, which binds to the basal plane, but not to the prism.

To assess the practical application of IBPs, ice creams containing AFP type III and winter rye extract were produced. An accelerated ice recrystallization inhibition assessment method was developed, and it confirmed that IBPs are inhibiting recrystallization in ice cream mixes. Moreover, IBPs have a synergistic effect with stabilizers increasing the activity. However, textural analysis of ice creams demonstrated that IBP ice cream is significantly harder, and feels more brittle, crystalline and rough when eaten. A microscopy method for visualizing ice cream microstructure was devised. It showed that while in the presence of IBPs ice crystals within the ice cream are smaller, the crystals are aggregated into a rigid three-dimensional network. This effect is associated with both tested IBP types. IBP modifies ice crystal surface, it renders the convex crystal area between IBP molecules thermodynamically unstable, resulting in fusion of adjacent crystals. This effect makes IBPs problematic to use in ice creams when a soft and smooth texture is desired. On the other hand, IBPs improve ice cream shape-preserving capability enabling longer consumption time; IBPs also allow production of more elaborately shaped products or novel frozen desserts where a harder texture is a feature of the product.

References

- Adar, C., Sirotinskaya, V., Bar Dolev, M., Friehmann, T., & Braslavsky, I. (2018). Falling water ice affinity purification of ice-binding proteins. *Scientific Reports*, *8*(1), 11046. doi:10.1038/s41598-018-29312-x
- Baardsnes, J., Kondejewski, L. H., Hodges, R. S., Chao, H., Kay, C., & Davies, P. L. (1999). New ice-binding face for type I antifreeze protein. *FEBS Letters*, *463*(1-2), 87–91. doi:10.1016/S0014-5793(99)01588-4
- Baardsnes, Jason, Kuiper, M. J., & Davies, P. L. (2003). Antifreeze protein dimer: when two ice-binding faces are better than one. *The Journal of Biological Chemistry*, *278*(40), 38942–38947. doi:10.1074/jbc.M306776200
- Bang, J. K., Lee, J. H., Murugan, R. N., Lee, S. G., Do, H., Koh, H. Y., ... Kim, H. J. (2013). Antifreeze peptides and glycopeptides, and their derivatives: potential uses in biotechnology. *Marine Drugs*, *11*(6), 2013–2041. doi:10.3390/md11062013
- Bar Dolev, M., Braslavsky, I., & Davies, P. L. (2016). Ice-Binding Proteins and Their Function. *Annual Review of Biochemistry*, *85*, 515–542. doi:10.1146/annurev-biochem-060815-014546
- Bar, M., Celik, Y., Fass, D., & Braslavsky, I. (2008). Interactions of β -Helical Antifreeze Protein Mutants with Ice. *Crystal Growth & Design*, *8*(8), 2954–2963. doi:10.1021/cg800066g
- Bar-Dolev, M., Celik, Y., Wettlaufer, J. S., Davies, P. L., & Braslavsky, I. (2012). New insights into ice growth and melting modifications by antifreeze proteins. *Journal of the Royal Society, Interface*, *9*(77), 3249–3259. doi:10.1098/rsif.2012.0388
- Barrett, J. (2001). Thermal hysteresis proteins. *The International Journal of Biochemistry & Cell Biology*, *33*(2), 105–117.
- Basu, K., Garnham, C. P., Nishimiya, Y., Tsuda, S., Braslavsky, I., & Davies, P. (2014). Determining the ice-binding planes of antifreeze proteins by fluorescence-based ice plane affinity. *Journal of Visualized Experiments*, (83), e51185. doi:10.3791/51185
- Bodyfelt, F. W., Tobias, J., & Trout, G. M. (1988). *The sensory evaluation of dairy products*. New York: Van Nostrand Reinhold.
- Bramley, A. S., Gray, S. J., Turan, S. M., Spors, D. D., & Frisch, S. M. (2011, August 23). Low fat frozen confectionery product. US patent 8003151.
- Braslavsky, I., & Drori, R. (2013). LabVIEW-operated novel nanoliter osmometer for ice binding protein investigations. *Journal of Visualized Experiments*, (72), e4189. doi:10.3791/4189
- Bredow, M., Tomalty, H. E., Smith, L., & Walker, V. K. (2018). Ice and anti-nucleating activities of an ice-binding protein from the annual grass, *Brachypodium distachyon*. *Plant, Cell & Environment*, *41*(5), 983–992. doi:10.1111/pce.12889
- Bredow, M., & Walker, V. K. (2017). Ice-Binding Proteins in Plants. *Frontiers in Plant Science*, *8*, 2153. doi:10.3389/fpls.2017.02153
- Bredow, M., Vanderbeld, B., & Walker, V. K. (2017). Ice-binding proteins confer freezing tolerance in transgenic *Arabidopsis thaliana*. *Plant Biotechnology Journal*, *15*(1), 68–81. doi:10.1111/pbi.12592
- Brockbank, K. G. M., Campbell, L. H., Greene, E. D., Brockbank, M. C. G., & Duman, J. G. (2011). Lessons from nature for preservation of mammalian cells, tissues, and organs. *In Vitro Cellular & Developmental Biology. Animal*, *47*(3), 210–217. doi:10.1007/s11626-010-9383-2

- Brumberg, A., Hammonds, K., Baker, I., Backus, E. H. G., Bisson, P. J., Bonn, M., ... Shultz, M. J. (2017). Single-crystal Ih ice surfaces unveil connection between macroscopic and molecular structure. *Proceedings of the National Academy of Sciences of the United States of America*, *114*(21), 5349–5354. doi:10.1073/pnas.1703056114
- Buckley, S. L., & Lillford, P. J. (2009). Antifreeze Proteins. In *Modern Biopolymer Science* (pp. 93–128). Elsevier. doi:10.1016/B978-0-12-374195-0.00003-3
- Budke, C., Heggemann, C., Koch, M., Sewald, N., & Koop, T. (2009). Ice recrystallization kinetics in the presence of synthetic antifreeze glycoprotein analogues using the framework of LSW theory. *The Journal of Physical Chemistry. B*, *113*(9), 2865–2873. doi:10.1021/jp805726e
- Budke, Carsten, Dreyer, A., Jaeger, J., Gimpel, K., Berkemeier, T., Bonin, A. S., ... Koop, T. (2014). Quantitative efficacy classification of ice recrystallization inhibition agents. *Crystal Growth & Design*, *14*(9), 4285–4294. doi:10.1021/cg5003308
- Budke, Carsten, & Koop, T. (2006). Ice recrystallization inhibition and molecular recognition of ice faces by poly(vinyl alcohol). *Chemphyschem*, *7*(12), 2601–2606. doi:10.1002/cphc.200600533
- Byass, L. J., Doucet, C. J., Fenn, R. A., McArthur, A. J., Sidebottom, C. M., & Smallwood, M. F. (2004, September 28). Carrot antifreeze polypeptides. US patent 6797690.
- Capicciotti, C. J., Poisson, J. S., Boddy, C. N., & Ben, R. N. (2015). Modulation of antifreeze activity and the effect upon post-thaw HepG2 cell viability after cryopreservation. *Cryobiology*, *70*(2), 79–89. doi:10.1016/j.cryobiol.2015.01.002
- Celik, Y., Drori, R., Pertaya-Braun, N., Altan, A., Barton, T., Bar-Dolev, M., ... Braslavsky, I. (2013). Microfluidic experiments reveal that antifreeze proteins bound to ice crystals suffice to prevent their growth. *Proceedings of the National Academy of Sciences of the United States of America*, *110*(4), 1309–1314. doi:10.1073/pnas.1213603110
- Celik, Y., Graham, L. A., Mok, Y.-F., Bar, M., Davies, P. L., & Braslavsky, I. (2010). Superheating of ice crystals in antifreeze protein solutions. *Proceedings of the National Academy of Sciences of the United States of America*, *107*(12), 5423–5428. doi:10.1073/pnas.0909456107
- Chao, H., DeLuca, C. I., & Davies, P. L. (1995). Mixing antifreeze protein types changes ice crystal morphology without affecting antifreeze activity. *FEBS Letters*, *357*(2), 183–186.
- Chapsky, L., & Rubinsky, B. (1997). Kinetics of antifreeze protein-induced ice growth inhibition. *FEBS Letters*, *412*(1), 241–244. doi:10.1016/S0014-5793(97)00787-4
- Cheng, J., Hanada, Y., Miura, A., Tsuda, S., & Kondo, H. (2016). Hydrophobic ice-binding sites confer hyperactivity of an antifreeze protein from a snow mold fungus. *The Biochemical Journal*, *473*(21), 4011–4026. doi:10.1042/BCJ20160543
- Chow, R., Blindt, R., Chivers, R., & Povey, M. (2005). A study on the primary and secondary nucleation of ice by power ultrasound. *Ultrasonics*, *43*(4), 227–230. doi:10.1016/j.ultras.2004.06.006
- Clarke, C. J., Buckley, S. L., & Lindner, N. (2002). Ice structuring proteins - a new name for antifreeze proteins. *Cryo Letters*, *23*(2), 89–92.
- Cox, S. J., Kathmann, S. M., Slater, B., & Michaelides, A. (2015). Molecular simulations of heterogeneous ice nucleation. II. Peeling back the layers. *The Journal of Chemical Physics*, *142*(18), 184705. doi:10.1063/1.4919715

- D'Amico, S., Collins, T., Marx, J.-C., Feller, G., & Gerday, C. (2006). Psychrophilic microorganisms: challenges for life. *EMBO Reports*, 7(4), 385–389. doi:10.1038/sj.embor.7400662
- Daniel, A., Hoddle, A., Jones, A., Oldroyd, J. R., & Singleton, S. (2004, May 12). Ice cream confection containing an antifreeze protein. EU patent 1417892.
- Darling, D. F., & Huddle, A. (2001, March 13). Frozen food product. US patent 6200622.
- Davies, P. L. (2014). Ice-binding proteins: a remarkable diversity of structures for stopping and starting ice growth. *Trends in Biochemical Sciences*, 39(11), 548–555. doi:10.1016/j.tibs.2014.09.005
- De Maayer, P., Anderson, D., Cary, C., & Cowan, D. A. (2014). Some like it cold: understanding the survival strategies of psychrophiles. *EMBO Reports*, 15(5), 508–517. doi:10.1002/embr.201338170
- DeLuca, C. I., Comley, R., & Davies, P. L. (1998). Antifreeze proteins bind independently to ice. *Biophysical Journal*, 74(3), 1502–1508. doi:10.1016/S0006-3495(98)77862-2
- DeVries, A. L., & Wohlschlag, D. E. (1969). Freezing resistance in some antarctic fishes. *Science*, 163(3871), 1073–1075. doi:10.1126/science.163.3871.1073
- Do, H., Kim, S.-J., Kim, H. J., & Lee, J. H. (2014). Structure-based characterization and antifreeze properties of a hyperactive ice-binding protein from the Antarctic bacterium *Flavobacterium frigoris* PS1. *Acta Crystallographica. Sect. D, Biological Crystallography*, 70(Pt 4), 1061–1073. doi:10.1107/S1399004714000996
- Donhowe, D. P., & Hartel, R. W. (1996). Recrystallization of ice during bulk storage of ice cream. *International Dairy Journal*, 6(11-12), 1209–1221. doi:10.1016/S0958-6946(96)00030-1
- Drori, R., Celik, Y., Davies, P. L., & Braslavsky, I. (2014). Ice-binding proteins that accumulate on different ice crystal planes produce distinct thermal hysteresis dynamics. *Journal of the Royal Society, Interface*, 11(98), 20140526. doi:10.1098/rsif.2014.0526
- Drori, R., Davies, P. L., & Braslavsky, I. (2015a). Experimental correlation between thermal hysteresis activity and the distance between antifreeze proteins on an ice surface. *RSC Adv.*, 5(11), 7848–7853. doi:10.1039/C4RA12638F
- Drori, R., Davies, P. L., & Braslavsky, I. (2015b). When are antifreeze proteins in solution essential for ice growth inhibition? *Langmuir: The ACS Journal of Surfaces and Colloids*, 31(21), 5805–5811. doi:10.1021/acs.langmuir.5b00345
- Drori, R., Li, C., Hu, C., Raiteri, P., Rohl, A. L., Ward, M. D., & Kahr, B. (2016). A supramolecular ice growth inhibitor. *Journal of the American Chemical Society*, 138(40), 13396–13401. doi:10.1021/jacs.6b08267
- Ewart, K. V., & Fletcher, G. L. (1990). Isolation and characterization of antifreeze proteins from smelt (*Osmerus mordax*) and Atlantic herring (*Clupea harengus harengus*). *Canadian Journal of Zoology*, 68(8), 1652–1658. doi:10.1139/z90-245
- Farr, R. S., Goudappel, G. J. W., Husken, H., Jarvis, D. A., Kuijk, A., Veen, S. J., ... Weg, P. B. (2017, December 21). Frozen confection. US patent 20170360063A1.
- Garnham, C. P., Nishimiya, Y., Tsuda, S., & Davies, P. L. (2012). Engineering a naturally inactive isoform of type III antifreeze protein into one that can stop the growth of ice. *FEBS Letters*, 586(21), 3876–3881. doi:10.1016/j.febslet.2012.09.017
- Graham, L. A., Liou, Y. C., Walker, V. K., & Davies, P. L. (1997). Hyperactive antifreeze protein from beetles. *Nature*, 388(6644), 727–728. doi:10.1038/41908

- Griffith, M., & Ewart, K. V. (1995). Antifreeze proteins and their potential use in frozen foods. *Biotechnology Advances*, *13*(3), 375–402.
- Guinard, J. X., Zoumas-Morse, C., Mori, L., Uatoni, B., Panyam, D., & Kilara, A. (1997). Sugar and fat effects on sensory properties of ice cream. *Journal of Food Science*, *62*(5), 1087–1094. doi:10.1111/j.1365-2621.1997.tb15044.x
- Guo, S., Garnham, C. P., Karunan Partha, S., Campbell, R. L., Allingham, J. S., & Davies, P. L. (2013). Role of Ca²⁺ in folding the tandem β -sandwich extender domains of a bacterial ice-binding adhesin. *The FEBS Journal*, *280*(22), 5919–5932. doi:10.1111/febs.12518
- Guo, S., Garnham, C. P., Whitney, J. C., Graham, L. A., & Davies, P. L. (2012). Re-evaluation of a bacterial antifreeze protein as an adhesin with ice-binding activity. *Plos One*, *7*(11), e48805. doi:10.1371/journal.pone.0048805
- Gurian-Sherman, D., & Lindow, S. E. (1993). Bacterial ice nucleation: significance and molecular basis. *The FASEB Journal*, *7*(14), 1338–1343.
- Gwak, Y., Park, J., Kim, M., Kim, H. S., Kwon, M. J., Oh, S. J., ... Jin, E. (2015). Creating Anticicing Surfaces via the Direct Immobilization of Antifreeze Proteins on Aluminum. *Scientific Reports*, *5*, 12019. doi:10.1038/srep12019
- Hakim, A., Nguyen, J. B., Basu, K., Zhu, D. F., Thakral, D., Davies, P. L., ... Meng, W. (2013). Crystal structure of an insect antifreeze protein and its implications for ice binding. *The Journal of Biological Chemistry*, *288*(17), 12295–12304. doi:10.1074/jbc.M113.450973
- Haleva, L., Celik, Y., Bar-Dolev, M., Pertaya-Braun, N., Kaner, A., Davies, P. L., & Braslavsky, I. (2016). Microfluidic Cold-Finger Device for the Investigation of Ice-Binding Proteins. *Biophysical Journal*, *111*(6), 1143–1150. doi:10.1016/j.bpj.2016.08.003
- Hanada, Y., Nishimiya, Y., Miura, A., Tsuda, S., & Kondo, H. (2014). Hyperactive antifreeze protein from an Antarctic sea ice bacterium *Colwellia* sp. has a compound ice-binding site without repetitive sequences. *The FEBS Journal*, *281*(16), 3576–3590. doi:10.1111/febs.12878
- Hanwell, M. D., Curtis, D. E., Lonie, D. C., Vandermeersch, T., Zurek, E., & Hutchison, G. R. (2012). Avogadro: an advanced semantic chemical editor, visualization, and analysis platform. *Journal of Cheminformatics*, *4*(1), 17. doi:10.1186/1758-2946-4-17
- Hashim, N. H. F., Sulaiman, S., Abu Bakar, F. D., Illias, R. M., Kawahara, H., Najimudin, N., ... Murad, A. M. A. (2014). Molecular cloning, expression and characterisation of Afp4, an antifreeze protein from *Glaciozyma antarctica*. *Polar Biology*, *37*(10), 1495–1505. doi:10.1007/s00300-014-1539-1
- Hassas-Roudsari, M., & Goff, H. D. (2012). Ice structuring proteins from plants: Mechanism of action and food application. *Food Research International*, *46*(1), 425–436. doi:10.1016/j.foodres.2011.12.018
- Hobbs, P. V. (2010). *Ice physics*. Oxford University Press.
- Huang, M. L., Ehre, D., Jiang, Q., Hu, C., Kirshenbaum, K., & Ward, M. D. (2012). Biomimetic peptoid oligomers as dual-action antifreeze agents. *Proceedings of the National Academy of Sciences of the United States of America*, *109*(49), 19922–19927. doi:10.1073/pnas.1212826109
- Hudait, A., Odendahl, N., Qiu, Y., Paesani, F., & Molinero, V. (2018). Ice-Nucleating and Antifreeze Proteins Recognize Ice through a Diversity of Anchored Clathrate and Ice-like Motifs. *Journal of the American Chemical Society*, *140*(14), 4905–4912. doi:10.1021/jacs.8b01246

- Inada, T., & Lu, S.-S. (2003). Inhibition of Recrystallization of Ice Grains by Adsorption of Poly(Vinyl Alcohol) onto Ice Surfaces. *Crystal Growth & Design*, 3(5), 747–752. doi:10.1021/cg0340300
- Johari, G. P. (1997). The Gibbs–Thomson effect and intergranular melting in ice emulsions: Interpreting the anomalous heat capacity and volume of supercooled water. *The Journal of Chemical Physics*, 107(23), 10154–10165. doi:10.1063/1.475322
- Kaneka Group. (2016). *KANEKA CSR Report 2016*. Retrieved from http://www.kaneka.co.jp/en/csr/backnumber/pdf/csr_2016_01.pdf
- Kansai University. (2014, October 29). Professor Kawahara's team announces the development of a new product. Retrieved July 2, 2018, from <http://www.kansai-u.ac.jp/English/archives/2014/10/professor-kawaharas-team-announces-the-development-of-a-new-product.html>
- Kiani, H., & Sun, D.-W. (2011). Water crystallization and its importance to freezing of foods: A review. *Trends in Food Science & Technology*, 22(8), 407–426. doi:10.1016/j.tifs.2011.04.011
- Kim, H. J., Lee, J. H., Hur, Y. B., Lee, C. W., Park, S.-H., & Koo, B.-W. (2017). Marine antifreeze proteins: structure, function, and application to cryopreservation as a potential cryoprotectant. *Marine Drugs*, 15(2). doi:10.3390/md15020027
- Kim, M., Gwak, Y., Jung, W., & Jin, E. (2017). Identification and Characterization of an Isoform Antifreeze Protein from the Antarctic Marine Diatom, *Chaetoceros neogracile* and Suggestion of the Core Region. *Marine Drugs*, 15(10). doi:10.3390/md15100318
- Knight, C A. (2000). Structural biology. Adding to the antifreeze agenda. *Nature*, 406(6793), 249, 251. doi:10.1038/35018671
- Knight, C A, Cheng, C. C., & DeVries, A. L. (1991). Adsorption of alpha-helical antifreeze peptides on specific ice crystal surface planes. *Biophysical Journal*, 59(2), 409–418. doi:10.1016/S0006-3495(91)82234-2
- Knight, C A, & Devries, A. L. (1989). Melting inhibition and superheating of ice by an antifreeze glycopeptide. *Science*, 245(4917), 505–507. doi:10.1126/science.245.4917.505
- Knight, C A, DeVries, A. L., & Oolman, L. D. (1984). Fish antifreeze protein and the freezing and recrystallization of ice. *Nature*, 308(5956), 295–296. doi:10.1038/308295a0
- Knight, Charles A., & Duman, J. G. (1986). Inhibition of recrystallization of ice by insect thermal hysteresis proteins: A possible cryoprotective role. *Cryobiology*, 23(3), 256–262. doi:10.1016/0011-2240(86)90051-9
- Knight, Charles A., Wierzbicki, A., Laursen, R. A., & Zhang, W. (2001). Adsorption of Biomolecules to Ice and Their Effects upon Ice Growth. 1. Measuring Adsorption Orientations and Initial Results. *Crystal Growth & Design*, 1(6), 429–438. doi:10.1021/cg015531t
- Kondo, H., Hanada, Y., Sugimoto, H., Hoshino, T., Garnham, C. P., Davies, P. L., & Tsuda, S. (2012). Ice-binding site of snow mold fungus antifreeze protein deviates from structural regularity and high conservation. *Proceedings of the National Academy of Sciences of the United States of America*, 109(24), 9360–9365. doi:10.1073/pnas.1121607109
- Koushafar, H., & Rubinsky, B. (1997). Effect of antifreeze proteins on frozen primary prostatic adenocarcinoma cells. *Urology*, 49(3), 421–425. doi:10.1016/S0090-4295(96)00572-9

- Kristiansen, E., & Zachariassen, K. E. (2005). The mechanism by which fish antifreeze proteins cause thermal hysteresis. *Cryobiology*, *51*(3), 262–280. doi:10.1016/j.cryobiol.2005.07.007
- Kubota, N. (2011). Effects of cooling rate, annealing time and biological antifreeze concentration on thermal hysteresis reading. *Cryobiology*, *63*(3), 198–209. doi:10.1016/j.cryobiol.2011.06.005
- Kuiper, M. J., Lankin, C., Gauthier, S. Y., Walker, V. K., & Davies, P. L. (2003). Purification of antifreeze proteins by adsorption to ice. *Biochemical and Biophysical Research Communications*, *300*(3), 645–648. doi:10.1016/S0006-291X(02)02900-5
- Laursen, R. A., Wen, D., & Knight, C. A. (1994). Enantioselective Adsorption of the D- and L-Forms of an α -Helical Antifreeze Polypeptide to the {20-21} Planes of Ice. *Journal of the American Chemical Society*, *116*(26), 12057–12058. doi:10.1021/ja00105a058
- Lee, J. H., Park, A. K., Do, H., Park, K. S., Moh, S. H., Chi, Y. M., & Kim, H. J. (2012). Structural basis for antifreeze activity of ice-binding protein from arctic yeast. *The Journal of Biological Chemistry*, *287*(14), 11460–11468. doi:10.1074/jbc.M111.331835
- Lee, J. K., Park, K. S., Park, S., Park, H., Song, Y. H., Kang, S.-H., & Kim, H. J. (2010). An extracellular ice-binding glycoprotein from an Arctic psychrophilic yeast. *Cryobiology*, *60*(2), 222–228. doi:10.1016/j.cryobiol.2010.01.002
- Leinala, E. K., Davies, P. L., Doucet, D., Tyshenko, M. G., Walker, V. K., & Jia, Z. (2002). A beta-helical antifreeze protein isoform with increased activity. Structural and functional insights. *The Journal of Biological Chemistry*, *277*(36), 33349–33352. doi:10.1074/jbc.M205575200
- Mahatabuddin, S., Fukami, D., Arai, T., Nishimiya, Y., Shimizu, R., Shibasaki, C., ... Tsuda, S. (2018). Polypentagonal ice-like water networks emerge solely in an activity-improved variant of ice-binding protein. *Proceedings of the National Academy of Sciences of the United States of America*, *115*(21), 5456–5461. doi:10.1073/pnas.1800635115
- Marshall, C. J., Basu, K., & Davies, P. L. (2016). Ice-shell purification of ice-binding proteins. *Cryobiology*, *72*(3), 258–263. doi:10.1016/j.cryobiol.2016.03.009
- Meister, K., Lotze, S., Olijve, L. L. C., DeVries, A. L., Duman, J. G., Voets, I. K., & Bakker, H. J. (2015). Investigation of the Ice-Binding Site of an Insect Antifreeze Protein Using Sum-Frequency Generation Spectroscopy. *The Journal of Physical Chemistry Letters*, *6*(7), 1162–1167. doi:10.1021/acs.jpcllett.5b00281
- Midya, U. S., & Bandyopadhyay, S. (2014). Hydration behavior at the ice-binding surface of the *Tenebrio molitor* antifreeze protein. *The Journal of Physical Chemistry. B*, *118*(18), 4743–4752. doi:10.1021/jp412528b
- Mizrahy, O., Bar-Dolev, M., Guy, S., & Braslavsky, I. (2013). Inhibition of ice growth and recrystallization by zirconium acetate and zirconium acetate hydroxide. *Plos One*, *8*(3), e59540. doi:10.1371/journal.pone.0059540
- Mitchell, D. E., Clarkson, G., Fox, D. J., Vipond, R. A., Scott, P., & Gibson, M. I. (2017). Antifreeze Protein Mimetic Metallohelices with Potent Ice Recrystallization Inhibition Activity. *Journal of the American Chemical Society*, *139*(29), 9835–9838. doi:10.1021/jacs.7b05822

- Mochizuki, K., & Molinero, V. (2018). Antifreeze glycoproteins bind reversibly to ice via hydrophobic groups. *Journal of the American Chemical Society*, *140*(14), 4803–4811. doi:10.1021/jacs.7b13630
- Naullage, P. M., Qiu, Y., & Molinero, V. (2018). What controls the limit of supercooling and superheating of pinned ice surfaces? *The Journal of Physical Chemistry Letters*, *9*(7), 1712–1720. doi:10.1021/acs.jpcclett.8b00300
- Ndoye, F. T., & Alvarez, G. (2015). Characterization of ice recrystallization in ice cream during storage using the focused beam reflectance measurement. *Journal of Food Engineering*, *148*, 24–34. doi:10.1016/j.jfoodeng.2014.09.014
- Nishijima, K., Tanaka, M., Sakai, Y., Koshimoto, C., Morimoto, M., Watanabe, T., ... Kitajima, S. (2014). Effects of type III antifreeze protein on sperm and embryo cryopreservation in rabbit. *Cryobiology*, *69*(1), 22–25. doi:10.1016/j.cryobiol.2014.04.014
- Nutt, D. R., & Smith, J. C. (2008). Dual function of the hydration layer around an antifreeze protein revealed by atomistic molecular dynamics simulations. *Journal of the American Chemical Society*, *130*(39), 13066–13073. doi:10.1021/ja8034027
- Olijve, Luuk L C, Meister, K., DeVries, A. L., Duman, J. G., Guo, S., Bakker, H. J., & Voets, I. K. (2016). Blocking rapid ice crystal growth through nonbasal plane adsorption of antifreeze proteins. *Proceedings of the National Academy of Sciences of the United States of America*, *113*(14), 3740–3745. doi:10.1073/pnas.1524109113
- Olijve, Luuk L. C., Oude Vrielink, A. S., & Voets, I. K. (2016). A simple and quantitative method to evaluate ice recrystallization kinetics using the circle hough transform algorithm. *Crystal Growth & Design*, *16*(8), 4190–4195. doi:10.1021/acs.cgd.5b01637
- Oude Vrielink, A. S., Aloï, A., Olijve, L. L. C., & Voets, I. K. (2016). Interaction of ice binding proteins with ice, water and ions. *Biointerphases*, *11*(1), 018906. doi:10.1116/1.4939462
- Pandey, R., Usui, K., Livingstone, R. A., Fischer, S. A., Pfäendtner, J., Backus, E. H. G., ... Weidner, T. (2016). Ice-nucleating bacteria control the order and dynamics of interfacial water. *Science Advances*, *2*(4), e1501630. doi:10.1126/sciadv.1501630
- Payne, S. R., Sandford, D., Harris, A., & Young, O. A. (1994). The effects of antifreeze proteins on chilled and frozen meat. *Meat Science*, *37*(3), 429–438. doi:10.1016/0309-1740(94)90058-2
- Pertaya, N., Marshall, C. B., Celik, Y., Davies, P. L., & Braslavsky, I. (2008). Direct visualization of spruce budworm antifreeze protein interacting with ice crystals: basal plane affinity confers hyperactivity. *Biophysical Journal*, *95*(1), 333–341. doi:10.1529/biophysj.107.125328
- Pertaya, N., Marshall, C. B., DiPrinzio, C. L., Wilen, L., Thomson, E. S., Wettlaufer, J. S., ... Braslavsky, I. (2007). Fluorescence microscopy evidence for quasi-permanent attachment of antifreeze proteins to ice surfaces. *Biophysical Journal*, *92*(10), 3663–3673. doi:10.1529/biophysj.106.096297
- Petrenko, V. F., & Whitworth, R. W. (2002). *Physics of Ice*. Oxford University Press. doi:10.1093/acprof:oso/9780198518945.001.0001
- Phippen, S. W., Stevens, C. A., Vance, T. D. R., King, N. P., Baker, D., & Davies, P. L. (2016). Multivalent Display of Antifreeze Proteins by Fusion to Self-Assembling Protein Cages Enhances Ice-Binding Activities. *Biochemistry*, *55*(49), 6811–6820. doi:10.1021/acs.biochem.6b00864

- Raymond, J. A., Fritsen, C., & Shen, K. (2007). An ice-binding protein from an Antarctic sea ice bacterium. *FEMS Microbiology Ecology*, *61*(2), 214–221. doi:10.1111/j.1574-6941.2007.00345.x
- Raymond, J. A., Janech, M. G., & Fritsen, C. H. (2009). Novel ice-binding proteins from a psychrophilic Antarctic alga (*Chlamydomonadaceae*, *Chlorophyceae*). *Journal of Phycology*, *45*(1), 130–136. doi:10.1111/j.1529-8817.2008.00623.x
- Regand, A., & Goff, H. D. (2006). Ice recrystallization inhibition in ice cream as affected by ice structuring proteins from winter wheat grass. *Journal of Dairy Science*, *89*(1), 49–57. doi:10.3168/jds.S0022-0302(06)72068-9
- Regand, Alejandra, & Goff, H. D. (2006). Freezing and Ice Recrystallization Properties of Sucrose Solutions Containing Ice Structuring Proteins from Cold-Acclimated Winter Wheat Grass Extract. *Journal of Food Science*, *70*(9), E552–E556. doi:10.1111/j.1365-2621.2005.tb08318.x
- Röttger, K., Endriss, A., Ihringer, J., Doyle, S., & Kuhs, W. F. (1994). Lattice constants and thermal expansion of H₂ O and D₂ O ice Ih between 10 and 265 K. *Acta Crystallographica Section B Structural Science*, *50*(6), 644–648. doi:10.1107/S0108768194004933
- Schauperl, M., Podewitz, M., Ortner, T. S., Waibl, F., Thoeny, A., Loerting, T., & Liedl, K. R. (2017). Balance between hydration enthalpy and entropy is important for ice binding surfaces in Antifreeze Proteins. *Scientific Reports*, *7*(1), 11901. doi:10.1038/s41598-017-11982-8
- Schauperl, M., Podewitz, M., Waldner, B. J., & Liedl, K. R. (2016). Enthalpic and entropic contributions to hydrophobicity. *Journal of Chemical Theory and Computation*, *12*(9), 4600–4610. doi:10.1021/acs.jctc.6b00422
- Schindelin, J., Arganda-Carreras, I., Frise, E., Kaynig, V., Longair, M., Pietzsch, T., ... Cardona, A. (2012). Fiji: an open-source platform for biological-image analysis. *Nature Methods*, *9*(7), 676–682. doi:10.1038/nmeth.2019
- Scotter, A. J., Marshall, C. B., Graham, L. A., Gilbert, J. A., Garnham, C. P., & Davies, P. L. (2006). The basis for hyperactivity of antifreeze proteins. *Cryobiology*, *53*(2), 229–239. doi:10.1016/j.cryobiol.2006.06.006
- Shi, M., Gao, J., & Zhang, M. Q. (2017). Web3DMol: interactive protein structure visualization based on WebGL. *Nucleic Acids Research*, *45*(W1), W523–W527. doi:10.1093/nar/gkx383
- Sidebottom, C., Buckley, S., Pudney, P., Twigg, S., Jarman, C., Holt, C., ... Lillford, P. (2000). Heat-stable antifreeze protein from grass. *Nature*, *406*(6793), 256. doi:10.1038/35018639
- Smolin, N., & Daggett, V. (2008). Formation of ice-like water structure on the surface of an antifreeze protein. *The Journal of Physical Chemistry. B*, *112*(19), 6193–6202. doi:10.1021/jp710546e
- Sproncken, C. C. M., Surís-Valls, R., Cingil, H. E., Detrembleur, C., & Voets, I. K. (2018). Complex Coacervate Core Micelles Containing Poly(vinyl alcohol) Inhibit Ice Recrystallization. *Macromolecular Rapid Communications*, e1700814. doi:10.1002/marc.201700814
- Strom, C. S., Liu, X. Y., & Jia, Z. (2005). Why does insect antifreeze protein from *Tenebrio molitor* produce pyramidal ice crystallites? *Biophysical Journal*, *89*(4), 2618–2627. doi:10.1529/biophysj.104.056770

- Sun, T., Lin, F.-H., Campbell, R. L., Allingham, J. S., & Davies, P. L. (2014). An antifreeze protein folds with an interior network of more than 400 semi-clathrate waters. *Science*, *343*(6172), 795–798. doi:10.1126/science.1247407
- Sönnichsen, F. D., DeLuca, C. I., Davies, P. L., & Sykes, B. D. (1996). Refined solution structure of type III antifreeze protein: hydrophobic groups may be involved in the energetics of the protein-ice interaction. *Structure*, *4*(11), 1325–1337. doi:10.1016/S0969-2126(96)00140-2
- Zachariassen, K. E., & Kristiansen, E. (2000). Ice nucleation and antinucleation in nature. *Cryobiology*, *41*(4), 257–279. doi:10.1006/cryo.2000.2289
- Zepeda, S., Yokoyama, E., Uda, Y., Katagiri, C., & Furukawa, Y. (2008). In Situ Observation of Antifreeze Glycoprotein Kinetics at the Ice Interface Reveals a Two-Step Reversible Adsorption Mechanism. *Crystal Growth & Design*, *8*(10), 3666–3672. doi:10.1021/cg800269w
- Zhang, W., & Laursen, R. A. (1999). Artificial antifreeze polypeptides: alpha-helical peptides with KAAK motifs have antifreeze and ice crystal morphology modifying properties. *FEBS Letters*, *455*(3), 372–376.
- Takamichi, M., Nishimiya, Y., Miura, A., & Tsuda, S. (2007). Effect of annealing time of an ice crystal on the activity of type III antifreeze protein. *The FEBS Journal*, *274*(24), 6469–6476. doi:10.1111/j.1742-4658.2007.06164.x
- Takamichi, M., Nishimiya, Y., Miura, A., & Tsuda, S. (2009). Fully active QAE isoform confers thermal hysteresis activity on a defective SP isoform of type III antifreeze protein. *The FEBS Journal*, *276*(5), 1471–1479. doi:10.1111/j.1742-4658.2009.06887.x
- Walters, K. R., Serianni, A. S., Sformo, T., Barnes, B. M., & Duman, J. G. (2009). A nonprotein thermal hysteresis-producing xylomannan antifreeze in the freeze-tolerant Alaskan beetle *Upis ceramboides*. *Proceedings of the National Academy of Sciences of the United States of America*, *106*(48), 20210–20215. doi:10.1073/pnas.0909872106
- Vance, T. D. R., Graham, L. A., & Davies, P. L. (2018). An ice-binding and tandem beta-sandwich domain-containing protein in *Shewanella frigidimarina* is a potential new type of ice adhesin. *The FEBS Journal*, *285*(8), 1511–1527. doi:10.1111/febs.14424
- Vance, T. D. R., Olijve, L. L. C., Campbell, R. L., Voets, I. K., Davies, P. L., & Guo, S. (2014). Ca²⁺-stabilized adhesin helps an Antarctic bacterium reach out and bind ice. *Bioscience Reports*, *34*(4). doi:10.1042/BSR20140083
- Wang, C., Pakhomova, S., Newcomer, M. E., Christner, B. C., & Luo, B.-H. (2017). Structural basis of antifreeze activity of a bacterial multi-domain antifreeze protein. *Plos One*, *12*(11), e0187169. doi:10.1371/journal.pone.0187169
- Wang, R., Zhang, P., Gong, Z., & Hew, C. L. (1995). Expression of the antifreeze protein gene in transgenic goldfish (*Carassius auratus*) and its implication in cold adaptation. *Molecular Marine Biology and Biotechnology*, *4*(1), 20–26.
- Varela, P., Pintor, A., & Fiszman, S. (2014). How hydrocolloids affect the temporal oral perception of ice cream. *Food Hydrocolloids*, *36*, 220–228. doi:10.1016/j.foodhyd.2013.10.005
- Venketesh, S., & Dayananda, C. (2008). Properties, potentials, and prospects of antifreeze proteins. *Critical Reviews in Biotechnology*, *28*(1), 57–82. doi:10.1080/07388550801891152

- Wierzbicki, A., Knight, C. A., Rutland, T. J., Muccio, D. D., Pybus, B. S., & Sikes, C. S. (2000). Structure-function relationship in the antifreeze activity of synthetic alanine-lysine antifreeze polypeptides. *Biomacromolecules*, *1*(2), 268–274. doi:10.1021/bm000004w
- Wilson, P. W., Beaglehole, D., & Devries, A. L. (1993). Antifreeze glycopeptide adsorption on single crystal ice surfaces using ellipsometry. *Biophysical Journal*, *64*(6), 1878–1884. doi:10.1016/S0006-3495(93)81559-5
- Xiao, N., Hanada, Y., Seki, H., Kondo, H., Tsuda, S., & Hoshino, T. (2014). Annealing condition influences thermal hysteresis of fungal type ice-binding proteins. *Cryobiology*, *68*(1), 159–161. doi:10.1016/j.cryobiol.2013.10.008
- Xiao, N., Suzuki, K., Nishimiya, Y., Kondo, H., Miura, A., Tsuda, S., & Hoshino, T. (2010). Comparison of functional properties of two fungal antifreeze proteins from *Antarctomyces psychrotrophicus* and *Typhula ishikariensis*. *The FEBS Journal*, *277*(2), 394–403. doi:10.1111/j.1742-4658.2009.07490.x
- Yeh, C.-M., Kao, B.-Y., & Peng, H.-J. (2009). Production of a recombinant type 1 antifreeze protein analogue by *L. lactis* and its applications on frozen meat and frozen dough. *Journal of Agricultural and Food Chemistry*, *57*(14), 6216–6223. doi:10.1021/jf900924f
- Yeh, Y., & Feeney, R. E. (1996). Antifreeze proteins: structures and mechanisms of function. *Chemical Reviews*, *96*(2), 601–618. doi:10.1021/cr950260c
- Yu, S. O., Brown, A., Middleton, A. J., Tomczak, M. M., Walker, V. K., & Davies, P. L. (2010). Ice restructuring inhibition activities in antifreeze proteins with distinct differences in thermal hysteresis. *Cryobiology*, *61*(3), 327–334. doi:10.1016/j.cryobiol.2010.10.158
- Yu, X. M., Griffith, M., & Wiseman, S. B. (2001). Ethylene induces antifreeze activity in winter rye leaves. *Plant Physiology*, *126*(3), 1232–1240.

Acknowledgments

I would like to thank my supervisor Katrin Laos for the support and guidance throughout the years. And express my deepest gratitude to Ido Braslavsky for taking me in and showing me an exciting new world of ice-binding proteins.

The *EfcIBP* studies presented here were carried out in Ido Braslavsky's laboratory at The Hebrew University of Jerusalem, Rehovot, Israel. The ice cream experiments were done in the Centre of Food and Fermentation Technologies, Tallinn and at the Tallinn University of Technology.

This work was partially supported by ASTRA "TUT Institutional Development Programme for 2016-2022" Graduate School of Functional Materials and Technologies (2014-2020.4.01.16-0032).

Publication I was supported by the Estonian national scholarship program Kristjan Jaak.

Publications II and III were supported by a scholarship from the European Regional Development Fund.

Publication IV was supported by the European Regional Development Fund (project EU48667) and Estonian Ministry of Education (project IUT19-27).

Abstract

Functional Analysis of Ice-Binding Proteins and Practical Application in Ice Cream

Ice-binding proteins (IBPs) are unique natural molecules that can adsorb to ice. The binding forces the ice to grow in between the bound molecules, creating rippled surfaces that according to the Gibbs-Thomson effect make further growth unfavorable. Consequently, the macroscopic growth of ice crystals is arrested in a temperature gap called thermal hysteresis that appears between melting and freezing points. In addition, ice recrystallization is also prevented. These effects are used by many organisms to survive in cold environments.

A bacterial ice-binding protein was found in the metagenome of an Antarctic ciliate *Euplotes focardii* consortium (*EfcIBP*) and recombinantly produced in *Escherichia coli*. The first aim of this work was to functionally characterize this protein.

Thermal hysteresis (TH) and ice recrystallization inhibition (IRI) activity measurements demonstrated that the protein has moderate TH (0.46 °C at 40 μM), but extremely good IRI activity (50% recrystallization inhibition point at 2.5 nM). *EfcIBP* also creates ice crystals with an unusually wide truncated trapezohedron shape that burst into even wider Saturn-like shape with a thin “ring” around it. Bursting in this direction was typically attributed to hyperactive, but not moderate IBPs. To inquire into this peculiar behavior a fluorescence-based ice plane affinity method was applied to reveal that *EfcIBP* binds to most pyramidal ice crystal planes, weakly to the basal plane and doesn't bind to the prismatic plane. *EfcIBP* also has higher affinity on two specific planes. First is located close to the secondary pyramidal plane, but the other is a pyramidal plane at a very small angle to the basal. This low angle near-basal plane has not been demonstrated in other IBPs before. Even though the protein showed lower affinity to the basal plane, in fluorescent microscopy between two coverslips the crystals demonstrated a high affinity to the basal plane enabling accumulation kinetics measurements. These measurements showed that *EfcIBP* is a very fast basal binder, accumulating on ice in approximately one minute. The basal plane adsorption constant is $4 \pm 1 \text{ mM}^{-1} \text{ s}^{-1}$, which is close to the adsorption constant measured in fish type III AFP (antifreeze protein, a subclass of IBP). The difference, however, is that this moderate fish IBP accumulates on the prism plane. In comparison, hyperactive IBPs were shown to accumulate on the basal plane for hours with the adsorption constant order of magnitude lower. Following the results of docking and protein structure studies, a series of *EfcIBP* mutants was designed. TH and IRI measurements showed a significant decrease in activity and confirmed that the protein binds through two of its faces.

These results helped to explain the unusual combination of TH, IRI, and shaping activities. In addition, a new class of moderate IBPs is defined, which has basal ice plane affinity, but no prismatic.

The second aim of this work was to assess the practical application of IBPs in ice cream. Ice cream is a sensitive product that needs to be maintained at a constant freezing temperature, otherwise, ice crystals might grow, thus reducing texture quality of ice cream. IBPs can potentially improve texture by reducing ice crystal size and lengthen shelf life by preventing recrystallization.

AFP type III was recombinantly produced and winter rye extract containing IBPs was made from cold-acclimated leaves. Low-fat ice creams containing AFP type III and winter

rye extract were prepared. Microscopical studies showed that both IBPs can stop ice recrystallization in the ice cream mixes; however, they also cause an additional effect of ice crystal aggregation into rigid networks. The aggregation causes significant changes in the ice cream texture, as evidenced by increased hardness and friability. Addition of only 3 mg L⁻¹ of AFP type III increased hardness from 5 N (control ice cream) to 24 N. On the other hand, this internal crystal network helps to preserve ice cream shape during melting.

Overall, the inclusion of IBPs into ice cream as a novel ingredient is not straightforward. It causes a mostly undesired effect of texture hardening, but this effect can be potentially employed in new types of frozen desserts which instead can have a harder texture in combination with a longer consumption time.

Lühikokkuvõte

Jääga seonduvate valkude funktsionaalne analüüs ja kasutamine jäätises

Jääga seonduvad valgud (IBP) on ainulaadsed looduslikud molekulid, millel on võime adsorbeeruda jääle. IBP adsorbeerumine sunnib jääd IBP molekulide vahel kasvama, tekitades kumeraid pindu ja takistades vastavalt Gibbs-Thomsoni efektile jää edasist kasvu. Selle tulemusena peatub ka jääkristallide makroskoopiline kasv sulamis- ja külmumistemperatuuri vahele jäävas temperatuuri vahemikus (terminaalne hüsterees). Lisaks takistavad IBPd ka jää rekristallisatsiooni. Selliseid omadusi kasutavad mitmed organismid külmas keskkonnas ellu jäämiseks.

Nii on leitud Antarktika ripslooma *Euplotes focardii* konsortsiumi metagenoomis bakteriaalne jääd siduv valk (*EfcIBP*), mida on võimalik rekombinantsetl toota *Escherichia coli* abil. Käesoleva töö esimene eesmärk oligi selle valgu funktsionaalne iseloomustamine.

Vastavalt terminaalsete hüstereesi (TH) ja jää rekristalliseerimise inhibeerimise (IRI) aktiivsuse mõõtmiskatsetele leiti, et valk on mõõduka TH aktiivsusega (0,46 °C 40 µM juures), kuid väga hea IRI aktiivsusega (2,5 nM vähendab jää rekristalliseerumist 50%). *EfcIBP* põhjustab ebatavalise laia kärbitud trapetsoeedri kujuga jääkristallide teket, mis järgneval jahutamisel kasvavad veelgi laiemaks õhukese rõngaga ümbritsetud Saturni-kujulisteks kristallideks. Sellises suunas toimuvat jää kasvu seostati varasemalt peamiselt hüperaktiivsete, mitte aga mõõdukate IBP-dega. Selle omapärase käitumise mõistmiseks viidi läbi fluorestsentsil põhinev jää kristallitasandite afiinsuse katse, mis näitas, et *EfcIBP* seondub peamiselt püramiidsete jääkristallide tasanditega, nõrgalt basaaltasandiga ja ei seondu prismaatilise tasandiga. *EfcIBP*-l on ka kõrgem afiinsus kahel kindlal tasapinnal. Esimene asub sekundaarse püramiidtasandi lähedal, teine on aga püramiidi tasand, mis asub basaaltasandist väga väikese nurga all. Sellist madala nurgaga püramiidtasandit ei ole varasemalt teiste IBP-dega seostatud. Kuigi valgul leiti esmalt madalam afiinsus basaaltasandil, näitas fluorestsentsmikroskoopia *EfcIBP* kõrgemat afiinsust basaaltasandil, võimaldades mõõta akumulereerimiskineetikat. Need mõõtmised näitasid, et *EfcIBP* adsorbeerub basaaltasandile väga kiiresti, umbes ühe minuti jooksul. Basaaltasandi adsorptsiooni konstant on $4 \pm 1 \text{ mM}^{-1} \text{ s}^{-1}$, mis on lähedane tüüp III kala AFP (antifriisvalk, IBP alamklass) mõõdetud adsorptsioonikonstandile. Erinevus seisneb aga selles, et see mõõdukas kala AFP akumulereerub prismatasandile. Võrdlusena uuriti hüperaktiivseid IBP-d, mille akumulereerumine basaaltasandile toimus tundide jooksul ning mille adsorptsioonikonstant oli suurusjärgu võrra väiksem. Lähtudes arvutisimulatsioonide ja valgu struktuuriuuringute tulemustest, loodi mitu *EfcIBP* mutanti. Nende TH ja IRI mõõtmistulemused näitasid märkimisväärset aktiivsuse vähenemist ja kinnitasid, et valk seondub jää pinnaga oma kahe külje kaudu.

Töö tulemused aitavad selgitada TH, IRI ja kuju ebatavalist kombinatsiooni. Lisaks defineeriti uus mõõdukate IBP-de klass, millel on afiinsus basaaltasandile, kuid mitte prismatasandile.

Käesoleva töö teine eesmärk oli hinnata IBP-de sobivust jäätises. Jäätis on külmutatud magustoit, mis on tundlik temperatuuri kõikumistele. Sellised temperatuuri kõikumised põhjustavad jäätises jääkristallide kasvu, alandades jäätise tekstuuri kvaliteeti. Kuna IBP-del on omadus takistada jääkristallide kasvu ja rekristalliseerumist, võimaldaks nende lisamine jäätisesse parandada jäätise tekstuuri ja pikendada säilivusaega.

Sobivuse uurimiseks valmistati rekombinantne AFP tüüp III ning IBP sisaldav talirukki ekstrakt, mis lisati madala rasvasisaldusega jäätistesse.

Mikroskoopilised uuringud näitasid, et mõlemad IBPd võimaldavad peatada jäätise segudes jää rekristalliseerumist, kuid lisaks põhjustavad nad jääkristallide agregeerumise jäikades kristallvõrgustikeks. Agregeerumine põhjustab jäätise tekstuuri olulisi muutusi, suureneb kõvadus ja rabadus. Vaid 3 mg L⁻¹ AFP tüüp III lisamine suurendas kõvadust 5 N-lt (kontrolljäätis) 24 N-ni. Teisest küljest aitab see sisemine kristallvõrgustik jäätise sulatamisel säilitada kuju.

Seega IBP-de lisamine jäätisesse uudse koostisosana põhjustab ebasoovitavat tekstuuri kõvenemist, samas on võimalik seda kasutada uut tüüpi külmutatud magustoitude väljatöötamisel, mis võivad olla kõvema tekstuuriga ja pikema tarbimisajaga.

Appendix 1

Publication I

Mangiagalli, M., Bar-Dolev, M., Tedesco, P., Natalello, A., **Kaleda, A.**, Brocca, S., Pascale, D., Pucciarelli, S., Miceli, C., Braslavsky, I., Lotti, M. (2017), Cryo-protective effect of an ice-binding protein derived from Antarctic bacteria. *FEBS J*, 284: 163-177. doi:10.1111/febs.13965

Cryo-protective effect of an ice-binding protein derived from Antarctic bacteria

Marco Mangiagalli¹, Maya Bar-Dolev², Pietro Tedesco³, Antonino Natalello¹ , Aleksei Kaleda^{2,4}, Stefania Brocca¹, Donatella de Pascale³, Sandra Pucciarelli⁵, Cristina Miceli⁵, Ido Bravslavsky²  and Marina Lotti¹

1 Department of Biotechnology and Biosciences, State University of Milano-Bicocca, Italy

2 Institute of Biochemistry, Food Science and Nutrition, The Robert H. Smith Faculty of Agriculture, Food and Environment, The Hebrew University of Jerusalem, Rehovot, Israel

3 Institute of Protein Biochemistry, National Research Council, Naples, Italy

4 Department of Food Processing, Faculty of Chemical and Materials Technology, Tallinn University of Technology, Estonia

5 School of Biosciences and Veterinary Medicine, University of Camerino, Italy

Keywords

cold adaptation; *Euplotes focardii* consortium; ice binding protein; ice recrystallization inhibition; thermal hysteresis

Correspondence

M. Lotti, Department of Biotechnology and Biosciences, State University of Milano Bicocca, Piazza della Scienza 2, 20126 Milano, Italy
Fax: +39 02 6448 3565
Tel: +39 02 6448 3527
E-mail: marina.lotti@unimib.it

(Received 27 July 2016, revised 31 October 2016, accepted 14 November 2016)

doi:10.1111/febs.13965

Cold environments are populated by organisms able to contravene deleterious effects of low temperature by diverse adaptive strategies, including the production of ice binding proteins (IBPs) that inhibit the growth of ice crystals inside and outside cells. We describe the properties of such a protein (*EfcIBP*) identified in the metagenome of an Antarctic biological consortium composed of the ciliate *Euplotes focardii* and psychrophilic non-cultured bacteria. Recombinant *EfcIBP* can resist freezing without any conformational damage and is moderately heat stable, with a midpoint temperature of 66.4 °C. Tested for its effects on ice, *EfcIBP* shows an unusual combination of properties not reported in other bacterial IBPs. First, it is one of the best-performing IBPs described to date in the inhibition of ice recrystallization, with effective concentrations in the nanomolar range. Moreover, *EfcIBP* has thermal hysteresis activity (0.53 °C at 50 µM) and it can stop a crystal from growing when held at a constant temperature within the thermal hysteresis gap. *EfcIBP* protects purified proteins and bacterial cells from freezing damage when exposed to challenging temperatures. *EfcIBP* also possesses a potential N-terminal signal sequence for protein transport and a DUF3494 domain that is common to secreted IBPs. These features lead us to hypothesize that the protein is either anchored at the outer cell surface or concentrated around cells to provide survival advantage to the whole cell consortium.

Introduction

Earth is a cold place where the temperature of over 85% of soil and water environments is close to the freezing point of water. Under these conditions, challenges for life are multifaceted, as temperature affects several key biological processes. In the cold, the

fluidity of cell membranes decreases and protein folding is impaired because hydrophobic interactions weaken. Moreover, the rates of transcription, translation, cell division and chemical reactions slow down. Nevertheless, a rich variety of organisms widely spread

Abbreviations

AFP, antifreeze protein; CFU, colony forming unit; DUF, domain of unknown function; *EfcIBP*, *Euplotes focardii* consortium ice binding protein; FT, freezing and thawing; GFP, green fluorescent protein; IBP, ice binding protein; IBS, ice binding site; IR, ice recrystallization; IRI, ice recrystallization inhibition; LB, Luria–Bertani; PB, phosphate buffer; TB, terrific broth; TH, thermal hysteresis.

across the natural kingdoms thrive in cold habitats [1]. To cope with the constraints mentioned above, the so-called cold-adapted or psychrophilic organisms have evolved different adaptive strategies, for example changes in the composition of cell membranes towards a higher content of unsaturated lipids, and the synthesis of cold-shock proteins and cold-active enzymes [2].

In the extreme condition of permanent subzero temperature, as occurs in permafrost soils and ice seas, or with seasonal fall in temperature another risk threatens even cold-adapted organisms: freezing. The formation of ice crystals both inside and outside cells is a cause of cell damage and death [3]. Fish, insects, plants, algae, diatoms, yeasts and bacteria that colonize very cold habitats, for example Arctic and Antarctic regions, avoid ice injuries by producing ice binding proteins (IBPs), which inhibit the growth of ice crystals [4]. Though all IBPs bind the same ligand – ice – their molecular and functional diversity is astonishing; what surmises recent evolution [4] and makes it difficult to draft a picture of structure–function relationships in this group of proteins. The identification and detailed characterization of novel proteins is expected to add information useful for rationalizing the properties and functions of the IBPs. To this end, this work investigates an IBP from a peculiar biological source, the bacterial community (consortium) that lives in association with a cold-adapted ciliate isolated from cold seawaters at Terranova Bay on the coast of Antarctica.

IBPs decrease the water freezing temperature in a non-colligative manner, thereby creating a hysteresis between the melting and the freezing temperature (thermal hysteresis; TH) [5,6]. TH derives from binding of IBPs to water molecules at the outer layer of ice and inhibiting further ice growth at the position of binding. This local pinning of the surface induces a microcurvature of the rest of the ice surface in between the pinned positions, and makes the association of other water molecules unfavorable from a thermodynamic point of view and *de facto* decreases the water freezing point. IBPs are classified based on their effectiveness in TH. For example, ‘hyperactive’ IBPs from insects and from some bacteria induce TH of 2–13 °C. As the main function of many IBPs is to prevent cell freezing, they are often referred to as ‘antifreeze proteins’. However, IBPs are present also in living beings that have ice crystals within cells or fluids and, therefore, their function is to help cells in tolerating freezing rather than resisting it. In this context, the most remarkable effect of IBPs is the inhibition of ice recrystallization (IR). IR is the growth of large ice crystals at the expenses of smaller ones [7] and is very

harmful for biological matter since it causes dehydration and cellular damage, particularly of cell membranes. Moreover, several microorganisms such as bacteria, fungi, algae and diatoms secrete IBPs to create channels in iced water around cells to allow for the uptake of oxygen and nutrients [8]. Extracellular IBPs contain a conserved region classified in the Pfam database (<http://pfam.xfam.org/>) as ‘domain of unknown function’ (DUF) 3494, and most of them carry a signal peptide for secretion at their amino terminus [8–10].

Crystallographic structures available to date classify IBPs in at least 11 different folds, utilizing different strategies of structural stabilization such as networks of hydrogen bonds and/or disulfide bonds, and/or Ca²⁺ stabilization, whereas the usual hydrophobic core of globular proteins is less relevant [11]. The active site of IBPs is the protein surface devoted to interaction with ice and is called the ice binding site (IBS). Again, different proteins adopt different solutions. Still, common features to most IBSs described to date are that they are quite extended, flat and hydrophobic surfaces and include threonine residues [11]. IBSs are mostly devoid of charged residues and often contain repeated amino acid sequences, consistent with their ability to mimic ice surface [4]. Even more puzzling than structural diversity are the effects of binding of IBPs to ice crystals, since some IBPs are more active in TH and others in IR. Explaining the rationale of such differences is not straightforward [4]. Since it was reported that moderate and hyperactive IBPs bind to different planes of ice crystals [12], the concept was developed that IBP properties depend on their specific spatial interaction with ice [4]. However, what drives IBPs to associate to a specific crystal face is still an open issue.

Here we describe the features of a bacterial ice binding protein, whose coding sequence was found in the metagenome of bacterial symbionts of *Euplotes focardii*, a free-swimming psychrophilic ciliate endemic of the oligotrophic coastal sediments of Terra Nova Bay in Antarctica. Previous studies on this single-cell organism contributed to the understanding of the molecular bases of cold adaptation and suggested a pivotal role for IBPs [13–15]. The sequence studied in this work was identified upon sequencing the *E. focardii* genome. Data analysis showed that out of the 201 918 contigs identified, 11 179 (from 100 to 25 584 bps) did not contain the telomeric repeats typical of *Euplotes* nanochromosomes (CCCCAAA-3′/3′-GGGGTTTT-5′) and were attributed to marine bacteria on the basis of a comparison with all bacterial genomes available in the NCBI data bank. Analysis of the 16S RNA sequences [16] revealed that the major

bacterial genera were either Bacteroidetes (16%) or Proteobacteria (78%). Search of IBP sequences within genomic contigs was carried out by Blast analysis, using IBP genes from the diatom *Fragilariopsis cylindrus* as the query. A contig of 3221 bps was found to contain an ORF for a putative IBP of 253 amino acids (GenBank code [AHG59376](#) [15]). In this work, we show that the recombinant protein *E. focardii* consortium IBP (*Efc*IBP) is stable to freezing and thawing, exerts a moderate effect of cryo-protection of pure proteins and whole bacterial cells and displays a remarkable activity in inhibiting ice recrystallization even at very low concentration.

Results

Attempts to produce the recombinant protein *E. focardii* consortium IBP in *Escherichia coli* failed whatever the conditions applied (data not shown). Analysis of sequence AHG59376 by Prosite [17] and SignalP 4.1 [18] suggested that an N-terminal stretch of 23 amino acid residues (MKKIKITMLTATVLFGLLTVVGC) may be a signal for anchorage to the cell surface or for protein transport [15]. Therefore, we designed a sequence devoid of the N-terminal stretch that is referred to in this paper as *Efc*IBP. Production of the recombinant protein was assayed in *E. coli*, at different temperatures and in different growth media as reported in 'Materials and methods'. The highest yield of soluble *Efc*IBP was achieved after 16 h incubation at 25 °C in ZYM-5052 medium [19]. The yield of *Efc*IBP, determined after affinity chromatography purification, was ~ 2 mg from 1 L of culture. Under the same conditions we obtained ~ 8 mg

of green fluorescent protein (GFP) from 1 L of culture (Fig. 1).

Secondary structure and conformational properties of *Efc*IBP

Fourier transform infrared (FTIR) and circular dichroism (CD) spectroscopies were applied to investigate the composition in secondary structure and the conformational stability of *Efc*IBP (Fig. 2). FTIR analysis was performed in the amide I region, where the signal is mainly due to C=O stretching vibrations of the peptide bond, which is particularly sensitive to the polypeptide secondary structures. Figure 2A shows the second derivative spectrum [20] of *Efc*IBP and bands are assigned as described in [21]. The spectrum is dominated by a component at ~ 1634 cm^{-1} , assigned to native β -sheet structures. The component at about 1653 cm^{-1} occurs in the spectral region of α -helices and random coils, and peaks at ~ 1669 and ~ 1689 cm^{-1} can be assigned to turn and turn/ β -sheet structures, respectively. The ratio of peak intensity at ~ 1689 and ~ 1634 cm^{-1} indicates a parallel orientation of the β -sheet structures. Indeed, as suggested by theoretical and experimental works [21,22], in the amide I region the presence of parallel β -sheets is revealed by either a single band at 1640–1623 cm^{-1} or by this signal together with a very low intensity peak at 1695–1675 cm^{-1} . The high content of β -sheet structures in the *Efc*IBP protein is also highlighted by its CD spectrum displaying a negative band at ~ 219 nm and positive ellipticity at ~ 195 nm (Fig. 2B). Accordingly, the 3D structural model (see later) built using the structure of the IBP from *Flavobacterium frigidis* (33.5% sequence identity) as the template predicts a mainly beta structure.

In order to investigate the robustness of the *Efc*IBP structure towards freezing and towards repeated freezing and thawing (FT) steps, we analysed by FTIR and near-UV CD spectroscopies the structure of the protein stressed by up to 14 FT cycles followed by overnight freezing, as described in 'Materials and methods'.

For the sake of completeness, we show also results obtained with GFP, used as a probe to assess the performance of *Efc*IBP as a cryoprotectant (see later). GFP is similar to *Efc*IBP in size and in the prevalence of beta elements in the secondary structure. Changes in the secondary structure of both proteins revealed by FTIR spectra are hardly detectable (data not shown), whereas effects on the tertiary structures are different and protein dependent (Fig. 3). Indeed, after FT cycles, we observed a small loss of intensity (15% at

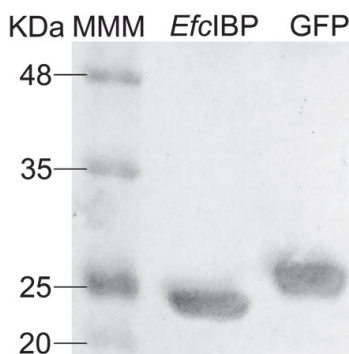


Fig. 1. SDS/PAGE of recombinant proteins purified by affinity chromatography. MMM: molecular mass marker. Each lane contains ~ 5 μg of purified protein.

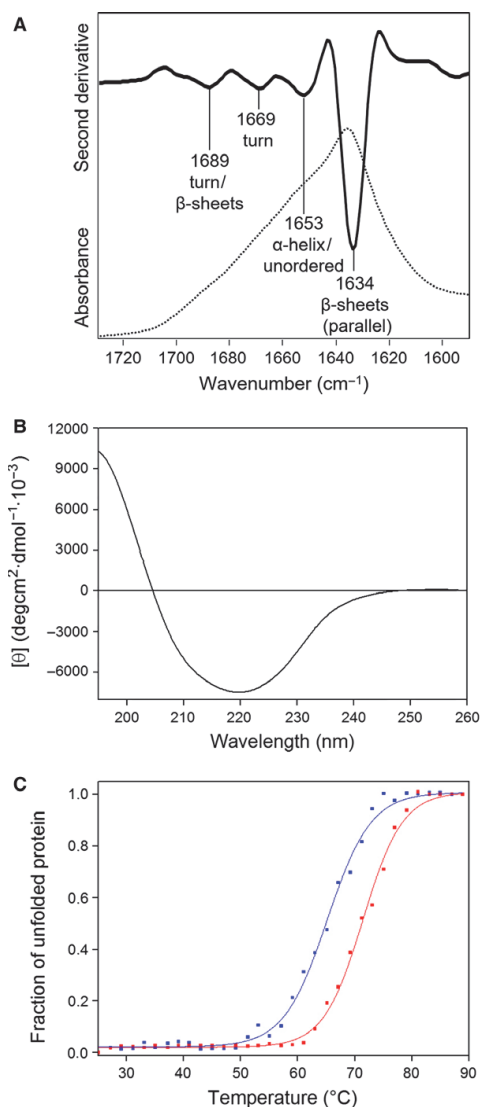


Fig. 2. Secondary structure analysis of *EfdBP*. (A) FTIR absorption spectrum (dotted line) and second derivative spectrum (continuous line) of *EfdBP* (40 μM). (B) far-UV CD spectrum of *EfdBP* (8 μM). (C) Heat stability of *EfdBP* (blue) and GFP (red) (8 μM). Ellipticity at 215 nm was recorded during heating from 25 to 90 °C. Initial CD signal was normalized to 100%.

287 nm) in the near-UV CD spectra of *EfcIBP* (Fig. 3A). Under the same conditions of freeze–thaw cycles, the TH values were not affected. These results

show that structural and functional properties of this IBP are suitable to cope with low temperature and freezing stresses. On the other hand, the spectrum of native GFP revealed a marked flattening of the signal, mainly around 279 nm, where the signal loss is 70% (Fig. 3B).

To gain a more complete view of the protein's temperature sensitivity, we analysed both *EfcIBP* and GFP by CD spectroscopy, monitoring ellipticity changes at 215 nm in samples heated from 25 to 90 °C (Fig. 2C). Above ~60 °C, the ellipticity signal of *EfcIBP* was rapidly lost with the midpoint at 66.4 ± 2.7 °C. The appearance of visible protein precipitates in the cuvette suggested that aggregation occurs. Similar behavior has been reported for *LeIBP* and *FjIBP*, two homologs of *EfcIBP* with midpoint temperature of 61 and 56.4 °C, respectively (Table 1) [23]. GFP displayed higher thermal stability with a

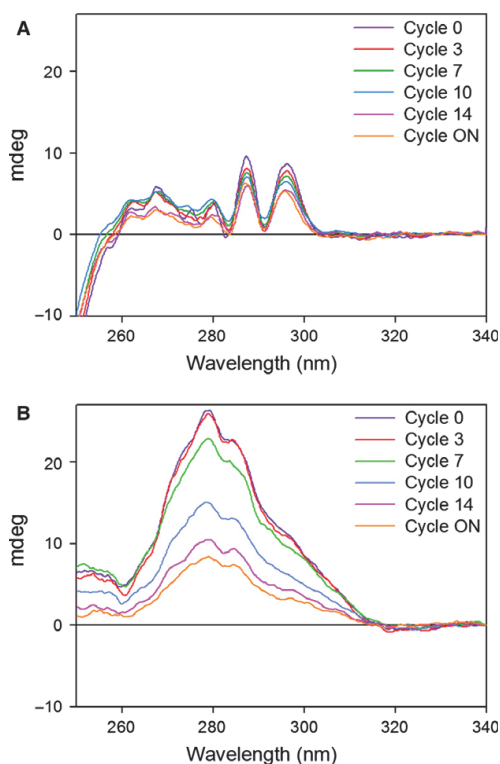


Fig. 3. Robustness of *EfdBP* (A) and GFP (B) analysed by near-UV CD spectroscopy. Spectra were acquired in phosphate buffer before freezing (cycle 0), upon several cycles of FT and upon further overnight freezing following the 14th FT cycle (cycle ON).

midpoint of signal loss at 71.4 ± 0.8 °C. From these data we surmise that *Efc*IBP not only well withstands repeated freezing and melting, but is also surprisingly thermostable, although less than GFP. Temperature stability of proteins from psychrophilic organisms may sound counterintuitive; however, stability may be a side effect of the rigidity necessary for IBPs when binding to ice crystals. In fact, according to the anchored clathrate waters mechanism, the ice binding sites of IBPs need to be well positioned to allow water molecules to be arranged on top of them in an ice-like structure that mimics ice crystals and allows binding of anchored water to a nearby ice crystal [24].

Ice-binding properties

The thermal hysteresis values of *Efc*IBP are similar to those of moderate fish antifreeze proteins (AFPs) [11] with activity of 0.53 °C at 50 μM concentration, as shown in the TH plot in Fig. 4A. The activity at this concentration did not reach a plateau, indicating that higher concentrations may yield higher TH values. However, higher concentrations are more difficult to measure due to fast melting of superheated crystals. The same TH was obtained with 300 μM (2.1 $\text{mg}\cdot\text{mL}^{-1}$) of AFP type III. In comparison, 40 μM at 8 min incubation time yielded 1.1 °C for the *Tenebrio molitor* AFP, a representative of the hyperactive proteins [25].

The growth and melting patterns observed with *Efc*IBP differ from the bipyramidal patterns obtained with fish AFPs, and have some features similar to the shapes observed with hyperactive insect AFPs [26] and the ryegrass IBP [27] (Fig. 4B). Ice in the presence of *Efc*IBP appears to grow and melt layer by layer in the direction of the basal planes, leading to very thin ice crystals (Video S1). Although the crystals do not grow when held at constant temperatures within the

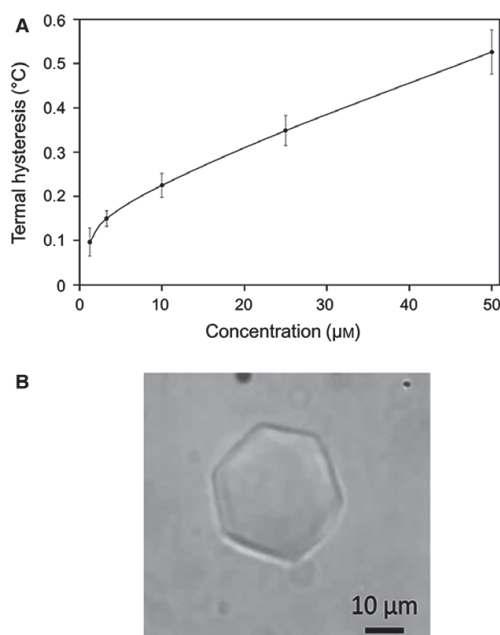


Fig. 4. (A) Thermal hysteresis activity of *Efc*IBP. See text for details. Each data point is the average of at least three measurements. The error bars represent standard deviations ($n = 6$). (B) Ice morphology in the presence of *Efc*IBP (~ 1 μM).

hysteresis gap, stepwise lowering of the temperature leads to step growth of the crystals, until the freezing point is reached and the crystals burst. A similar phenomenon was noted with fish antifreeze glycoproteins, despite differences in crystal morphologies [26]. The step growth was less pronounced at higher concentrations, although it still occurred at 50 μM (1.2 $\text{mg}\cdot\text{mL}^{-1}$). Crystals that grew new ice layers

Table 1. TH activities of *Efc*IBP homologs. Identity with *Efc*IBP was calculated on full-length sequences.

Protein ID	Organism	Identity	TH activity	Reference
<i>Efc</i> IBP	Bacterial consortium of <i>Euplotes focardii</i>	—	0.53 °C at 50 μM	This work
<i>Col</i> AFP	<i>Colwellia</i> sp. strain SLW05	37.3%	3.8 °C at 0.14 mM	[35]
<i>F</i> IBP	<i>Flavobacterium frigidis</i> PS1	33.5%	2.5 °C at 50 μM	[23]
<i>Fc</i> AFP	<i>Fragilariopsis cylindrus</i>	30.9%	0.9 °C at 350 μM	[34]
<i>Ch</i> AFP	<i>Chaetoceros neogracile</i>	36.3%	0.8 °C at 40 μM	[39]
<i>Nag</i> IBP	<i>Navicula glaciei</i>	33.5%	3.2 °C at 1.6 mM	[37]
<i>Tis</i> AFP8	<i>Typhula ishikariensis</i>	35.4%	2 °C at 180 μM	[36]
<i>Afp</i> 4	<i>Glaciozyma antarctica</i>	31.3%	0.08 °C at 200 μM	[38]
<i>Lel</i> IBP	<i>Leucosporidium</i> sp. AY30	33.2%	0.35 °C at 370 μM	[33]

within the TH gap did not continue to grow if held at a constant temperature. To check whether the protein accumulates on the ice surface over time, we incubated the crystal in 50 μM *Efc*IBP for 1 or 10 min before temperature lowering. We did not detect any significant difference in TH values, indicating that *Efc*IBP binds quickly (within the first minute) on the crystal surface. Still, after both annealing times, we observed step growth during the temperature decrease.

The IRI activity of *Efc*IBP is shown in Fig. 5. We observed that 0.1 μM of protein was overall sufficient to inhibit IR, but some crystals did grow. At 1 μM *Efc*IBP, IR was completely inhibited. We calculated the IRI efficacy of *Efc*IBP following the analysis derived by Budke *et al.* [28] and compared it with the efficacy of type III AFP from ocean pout (*Zoarces americanus*, QAE (QAE is a particular subgroup of IBPs from ocean pout *Macrozoarces americanus*) isoform named HPLC12) [4]. This fish IBP was chosen as a control since its TH activity is in the same range. The IRI efficacy (C_i) is the inflection point of a curve that describes the dependence of IR rate on protein concentration (Fig. 6). The C_i value represents the concentration of *Efc*IBP below which the IRI is not effective. We found that the C_i of *Efc*IBP is $0.0025 \pm 0.0006 \mu\text{M}$. For comparison, we measured IRI for ocean pout type III AFP and found a C_i value of $0.05 \pm 0.02 \mu\text{M}$. The effectivity of *Efc*IBP in IRI is 20-fold higher than type III AFP and it is also very high compared with other IBPs [29,30]. Values of C_i in the nanomolar range were previously reported only for antifreeze glycoproteins [29].

Cryoprotection assays

The biological activity of *Efc*IBP was explored in experiments of cryoprotection of a single pure protein (GFP) and of whole *E. coli* cells. In the first set of experiments, purified GFP was exposed to FT treatment in the presence of 0.6 μM *Efc*IBP or other proteins known to be either active (BSA) or inactive (lysozyme) as cryo-protectors [31]. GFP fluorescence was measured before freezing, after 7 and 14 cycles of FT, and finally after 14 FT cycles and overnight freezing. Under these conditions, we observed a rapid loss of intrinsic fluorescence in GFP (Fig. 7A) likely as a result of denaturation induced by FT treatment and consistent with the results reported in Fig. 3B. The fluorescence decay was milder in the presence of *Efc*IBP and of BSA, but not in the presence of lysozyme, used as a negative control (Fig. 7A).

To evaluate the protection effect of *Efc*IBP on whole cells, we had to perform experiments at less

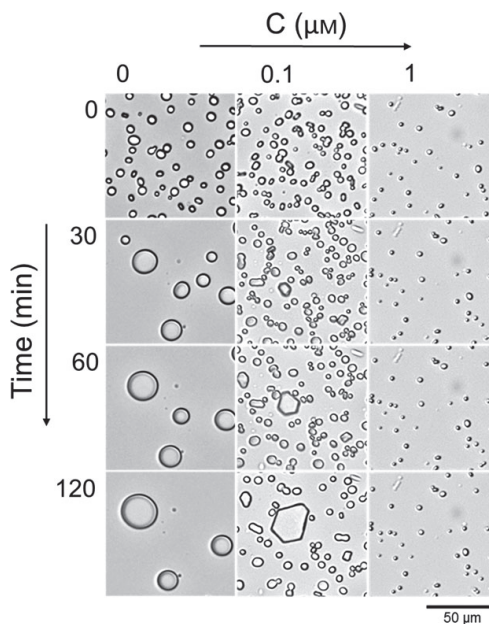


Fig. 5. Ice recrystallization inhibition by *Efc*IBP. A sucrose sandwich assay with and without *Efc*IBP was carried out for 2 h at an annealing temperature of -7.4°C . Snapshots along the experiment are presented. The time lapse is noted to the left. Protein concentration in 45% sucrose solution is noted at the top.

severe temperature, since *E. coli* exposed to FT according to the previous schema was not viable. *E. coli* BL21 (DE3) cells were incubated at a temperature close to the water freezing point in the presence of either 50% (v/v) glycerol or different proteins ($1 \text{ mg}\cdot\text{mL}^{-1}$) as in the previous experiment. Cell viability was assayed every 2 days, by counting colony forming units (CFUs) formed by cells exposed to cold treatment (Fig. 7B). After 12 days, the percentage of viable cells was 6.50% for cells in phosphate buffer (PB) and lysozyme, 9.21% for samples with BSA, 24.6% for samples containing *Efc*IBP and 35% for those with glycerol.

Structure and function in the context of IBP evolution

The maximum likelihood phylogenetic tree (Fig. 8) built with 29 selected sequences from bacteria and eukaryotic microorganism (mostly cold adapted) placed *Efc*IBP within the *Stigmatella aurantica* AFP/

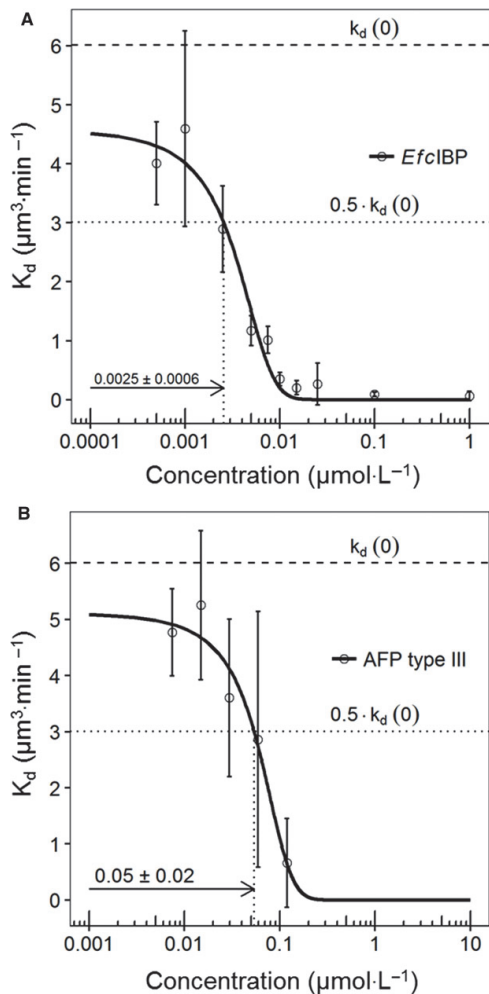


Fig. 6. Quantitative ice recrystallization efficacy of *EfcIBP* and type III AFP. The recrystallization rate constant K_d was measured as a function of protein concentration. Standard deviations are shown ($n = 3$). The inflection point of the curve is the intercept of the dotted lines. The C_i values with 95% confidence intervals are noted at the bottom left. (A) *EfcIBP*. (B) Type III AFP (HPLC12 isoform from ocean pout).

IBP lineage. With the exception of *Fimbriimonas ginsengisoli*, the members of the cluster are Antarctic or cryophilic microbes. The same result was obtained when aligned sequences were restricted to 23 IBPs containing a domain of unknown function (DUF) 3494 retrieved from the Pfam server [32] using the *EfcIBP*

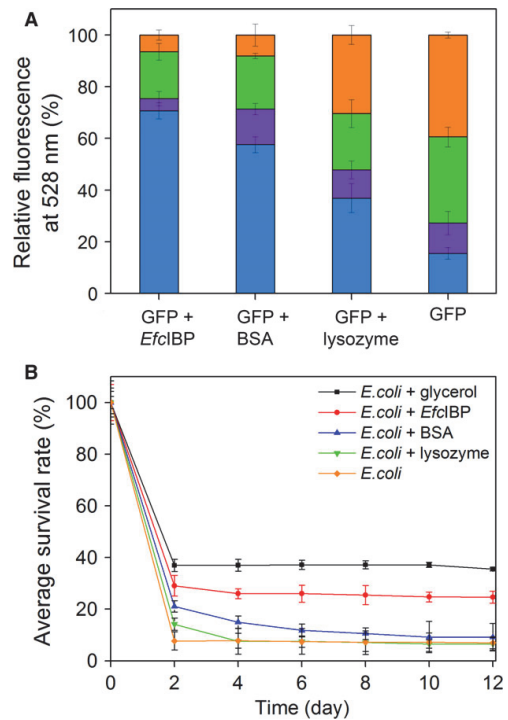


Fig. 7. Cryoprotection assay. (A) Cryoprotection of GFP. GFP fluorescence in the presence of cryoprotectants was acquired before freezing (orange), after 7 (green) and 14 cycles (purple) of FT and after a further overnight freezing following the 14th FT cycle (blue). Initial fluorescence was normalized to 100%. Excitation was at 474 nm and spectra were recorded at 528 nm in PB. Each data point is the average of four measurements. Standard deviations are shown. (B) Cryoprotection of *E. coli* BL21 (DE3) cells. Cells viability in the presence of cryoprotectants was determined in terms of CFUs at different time points in the course of a 12-day incubation at ca. 0 °C. For each sample, the number of viable cells before chilling was taken as 100%. Each data point is the average of three measurements. Standard deviations are shown.

amino acid sequence as the query (bracketed in Fig. 8).

To integrate functional and structural analyses, we restricted the cluster to eight IBPs with over 30% sequence identity to *EfcIBP* and whose TH activity had been determined (Table 1) [23,33–39]. The 3D structure of three IBPs included in the comparison (*FfIBP*, *LeIBP* and *ColAFP*) is known and consists of a β -helix with an α -helix alongside the main axes of the protein [23,33,35]. Structural information allowed building the structure-driven multiple

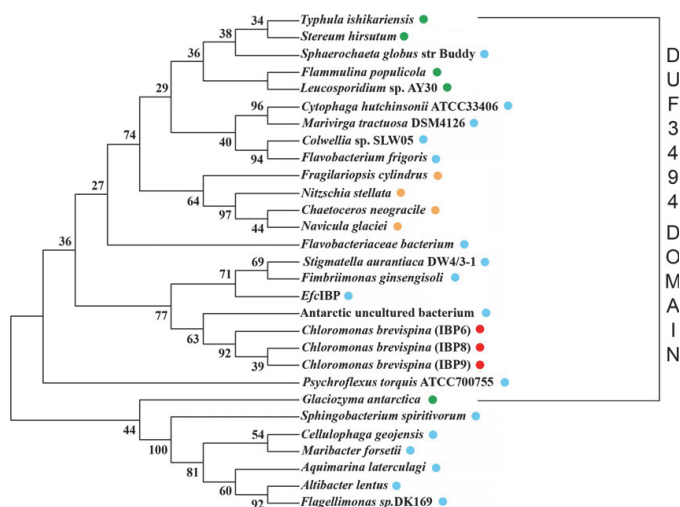


Fig. 8. Phylogenetic tree based on amino acid sequences of ice binding proteins from fungi, bacteria, diatoms and algae (maximum likelihood method on JTT matrix, 1050 bootstraps). Branches reproduced in < 50% of bootstrap replicates are collapsed. The percentage of bootstraps in which the associated taxa clustered together are shown next to the branches. The bullets indicate the sequences obtained from fungi (green), bacteria (blue), diatoms (orange) and algae (red). The sequences were obtained from the NCBI database with the following codes: *Sphaerochaeta globus* (strain Buddy), YP_004248731; *Navicula glaciei*, AAZ76251; *Fragilariopsis cylindrus*, CN212299; *Fragilariopsis curta*, ACT99634; *Chlamydomonas* sp., EU190445; *Typhula ishkarioensis*, BAD02897; *Flammulina populicola*, ACL27144; *Lentiniulaedodes edodes*, ACL27145; *Glaciozyma antarctica* ACX31168; *Psychromona ingrahamii*, ZP_01349469; *Colwellia* sp., DQ788793; *Deschampsia antarctica*, ACN38296; *Lolium perenne*, ACN38303; *Marivirga tractuosa* (strain DSM4126), YP_004052221; *Cytophaga hutchinsonii* (strain ATCC33406), YP_676864; *Chaetoceros neogracile*, ACU09498; *Nitzschia stellata*, AEY75833; *Psychroflexus torquis* (strain ATCC700755), YP_006867144; *Stigmatella aurantiaca* (strain DW4/3-1), gL_115375670; an uncultured bacterium (EKD52074.1), *Stereum hirsutum* FP-91666 SS1, XP_007299923.1; Antarctic unidentified bacterium, gij930810610|gb|ALG05165.1; *Chloromonas brevispina* IBP 6, 8, 9, gij649907359|gb|AIC65766.1, gij649907413|gb|AIC65768.1, gij649907440|gb|AIC65769.1; *Fimbriimonas ginsengisoli* Gsoil 348, gij663071654|gb|AIE83809.1; *Leucosporidium* sp. AY30gij255709878|gb|ACU30806.1.

alignment shown in Fig. 9. The alignment highlights high conservation in both primary and secondary structures, as well as in the sequence of IBSS (Fig. 10A), with a mean sequence identity of 26.3%, 23.7% and 23.9% with the IBSSs of *FfIBP*, *LeIBP* and *ColAFP*, respectively. A high content of polar residues is observed, in particular threonine and serine. In the structural model, some of these polar amino acids (highlighted in cyan in Fig. 10A) line up on β -sheets, on the same face of the protein, suggesting a putative ice binding face (Fig. 10B). We observed that, in spite of sequence and structure conservation, considered IBPs display different TH activity. We are aware that comparison of TH determined by different authors is not straightforward because of possible discrepancies in concentration and analytical methods. However, with all due caution, data available point to a non-relatedness of general structural organization and TH. Data on IRI, unfortunately, are still too sporadic to be

included in the analysis. In case of *FcAFP*, IRI activity is 1.2 μM and 0.12 μM in low- and high-salinity conditions, respectively [34].

Discussion

As the body of knowledge increases, the heterogeneity of proteins able to bind to ice becomes more and more evident. The widespread occurrence of IBPs within organisms unrelated to each other and the striking variety of sequences, structures and functional strategies is considered proof of recent evolutionary pathways aimed at providing cells and tissues with defences against intracellular and environmental freezing. Polar marine environments are being intensively investigated in the frame of programs for the study and exploitation of biodiversity and provide a rich reservoir of novel organisms.

EfcIBP shows structural and functional properties common to IBPs, but also a combination of TH and

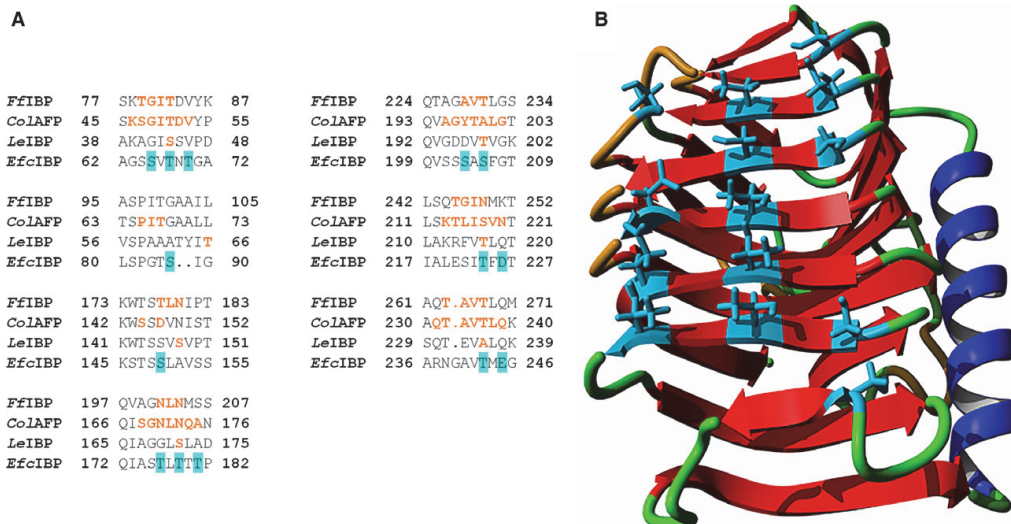


Fig. 10. Ice binding site prediction. (A) Sequence alignment of the IBSSs from *FfIBP* [23], *CoIAFP* [35], *LeIBP* [33] and *EfcIBP*. The residues involved in ice binding are shown in orange bold. The polar residues located in β -sheet on the same face of *EfcIBP* are highlighted in cyan. The alignment includes the full-length sequence of each protein. (B) Molecular model of *EfcIBP*. The 3D structure was modelled with swiss-MODEL [51] using *FfIBP* as a template [23]. β -Sheets are indicated in red, α -helices in blue, coils in orange and turns in green; sidechains of polar residues predicted to belong to IBS are in cyan.

this IBP. Rather, *EfcIBP* may serve to depress ice recrystallization or have an effect on preservation of the liquid environment in the vicinity of the consortium. IRI activity was demonstrated in several IBPs secreted by microorganisms that inhabit icy niches, in particular in communities of microorganisms living in sea ice [40]. Such a role would support the importance for *E. focardii* of living together with a bacterial community able to secrete an IBP or at least to export it to the cell surface and is consistent with the cryoprotection effect observed when the IBP is supplemented in sufficient amounts. In the absence of direct evidence about protein transport, the hypothesis of secretion is substantiated by two observations, namely the presence of a putative sequence of transport/anchorage to the cell membrane at the amino terminus and the identification of a DUF3494 domain common to several secreted IBPs [9]. Still to be clarified is the function of this IBP within the cell consortium as it might well be active in the structuring of ice around the ciliate cells but could also play a role when in association with the ciliate cells surface. Such a function has been shown for the Antarctic moss *Bryum argenteum*, which accumulates proteins on its surface [10]. Either anchored at the outer cell surface or concentrated around cells, this protein might provide survival advantages to the entire

consortium and may have contributed to the successful colonization of the Antarctic habitat by the ciliate.

Materials and methods

Strains, media and production assays

E. coli BL21[DE3] (EMD Millipore, Billerica, MA, USA) was used as the host for heterologous expression. Production assays of recombinant *EfcIBP* were carried out in low-salt Luria-Bertani (LB) medium (tryptone 1%, yeast extract 0.5%, sodium chloride 0.5%), terrific broth (TB; tryptone 12%, yeast extract 24%, glycerol 4%, potassium phosphate monobasic 0.17 mM, potassium phosphate dibasic 0.72 mM) or ZYM-5052 medium [19], with addition of 100 mg·L⁻¹ ampicillin. In these analytical experiments, pre-cultures were grown in LB medium to $D_{600} \sim 0.6$ –0.8 and diluted 1 : 25 in different media. Cultures in LB or TB medium were incubated at 30 °C to reach D_{600} 0.6–0.8 before adding 0.2 μ M isopropylthio- β -D-galactoside as inducer. Each induced culture was subdivided in three shaking flasks and incubated at different temperatures (13, 30 and 37 °C). Samples were withdrawn after 2, 4 and 18 h, with additional samples obtained after 48 and 72 h from the 13 °C cultures. Analytical cultures in ZYM-5052 medium were incubated at 13 and 25 °C, for 16–72 h, depending on incubation temperature and samples withdrawn at the end of incubation.

Cloning of the *EfcIBP* coding sequence

The *EfcIBP* gene corresponds to nucleotides 70–762 of the genomic sequence *EfsymbAFP* previously described by [13]. The sequence encoding *EfcIBP* was amplified by PCR using a forward primer (5'-CATATGAAGAAAGAAAAGAAC-GAT-3') that inserts in 5' the initial ATG along with the restriction site for *NdeI* (underlined) and a reverse primer (5'-CTCGAGCGGCAGAACAAA-3') that inserts in 3' the restriction site for *XhoI* (underlined). Reactions were carried out using MyCycler (Bio-Rad, Hercules, CA, USA) under the following conditions: 1 cycle (95 °C for 5 min), 30 cycles (95 °C 1 min, 54 °C 1 min, and 72 °C 1 min), and a final cycle of 72 °C for 7 min. PCR products were cloned in frame with a sequence coding for C-terminal 6xHis-Tag into the pET-21a expression vector previously cleaved with *NdeI* and *XhoI* to obtain pET-21a[*EfcIBP*]. The sequence of cloned DNA was verified by bidirectional DNA sequencing.

GFP was produced from pET-19b [GFP] [41]. Type III AFP is a recombinant version of HPLC12, a type III isoform that belongs to the QAE subgroup of IBPs from ocean pout *M. americanus*. The protein was produced in *E. coli* and purified as described elsewhere [42].

Production and purification of recombinant proteins

Production of recombinant *EfcIBP* and GFP was in ZYM-5052 [19] with addition of 100 mg·L⁻¹ ampicillin. Pre-cultures were grown in low-salt LB medium up to $D_{600} \sim 0.6$ – 0.8 , diluted 1 : 25 in ZYM-5052 and incubated overnight at 25 °C.

Proteins were purified by affinity chromatography using resin of nickel–nitrilotriacetic acid agarose. Elution fractions containing the highest protein concentrations were pooled and buffer was exchanged for 10 mM ammonium acetate pH 7.0 by two consecutive gel filtrations on PD-10 columns (GE Healthcare, Little Chalfont, UK) according to the manufacturer's instructions. Samples were lyophilized in a freeze-dryer (Heto FD1.0, Gemini BV, Apeldoorn, the Netherlands) and stored at –20 °C or re-suspended in PB (25 mM sodium phosphate pH 7.0).

Protein concentration was determined by the Bradford protein assay (Bio-Rad), using bovine serum albumin as the standard. SDS/PAGE was on 14% acrylamide gels [43] stained with Coomassie dye (Bio-Rad) after electrophoresis. Broad-range, pre-stained molecular-mass markers (Gene-Spin, Milan, Italy) were used as standards.

Analysis of protein conformation and stability

CD spectroscopy

CD spectra of proteins dissolved in PB (8 μM for far-UV measurements and 40 μM for near-UV measurements) were

recorded with a J-815 spectropolarimeter (Jasco Corp., Easton, MD, USA), using either 0.1 cm (for far-UV) or 1 cm path length quartz cuvettes (for near-UV). Experiments were in duplicate.

Spectra in the far-UV were measured in the range 195–260 nm, while near-UV measurements were at 240–340 nm, with 0.1 nm data pitch and 20 nm·min⁻¹ scanning speed. All spectra were corrected for buffer contribution, averaged from two independent acquisitions, and smoothed by using a third-order least square polynomial fit.

Thermal denaturation spectra were obtained measuring the CD signal at 215 nm fixed wavelength when progressively heating the sample from 25 to 90 °C. Measurements were performed with a data pitch of 0.2 °C and a temperature slope of 5 °C·min⁻¹.

Molar mean ellipticity values per residue $[\theta]$ were calculated as:

$$[\theta] = \frac{3300 \cdot m \cdot \Delta A}{c \cdot n \cdot l}$$

where ΔA is the difference in the absorption between circularly polarized right and left light of the protein corrected for blank, m is the protein molecular mass in daltons, l is the path length (0.1 cm), c is the protein concentration (mg·mL⁻¹) and n is the number of residues [41].

FTIR spectroscopy

FTIR spectra in attenuated total reflection (ATR) were collected by using the Quest device (Specac, UK) equipped with a single reflection diamond element. Aliquots of 2 μL of protein solution (40 μM in PB) were deposited on the ATR plate and dried at room temperature in order to obtain a protein film. ATR/FTIR spectra were then measured using a Varian 670-IR spectrometer (Varian Australia Pty Ltd, Mulgrave, Victoria, Australia) under the following conditions: 2 cm⁻¹ spectral resolution, 25 kHz scan speed, 512 scan co-additions, triangular apodization and nitrogen-cooled mercury cadmium telluride detector. Absorption spectra were corrected for buffer contribution, and normalized to the amide I band intensity. Analyses of spectra were performed with the software Resolutions-Pro (Varian Australia).

Assessment of stability to freezing and thawing

IBP and GFP samples (40 μM) were subjected to up to 14 cycles of freezing (–20 °C for 20 min) and thawing (25 °C for 10 min) or to 14 cycles of FT followed by overnight freezing (–20 °C for 16 h). Effects on protein structure were assessed by near-UV CD and FTIR spectroscopies.

Ice binding assays

Thermal hysteresis and ice crystal morphology

We observed ice morphologies and determined TH using a LabVIEW (National Instruments Corp., Austin, TX, USA)-operated custom-designed nanoliter osmometer as described [44,45]. Lyophilized proteins were recovered in double distilled water to 50 μM solution and diluted in 20 mM ammonium bicarbonate (pH 8.5). Rehydrated proteins exhibit the same secondary structure of freshly prepared, soluble samples, as revealed by FTIR spectra (data not shown). Samples of ~ 10 nL immersed in oil were cooled until freezing (~ -30 °C) and then warmed until a single ice crystal of < 20 μm diameter remained. The melting temperature of the crystal was measured and then the crystal was incubated for 1 or 10 min at a few hundredths of a degree below the melting point. After incubation, the temperature was reduced by 0.01 °C every 4 or 10 s and the crystal image was recorded. The temperature at which fast growth commenced was determined as the freezing point. The difference between the melting point and the hysteresis freezing points is the TH value.

Ice recrystallization inhibition

Ice recrystallization inhibition (IRI) was conducted using a sucrose-sandwich assay [46] with some modifications [28]. The final solutions contained 45% sucrose, 50 mM NaCl, 10 mM Tris (pH 8.0) and up to 1 μM of protein. Samples of 1 μL were placed on a sapphire sample holder and covered with a 13-mm diameter circular glass coverslip. The sapphire was used to reduce temperature gradients. The sample was sealed with type-B immersion oil (Sigma-Aldrich, St. Louis, MO, USA) to avoid evaporation and mounted on the stage of a Motorized Cryobiology System (model MDBCS196, Linkam Scientific, Tadworth, UK). A copper plate with a 2.5-mm diameter slit was placed on top of the sample to further reduce temperature gradients. Immersion oil was used between the sample, the stage and the slit to improve thermal contact. The Linkam stage was placed on a light microscope (BX41, Olympus America Inc., Melville, NY, USA) and operated using a Labview interface. The system was cooled from room temperature to -50 °C at a rate of 130 °C $\cdot\text{min}^{-1}$ and sustained at -50 °C for 1 min. The temperature was then elevated to -20 °C at a warming rate of 130 °C $\cdot\text{min}^{-1}$ and then warming continued to -10 °C at a rate of 10 °C $\cdot\text{min}^{-1}$. The final stage of heating up to the annealing temperature of -7.4 °C was conducted at a slow rate of 1 °C $\cdot\text{min}^{-1}$ to avoid overheating. The sample was maintained at this temperature for 60 min. During this period, recrystallization was recorded using an EXi Aqua bio-Imaging camera (QImaging, Surrey, Canada) every 1 min. The experiment was carried out with different concentrations of protein and repeated at least three times for each concentration.

The IRI was calculated following the mathematical description derived by Budke *et al.* [28]. The images were processed using Fiji (R Foundation for Statistical Computing, Vienna, Austria) to calculate the number of crystals, the mean radius of the crystals and the total crystal volume. The cube of the mean crystal radius was calculated for all images in each data set and plotted against time. The slope of the curve obtained from time points 30–60 min was taken as the recrystallization rate constant. The ice volume fraction (Q) was also calculated for all images in each data set and only experiments with $< 1\%$ variation in Q were considered. In all experiments the ice volume fraction was up to 9% (in high volume fraction the theory for IRI calculation is not legitimate). The recrystallization rates (K_d) were plotted against protein concentration, with at least three replicates for each concentration. This data set was fitted to a sigmoidal curve using R (R Foundation for Statistical Computing, Vienna, Austria). The inflection point of the curve, termed the C_i value, represents the effective protein concentration below which recrystallization is not efficiently inhibited [28]. A profile likelihood confidence interval ($\alpha = 0.05$) for the C_i point was calculated using the 'nlstools' R package. The rate constant in the absence of protein ($K_d(Q)$ at $[C] = 0$) was determined by measuring the recrystallization rate of buffer without protein. This experiment was repeated eight times and the averaged $K_d(Q)$ value was used for curve fitting. To accommodate the possible effects of different Q , we extrapolated all K_d values for zero volume fraction $Q = 0$ as described [28] and plotted the new K_{i0} values against protein concentration (data not shown). The difference between the original C_i value and the corrected C_i value was very small.

Cryoprotection assays

Cryoprotection of GFP

Fluorescence spectroscopy experiments were carried out to detect the effects of FT on GFP fluorescence in either the presence or the absence of the *EfcIBP*. All protein samples were dissolved or prepared in PB. Samples of GFP (0.6 μM) were mixed with equimolar concentrations of *EfcIBP*, BSA (Sigma-Aldrich), or lysozyme (Sigma-Aldrich) or with PB alone, in a final volume of 500 μL in PB. Samples were divided into four 100 μL aliquots and deposited in a 96-multiwell plate to replicate each measurement. Plates were then frozen and thawed according to the scheme previously described above in 'Assessment of stability to freezing and thawing'. Emission spectra were recorded before freezing, after 7 and 14 FT cycles and finally after overnight freezing. Fluorescence emitted from GFP was measured by a Cary Eclipse (Varian Inc., Palo Alto, CA, USA) spectrofluorimeter using 96-multiwell plates. GFP fluorescence was recorded at room temperature

with excitation at 474 nm and emission at 528 nm. The experiment was repeated three times.

Cold-tolerance assays were carried out on *E. coli* BL21 (DE3) cells exposed to low temperature in the presence or in the absence of *Efc*IBP. Cells carrying empty plasmid pET21 (to confer ampicillin resistance) were grown in ZYM-5052 medium and incubated overnight at 25 °C until they reached a D_{600} of ~ 3 . Aliquots of 1 mL of fresh culture were mixed with equal volumes of 1 mg·mL⁻¹ PB solutions of *Efc*IBP, BSA (Sigma-Aldrich), lysozyme (Sigma-Aldrich), or glycerol (50%) (Euroclone, Pero, Italy), or with PB alone as a control. Cell aliquots in 1.5-mL plastic tubes were kept submerged in ice for several days at a temperature of -0.5 °C. After 0, 2, 4, 6, 8, 10 and 12 days, samples were diluted in LB medium with addition of 100 mg·L⁻¹ ampicillin, and inoculated on LB-agar plates to count CFUs after 16 h incubation at 37 °C. Plates were inoculated in three replicates for each point.

Sequence analysis and modelling of 3D structure

The evolutionary history was inferred by using the maximum likelihood method based on the JTT matrix-based model [47]. The bootstrap consensus tree was inferred from 1050 replicates and assumed to describe the evolutionary history of the analyzed taxa [48]. An initial tree for the heuristic search was obtained by applying the neighbor-joining method to a matrix of pairwise distances estimated using a JTT model. The analysis involved 29 amino acid sequences. There was a total of 792 positions in the final dataset. Evolutionary analyses were conducted with MEGA5 [49]. Multiple alignments were performed by ESPRIT [50]. The 3D structure of *Efc*IBP was modelled on the structure of *F*IBP (PDB: 4NU2 [23]) using SWISS-MODEL [51]. *Efc*IBP displays a sequence identity of 33.5% compared with the *F*IBP. The resulting model was visualized using YASARA (www.yasara.org) and POVray (www.povray.org).

Acknowledgements

This work was supported by a grant of the Progetto Nazionale di Ricerche in Antartide PEA 2014-2016 entitled 'Genome scanning and characterization of novel antifreeze proteins for industrial application' coordinated by DdP and by a grant of ERC to IB. AK acknowledges support by the Estonian national scholarship program Kristjan Jaak. We thank Dr Victor Yashunsky (The Hebrew University of Jerusalem, Israel), and Dr Lior Segev (Weizmann Institute of Science, Israel) for LabVIEW programming and Lotem Haleva for her contribution to TH thermal stability analysis.

Author contributions

MM and SB carried out production and purification of the recombinant proteins and assessed stability and cryoprotection activity; AN performed analyses by infrared spectroscopy; MB-D, AK and IB characterized the TH and IRI activity and studied ice crystals morphology; PT and DdeP designed and produced the coding sequence; SP and CM performed evolutionary analysis; DdeP and ML conceived and supervised the project; ML wrote the paper. All Authors have read and approved the content of the manuscript.

References

- De Maayer P, Anderson D, Cary C & Cowan DA (2014) Some like it cold: understanding the survival strategies of psychrophiles. *EMBO Rep* **15**, e201338170.
- D'Amico S, Collins T, Marx JC, Feller G & Gerday C (2006) Psychrophilic microorganisms: challenges for life. *EMBO Rep* **7**, 385–389.
- Bouvet V & Ben RN (2003) Antifreeze glycoproteins – Structure, conformation, and biological applications. *Cell Biochem Biophys* **39**, 133–144.
- Bar Dolev M, Braslavsky I & Davies PL (2016) Ice-binding proteins and their function. *Annu Rev Biochem* **85**, 515–542.
- Raymond JA & DeVries AL (1977) Adsorption inhibition as a mechanism of freezing resistance in polar fishes. *Proc Natl Acad Sci USA* **74**, 2589–2593.
- DeVries AL, Komatsu SK & Feeney RE (1970) Chemical and physical properties of freezing point-depressing glycoproteins from Antarctic fishes. *J Biol Chem* **245**, 2901–2908.
- Knight CA, DeVries AL & Oolman LD (1984) Fish antifreeze protein and the freezing and recrystallization of ice. *Nature* **308**, 295–296.
- Davies PL (2016) Antarctic moss is home to many epiphytic bacteria that secrete antifreeze proteins. *Environ Microbiol Rep* **8**, 1–2.
- Raymond JA (2014) The ice-binding proteins of a snow alga, *Chloromonas brevispina*: probable acquisition by horizontal gene transfer. *Extremophiles* **18**, 987–994.
- Raymond JA (2015) Dependence on epiphytic bacteria for freezing protection in an Antarctic moss, *Bryum Argenteum*. *Environ Microbiol Rep* **8**, 14–19.
- Davies PL (2014) Ice-binding proteins: a remarkable diversity of structures for stopping and starting ice growth. *Trends Biochem Sci* **39**, 548–555.
- Drori R, Celik Y, Davies PL & Braslavsky I (2014) Ice-binding proteins that accumulate on different ice crystal planes produce distinct thermal hysteresis dynamics. *J R Soc Interface* **11**, 20140526.

- 13 Pucciarelli S, La Terza A, Ballarini P, Barchetta S, Yu T, Marziale F, Passini V, Methe B, Detrich HW III & Miceli C (2009) Molecular cold-adaptation of protein function and gene regulation: the case for comparative genomic analyses in marine ciliated protozoa. *Mar Genomics* **2**, 57–66.
- 14 Yang G, De Santi C, de Pascale D, Pucciarelli S, Pucciarelli S & Miceli C (2013) Characterization of the first eukaryotic cold-adapted patatin-like phospholipase from the psychrophilic Euplotes focardii: identification of putative determinants of thermal-adaptation by comparison with the homologous protein from the mesophilic Euplotes crassus. *Biochimie* **95**, 1795–1806.
- 15 Pucciarelli S, Chiappori F, Devaraj RR, Yang G, Yu T, Ballarini P & Miceli C (2014) Identification and analysis of two sequences encoding ice-binding proteins obtained from a putative bacterial symbiont of the psychrophilic Antarctic ciliate Euplotes focardii. *Antarct Sci* **26**, 491–501.
- 16 Pucciarelli S, Devaraj RR, Mancini A, Ballarini P, Castelli M, Schrällhammer M, Petroni G & Miceli C (2015) Microbial Consortium Associated with the Antarctic Marine Ciliate Euplotes focardii: an investigation from genomic sequences. *Microb Ecol* **70**, 484–497.
- 17 Sigrist CJA, de Castro E, Cerutti L, Cuche BA, Hulo N, Bridge A, Bougueleret L & Xenarios I (2013) New and continuing developments at PROSITE. *Nucleic Acids Res* **41**, E344–E347.
- 18 Petersen TN, Brunak S, von Heijne G & Nielsen H (2011) SignalP 4.0: discriminating signal peptides from transmembrane regions. *Nat Methods* **8**, 785–786.
- 19 Studier FW (2005) Protein production by auto-induction in high-density shaking cultures. *Protein Expr Purif* **41**, 207–234.
- 20 Byler DM & Susi H (1986) Examination of the secondary structure of proteins by deconvolved FTIR spectra. *Biopolymers* **25**, 469–487.
- 21 Barth A (2007) Infrared spectroscopy of proteins. *Biochim Biophys Acta* **1767**, 1073–1101.
- 22 Cerf E, Sarroukh R, Tamamizu-Kato S, Breydo L, Derclaye S, Dufrène Y, Narayanaswami V, Goormaghtigh E, Ruyschaert J & Raussens V (2009) Antiparallel beta-sheet: a signature structure of the oligomeric amyloid beta-peptide. *Biochem J* **421**, 415–423.
- 23 Do H, Kim SJ, Kim HJ & Lee JH (2014) Structure-based characterization and antifreeze properties of a hyperactive ice-binding protein from the Antarctic bacterium *Flavobacterium frigoris* PS1. *Acta Crystallogr D* **70**, 1061–1073.
- 24 Garnham CP, Campbell RL & Davies PL (2011) Anchored clathrate waters bind antifreeze proteins to ice. *Proc Natl Acad Sci USA* **108**, 7363–7367.
- 25 Graham LA, Liou YC, Walker VK & Davies PL (1997) Hyperactive antifreeze protein from beetles. *Nature* **388**, 727–728.
- 26 Bar-Dolev M, Celik Y, Wettlaufer JS, Davies PL & Braslavsky I (2012) New insights into ice growth and melting modifications by antifreeze proteins. *J R Soc Interface* **9**, 3249–3259.
- 27 Middleton AJ, Marshall CB, Faucher F, Bar-Dolev M, Braslavsky I, Campbell RL, Walker VK & Davies PL (2012) Antifreeze protein from freeze-tolerant grass has a beta-roll fold with an irregularly structured ice-binding site. *J Mol Biol* **416**, 713–724.
- 28 Budke C, Heggemann C, Koch M, Sewald N & Koop T (2009) Ice recrystallization kinetics in the presence of synthetic antifreeze glycoprotein analogues using the framework of LSW theory. *J Phys Chem B* **113**, 2865–2873.
- 29 Budke C, Dreyer A, Jaeger J, Gimpel K, Berkemeier T, Bonin AS, Nagel L, Plattner C, DeVries AL & Sewald N (2014) Quantitative efficacy classification of ice recrystallization inhibition agents. *Cryst Growth Des* **14**, 4285–4294.
- 30 Olijve LLC, Meister K, DeVries AL, Duman JG, Guo S, Bakker HJ & Voets IK (2016) Blocking rapid ice crystal growth through nonbasal plane adsorption of antifreeze proteins. *Proc Natl Acad Sci USA* **113**, 3740–3745.
- 31 Hughes S & Graether SP (2011) Cryoprotective mechanism of a small intrinsically disordered dehydrin protein. *Protein Sci* **20**, 42–50.
- 32 Finn RD, Coghill P, Eberhardt RY, Eddy SR, Mistry J, Mitchell AL, Potter SC, Punta M, Qureshi M & Sangrador-Vegas A (2016) The Pfam protein families database: towards a more sustainable future. *Nucleic Acids Res* **44**, D279–D285.
- 33 Lee JH, Park AK, Do H, Park KS, Moh SH, Chi YM & Kim HJ (2012) Structural basis for antifreeze activity of ice-binding protein from arctic yeast. *J Biol Chem* **287**, 11460–11468.
- 34 Bayer-Giraldi M, Weikusat I, Besir H & Dieckmann G (2011) Characterization of an antifreeze protein from the polar diatom *Fragilariopsis cylindrus* and its relevance in sea ice. *Cryobiology* **63**, 210–219.
- 35 Hanada Y, Nishimiya Y, Miura A, Tsuda S & Kondo H (2014) Hyperactive antifreeze protein from an Antarctic sea ice bacterium *Colwellia* sp has a compound ice-binding site without repetitive sequences. *FEBS J* **281**, 3576–3590.
- 36 Xiao N, Suzuki K, Nishimiya Y, Kondo H, Miura A, Tsuda S & Hoshino T (2010) Comparison of functional properties of two fungal antifreeze proteins from *Antarctomyces psychrotrophicus* and *Typhula ishikariensis*. *FEBS J* **277**, 394–403.
- 37 Xiao N, Hanada Y, Seki H, Kondo H, Tsuda S & Hoshino T (2014) Annealing condition influences

- thermal hysteresis of fungal type ice-binding proteins. *Cryobiology* **68**, 159–161.
- 38 Hashim NHF, Sulaiman S, Bakar FDA, Illias RM, Kawahara H, Najimudin N, Mahadi NM & Murad AMA (2014) Molecular cloning, expression and characterisation of Afp4, an antifreeze protein from *Glaciozyma antarctica*. *Polar Biol* **37**, 1495–1505.
- 39 Gwak IG, sic Jung W, Kim HJ, Kang S-H & Jin E (2010) Antifreeze protein in Antarctic marine diatom, *Chaetoceros Neogracile*. *Mar Biotechnol* **12**, 630–639.
- 40 Uhlig C, Kilpert F, Frickenhaus S, Kegel JU, Krell A, Mock T, Valentin K & Beszteri B (2015) In situ expression of eukaryotic ice-binding proteins in microbial communities of Arctic and Antarctic sea ice. *ISME J* **9**, 2537–2540.
- 41 Sambti I, Gatti-Lafranconi P, Longhi S & Lotti M (2010) How disorder influences order and vice versa – mutual effects in fusion proteins containing an intrinsically disordered and a globular protein. *FEBS J* **277**, 4438–4451.
- 42 DeLuca CI, Comley R & Davies PL (1998) Antifreeze proteins bind independently to ice. *Biophys J* **74**, 1502–1508.
- 43 Laemmli UK (1970) Cleavage of structural proteins during the assembly of the head of bacteriophage T4. *Nature* **227**, 680–685.
- 44 Braslavsky I & Drori R (2013) LabVIEW-operated novel nanoliter osmometer for ice binding protein investigations. *J Vis Exp* **72**, e4189.
- 45 Pertaya N, Celik Y, DiPrinzio CL, Wettlaufer JS, Davies PL & Braslavsky I (2007) Growth-melt asymmetry in ice crystals under the influence of spruce budworm antifreeze protein. *J Phys Condens Matter* **19**, 412101.
- 46 Regand A & Goff HD (2006) Ice recrystallization inhibition in ice cream as affected by ice structuring proteins from winter wheat grass. *J Dairy Sci* **89**, 49–57.
- 47 Jones DT, Taylor WR & Thornton JM (1992) The rapid generation of mutation data matrices from protein sequences. *Comput Appl Biosci* **8**, 275–282.
- 48 Felsenstein J (1985) Confidence limits on phylogenies: an approach using the bootstrap. *Evolution* **39**, 783–791.
- 49 Tamura K, Peterson D, Peterson N, Stecher G, Nei M & Kumar S (2011) MEGA5: molecular evolutionary genetics analysis using maximum likelihood, evolutionary distance, and maximum parsimony methods. *Mol Biol Evol* **28**, 2731–2739.
- 50 Robert X & Gouet P (2014) Deciphering key features in protein structures with the new ENDscript server. *Nucleic Acids Res* **42**, W320–W324.
- 51 Biasini M, Bienert S, Waterhouse A, Arnold K, Studer G, Schmidt T, Kiefer F, Cassarino TG, Bertoni M & Bordoli L (2014) SWISS-MODEL: modelling protein tertiary and quaternary structure using evolutionary information. *Nucleic Acids Res* **42**, W252–W258.

Supporting information

Additional Supporting Information may be found online in the supporting information tab for this article: **Video S1**. Ice crystal growth. A single ice crystal grown in a solution containing 3.3 μM *Efc*IBP (melting temperature = -0.02).

Appendix 2

Publication II

Mangiagalli, M., Sarusi, G., **Kaleda, A.**, Bar Dolev, M., Nardone, V., Vena, V. F., Braslavsky, I., Lotti, M., Nardini, M. (2018), Structure of a bacterial ice binding protein with two faces of interaction with ice. *FEBS J*, 285: 1653-1666. doi:10.1111/febs.14434

Structure of a bacterial ice binding protein with two faces of interaction with ice

Marco Mangiagalli¹ , Guy Sarusi², Aleksei Kaleda^{2,3}, Maya Bar Dolev², Valentina Nardone⁴, Vittoria Federica Vena¹, Ido Braslavsky² , Marina Lotti¹  and Marco Nardini⁴ 

¹ Department of Biotechnology and Biosciences, University of Milano-Bicocca, Italy

² Institute of Biochemistry, Food Science and Nutrition, The Robert H. Smith Faculty of Agriculture, Food and Environment, The Hebrew University of Jerusalem, Rehovot, Israel

³ Department of Chemistry and Biotechnology, School of Science, Tallinn University of Technology, Estonia

⁴ Department of Biosciences, University of Milano, Italy

Keywords

cold adaptation; DUF3494; IBP-1 fold; ice recrystallization inhibition; thermal hysteresis

Correspondence

M. Lotti, Department of Biotechnology and Biosciences, University of Milano-Bicocca, Piazza della Scienza 2, 20126 Milan, Italy
Tel: +39 02 6448 3527

E-mail: marina.lotti@unimib.it
and

M. Nardini Department of Biosciences, University of Milano, Via Celoria 26, 20133 Milan, Italy

Fax: +39 02 503 14895

Tel: +39 02 503 14898-14894

E-mail: marco.nardini@unimi.it

(Received 30 January 2018, revised 1 March 2018, accepted 8 March 2018)

doi:10.1111/febs.14434

Ice-binding proteins (IBPs) contribute to the survival of many living beings at subzero temperature by controlling the formation and growth of ice crystals. This work investigates the structural basis of the ice-binding properties of *Efc*IBP, obtained from Antarctic bacteria. *Efc*IBP is endowed with a unique combination of thermal hysteresis and ice recrystallization inhibition activity. The three-dimensional structure, solved at 0.84 Å resolution, shows that *Efc*IBP belongs to the IBP-1 fold family, and is organized in a right-handed β-solenoid with a triangular cross-section that forms three protein surfaces, named A, B, and C faces. However, *Efc*IBP diverges from other IBP-1 fold proteins in relevant structural features including the lack of a ‘capping’ region on top of the β-solenoid, and in the sequence and organization of the regions exposed to ice that, in *Efc*IBP, reveal the presence of threonine-rich ice-binding motifs. Docking experiments and site-directed mutagenesis pinpoint that *Efc*IBP binds ice crystals not only via its B face, as common to other IBPs, but also via ice-binding sites on the C face.

Database

Coordinates and structure factors have been deposited in the Protein Data Bank under accession number 6EIO.

Introduction

Organisms living in cold habitats such as polar regions, high mountains, oceans or other cold environments of the Earth, permanently or seasonally have to cope with subzero temperatures. In several cases protection toward freezing and ice injuries is provided by ‘ice binding proteins’ (IBPs) that bind ice crystals and control their growth and shape [1,2]. Since the first

description of an IBP from an Antarctic fish back in the 1960s [3], these proteins have been identified in a number of fishes, insects, diatoms, algae, yeasts, fungi, and bacteria [4,5]. Over the years, the growing body of information available fostered the development of models and hypotheses to explain the peculiar features and properties of IBPs. Particularly challenging are the

Abbreviations

ColAFP, *Colwellia* sp. strain SLW05 antifreeze protein; *Efc*IBP, *Euplotes focardii* bacterial consortium ice-binding protein; *F1*BP, *Flavobacterium frigidum* PS1 ice-binding protein; IBP, ice-binding protein; IBPv, *Flavobacteriaceae* bacterium 3519-10 ice-binding protein; IBS, ice-binding site; IRI, ice recrystallization inhibition; *Le*IBP, *Leucosporidium* sp. AY30 ice-binding protein; TH, thermal hysteresis; *TisAFP6*, *Typhula ishikariensis* antifreeze protein isoform 6; *TisAFP8*, *Typhula ishikariensis* antifreeze protein isoform 8; wt, wild-type.

relationships between structure and activity. In fact, while IBP structures are classified in at least 11 different folds [5], all of them associate to the very same ligand: ice crystals. This apparent paradox is justified by the presence of specific ice-binding sites (IBSs) in all IBPs that share similar structural properties. IBSs are typically flat and extended surfaces, relatively hydrophobic, able to organize water into an ice-like arrangement that merges and freezes with the quasi-liquid layer next to the ice lattice [4]. In many cases, IBSs are also characterized by the presence of threonine-rich repeats, such as Thr–X–Thr or Thr–X–Asx, whose involvement in ice binding has been recognized by site-directed mutagenesis studies [6–11].

Nevertheless, the correlation between structural differences and effects induced by IBPs on ice crystals growth and structuring, that is thermal hysteresis (TH) and inhibition of ice recrystallization (IRI), still wait for a comprehensive explanation. TH is the gap between the melting and the freezing points of ice produced by the adsorption of IBPs to crystals. The bound IBPs induce microcurvatures on the growing ice front and, following the Gibbs–Thomson effect, the association of additional water molecules on the ice is less favorable, leading to reduction of the freezing point below the melting point. IRI, instead, refers to the ability of IBPs to contrast the formation of large ice crystals from small ones [5,12]. While TH is relevant in avoiding freezing, IRI activity seems to be related to freeze tolerance, since injuries to living matter by large crystals are by far more severe than those produced by small ice particles, that can be tolerated inside or between cells [13]. On the basis of TH activity, IBPs are classified as moderate, with TH of 0.1–2.0 °C, or as hyperactive, with TH of 2–13 °C. Several lines of evidence support the idea that the extent of TH activity may depend on the specific plane of ice crystals to which the IBPs adsorb. Most hyperactive IBPs bind to the basal plane of ice, in addition to the prismatic and pyramidal crystal planes to which moderate IBPs associate [5,14]. Data of IRI activity have been reported only for a subset of IBPs. Nevertheless, information available raises questions and issues about the mechanistic basis of TH and IRI which, in all major classes of IBPs, seem to be nonrelated [15]. This conclusion is also supported by mutagenesis experiments on an IBP from *Lolium perenne* showing that amino acid substitutions may decrease or increase IRI activity without changing TH [16].

A deeper insight in the molecular basis of IBP properties is required to advance our understanding of the evolution of this very peculiar cold adaptation strategy and of the IBP biological function. In fact, IBPs play

different roles in distinct organisms, for example, they can restrain body fluids from freezing, promote ice structuring to preserve a liquid environment around cells, or mediate cells adhesion to ice [4,5,17].

In this work, we tackle IBP function from a structural viewpoint and we report the 3D structure at 0.84 Å resolution of an IBP derived from the metagenome of bacterial symbionts of the Antarctic ciliate *Euplotes focardii* (*Efc*IBP). *Efc*IBP shows atypical combination of TH and IRI activities, not reported for other bacterial IBPs, with moderate TH activity (0.53 °C 50 µM) and one of the highest IRI activity (2.5 nm) described to date. According to primary sequence analysis, *Efc*IBP contains a domain of unknown function DUF3494, which was predicted to fold in a discontinuous β -solenoid structure [18]. This fold is typical of bacterial IBPs, where it is defined as IBP-1 fold [5], and it might have been horizontally transferred to other organisms sharing the same environment, such as algae, fungi, yeasts, and diatoms [19–22]. Our results show that *Efc*IBP is a novel member of IBP-1 family with a modified fold and the presence of repetitive IBS sequence motifs. Site-directed mutagenesis and docking simulations reveal how *Efc*IBP exerts its moderate TH activity. The IBS of *Efc*IBP presumably has two different protein surfaces characterized by low hydrophobicity and repetitive sequence motifs. This composite IBS allows binding to multiple ice planes, including the basal plane.

Results and Discussion

*Efd*BP structure

Recombinant *Efc*IBP was crystallized as described in the Experimental Procedures section. Crystals belong to the orthorhombic $P2_12_12_1$ space group and diffracted to the atomic resolution of 0.84 Å using synchrotron radiation (ESRF, Grenoble), one of the highest resolution reached for this kind of protein so far. The final model was refined to a final $R_{\text{work}} = 11.5\%$ and $R_{\text{free}} = 12.8\%$ with good stereochemical parameters, and contains 223 amino acids (including the *Efc*IBP residues 37–253, and the C-terminal 6His-tag), 411 water molecules, 4 sulfate ions, and 1 glycerol molecule. Data collection analysis and refinement statistics are summarized in Table 1.

The *Efc*IBP displays an IBP-1 fold [5], consisting of a right-handed β -helix with a triangular cross-section formed by three parallel β -sheets (here named A, B, and C faces) and by an additional single α -helix ($\alpha 1$) aligned along the axis of the β -helix (Fig. 1). The A face is formed by nine β -strands and is not directly

Table 1. Data collection and structure refinement statistics.

Data collection	
Space group	$P2_12_12_1$
a, b, c (Å)	45.48, 50.72, 92.45
α, β, γ (°)	90.0, 90.0, 90.0
Wavelength (Å)	0.82658
Resolution (Å)	46.23–0.84 (0.89–0.84) ^a
R_{merge}^b	0.108 (0.577)
R_{pim}^c	0.046 (0.360)
$\langle I/\sigma(I) \rangle$	10.0 (1.8)
Completeness (%)	94.5 (68.8)
Redundancy	5.5 (3.1)
Refinement	
Resolution (Å)	46.23–0.84
Number of reflections	183713
$R_{\text{work}}/R_{\text{free}}$ (%) ^d	11.5/12.8
Number of molecules	
Copies in the AU	1
Protein residues	223
Sulfate ions	4
Glycerol molecules	1
Water molecules	411
Average B-factors (Å ²)	11.7
RMSD	
Bond lengths (Å)	0.008
Bond angles (°)	1.17
Ramachandran plot statistics	
	96.3% in favoured regions
	3.7% in allowed regions
	0.0% outliers

^a Highest resolution shell is shown in parentheses.

^b $R_{\text{merge}} = \sum_{\text{hkl}} |h_{\text{hkl}} - \langle I_{\text{hkl}} \rangle| / \sum_{\text{hkl}} I_{\text{hkl}}$.

^c $R_{\text{pim}} = \sum_{\text{hkl}} \sqrt{1/(n-1)} \sum_{j=1}^n |h_{\text{hkl}} - \langle I_{\text{hkl}} \rangle| / \sum_{\text{hkl}} \sum_{j=1}^n I_{\text{hkl},j}$.

^d $R_{\text{work}} = \sum_{\text{hkl}} |F_{\text{O}} - F_{\text{C}}| / \sum_{\text{hkl}} |F_{\text{O}}|$. R_{free} is calculated from 5% randomly selected data for cross-validation.

exposed to the solvent region, but screened by the $\alpha 1$ helix and by the N-terminal region (residues 44–54) preceding the $\beta 1$ strand (Figs 1 and 2). This protein surface is, therefore, not suited for the interaction with ice crystals. The B and C faces are each formed by eight β -strands. The B face is flat and regular, while the C face is divided into two regions. The first region consists of strands $\beta 3$, $\beta 6$, $\beta 10$, $\beta 19$, $\beta 22$, and $\beta 25$, forming a flat surface that maintains the triangular section of the structure. Instead, strands $\beta 13$ and $\beta 16$ markedly diverge toward the exterior of the protein body (Fig. 1). The B and C faces are both fully exposed to the solvent region and, therefore, potentially involved in ice binding. Two short 3_{10} helices (one turn each) are also present in the *EfcIBP* structure. They are located just after a long loop region running outside of the protein solenoid and they seem to help the following β -strands ($\beta 1$ and $\beta 17$, respectively) to insert back into the β -helix core structure (Figs 1 and 2).

The *EfcIBP* structure is very similar to other single domain IBP-1 fold proteins, specifically to those from *Colwellia* sp. (*ColAFP*; DALI Z-score of 32.3, residue identity of 38%) [23], from *Flavobacterium frigidis* (*FfIBP*; DALI Z-score of 32.4, residue identity of 35%) [24], from *Typhula ishikariensis* (*TisAFP6* and *TisAFP8* isoforms; DALI Z-score of 31.0, residue identity of 37%) [25,26], and from *Leucosporidium* sp. (*LeIBP*; DALI Z-score of 30.8, residue identity of 35%) [27]. Furthermore, *EfcIBP* matches well the structure of each domain of the two-domain IBP secreted by a *Flavobacteriaceae* bacterium (IBPv; DALI Z-score of 31.9 and 32.8, residue identity of 35% and 32%, for domain A and B, respectively) [28] (Fig. 2). Backbone comparison among these IBPs highlights an excellent conservation of secondary structure elements within the central core of the β -helix and helix $\alpha 1$, with an RMSD in the 0.9–1.2 Å range, calculated over 198 C α pairs (Figs 2 and 3).

Alongside the similarities between *EfcIBP* and other proteins with an IBP-1 fold, clear structural differences are present in the region from the end of strand $\beta 5$ and the start of helix $\alpha 1$ (Figs 1 and 2). The loop between strands $\beta 5$ and $\beta 6$ is 11 amino acids longer in *TisAFP6*, *TisAFP8*, and *LeIBP*, while in *ColAFP*, *FfIBP*, and in both domains of IBPv, its length is similar but with different structure when compared to *EfcIBP*. The connection between $\beta 7$ and $\alpha 1$ is also different, with an insertion of 12 amino acids in *ColAFP*, 11 in *FfIBP*, and 6 in *TisAFP6*, *TisAFP8* and *LeIBP*. This loop is similar in *EfcIBP* and in the A domain of IBPv, while the IBPv B domain has an insertion of one amino acid (Fig. 2). As a result, a cap subdomain is present between $\beta 5$ and $\alpha 1$ in *ColAFP*, *FfIBP*, *TisAFP6*, *TisAFP8*, and *LeIBP*, but not in *EfcIBP* and in the two domains of IBPv (Fig. 3). Within IBP-1 fold proteins, this cap region has been classified into two groups [24], depending on the presence (group 1: *ColAFP* and *FfIBP*) or absence (group 2: *TisAFP6*, *TisAFP8*, and *LeIBP*) of a disulfide bridge between Cys residues belonging to the $\beta 5$ – $\beta 6$ and $\beta 7$ – $\alpha 1$ loops. With this respect, *EfcIBP*, together with IBPv, can be classified as a novel third group, where the cap subdomain is totally absent. The role of the capping region in IBP protein is debated. Studies on chimeras of *FfIBP* and *LeIBP* showed that the capping region plays an important role in structure stabilization. The *FfIBP* chimera, with the cap from *LeIBP*, has a Tm value of 47.4 °C, significantly lower than the wild-type (wt) *FfIBP* (Tm value of 56.4 °C), with a concomitant decrease in TH activity (greater than sevenfold). On the contrary, chimeric *LeIBP*, with the capping head region of *FfIBP*, had a slightly increased TH activity

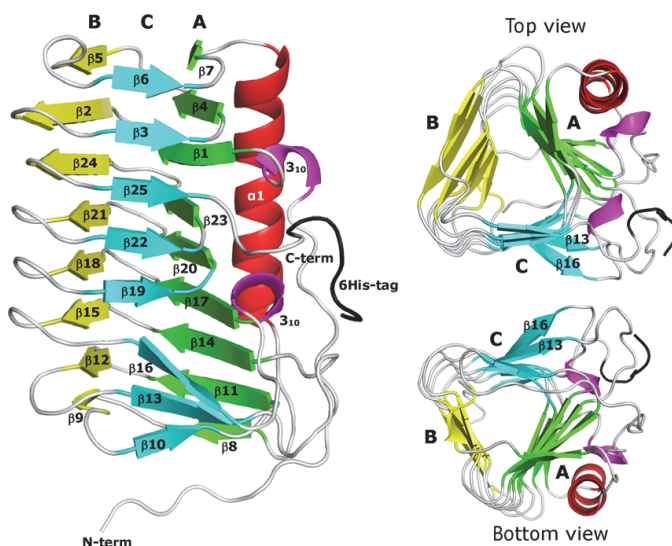


Fig. 1. Three-dimensional structure of *EfcIBP*. Ribbon diagram showing the secondary structure elements of *EfcIBP*: β strands belonging to the A, B, and C faces of the β -helix are in green, yellow, and cyan, respectively. The helix $\alpha 1$ is in red and the 3_{10} helices in magenta. The triangular section of the *EfcIBP* structure is evident in the top and the bottom views. The $\beta 13$ e $\beta 16$ strands, which diverge toward the outside from the core of the β -helix, are indicated.

compared with wt *LeIBP* and a higher T_m value (66.4 °C vs 61 °C). Thus, the capping head region of *F/IBP* is more stable than that of *LeIBP*, likely due to the presence of the disulfide bond, and is important for the overall stability of IBP [24]. Interestingly, recombinant *EfcIBP* is very stable to heat, with a T_m of 66.4 °C, despite the absence of the capping region [18].

Further structural differences that characterize *EfcIBP* compared to IBP-1 fold proteins are located at the N- and C-terminal regions. In particular, the N-terminal extension Thr37–Thr45 is unique for *EfcIBP*, and it has an elongated structure that runs almost parallel to the β -strands of the C face, being anchored to the core of the protein through both polar and nonpolar interactions with residues belonging to $\beta 8$ (B face) and $\beta 10$ (C face; Figs 1, 2 and 3).

In summary, the structure of *EfcIBP* appears to be more compact than homologous IBP-1 proteins, with the absence of the capping region between $\beta 5$ and $\alpha 1$, and the B face more regular at its terminal filaments ($\beta 5$ and $\beta 9$; Figs 2 and 3). Overall, *EfcIBP* is much more similar to the two-domain IBPv, where each IBPv domain also misses the capping region, than to other IBP-1 fold proteins.

Structural insights for IBS identification in *EfcIBP*

The identification of the *EfcIBP* IBS was driven by previous studies on other IBP-1 fold proteins. Mutagenesis experiments and virtual docking to ice planes

based on the crystal structures of *ColAFP*, *F/IBP*, *TisAFP6*, *TisAFP8*, *LeIBP*, and IBPv reveal that the IBS is located on the flattest surface of the β -helix (B face), while the other faces (A and C) are not involved in ice binding (Fig. 2) [23–28]. These IBP-1 fold proteins typically lack regular ice-binding motifs, such as the Thr–X–Thr and the Thr–X–Asx repeats (X = any residue, Asx = Asn or Asp), typically found in insect and bacterial hyperactive IBPs [8,29].

Furthermore, the B face of IBP-1 proteins is always quite hydrophobic, with polar residues being only between ~30% and 60% of the total solvent-exposed residues. Indeed, the hydrophobic effect is thought to be a pivotal driving force when considering the general functional mechanism of IBPs, with restrained water molecules forming hydrogen bond networks and producing ‘cages’ around hydrophobic groups, especially the methyl groups of Thr residues. Then, these anchored waters allow IBPs to bind ice by matching its specific plane(s). The organized solvation shell around the IBSs is involved in the initial recognition and binding of IBPs to ice by lowering the barrier for binding and consolidation of the protein–ice interaction surface [10,30].

Despite the high structural homology with other IBP-1 fold proteins (Figs 2 and 3), the *EfcIBP* residue distribution on the surface of the β -helix has different properties. A clear pattern of putative IBS repeats, three Thr–X–Thr and three Thr–X–Asx motifs, can be recognized in *EfcIBP* (Figs 2 and 4). Interestingly, they are mostly located on the B face (on strands $\beta 2$, $\beta 15$,

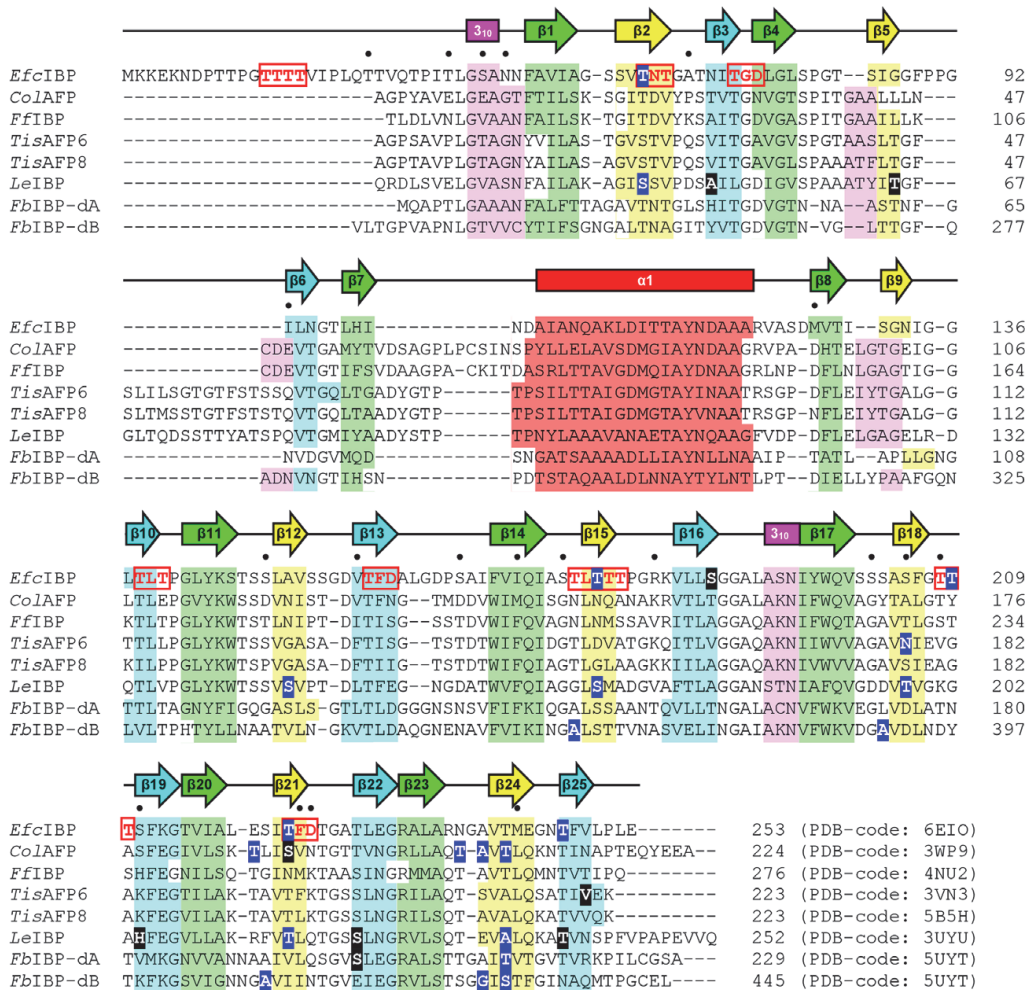


Fig. 2. Structural-base sequence alignment of *EfcIBP* with related IBP-1 fold proteins. *EfcIBP* is aligned with *ColAfp* [23], *FfIBP* [24], *TisAfp6*, and *TisAfp8* isoforms [25,26], *LeIBP* [27], and with the two domains (dA and dB) of IBPv [28]. The sequence alignment has been performed using the MUSCLE program (<https://www.ebi.ac.uk/Tools/msa/muscle/>) and manually corrected based on their 3D structure comparison. Secondary structure elements are indicated on top for *EfcIBP* and shaded (color code as in Fig. 1) for all aligned proteins. Residues mutated in *EfcIBP*, *ColAfp*, *FfIBP*, *TisAfp6*, *TisAfp8*, *LeIBP*, and IBPv with decreased/unaltered ice-binding properties are shaded in blue/black, respectively. The *EfcIBP* repeat motifs Thr-X-Thr and Thr-X-Asx (X = any residue and Asx = Asn or Asp) are indicated in bold and boxed in red. *EfcIBP* amino acids with side chains in a double conformation are indicated by a black dot.

and $\beta 21$), but some of them are also present on the C face (strands $\beta 10$ and $\beta 13$), in the connecting regions between β strands belonging to different faces (between $\beta 3$ and $\beta 4$, and between $\beta 18$ and $\beta 19$), and in the N-terminal extension (Figs 2 and 4). These observations suggest that not only the B face is involved in ice binding in *EfcIBP*.

The B face of *EfcIBP* is formed mainly by seven parallel β -strands ($\beta 12$, $\beta 15$, $\beta 18$, $\beta 21$, $\beta 24$, $\beta 2$, and $\beta 5$) composed of three to five residues, with a further minor contribution of the short $\beta 9$ (Fig. 4). Three Thr-X-Thr and one Thr-X-Asx IBS motifs are homogeneously distributed along the different parallel β -strands ($\beta 2$, $\beta 15$, and $\beta 21$) and converge to form a row of four Thr

residues at the center of the B face, with the presence of an additional Ser in the middle and terminated by Ala and Gly residues (Fig. 4). This row is the most repetitive organization in the *Efc*IBP structure and it might be responsible for much of the ice-binding capacity of the protein. On the other hand, the presence of several putative IBSs on the B face of *Efc*IBP decreases dramatically its hydrophobicity (73.6% of the residues exposed to the solvent are polar) relative to other homologous IBP-1 fold proteins.

The *Efc*IBP C face is less flat and regularly organized than the B face (Fig. 4). However, as found for the B face, it contains putative Thr-rich IBS motifs and the residues pointing toward the solvent are mostly polar (80%). These structural features indicate that the B face is the most likely surface for ice binding, but suggest that the C face might be involved too. Furthermore, the low surface hydrophobicity coupled with the presence of IBS motifs might be the reason of the moderate, and not hyperactive, TH activity of *Efc*IBP.

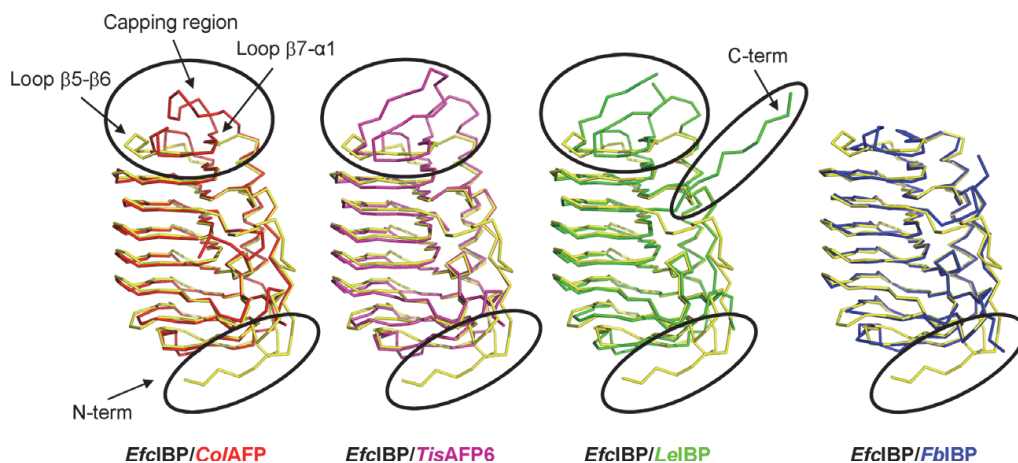


Fig. 3. Structural superposition of *Efc*IBP with related IBP-1 fold proteins. Superposition of *Efc*IBP (yellow) with the structures of *Col*/AFP (red), *Tis*/AFP6 (magenta), *Lel*BP (green), and IBPv (domain B, blue). Regions with high structural divergence are highlighted. The *Efc*IBP C-terminal 6His-tag has been omitted.

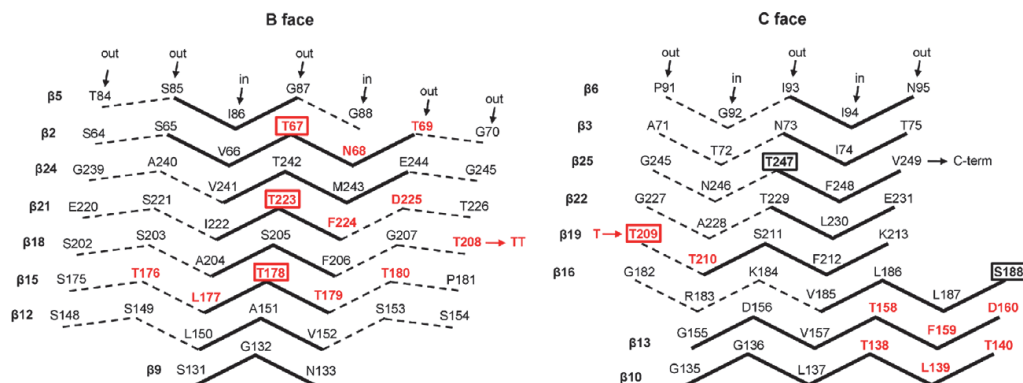


Fig. 4. IBS at the B and C faces of *Efc*IBP. Schematic representation of the amino acid distribution on the (left) B face and on the (right) C face of *Efc*IBP. Residues belonging to the Thr-X-Thr and Thr-X-Asx IBS motifs are in red. Residues mutated to Tyr are squared. Solid lines indicate β strands, whose numbering is shown on the left side.

Interestingly, most of the residues potentially involved in ice binding (typically Thr and Ser) on the B and C faces are with side chains in alternative conformations in our high-resolution *Efc*IBP crystal structure (Figs 2 and 4). This observation suggests that *Efc*IBP can reorganize the water molecules on its first hydration shell of both faces with high plasticity, thus reproducing the water molecule organization typically found on both the basal and prismatic planes of hexagonal ice crystals. In this respect, however, the position and the spacing of crystallographic water molecules at the protein surface only partly match those typically found in ice crystal planes, due to the involvement in crystal contacts of both B and C faces, with consequent reorganization of the water molecules at the protein–protein interface.

Ice docking study

Molecular docking techniques were employed to get insights into the interactions of *Efc*IBP with ice. Although many moderately active IBPs are known to bind to primary prism plane of ice crystal, but not to basal plane, we decided to test both planes as possible interaction partners of *Efc*IBP, and the surface complementarity (Sc) between the *Efc*IBP IBS and ice was evaluated to validate the docking [31]. As it is known that some hydration water molecules on the IBS are directly involved in binding to ice in certain IBPs [10,11], a series of *Efc*IBP structures in which the crystallographic water molecules were gradually deleted (starting from those belonging to the most external water shell) was prepared and used for the docking study and Sc calculation. The resulting best docking poses (highest score in terms of steric and electrostatic correlations) indicated that *Efc*IBP binds both ice planes through the B face IBS with Sc values of 0.46 and 0.34 for basal and primary prism planes, respectively. Interestingly, the presence of few (26) crystallographic water molecules located in the troughs of the B face protein surface is sufficient to significantly improve the shape complementarity of this face with

ice planes, with Sc values of 0.53 for basal plane and 0.39 for primary prism plane (Fig. 5A,B). Both these values are higher than 0.38, which was previously determined as a Sc threshold for IBPs [8,23]. The interaction models were further validated by calculating the contact surface areas, which are 1390 and 1163 Å² for basal and prism primary planes, respectively. These values are large and in line with those found for other IBPs of similar fold and size [23,24,26]. The B face residues directly interact with ice, with the hydration water molecules contributing to increase the shape complementarity with both ice basal and primary prism planes.

Surprisingly, the docking simulations indicate that the primary prism plane of ice, but not the basal plane, can be bound also by the *Efc*IBP C face, with a Sc value of 0.31 which increases to 0.40 if some (61) water molecules are used in the calculation (Fig. 5C). In this scenario, the included crystallographic water molecules compensate for the flatness distortions of the protein C face induced by the presence of filaments β 13 and β 16 (Fig. 1). The contact surface area between the protein C face and the prism primary plane is 1265 Å² and the majority of the ice–protein contacts are water mediated.

Site-directed mutagenesis of *Efd*BP IBS residues

In order to investigate which part of the *Efc*IBP surface is involved in ice binding, we designed and expressed a series of single point mutants and evaluated their TH and IRI activities. Based on structural and docking analyses we focused on the putative IBS located on the B and C faces of the protein. The selected B face residues (T67, T178, and T223) belong to three Thr–X–Thr and Thr–X–Asx motifs and are centered on the B face (Figs 4 and 6). The C face mutations involve residues S188, T209, and T247. T247 was selected because it is located at the center of the C face, while T209 is of interest since it is part of a Thr–X–Thr motif laterally located on the C face (Figs 4 and 6). In order to check if the divergent

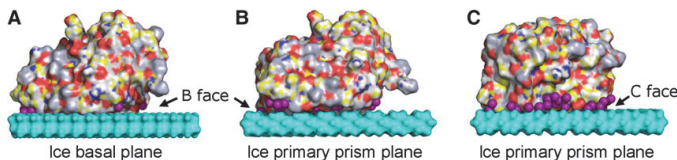


Fig. 5. Docking of *Efd*BP to ice planes. Interface between the B face of *Efd*BP and ice (A) basal and (B) primary prism planes. (C) Interface between the C face of *Efd*BP and the ice primary prism plane. Residues are colored in yellow for carbon, red for oxygen, blue for nitrogen, green for sulfur and gray for hydrogens. Bound crystallographic water molecules are colored in magenta, ice molecules in cyan.

region $\beta 10$ – $\beta 13$ – $\beta 16$ forms an IBS, S188 was also substituted. This residue is located on $\beta 16$, adjacent to the Thr–X–Thr and Thr–X–Asx motifs of strands $\beta 10$ and $\beta 13$. Yet $\beta 10$ and $\beta 13$ are less solvent exposed and, therefore, less likely to take part in ice binding. The selected residues were replaced by Tyr, a bulky residue that would disrupt the flatness of the protein surface and hinder the ability of the protein to bind ice in case it is located on the IBS [23,25,26].

All mutants were produced in Zym-5052 medium and purified at high yield (~2 mg from 1 L of culture). The degree of purification was comparable to the wt *EfcIBP*. The CD spectra of *EfcIBP* variants, except T247Y mutant, were highly similar to those of the wt (Fig. 7A,B), indicating that substitutions did not affect the protein secondary structure. The spectra showed a minimum ellipticity at approximately 219 nm and positive ellipticity at ~195 nm, which are characteristic of β sheet-rich proteins. In the case of T247Y mutant, the overall CD spectrum was similar to that of the wt, indicating that the protein retained its fold. However, the minimum ellipticity was shifted to 217 nm and the amplitude was slightly lower relative to the other mutants and to the wt (purple line in Fig. 7B). These minor changes possibly indicate a slight decrease in β structure. It should be noted that the T247Y mutation

site is located very close to the C terminus of the protein (Leu253), where the 6His-tag tail is present (Fig. 6). A reorientation of this C-terminal tail, due to the T247Y mutation, might partly disturb the N-terminal region of the protein (on the A face) located in front of it, where the protein backbone has an extended β -like structure (Fig. 1). Still, the experimental evidence that the thermal stability of the protein remains similar to the wt in all mutants, including the T247Y variant (Fig. 7C,D), indicates that the Tyr substitutions did not alter the β -helix structure in the core of the protein, which remains compact and stable.

Activity measurements of *EfdIBP* mutants

Following our findings that amino acid substitutions neither disrupt the protein folding nor affect its stability, and with the aim to determine the IBS of *EfcIBP*, we measured the TH activity of the mutants. Figure 8 shows the TH of all variants in comparison to the wt protein. All B face mutants show TH levels of 10–30% of the wt TH in equivalent protein concentrations. On the C face, S188Y retains 50–60% of activity, indicating that the $\beta 10$ – $\beta 13$ – $\beta 16$ region is not the major part of the IBS. Instead, T209Y retains only 30% activity, while T247Y is barely active, with no activity at 10 μ M and 4–5% activity at higher concentrations. Therefore, our TH measurements on *EfcIBP* mutants indicate the B face as the major IBS (including the Thr–X–Thr and Thr–X–Asx motifs), and the C face also partly involved in ice binding, in agreement with the docking simulations.

We measured the IRI activity of the *EfcIBP* mutants in order to obtain more information on the location of the IBS and the effects of the surface-exposed positions on ice binding (Fig. 9). All mutants show low IRI activity at a concentration of 0.02 μ M, reducing the recrystallization rate in the range of 0–50% compared to no IBP, with T247Y having no IRI activity. At a higher concentration, 0.1 μ M, the IRI activity of all mutants, including T247Y, is more pronounced, in the range 30–95% reduction of the recrystallization rate. In both concentrations, the wt reduced the recrystallization rate by 100%. This supports the TH and docking results, suggesting that *EfcIBP* interacts with ice through both B and C faces. It is likely that each face is responsible for binding of *EfcIBP* to specific sites or planes of ice. Another such case was demonstrated in a study of isoforms of type III AFP from ocean pout. The authors showed by single point mutations that the IBS of the protein is composed of two adjacent surfaces, each responsible for binding to different ice planes [32].

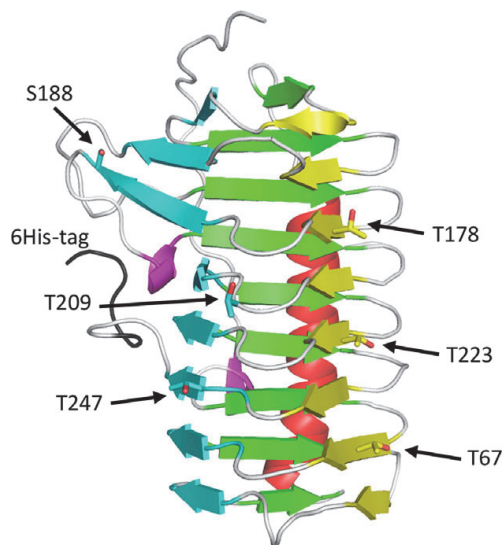


Fig. 6. *EfdIBP* mutation sites. Mutated residues on the B (yellow) and C (cyan) faces of the *EfdIBP* structure are shown as sticks and indicated by arrows and labels. The C-terminal 6His-tag is shown in black.

A puzzling finding is that there is no obvious correlation between the effects of the mutations on TH and their effects on IRI. Since both IRI and TH depend on the ice-binding properties of the proteins [15,33], one would expect the mutants with high TH to have also high IRI. Such a correlation was shown in a study of a series of mutants of the ryegrass IBP [33]. In the case of *EfcIBP* mutants, each mutation most probably affected the binding rates of the protein to particular ice planes in a different manner. It is possible that binding to certain ice planes is more crucial for IRI and less for TH, or vice versa. Furthermore, each face requires appropriate water organization for ice binding and reacts differently to surface perturbations. In particular, the S188Y mutant had the highest TH activity among the mutants (49% of the wt), and the lowest IRI activity (only 25% or 52% reduction of recrystallization rate at 0.02 and 0.1 μM concentrations,

respectively) after T247Y. One explanation for this effect is that the Tyr introduced into strand $\beta 16$ induces local organization of water molecules that disrupted binding to a certain ice plane important for IRI more than for TH. Yet, this and any other explanation are highly speculative at this stage. While *EfcIBP* presents a nontrivial case of ice recognition, all our findings so far point out that the protein has a compound IBS that involves both the B and the C faces with yet unknown specificities.

To summarize, the structural analysis of *EfcIBP* provided new insight into its functional features. The *EfcIBP* tertiary structure consists of a right-handed β -helix which conforms to the IBP-1 fold with some important differences. *EfcIBP* misses the cap subdomain between $\beta 5$ and $\alpha 1$, typically present in many IBP-1 fold protein. Considering that *EfcIBP* is very stable to heat, with a T_m of 66.4 $^{\circ}\text{C}$ [18], the proposed

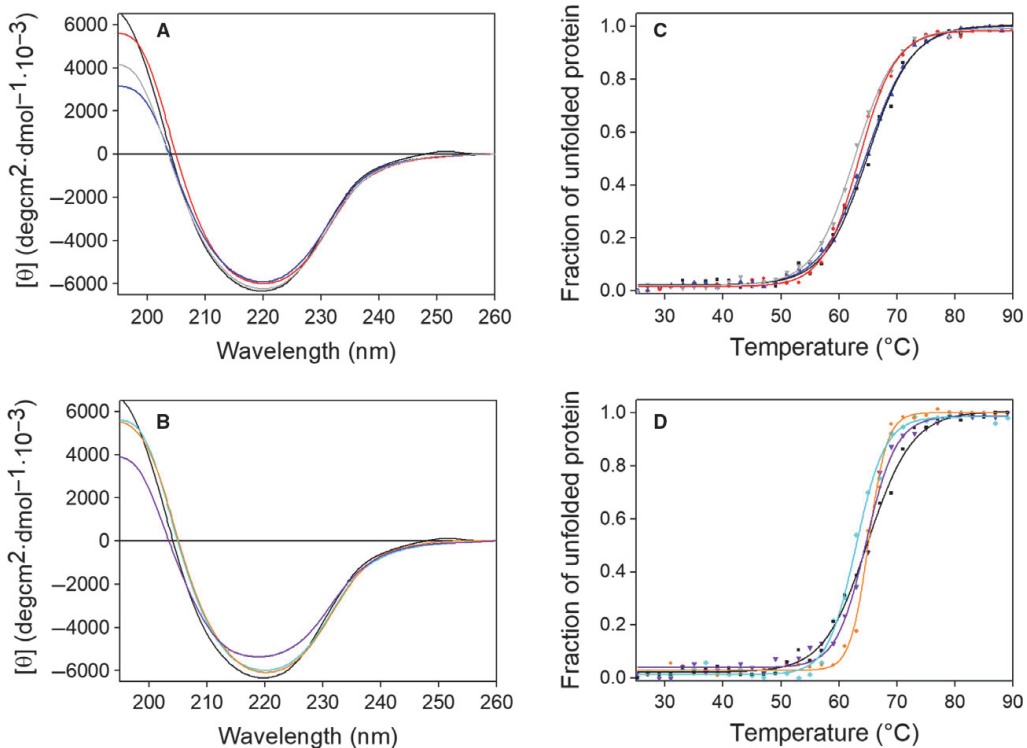


Fig. 7. Far-UV CD spectra of *EfcIBP* and its mutants. CD spectra (A) and denaturation profile (C) of face B mutants: in black wt *EfcIBP*, in red T67Y, in blue T178Y, in gray T223Y. CD spectra (B) and denaturation profile (D) of face C mutants: in black wt *EfcIBP*, in cyan S188Y, in orange T209Y and in purple T247Y.

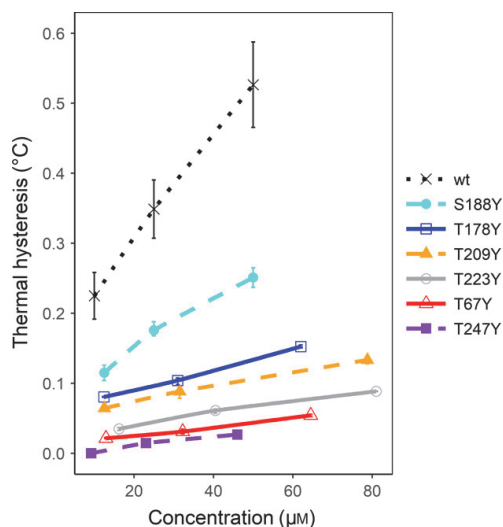


Fig. 8. TH activity of *EfcIBP* and mutants. The TH activity as a function of protein concentration is presented for the wt protein (black dotted line), the B face mutants (solid lines, empty markers) and the C face mutants (dashed lines, filled markers). Each point presents the average of three independent measurements, with standard deviations.

role of the cap subdomain in the overall stability of IBP [24] seem to be scaled down. This conclusion is further supported by the structure of the recently published two-domain protein IBPv [28], where each β -helix domain misses the cap subdomain but the protein has a T_m of 53.5 °C [34], similar to that of capped IBP-1 fold proteins [23–27]. Overall, the low hydrophobicity of B and C faces might explain the only moderate TH activity of the protein.

Docking simulation and mutational studies indicate that the *EfcIBP* has a compound IBS that consists of both the B and the C faces. In fact, most mutations on both faces heavily affect TH and IRI activities of the IBP. In some instances, the two effects appear to be fully or partly uncoupled. Although only a few amino acids have been changed, it emerges that TH and IRI depend at least partly on different features of the binding sites. To date, studies about the correlation of TH and IRI in IBPs are still too scarce to allow drawing general hypotheses. However, a recent study showed that also in LeIBP TH and IRI are not necessarily coupled, in fact also in this case a single mutation increases the IRI without affecting the TH [16]. This information calls for further studies aimed at a deeper understanding of IRI, especially in view of developing IBP-based methods for cryoprotection.

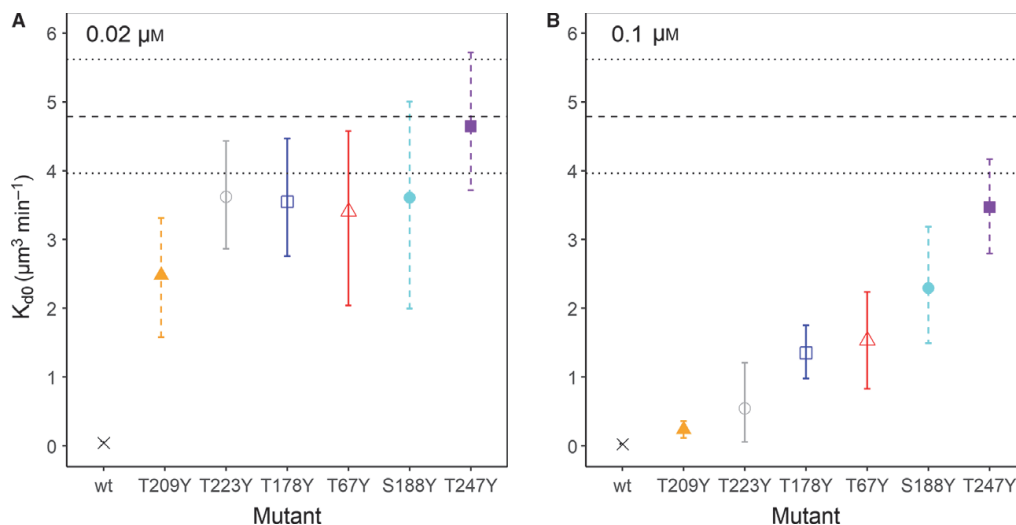


Fig. 9. Ice recrystallization efficacy of *EfcIBP* mutants and wt protein. Quantitative analyses of sucrose sandwich assays were performed at concentrations of A) 0.02 μM and B) 0.1 μM . K_{d0} represent the recrystallization rates. Vertical lines are 95% confidence intervals ($n = 5$). Horizontal dashed and dotted lines represent mean and 95% confidence interval for recrystallization constant of sucrose buffer without protein. Colors and shape codes are the same as in Fig. 8.

Experimental procedures

Strain and materials

Escherichia coli strain DH5 α TM (Invitrogen, Waltham, MA, USA) was used for plasmid amplification, while BL21 (DE3; EMD Millipore, Billerica, MA, USA) was used as the host strain for heterologous expression. Oligonucleotides are from Metabion (Metabion International, Planegg, AG, Germany) and Q5[®] High-Fidelity DNA Polymerase is from New England Biolabs (Ipswich, MA, USA).

Cloning and mutagenesis

pET-21a (*EfcIBP*) was described in a previous work [18]. The recombinant protein carries a 6His-tag at the C terminus. Mutagenesis of *EfcIBP* was carried out by Quick-Change[®] PCR. The forward and reverse primers are described in Table 2. Reactions were carried out using Q5[®] High-Fidelity DNA Polymerase and Eppendorf Master-cycler (Eppendorf, Hamburg, Germany) under the following conditions: 1 cycle (98 °C for 2 min), 25 cycles (98 °C for 10 s, annealing temperature for 25 s and 72 °C for 180 s), and a final cycle at 72 °C for 3 min. The annealing temperatures (T_A) used for each PCR reaction are indicated in Table 2. Mutations were verified by DNA bidirectional DNA sequencing.

Production and purification of recombinant proteins

Recombinant 6His-tagged proteins were produced in Zym-5052 medium [35] and purified from the soluble fraction of cell extracts by affinity chromatography as described previously [18]. Samples containing highest protein concentrations were pooled and buffer exchanged to 10 mM ammonium acetate (pH 7.0) by gel filtration using a PD10 column (GE Healthcare, Little Chalfont, UK). Purified proteins were lyophilized and stored at -20 °C. Protein

concentration was determined by the Bradford protein assay (Bio-Rad, Hercules, CA, USA), using bovine serum albumin as the standard.

Crystallization, structure determination, and refinement

Crystallization trials of *EfcIBP* (5 mg mL⁻¹ in pure water) were performed with vapor diffusion techniques (sitting drop) using an Oryx-8 crystallization robot (Douglas Instruments, East Garston, UK). Already after 1 day crystals were observed under several growth conditions, both at 4 and at 20 °C. The best crystals were obtained with the precipitant solution 2.2 M (NH₄)₂SO₄, 0.1 M HEPES buffer (pH 7.5), at 20 °C. Crystals were cryoprotected in their mother liquor, supplemented with 25% glycerol and flash-frozen in liquid nitrogen.

EfcIBP crystals diffracted up to 0.84 Å resolution with space group $P2_12_12_1$ and one protein molecule in the asymmetric unit (Matthews coefficient 2.12 Å³ Da⁻¹, estimated solvent content 42%). Diffraction data were collected at the ID-29 beamline of the European Synchrotron Radiation Facility (ESRF, Grenoble, France) and processed with XDS [36] and SCALA [37]. Data reduction statistics are reported in Table 1.

The *EfcIBP* crystal structure was solved by molecular replacement using Phaser [38], with the *ColAFP* structure (PDB code: 3WP9) [23] as a search model (36% sequence identity with *EfcIBP*). The *EfcIBP* sequence was then model built into the electron density using Coot [39] and restrained-refined with H atoms and anisotropic B-factors using Refmac5 [40] and Phenix [41]. All refinement statistics are reported in detail in Table 1. The stereochemical quality of the model was assessed using MolProbity [42].

Docking modeling to ice

Docked model for *EfcIBP* (without the C-terminal 6His-tag) and ice planes with the minimum overall docking score was searched with the program HEX 8.0.0 [43], using

Table 2. Primer sequences utilized for generation of *EfcIBP* variants. The mutation sites are underlined.

Primer ID	Sequence	Length	T_A (°C)
T67Y Forward	5' ACCAACATTACCGGAGATCTGGGC 3'	24	66.9
T67Y Reverse	5' CGCACCAGTGTTGTA <u>AA</u> CAGAAAGAAC 3'	26	66.2
T179Y Forward	5' CGCAAGGTGCTGCTGAGCGGT 3'	21	67.3
T179Y Reverse	5' ACCCGGTGTGGTGTACAGGGTAG 3'	23	68.3
T223Y Forward	5' CTGGAATCTATCTACTTCGATACCGGC 3'	27	68.2
T223Y Reverse	5' TCGGATCACGGTACCTTTGAAAGAGG 3'	26	67.9
S188Y Forward	5' GTGCTGCTGT <u>AC</u> GGTGGTGCGCTG 3'	24	67.0
S188Y Reverse	5' CTGCGACCTGGGGTGGTGGTCAG 3'	24	67.0
T209Y Forward	5' TTTAAAGGAACCGTGATGCA 3'	21	63.0
T209Y Reverse	5' AGAGGTAGTATA <u>AC</u> CGAAAGACG 3'	24	65.0
T247Y Forward	5' TTTGTTCTGCCGCTAGAGCACCACCAC 3'	27	74.0
T247Y Reverse	5' GGTGTTACCTCCATGT <u>AC</u> ACTGCGCC 3'	27	74.0

default parameters except for correlation type (shape + electrostatics). The shape complementarities of the IBP–ice interfaces for the resulting models were evaluated using the SC program [31].

CD spectroscopy

Lyophilized proteins were suspended in 25 mM phosphate buffer (pH 7.0) to a concentration of 8 μM . CD spectra were measured using a J-815 spectropolarimeter (Jasco Corp., Easton, MD, USA) in 1-mm path length cuvette as described [44]. In experiments aimed to assess thermal stability spectra were collected by measuring the CD signal at 215 nm fixed wavelength, and the sample was progressively heated from 25 to 90 °C. Measurements were performed with a data pitch of 2 °C and a temperature slope of 0.5 °C·min⁻¹. Experiments were performed in triplicate.

Thermal hysteresis

Protein samples were prepared by dissolving lyophilized proteins in 20 mM ammonium bicarbonate buffer (pH 8.5) and diluting them to the desired concentration in the same buffer. TH measurements were performed using a custom nanoliter osmometer as described previously [45]. Single crystals of typically 10- μm diameter were obtained and incubated for 1 min slightly below their melting temperature. Then the temperature was dropped at a cooling rate of 0.01 °C every 4 s. The freezing point was determined as the temperature at which the crystal grew continuously. Each measurement was repeated at least three independent times.

Ice recrystallization inhibition

Ice recrystallization inhibition activity was measured by a sucrose sandwich assay [46] with some modifications [47]. The sample solutions contained 45% sucrose, 50 mM NaCl, 10 mM Tris buffer (pH 8.0) and 0 or 0.02 μM or 0.1 μM of protein. Samples of 1.4 μL were placed on a sapphire sample holder and covered with a 13-mm-diameter circular glass coverslip. The sample was sealed with type B immersion oil (Sigma-Aldrich, St. Louis, MO, USA) to avoid evaporation and mounted on a copper plate with a 2.5-mm diameter slit placed on the stage of the nanoliter osmometer [45]. The sample was cooled from room temperature to -35 °C by the Peltier element of the nanoliter osmometer while slowly pouring liquid nitrogen on top of the sample. Fast rate of cooling was necessary to form polycrystalline ice. The temperature was then elevated to -10 °C at a warming rate of 150 °C·min⁻¹ and then warming continued to -8 °C at a rate of 6 °C·min⁻¹. The final stage of heating up to the annealing temperature of -7.4 °C was conducted at a slow rate of 1 °C·min⁻¹ to avoid overheating. The sample was maintained at this temperature for 60 min.

During this period, recrystallization was recorded using a Basler ace acA1920-155um camera (Basler, Ahrensburg, Germany) every 10 s. The experiment was repeated at least five times for each concentration.

The IRI was quantified following the mathematical description derived by Budke *et al.* [47]. The images were processed using Fiji software [48] to calculate the mean radius of the crystals and the total crystal volume. The cube of the mean crystal radius was calculated and plotted against time. The slope of the curve obtained from time points 30–60 min was taken as the recrystallization rate constant (K_d). The average ice volume fraction of this period was used to extrapolate K_d constant to zero ice fraction (K_{d0}), as described by Budke *et al.* [47]. In all experiments, the ice volume fraction was < 10%.

Statistical analysis and plotting were performed using R 3.4.3 (R Foundation for Statistical Computing, Vienna, Austria). Mean values and 95% confidence intervals were calculated by nonparametric bootstrapping method from R package 'Hmisc' 4.0-3 using 1000 resamples.

Acknowledgements

We thank Daniele de Sanctis for data collection support at the ID29 beamline of the European Synchrotron Radiation Facility (ESRF, Grenoble, France). This work was partly supported by a grant Progetto Nazionale di Ricerche in Antartide PEA 2014–2016 and the RISE-MSCA Project 'Metable' to ML. IB acknowledges support by European Research Council (grant No. 281595) and by Israel Science Foundation (grant No. 930/16). AK acknowledges support by European Regional Development Fund.

Author contributions

Biochemical and biophysical experiments on the native and mutant proteins were performed by MM (protein expression and purification, CD), AK and GS (IRI and TH); VN, VFV, and MN grew the protein crystals, collected the diffraction data, and solved the structure of the protein; MN performed the *in silico* docking experiments; MBD and IB designed and analyzed the activity measurements; ML, IB, and MN conceived the project; MBD, MN, and ML wrote the paper. All authors have read and approved the manuscript.

References

- 1 DeVries AL, Komatsu SK & Feeney RE (1970) Chemical and physical properties of freezing point-depressing glycoproteins from Antarctic fishes. *J Biol Chem* **245**, 2901–2908.

- 2 DeVries AL & Lin Y (1977) Structure of a peptide antifreeze and mechanism of adsorption to ice. *Biochim Biophys Acta* **495**, 388–392.
- 3 DeVries AL & Wohlschlag DE (1969) Freezing resistance in some Antarctic fishes. *Science (New York, NY)* **163**, 1073–1075.
- 4 Davies PL (2014) Ice-binding proteins: a remarkable diversity of structures for stopping and starting ice growth. *Trends Biochem Sci* **39**, 548–555.
- 5 Bar Dolev M, Braslavsky I & Davies PL (2016) Ice-binding proteins and their function. *Ann Rev Biochem* **85**, 515–542.
- 6 Graether SP, Kuiper MJ, Gagné SM, Walker VK, Jia Z, Sykes BD & Davies PL (2000) Beta-helix structure and ice-binding properties of a hyperactive antifreeze protein from an insect. *Nature* **406**, 325–328.
- 7 Liou YC, Tocilj A, Davies PL & Jia Z (2000) Mimicry of ice structure by surface hydroxyls and water of a β -helix antifreeze protein. *Nature* **406**, 322–324.
- 8 Leinala EK, Davies PL & Jia ZC (2002) Crystal structure of beta-helical antifreeze protein points to a general ice binding model. *Structure* **10**, 619–627.
- 9 Marshall CB, Daley ME, Graham LA, Sykes BD & Davies PL (2002) Identification of the ice-binding face of antifreeze protein from *Tenebrio molitor*. *FEBS Lett* **529**, 261–267.
- 10 Garnham CP, Campbell RL & Davies PL (2011) Anchored clathrate waters bind antifreeze proteins to ice. *Proc Natl Acad Sci USA* **108**, 7363–7367.
- 11 Hakim A, Nguyen JB, Basu K, Zhu DF, Thakral D, Davies PL, Isaacs FJ, Modis Y & Meng W (2013) Crystal structure of an insect antifreeze protein and its implications for ice binding. *J Biol Chem* **288**, 12295–12304.
- 12 Knight CA, De Vries AL & Oolman LD (1984) Fish antifreeze protein and the freezing and recrystallization of ice. *Nature* **308**, 295–296.
- 13 Mazur P (1984) Freezing of living cells: mechanisms and implications. *Am J Physiol Cell Physiol* **247**, C125–C142.
- 14 Basu K, Wasserman SS, Jeronimo PS, Graham LA & Davies PL (2016) Intermediate activity of midge antifreeze protein is due to a tyrosine-rich ice-binding site and atypical ice plane affinity. *FEBS J* **283**, 1504–1515.
- 15 Olijve LLC, Meister K, DeVries AL, Duman JG, Guo S, Bakker HJ & Voets IK (2016) Blocking rapid ice crystal growth through nonbasal plane adsorption of antifreeze proteins. *Proc Natl Acad Sci USA* **113**, 3740–3745.
- 16 Capicciotti CJ, Poisson JS, Boddy CN & Ben RN (2015) Modulation of antifreeze activity and the effect upon post-thaw HepG2 cell viability after cryopreservation. *Cryobiology* **70**, 79–89.
- 17 Voets IK (2017) From ice-binding proteins to bio-inspired antifreeze materials. *Soft Matter* **13**, 4808–4823.
- 18 Mangiagalli M, Bar-Dolev M, Tedesco P, Natalello A, Kaleda A, Brocca S, Pascale D, Pucciarelli S, Miceli C & Bravslavsky I (2017) Cryo-protective effect of an ice-binding protein derived from Antarctic bacteria. *FEBS J* **284**, 163–177.
- 19 Bayer-Giraldi M, Uhlig C, John U, Mock T & Valentin K (2010) Antifreeze proteins in polar sea ice diatoms: diversity and gene expression in the genus *Fragilariopsis*. *Environ Microbiol* **12**, 1041–1052.
- 20 Raymond JA & Kim HJ (2012) Possible role of horizontal gene transfer in the colonization of sea ice by algae. *PLoS ONE* **7**, e35968.
- 21 Uhlig C, Kilpert F, Frickenhaus S, Kegel JU, Krell A, Mock T, Valentin K & Beszteri B (2015) *In situ* expression of eukaryotic ice-binding proteins in microbial communities of Arctic and Antarctic sea ice. *ISME J* **9**, 2537–2540.
- 22 Davies PL (2016) Antarctic moss is home to many epiphytic bacteria that secrete antifreeze proteins. *Environ Microbiol Rep* **8**, 1–2.
- 23 Hanada Y, Nishimiya Y, Miura A, Tsuda S & Kondo H (2014) Hyperactive antifreeze protein from an Antarctic sea ice bacterium *Colwellia sp* has a compound ice-binding site without repetitive sequences. *FEBS J* **281**, 3576–3590.
- 24 Do H, Kim SJ, Kim HJ & Lee JH (2014) Structure-based characterization and antifreeze properties of a hyperactive ice-binding protein from the Antarctic bacterium *Flavobacterium frigoris* PS1. *Acta Crystallogr D Biol Crystallogr* **70**, 1061–1073.
- 25 Cheng J, Hanada Y, Miura A, Tsuda S & Kondo H (2016) Hydrophobic ice-binding sites confer hyperactivity of an antifreeze protein from a snow mold fungus. *Biochem J* **473**, 4011–4026.
- 26 Kondo H, Hanada Y, Sugimoto H, Hoshino T, Garnham CP, Davies PL & Tsuda S (2012) Ice-binding site of snow mold fungus antifreeze protein deviates from structural regularity and high conservation. *Proc Natl Acad Sci USA* **109**, 9360–9365.
- 27 Lee JH, Park AK, Do H, Park KS, Moh SH, Chi YM & Kim HJ (2012) Structural basis for antifreeze activity of ice-binding protein from arctic yeast. *J Biol Chem* **287**, 11460–11468.
- 28 Wang C, Pakhomova S, Newcomer ME, Christner BC & Luo B-H (2017) Structural basis of antifreeze activity of a bacterial multi-domain antifreeze protein. *PLoS ONE* **12**, e0187169.
- 29 Garnham CP, Gilbert JA, Hartman CP, Campbell RL, Laybourn-Parry J & Davies PL (2008) A Ca^{2+} -dependent bacterial antifreeze protein domain has a novel beta-helical ice-binding fold. *Biochem J* **411**, 171–180.
- 30 Nutt DR & Smith JC (2008) Dual function of the hydration layer around an antifreeze protein revealed by atomistic molecular dynamics simulations. *J Am Chem Soc* **130**, 13066–13073.

- 31 Lawrence MC & Colman PM (1993) Shape complementarity at protein/protein interfaces. *J Mol Biol* **234**, 946–950.
- 32 Garnham CP, Natarajan A, Middleton AJ, Kuiper MJ, Braslavsky I & Davies PL (2010) Compound ice-binding site of an antifreeze protein revealed by mutagenesis and fluorescent tagging. *Biochemistry* **49**, 9063–9071.
- 33 Yu SO, Brown A, Middleton AJ, Tomczak MM, Walker VK & Davies PL (2010) Ice restructuring inhibition activities in antifreeze proteins with distinct differences in thermal hysteresis. *Cryobiology* **61**, 327–334.
- 34 Wang C, Oliver EE, Christner BC & Luo BH (2016) Functional analysis of a bacterial antifreeze protein indicates a cooperative effect between its two ice-binding domains. *Biochemistry* **55**, 3975–3983.
- 35 Studier FW (2005) Protein production by auto-induction in high-density shaking cultures. *Protein Expr Purif* **41**, 207–234.
- 36 Kabsch W (2010) XDS. *Acta Crystallogr D Biol Crystallogr* **66**, 125–132.
- 37 Evans P (2006) Scaling and assessment of data quality. *Acta Crystallogr D Biol Crystallogr* **62**, 72–82.
- 38 Storoni LC, McCoy AJ & Read RJ (2004) Likelihood-enhanced fast rotation functions. *Acta Crystallogr D Biol Crystallogr* **60**, 432–438.
- 39 Emsley P & Cowtan K (2004) Coot: model-building tools for molecular graphics. *Acta Crystallogr D Biol Crystallogr* **60**, 2126–2132.
- 40 Murshudov GN, Vagin AA & Dodson EJ (1997) Refinement of macromolecular structures by the maximum-likelihood method. *Acta Crystallogr D Biol Crystallogr* **53**, 240–255.
- 41 Adams PD, Afonine PV, Bunkóczi G, Chen VB, Davis IW, Echols N, Headd JJ, Hung LW, Kapral GJ & Grosse-Kunstleve RW (2010) PHENIX: a comprehensive Python-based system for macromolecular structure solution. *Acta Crystallogr D Biol Crystallogr* **66**, 213–221.
- 42 Chen VB, Arendall WB, Headd JJ, Keedy DA, Immormino RM, Kapral GJ, Murray LW, Richardson JS & Richardson DC (2010) MolProbity: all-atom structure validation for macromolecular crystallography. *Acta Crystallogr D Biol Crystallogr* **66**, 12–21.
- 43 Ritchie DW & Venkatraman V (2010) Ultra-fast FFT protein docking on graphics processors. *Bioinformatics* **26**, 2398–2405.
- 44 Tedeschi G, Mangiagalli M, Chmielewska S, Lotti M, Natalello A & Brocca S (2017) Aggregation properties of a disordered protein are tunable by pH and depend on its net charge per residue. *Biochim Biophys Acta* **1861**, 2543–2550.
- 45 Braslavsky I & Drori R (2013) LabVIEW-operated novel nanoliter osmometer for ice binding protein investigations. *J Vis Exp* **72**, e4189.
- 46 Regand A & Goff HD (2006) Ice recrystallization inhibition in ice cream as affected by ice structuring proteins from winter wheat grass. *J Dairy Sci* **89**, 49–57.
- 47 Budke C, Heggemann C, Koch M, Sewald N & Koop T (2009) Ice recrystallization kinetics in the presence of synthetic antifreeze glycoprotein analogues using the framework of LSW theory. *J Phys Chem B* **113**, 2865–2873.
- 48 Schindelin J, Arganda-Carreras I, Frise E, Kaynig V, Longair M, Pietzsch T, Preibisch S, Rueden C, Saalfeld S, Schmid B *et al.* (2012) Fiji: an open-source platform for biological-image analysis. *Nat Methods* **9**, 676–682.

Appendix 3

Publication III

Kaleda, A., Haleva, L., Sarusi, G., Pinsky, T., Mangiagalli, M., Bar-Dolev, M., Lotti, M., Nardini, M., Braslavsky, I. (2018), Saturn-shaped ice burst pattern and fast basal binding of an ice-binding protein from an Antarctic bacterial consortium. *Langmuir*. doi:10.1021/acs.langmuir.8b01914

Saturn-Shaped Ice Burst Pattern and Fast Basal Binding of an Ice-Binding Protein from an Antarctic Bacterial Consortium

Aleksei Kaleda,^{†,‡,§,¶} Lotem Haleva,^{†,#} Guy Sarusi,^{†,¶} Tova Pinsky,^{†,#} Marco Mangiagalli,[§] Maya Bar Dolev,[†] Marina Lotti,[§] Marco Nardini,^{||} and Ido Braslavsky^{*,†,¶}

[†]Institute of Biochemistry, Food Science and Nutrition, The Robert H. Smith Faculty of Agriculture, Food and Environment, The Hebrew University of Jerusalem, Rehovot 7610001, Israel

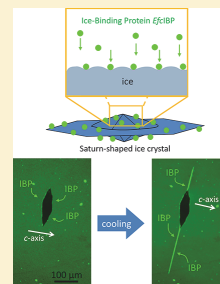
[‡]Department of Chemistry and Biotechnology, School of Science, Tallinn University of Technology, Ehitajate tee 5, 19086 Tallinn, Estonia

[§]Department of Biotechnology and Biosciences, University of Milano-Bicocca, Piazza della Scienza 2, 20126 Milan, Italy

^{||}Department of Biosciences, University of Milano, Via Celoria 26, 20133 Milan, Italy

Supporting Information

ABSTRACT: Ice-binding proteins (IBPs) bind to ice crystals and control their growth, enabling host organisms to adapt to subzero temperatures. By binding to ice, IBPs can affect the shape and recrystallization of ice crystals. The shapes of ice crystals produced by IBPs vary and are partially due to which ice planes the IBPs are bound to. Previously, we have described a bacterial IBP found in the metagenome of the symbionts of *Euplotes focardii* (*Efc*IBP). *Efc*IBP shows remarkable ice recrystallization inhibition activity. As recrystallization inhibition of IBPs and other materials are important to the cryopreservation of cells and tissues, we speculate that the *Efc*IBP can play a future role as an ice recrystallization inhibitor in cryopreservation applications. Here we show that *Efc*IBP results in a Saturn-shaped ice burst pattern, which may be due to the unique ice-plane affinity of the protein that we elucidated using the fluorescent-based ice-plane affinity analysis. *Efc*IBP binds to ice at a speed similar to that of other moderate IBPs ($5 \pm 2 \text{ mM}^{-1} \text{ s}^{-1}$); however, it is unique in that it binds to the basal and previously unobserved pyramidal near-basal planes, while other moderate IBPs typically bind to the prism and pyramidal planes and not basal or near-basal planes. These insights into *Efc*IBP allow a better understanding of the recrystallization inhibition for this unique protein.



INTRODUCTION

A key strategy of cold-adapted organisms that need to survive at low temperatures is the production of ice-binding proteins (IBPs). The general concept shared by all IBPs, as implied by their name, is the ability to directly adhere to ice crystals, thereby affecting different aspects of ice growth. IBPs have been identified and characterized in many organisms spanning different branches of the tree of life, including fish, terrestrial arthropods, plants, fungi, bacteria, and diatoms.¹

IBPs in freeze-avoidant organisms are thought to act by depressing the growth of ice crystals in supercooled solutions; thus, they are also known as antifreeze proteins (AFPs). Freezing point depression below the melting point is termed thermal hysteresis (TH).¹ AFPs have typically been classified into hyperactive and moderate AFPs, where moderate AFPs have TH up to 1 °C at millimolar concentrations while hyperactive AFPs produce higher TH in micromolar concentrations.^{2,3} In freeze-tolerant organisms, IBPs act as ice recrystallization inhibition (IRI) proteins, which can help to avoid damage caused by freezing.⁴ Research into bacterial and algal communities found at ice water interfaces led to the notion that the role of bacterial IBPs may be to sustain a liquid environment and prevent the freezing of brine pockets. This

idea is supported by the fact that many of these IBPs are secreted to the environment surrounding the organism.^{5,6} Extracellular IBPs contain a conserved region initially classified in the Pfam database (<http://pfam.xfam.org/>) as “domain of unknown function” (DUF) 3494, and most of them carry a signal peptide for secretion at their amino terminus.

Euplotes focardii, a free-swimming psychrophilic ciliate from the Terra Nova Bay in Antarctica lives in symbiosis with bacteria. Metagenome analysis of the symbionts of *E. focardii* revealed a coding sequence for a bacterial ice-binding protein (*Efc*IBP).⁷ This protein contains a DUF3494 domain and an N-terminal signal sequence for protein transport. The protein is folded in a right-handed β -helix with a triangular cross-section formed by three parallel β -sheets, named A, B, and C faces, and an additional single α -helix aligned along the axis of the β -helix.⁸ This fold is typical of bacterial IBPs, where it is defined as the IBP-1 fold.⁴ However, *Efc*IBP has a shorter β -

Special Issue: Interfaces and Biology 1: Mechanobiology and Cryobiology

Received: June 7, 2018

Revised: September 7, 2018

Published: September 10, 2018

solenoid, and the sequence and organization of the regions exposed to ice are also different from its homologues.

EfcIBP has a peculiar combination of TH and IRI activity. Its TH is 0.53 °C at 50 μ M, which is classified as a moderately active, but its ice recrystallization 50% inhibition concentration is 2.5 nM, making it one of the most potent IRI agents described in the literature to date.⁹ This attribute of *EfcIBP* makes it a candidate for an efficient recrystallization inhibition factor in cryobiology applications.

Ice growth inhibition mechanisms of hyperactive and moderate IBPs are not yet fully understood, and no comprehensive model that integrates different attributes of various IBPs exists to date. Drori et al.¹⁰ stated that the key property that delineates moderate and hyperactive IBPs is the ability of hyperactive IBPs to bind the basal ice plane, in addition to prismatic and pyramidal. However, a moderate IBP from the *Leucosporidium* species AY30 (*LeIBP*) is known to have low TH (0.2 °C at 50 μ M), but binds to the basal plane.¹¹ More exceptions to this rule are *LpIBP* from *Lolium perenne*,¹² *FcIBP* (isoform 11) from *Fragilariopsis cylindrus*,¹³ and *EfcIBP*, as discussed further in this paper.

Docking simulations demonstrated that both B and C faces of the protein employ water molecules to increase ice-binding site shape complementarity with an ice lattice, which is especially necessary for the nonflat C face of the protein. According to the simulations,⁸ the B face has a good shape complementarity (SC) to the basal plane (SC 0.53) and low complementarity for the primary prismatic plane (SC 0.39), and the C face has weak complementarity to the primary prismatic plane (SC 0.40). These SC values are higher than 0.38, which is considered a threshold for IBP¹⁴ and was previously used in *EfcIBP* docking study.⁸

On the basis of structural and simulated ice docking analyses, six mutants were designed with amino acid replacements on the putative ice-binding sites located on the B and C faces of the *EfcIBP*. TH and IRI analyses of B face mutants and C face mutants confirmed that both faces are vital for activity, as these mutants had significantly reduced TH and IRI. However, no clear distinction of which face is more important was found.⁸

Kinetics of IBP adsorption to ice have previously been studied, as have the ice surface affinities by moderate and hyperactive IBPs.^{15–20} Thermal hysteresis activity of hyperactive IBPs can increase up to 40 times with a longer incubation period, whereas incubation time only slightly affects moderate IBP TH activity.^{17,21} This was attributed to finding that some hyperactive IBPs adsorb slowly to the basal plane, reaching saturation only after more than 1 h. In contrast, moderate IBPs were demonstrated to adsorb to the prism plane rapidly.¹⁷

In a solution where IBPs are not present, ice crystals grow in a circular disc shape.²² When cooled below the melting point, ice crystals in moderate IBP solutions (such as type I–III AFP) form hexagonal bipyramid or trapezohedron shapes elongated in the direction of the *c*-axis. This growth along the *c*-axis proceeds continuously with diminishing size of the basal planes until the basal planes are almost eliminated, and the bipyramidal tips are formed. The bipyramidal crystal with the two tips is then stable until the freezing point is reached and the crystal bursts in the *c*-axis direction. In contrast, ice crystals in hyperactive IBP solutions, such as sbwAFP from spruce budworm, form bipyramidal or lemon shapes during

melting, stay in a constant size and shape in the TH gap, and burst in *a*-axis direction.^{2,23}

Ice crystal morphology and burst behavior induced by ice-binding proteins are closely related to the crystal planes to which they bind. Recently, an article describing moderate *FcIBP*11, a member of the DUF3494 family,¹³ demonstrated that basal binding affinity does not confer hyperactivity. In this article, we expand on the topic of basal-binding moderate IBPs and show that *EfcIBP*, a moderately active IBP from the DUF3494 family, binds to the basal and previously unobserved pyramidal planes at a rate comparable to other moderate IBPs. This causes growth and burst in the *a*-axis direction, which leads to peculiar Saturn-shaped ice crystals.

■ EXPERIMENTAL SECTION

Cloning and Mutagenesis. *EfcIBP* and its variants (T67Y, T178Y, T223Y, S188Y, T209Y, and T247Y) were cloned in a pET-21a vector.^{8,9} Briefly, the single-point mutations were introduced by QuickChange PCR using pET-21a [*EfcIBP*] as the template as previously described in Mangiagalli et al.⁸

The GFP-*EfcIBP* chimera was obtained by excision of green fluorescent protein (GFP) gene with *Nde*I (Jena Bioscience, Jena, Germany) from pUC18 [GFP]²⁴ and cloned into pET-21a [*EfcIBP*] linearized with the same enzyme. The cloning gave rise to pET-21a [GFP-*EfcIBP*] which was verified by restriction analysis and by bidirectional DNA sequencing.

Mutagenesis of GFP-*EfcIBP* to obtain GFP-T67Y, GFP-T223Y, and GFP-T247Y variants was carried out by QuickChange PCR using pET-21a [GFP-*EfcIBP*] as a template and the forward and reverse primers.⁸ Reactions were carried out using Q5 High-Fidelity DNA Polymerase (New England Biolabs, Ipswich, MA) and Eppendorf Master-cycler (Eppendorf, Hamburg, Germany) under the following conditions: 1 cycle (98 °C for 2 min), 25 cycles (98 °C for 10 s, T_A for 25 s, and 72 °C for 180 s), and a final cycle at 72 °C for 3 min. Here, T_A is the annealing temperature optimized for each mutant plasmid corresponding to the following temperatures: 66 °C for GFP-T67Y, 67.5 °C for GFP-T223Y, and 70 °C for GFP-T247Y. Mutations were verified by bidirectional DNA sequencing.

Production and Purification of Recombinant Proteins. *Escherichia coli* strain BL21[DE3] (EMD, Millipore, Billerica, MA, USA) was used as the host for heterologous production of proteins. All the His-tagged proteins used in this study were produced in Zym-5052 medium²⁵ and purified from the soluble fraction of cell extracts by affinity chromatography.⁹ Proteins from more concentrated samples were pooled and buffer exchanged by gel filtration on PD10 column (GE Healthcare, Little Chalfont, U.K.) against 10 mM ammonium acetate buffer pH 7.0. Purified proteins were lyophilized. *EfcIBP* and its variants were produced and purified at comparable yield (~2 mg from 1 L of culture), while the fusion proteins were produced and purified at higher yield (~5 mg from 1 L of culture).

Protein concentration was determined by the Bradford protein assay (Bio-Rad) or the Micro BCA protein assay kit (Thermo Scientific) using bovine serum albumin (BSA) as the standard.

Ice Growth Shapes by the Nanoliter Osmometer. Ice shaping of *EfcIBP* and its mutants was performed using a custom nanoliter osmometer.²⁶ Samples contained 3.3–50 μ M protein in 20 mM ammonium bicarbonate buffer (pH 8.5). Single crystals of typically 30 μ m diameter were obtained slightly below their melting temperature. Then the temperature was slowly dropped (-0.0025 °C s^{-1}), and the crystal shapes were observed during growth and burst, when growth suddenly becomes fast. Each experiment was repeated several times to observe growth from different *c*-axis orientations.

Fluorescence-Based Ice-Plane Affinity. Fluorescence-based ice-plane affinity (FIPA) was used to determine the IBP ice-plane binding preference. A modified method of Basu et al.²⁷ was used. Ice monocrystals were grown as described by Knight et al.²⁸ Plastic or glass beakers were insulated from the sides and filled with 2.5 L of degassed double distilled water. A weighted 50 mL tube with a small

hole in the cap was placed on the bottom of each beaker to reduce pressure buildup. The beakers were then left in a freezer at $-1\text{ }^{\circ}\text{C}$ for 3 days, and a slab of ice approximately 6 cm thick grew on top of the water. The ice was then examined through crossed polarizers, and large single crystals were cut out by melting the ice with hot metal plates. The orientation of the c -axis was established by careful observation of the birefringence color pattern that appears when looking through crossed polarizers.^{27,29}

A small oriented single ice crystal block was mounted on a brass coldfinger as described by Knight et al.²⁸ A hemispherical glass cup (diameter 60 mm) was filled with cold double distilled water, and the crystal was submerged in the water. The cup and coldfinger were enclosed within an isolated styrofoam box. The crystal was then allowed to grow into a 40 mm diameter hemisphere; then the water was replaced by 50 mL of $0.01\text{--}0.07\text{ mg mL}^{-1}$ protein solution in cold 10 mM Tris buffer (pH 8.4). The hemisphere was then allowed to grow at a constant temperature of $-4.5\text{ }^{\circ}\text{C}$, measured at the circulation bath that cooled the coldfinger, for 3.5 h until it reached approximately 46 mm in diameter, thus adding a 3 mm layer of ice to the hemisphere. The coldfinger with the hemisphere was then rotated upside down, and the flat part of the sphere was evened out by a warm metal plate. The temperature of the coldfinger was then set to $+1\text{ }^{\circ}\text{C}$, and the hemisphere was carefully wiped by a paper tissue to remove nonspecifically bound protein¹⁴ and was put into a $-18\text{ }^{\circ}\text{C}$ freezer as soon as it detached from the coldfinger. The hemisphere was allowed to etch at least overnight and then was imaged in fluorescent light and observed visually. The fluorescent imaging was done inside the $-18\text{ }^{\circ}\text{C}$ freezer with a 470 nm LED lamp with a 469 nm GFP excitation filter and a 525 nm GFP emission filter on The Imaging Source DMK 23UP031 (Bremen, Germany) camera.

Ice crystal a -axes orientation was determined by pit etching. The hemisphere was covered with plastic wrap, and a small hole was made with a needle in the center of the basal plane. The hemisphere was then put into a lyophilizer for 15–30 min until a clearly visible hexagonal hole appeared. Sides of the hexagonal pit coincide with the primary prism planes of the ice crystal lattice.³⁰

Microfluidic Coldfinger. The microfluidic coldfinger (MCF) system used here has been described previously in detail.³¹ Briefly, a microfluidic device containing a copper tip (coldfinger) was placed on a LabVIEW-controlled cold stage mounted on a fluorescence microscope (Ti Eclipse, Nikon, Japan), and a sCMOS camera (Neo 5.5 sCMOS, Andor) was used for video capture and analysis. The experiment started by flowing $5\text{ }\mu\text{L}$ of BSA solution (10 mg mL^{-1}) for 20 min. Then, double distilled water was flown through the MCF to remove unbound BSA. The stage temperature was then lowered until the water in the MCF was frozen around $-25\text{ }^{\circ}\text{C}$, after which the temperature of the stage was increased slowly to the ice melting point, while the temperature of the coldfinger was kept a few degrees below melting temperature. The temperature of the stage was then reduced to allow growth of the crystal, which was controlled by independently adjusting the temperatures of the coldfinger and the metal stage beneath the sample, forming a temperature gradient. The stage was warmed and cooled until only one or two parallel flat planes were observed, indicating the presence of a single crystal. At this point, GFP-*Efc*IBP or GFP-sbwAFP was injected in the MFC, surrounding and adsorbing to the ice crystal. Then the temperature was lowered to grow a new basal plane. The protein-bound ice crystal was observed by fluorescence microscopy for 20 min. Image analysis was performed using NIS Elements AR software (Nikon, Tokyo, Japan). Fluorescent measurements represent the difference between the fluorescence at a given time and the fluorescence at the time that the ice crystal stopped growing and started accumulating protein at the moment the basal plane became stationary.

Crystal Growth in 2D Confinement. The fluorescence experiment between two coverslips was also based on the cold stage setup described for MCF and followed the method by Pertaya et al.³² and Celik et al.³³ A $1.6\text{ }\mu\text{L}$ sample containing GFP-*Efc*IBP or GFP-sbwAFP (in 10 mM Tris-HCl pH 8.0, 20 mM NaCl) in different concentrations was placed on a sapphire slide and covered with a 16 mm diameter circular glass coverslip or was placed in a microfluidic

device similar to that described above, without a coldfinger, with a height of $40\text{ }\mu\text{m}$. The gap between the sapphire and the coverslip was sealed by immersion oil to prevent drying of the sample. The sapphire was placed on a copper slab with a 2 mm diameter hole to observe the fluorescence. The combination of sapphire and a small hole was designed to minimize temperature gradients in the sample. Oil was placed between the copper stage and the sapphire to improve the thermal contact. The stage temperature was then lowered until the solution froze, typically at $-25\text{ }^{\circ}\text{C}$. The temperature was then raised past the melting point until only a few crystals remained. The temperature of the stage was then slowly lowered until crystal growth and burst as “spicules”. The stationary protein-bound ice was observed for 15 min in fluorescent light. Image analysis was performed using NIS Elements AR software (Nikon, Tokyo, Japan). Fluorescent measurements represent the difference between the fluorescence at a given time and the fluorescence at the start of accumulation when the ice front became stationary. The binding kinetics of the IBPs were then calculated by fitting measured fluorescence intensity I to eq 1:

$$I = I_{\max}(1 - e^{-t/\tau}) \quad (1)$$

This equation was previously proposed to describe AFP type III accumulation kinetics on ice.¹⁷ Here τ is a typical accumulation time and is equal to $\frac{1}{k_{\text{on}}C}$.

Protein-Ice Docking. The docked model for *Efc*IBP and ice pyramidal plane (1,0,-1,4), with the minimum overall docking score, was performed with the program HEX 8.0.0,³⁴ using default parameters except for correlation type (shape + electrostatics). The shape complementarities (SC) of the *Efc*IBP-ice interfaces for the resulting models were calculated using the SC program,³⁵ and the surface contact was determined with the program ArealMol.³⁶

RESULTS AND DISCUSSION

*Efc*IBP is a unique IBP which has been shown to have high IRI, moderate TH activity, and two faces of binding.^{8,9} Here we describe several phenomena where *Efc*IBP displays uncommon ice shaping, binding kinetics, and binding plane affinity. In this section, we provide details about the different aspects and characteristics of the *Efc*IBP.

Ice Crystals in the Wild Type *Efc*IBP Solution. The unique effect of *Efc*IBP can first be noted in its effect on ice crystal shaping. The ice crystal shape of the wild type (wt) *Efc*IBP appears at the beginning of crystal growth as a wide hexagonal truncated trapezohedron (Figure 1A), a model for which is presented in Figure 1B. When the temperature of

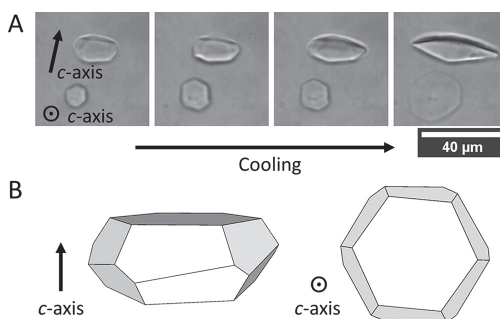


Figure 1. (A) Ice crystal shapes and their growth pattern during cooling in $5\text{ }\mu\text{M}$ solution of wt *Efc*IBP. (B) Simplified model of the wt *Efc*IBP ice crystal. The circled dot indicates c -axis normal to the image plane.

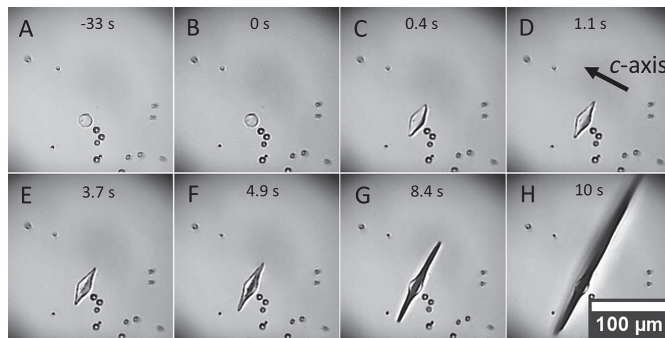


Figure 2. Selected video frames of ice crystal growth (A)–(F) and burst pattern (G)–(H) in wt *EfcIBP* 5 μM solution during cooling. The time from the beginning of growth is shown. The burst starts at 7.5 s. The full experiment can be seen in the Supporting Information, [Movie S1](#).

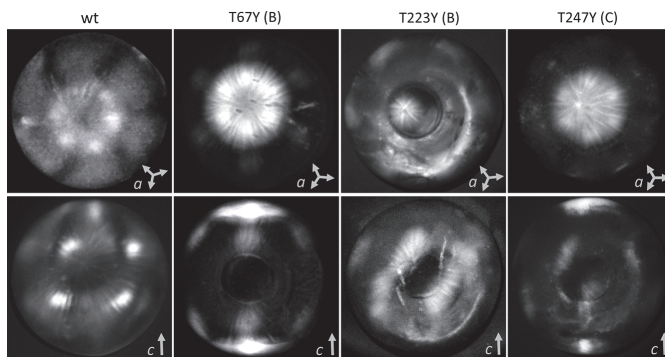


Figure 3. Fluorescence-based ice-plane affinity of wt GFP-*EfcIBP*, its B face mutants GFP-T67Y and GFP-T223Y, and C face mutant GFP-T247Y. Crystal axis directions were determined as described in methods and are indicated by arrows.

EfcIBP solution is lowered at a constant rate, ice crystals grow in small sharp steps in the *a*-axis direction, which was identified by the observed 6-fold crystal symmetry. Crystals grow, then stabilize and grow again, until a smoothed obtuse-angled bipyramidal crystal is formed (Figure 2A–F and [Movie S1](#)). When this growth is observed normal to the *c*-axis, it resembles a bipyramidal growth in the *c* direction that is commonly attributed to moderate IBPs (Figure 2D,E). However, it should be stressed that in the case of *EfcIBP*, ice is not a bipyramid pointing along the *c*-axis but a thin disc-shaped crystal which is longer in the *a* direction (with *c*- to *a*-axis ratio 1:4.5). In other words, unlike ice crystals of other IBPs that grow into thin bipyramids until basal planes are eliminated, in the presence of *EfcIBP*, ice crystals grow wider until prism planes are minimized.

EfcIBP has a unique burst behavior. Ice crystals obtained in the presence of *EfcIBP* have a biconvex shape. Upon continuous cooling, the burst happens as a rapid growth of a thin disc protruding from the edge of the crystal (Figure 2G,H). Note that Figure 2G offers a lateral view of the disc, observable as a line in the middle of the crystal. This supports that the burst pattern is in the *a* direction. Coherent with this interpretation, the bursting produces a circular disc when observed along the crystal's *c*-axis. This behavior was observed consistently dozens of times; more examples are in [Figure S1](#). A simplified model of such a burst is shown in [Figure S2](#). This

shape suggests that the crystal is blocked on the basal plane and not on the prism plane.

Homologue IBPs from the DUF3494 family, *ColAFP* from *Colwellia* sp. strain SLW05,¹⁴ *FfIBP* from *Flavobacterium frigidum* PS1,³⁷ *SfIBP_1* from *Shewanella frigidimarina*,³⁸ *LeIBP*,³⁹ and *TisAFP* from *Typhula ishikariensis*⁴⁰ produce different crystal shapes. The most similar shape is produced by *LeIBP*, although it forms a hexagonal truncated trapezohedron shape that is narrower and elongated along the *c*-axis (*c*:*a* ratio 2.4:1). When the burst pattern is compared to other DUF3494 IBPs, we note a difference in *SfIBP*,³⁸ *FfIBP*,³⁷ and *ColAFP*,¹⁴ which burst dendritically in the *a*-axis direction, as is common for hyperactive proteins.²³ The nondendritic burst pattern of the wt *EfcIBP* might be explained by the fact that it is a moderately active IBP and the supercooling of the solution is to a lesser degree than that of the hyperactive proteins, thus dendritic growth does not occur.

To further investigate ice crystal plane affinity of this protein, we produced GFP-*EfcIBP* and used the FIPA assay and other fluorescent microscopy methods. The fusion of GFP with the protein did not change the ice crystal shape or its burst behavior (Figure S1). However, the TH of GFP-*EfcIBP* is somewhat lower than that of the wt *EfcIBP* (by 35%, Figure S3), although there is no distinct effect of incubation time on TH for both proteins. In many cases, the fusion of GFP with AFP, such as type III AFP³² or sbwAFP¹⁶ does not negatively

affect the TH of the sample. In fact, the addition of GFP tends to raise the TH. The negative effect seen here is likely due to some shielding of the ice-binding sites by GFP. The cause of the lowered TH likely does not significantly affect the results presented further, as the ice shaping and burst behavior of GFP-*Efc*IBP are not different.

Ice-Plane Affinity of GFP-*Efc*IBP. Fluorescence-based ice-plane affinity analysis of GFP-*Efc*IBP demonstrated an intricate, roughly triangular binding pattern (Figure 3). GFP-*Efc*IBP has a general weak affinity toward most pyramidal plane angles (most of the hemisphere between the basal and prism planes is covered), with two sets of distinct small spots of higher affinity. The first is at a very low angle to the basal plane. By measuring the position of the spots, we estimate the Miller–Bravais indices²⁸ $(1,0,-1,x)$, where x is between 3 and 10. This position will be further named as pyramidal near-basal plane. The second set of spots is closer to the secondary pyramidal plane $(1,1,-2,1)$. Most of the crystal hemisphere is covered by the protein, except for slightly curved meridian lines running in the direction of the c -axis and an equatorial band on the prismatic planes. The darker spot directly on the basal plane suggests weaker affinity to the plane compared to the near-basal, which is also confirmed by visual observation of the hemisphere etching pattern (data not shown).

The six spots near the basal plane form a ring around the center of the basal plane with a symmetrical hexagonal pattern of 12 spots on the whole sphere in total, which is a feature of pyramidal plane binding.²⁷ This high index near-basal affinity spots are a novel pattern and have not been reported before. Other DUF3494 proteins that were studied either bind to the basal plane (*Le*IBP,¹¹ *Tis*AFP isoform 6,⁴¹ *Fc*IBP11¹³) or cover the hemisphere completely in FIPA experiments, including the basal plane (*Co*IAFP,¹⁴ *Sf*IBP_1³⁸).

The *Efc*IBP Saturn-like ice crystal shape and bursting direction is consistent with its plane binding specificity. Strong pyramidal near-basal (or basal) affinity, observed with FIPA, prevents the crystal basal plane growth. This makes the formation of a bipyramid with a long c -axis less likely. Furthermore, most pyramidal angles are covered by the protein, and only the prismatic plane is exposed to the solution. This allows growth of the ice crystals only along the a -axis direction and burst as a disc normal to the c -axis.

Ice crystals produced by *Le*IBP, a moderate IBP from the DUF3494 family, have been assumed to be bursting in the c -axis direction, even though this protein has basal plane affinity.^{11,41} However, the binding kinetics and affinity strength of this protein are unknown and might result in c -axis growth; otherwise, it might be that the growth pattern was incorrectly interpreted.

Here we established that the *Efc*IBP is indeed inhibiting basal growth through the near-basal binding and does not block prism direction. Still, we note that after the crystal burst, the ring is very thin. This suggests that the binding to the basal or near-basal plane is fast. To investigate the binding kinetics that are not observable by the FIPA analysis, we performed experiments with fluorescence microscopy of ice grown in a cold microscope stage.

Binding Dynamics of GFP-*Efc*IBP. The binding dynamics of GFP-*Efc*IBP were tested in the microfluidics coldfinger (MCF) device with fluorescence imaging and compared to those of hyperactive GFP-*sbw*AFP, known to bind to the basal plane of ice (Figure 4).^{16,31} Unlike that in FIPA, the dynamic of accumulation of GFP-*Efc*IBP can be monitored in the MCF.

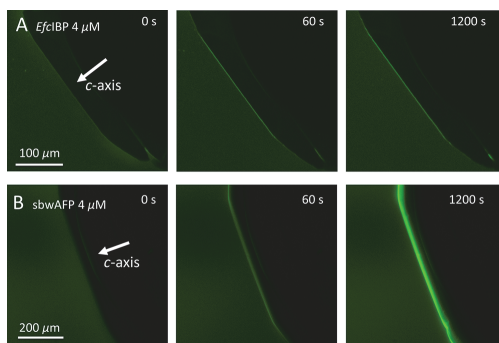


Figure 4. Accumulation of GFP-*Efc*IBP and GFP-*sbw*AFP on the flat stationary basal plane of ice using the MCF. The ice is the darker area on the top right side. (A) 4 μ M GFP-*Efc*IBP. (B) 4 μ M GFP-*sbw*AFP (part of this figure reprinted with permission from ref 31; copyright 2016 Elsevier). The time legend indicates the number of seconds from the time that the basal plane stopped growing and IBPs started accumulating on the ice front.

In FIPA, we note that the preferred accumulation is not exactly on the basal plane, but is in close proximity, while in MCF, we observe strong accumulation on the basal plane, which can be distinguished as a straight edge³¹ of a mostly round crystal (Figure 4). We acknowledge that in the MCF device, the crystallographic orientations of ice are not exposed as they are in the FIPA experiments; therefore, near-basal plane binding may be indistinguishable compared to basal plane binding. It is noted that there is no significant difference in the TH values of *Efc*IBP when incubation time is altered before cooling.⁹ This is indicative of a moderately active IBP, compared to some hyperactive IBPs, which may accumulate on the basal plane of ice for a few hours,¹⁷ thus increasing TH. GFP-*Efc*IBP accumulates on the crystal for approximately 1 min, after which it remains constant for at least 20 min (Figure 4A). GFP-*sbw*AFP accumulates on the basal plane for much longer, as is common in hyperactive AFPs (Figure 4B). We note that the higher fluorescence intensity next to the ice surface observed at 0 s is due to pushing protein off the surface of the growing ice front and not to accumulation.

A complementary method useful to study the accumulation kinetics on ice surfaces is to perform experiments between two coverslips and observe free growth of crystals and protein accumulation in semi-2D confinement using fluorescence microscopy. When grown between two coverslips, ice is forced into a height of 10 μ m, leading to the growth of truncated crystals when burst. This setup allows for protein accumulation measurements on ice but results in changes to the crystal shape because of the height constraint. Due to the height confinement, the observed crystals are cross-sections of the shapes that have been observed in the nanoliter osmometer (Figure 5A–F). The thin bright lines visible in Figure 5B,D,E,F are truncated ice sheets forced to grow in a very thin layer perpendicular to the image plane. The phenomenon of ice spicules has previously been documented with other IBPs, but in the c -axis direction when the growth in the a direction was blocked by the proteins.²⁰ In the case of *Efc*IBP, the geometric restriction transformed planar growth into spicule-like growth in the a direction on both sides of the crystal, exposing a large basal plane.²⁹ The crystals show two main orientations when

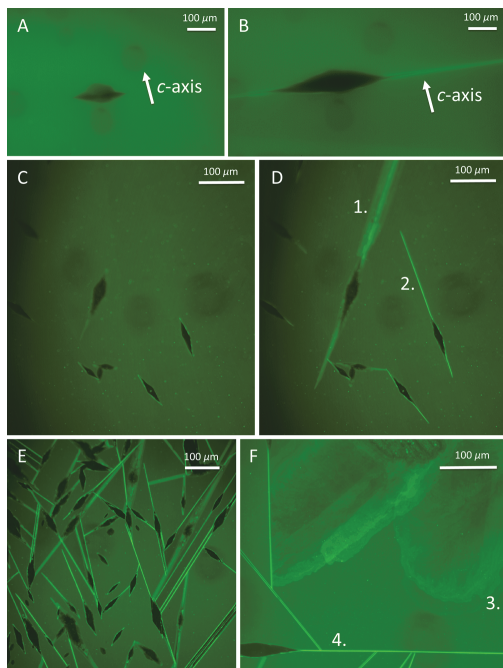


Figure 5. Experiments in 2D confinement in GFP-*EfcIBP* solution. (A) Single crystal is observed in the TH gap with the *c*-axis parallel to the coverslips. (B) Burst pattern of A is shown. (C) Multiple ice crystals observed in the TH gap. (D) Burst pattern of C is shown. The *c*-axis of crystal 1 is tilted to the coverslips, while those in the rest of the crystals, including crystal 2, are parallel. (E) and (F) Burst pattern of many crystals shows the ice sheet bursts to be both *c*-axis parallel (shown as a bright line) and tilted (shown as a sheet) in relation to the coverslips. (F) Crystals bursting perpendicular (crystal 4) to the coverslips can block the growth of neighboring ice (crystal 3, seen in [Movie S2](#)).

bursting: one in which the *c*-axis is at an angle to the coverslips ([Figure 5A,B](#)) and the other where the *c*-axis is nearly perpendicular in relation to the coverslips ([Figure 5B–F](#)). Flat, wide fluorescent ice sheets can be seen ([Figure 5D–F](#)) when the *c*-axis is nearly perpendicular to the coverslips. When the *c*-axis is at an angle to the coverslips, the burst “spicule” can block the growth of other crystals ([Figure 5E,F](#)), as the thin line is a sheet of ice (seen in [Figure S2B](#)) spanning from one coverslip to another. As the large ice sheet (crystal 3) seen in [Figure 5F](#) grows, it is blocked by a spanning ice sheet (crystal 4) which bends from the force of crystal 3. This is seen in [Movie S2](#) (18 s). When the two ice crystals collide, the spanning ice sheet is bent due to the force of the parallel ice ([Figure 5F](#), crystals 3 and 4). We also note that the large spanning ice sheet (crystal 3) is covered in fluorescent protein. The large sheet is likely the basal plane of ice, which is bound by GFP-*EfcIBP*. This experiment helps to validate the hypothesis that *EfcIBP* is a basal or near-basal binder.

Basal plane fluorescence intensity profiles of GFP-*EfcIBP* ([Figure 6A–C](#)) and GFP-*sbwAFP* ([Figure 6D](#)) were analyzed over time and compared to the results obtained from MCF. The accumulation rate value (K_{on}) of each protein can then be

calculated from [eq 1](#) in the [Experimental Section](#), as the concentration (C) and time (t) are known ([Figure 6E,F](#)).

The K_{on} values were calculated from both the MCF and coverslip methods separately. The K_{on} value for the basal plane of GFP-*EfcIBP* was found to be $4 \pm 1 \text{ mM}^{-1} \text{ s}^{-1}$ between coverslips (truncated sheets) (SD, $n = 3$ for all measurements) and $6 \pm 2 \text{ mM}^{-1} \text{ s}^{-1}$ in MCF, while on the pyramidal plane (crystal side, seen in [Figures 6E and S4](#)), the average K_{on} value was found to be $2 \pm 1 \text{ mM}^{-1} \text{ s}^{-1}$. The binding of GFP-*EfcIBP* on the pyramidal plane is, therefore, approximately the same rate as that on the basal plane; however, it has a significantly lower fluorescent intensity. The K_{on} value of GFP-*sbwAFP* on the basal plane was found to be an order of magnitude lower: $0.3 \pm 0.1 \text{ mM}^{-1} \text{ s}^{-1}$ (coverslips) and $0.6 \pm 0.3 \text{ mM}^{-1} \text{ s}^{-1}$ (MCF). These methods agree with one another for both the *EfcIBP* and for the *sbwAFP*, which show K_{on} values within the standard deviation range. To simplify these findings, we averaged the two rates obtained by each method with weights according to their accuracy. We concluded that the final K_{on} value for GFP-*sbwAFP* on the basal plane is $0.4 \pm 0.2 \text{ mM}^{-1} \text{ s}^{-1}$. The K_{on} value for GFP-*EfcIBP* on the basal plane is $5 \pm 2 \text{ mM}^{-1} \text{ s}^{-1}$.

The rapid binding of *EfcIBP* is comparable to the rapid binding of AFP type III, previously determined to be $8 \pm 1 \text{ mM}^{-1} \text{ s}^{-1}$.¹⁷ This indicates that *EfcIBP* and AFP type III bind to ice at a comparable rate. Yet the dramatic difference between the two proteins is which planes the proteins are binding to (basal vs prism). This is a direct and quantitative measurement of the fast accumulation of *EfcIBP* on the basal plane, which has not been noted before for any IBP. Future research should include elucidating the mechanism that allows this IBP to bind to the basal plane at such a rate.

Previous studies compared the differences between GFP-tagged moderate type III AFP and hyperactive *TmAFP* from *Tenebrio molitor* and *sbwAFP* and revealed that the hyperactive IBPs accumulate relatively slowly on both prism and basal planes and that the accumulation on the basal plane can take hours.^{10,16,17,33} In contrast, moderate IBPs that were represented by the type III AFP bind fast to the prism plane and cannot bind to the basal plane.^{10,17,31} Thus, basal plane affinity was denoted as a feature that characterized hyperactive IBPs with high TH. Yet, *EfcIBP* has low TH activity and is a fast basal binder compared to *sbwAFP* and reached a plateau after 1 min ([Figure 6E,F](#)). These findings, along with FIPA analysis, indicate that basal plane affinity on its own does not guarantee hyperactivity (high TH), as prismatic binding is important as well. It also demonstrates that basal affinity can be fast and not intrinsically slow as was found in several hyperactive proteins.

Asymmetrical Pyramidal Binding of GFP-*EfcIBP*. A notable feature of the wt *EfcIBP* FIPA is the overall asymmetry of the binding pattern, which is slightly rotated around the *c*-axis. The bright spots that are closer to the prismatic planes are located on the meridians of the *a*-axes and are not centered on them, but rather slightly shifted counterclockwise around the *c*-axis. This asymmetric binding observed in FIPA is reflected in the ice crystal shape, which appears as a trapezohedron instead of a symmetric bipyramid.

Such off-axis binding has been reported for fish AFP types I and III,^{27,42,43} yeast *LeIBP*,¹¹ mold fungus *TisAFP6*,⁴¹ and plant *DcAFP* (from *Daucus carota*).⁴⁴ All these proteins have a different degree of binding asymmetry even among mutants of the same protein⁴² and demonstrate corresponding twisting in

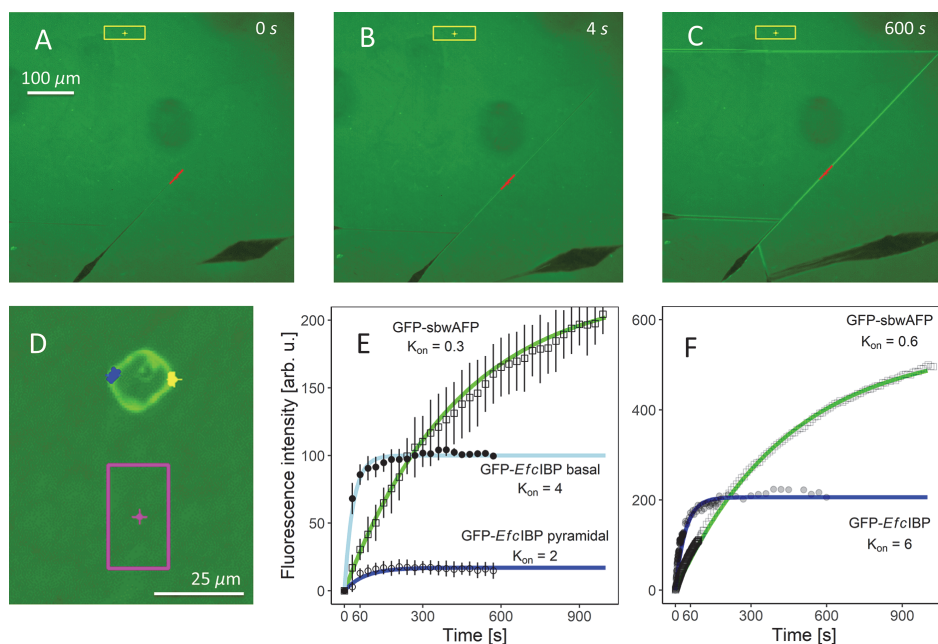


Figure 6. (A)–(C) Bursting ice crystals in 7.6 μM GFP-EfcIBP solution between coverslips. Fluorescent measurements represent the difference between the fluorescence of the basal plane (red line) at a given time and the fluorescence at the beginning of accumulation. The background fluorescence (yellow rectangle) was measured during the experiment to confirm that stable conditions were maintained. (D) Ice crystal grown in 7.6 μM GFP-sbwAFP solution within the TH gap. Fluorescent measurements represent the difference between the fluorescence of the basal plane (blue and yellow rectangles) at a given time and the fluorescence when the crystal stopped melting and began accumulating protein. The background fluorescence (pink rectangle) was measured during the experiment to confirm that stable conditions were maintained. (E) Fluorescence intensity over time of 10 μM GFP-EfcIBP (on basal and pyramidal planes) and 7.6 μM GFP-sbwAFP (on basal plane) measured between coverslips. The K_{on} values of GFP-sbwAFP and GFP-EfcIBP are shown ($\text{mM}^{-1} \text{s}^{-1}$). Vertical bars represent standard deviation ($n = 3$). (F) Fluorescence intensities of 4 μM GFP-EfcIBP and 4 μM GFP-sbwAFP in the MCF over time. The K_{on} values of GFP-EfcIBP and GFP-sbwAFP are shown ($\text{mM}^{-1} \text{s}^{-1}$).

the ice crystal shape. This emphasizes the importance of pyramidal binding for the ice crystal shape.

EfcIBP Mutants. To further understand the relation between ice-binding affinity and different aspects of IBP interaction with ice, we examined mutants of the EfcIBP, which were previously described (Figure S5).⁸ These mutants included modifications of ice-binding surfaces on the B and C faces, which drastically affected the TH activity of the mutants. Indeed, the TH activity at 40 μM of B face mutants is 0.04, 0.06, and 0.12 °C for T67Y, T223Y, and T178Y, respectively, while those of C face mutants is 0.22, 0.10, and 0.02 °C for S188Y, T209Y, and T247Y, respectively.⁸

The B face mutants T178Y and T223Y and C face mutants S188Y, T209Y, and T247Y had shapes similar to the wt ice crystal shape with a different degree of asymmetry (Figure S6). However, T67Y produced symmetrical and well-defined hexagonal bifurcations (Figure S6), a model for which is presented in Figure S2A. Accordingly, the GFP-T67Y mutant has an entirely symmetric FIPA pattern, with no twisting or tilting of spots that is observed in other mutants (Figure 3).

We note that the mutants least active in TH (GFP-T67Y, GFP-T223Y, and GFP-T247Y) retain affinity to the basal or near-basal plane and some generally weak affinity to other pyramidal angles (Figure 3). GFP-T223Y is missing the near-

basal ring of spots, indicating that this particular affinity is a feature of a specific region on the B face. The mutants still produce a wide ice crystal shape that grows in the *a*-axis direction (Figure S6), although their THs are an order of magnitude lower compared to that of the wt EfcIBP.⁸ Therefore, basal binding is not sufficient to achieve high TH when pyramidal or prism affinity is low, as seen in the mutants. Hemisphere area covered by the bound IBP in FIPA analysis has been correlated to the ice growth inhibition by IBPs.⁴⁵ In the FIPA picture of the weakest mutant GFP-T247Y, we observed a faint signal that covers most of the hemisphere with few stronger spots. Thus, IBP activity is determined not only by the specific ice planes bound by the protein but also by affinity strength and probably accumulation speed.

The FIPA patterns of the B and C face mutants (Figure 3) have affinity spots at positions different from those of the wt. This leads to the conclusion that tyrosine introduced on the B or C faces does not completely switch off the ice-binding site but instead modifies its plane affinity. It is possible that the water molecules participating in the ice recognition, particularly at the C face, can accommodate the disruption caused by the bulky amino acid.

Docking. To complement the docking studies already published on the wt EfcIBP interaction with basal and

prismatic planes,⁸ we provide here the corresponding docking simulation with a pyramidal plane (Figure 7). The docking

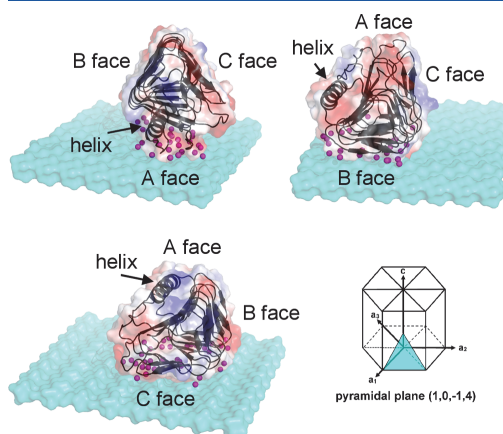


Figure 7. Docking of the wt *EfcIBP* to the ice pyramidal plane. The *EfcIBP* structure is shown as a black cartoon under the semi-transparent protein electrostatic surface. Bound crystallographic water molecules are colored in magenta; the ice molecule surface is in cyan. On the bottom right, the schematic view of the ice pyramidal plane (1,0,-1,4) is shown.

study was performed with the (1,0,-1,4) pyramidal plane, as representative of a pyramidal plane with low angle to the basal plane. Initial docking results (highest score in terms of steric and electrostatic correlations) show that *EfcIBP* binds the ice pyramidal plane through the B face, the C face, and also the surface corresponding to the A face, including the α -helix. The addition of a few crystallographic water molecules located in the troughs of the B, C, and A faces (26, 34, and 27 water molecules, respectively) is sufficient to reach a good shape complementarity between the ice pyramidal plane and the B and A faces (SC value of 0.45 for both) and a somewhat lower SC value (0.40) for the C face. The interaction models were further validated by calculating the contact surface areas, which are 1135, 1305, and 885 Å² for B, C, and A faces, respectively. These values are similar in size with those reported for other IBP-1 folded proteins.^{14,37,41} If compared with the docking results on basal and primary prism planes, the SC and interface analyses suggest that the wt *EfcIBP* binding on the pyramidal plane is less efficient than that on the basal plane (SC 0.53) but better than that hypothesized for the primary prism plane, which is marginally significant with SC 0.39.⁸

Crystal Growth Behavior. As mentioned before, *EfcIBP* ice crystals grow in a stepwise manner. This stepwise growth is more observable at medium IBP concentration (10 μ M), as at a higher concentration there are fewer steps (sometimes no more than one), and at a lower concentration there is less stabilization between burst steps and growth becomes more continuous. In contrast to *EfcIBP*, hyperactive IBPs do not grow in steps as the cooling progresses to the hysteresis freezing point. Nevertheless, the phenomenon of growth by steps was also observed in other IBPs, but in the *c*-axis direction.²³ When crystals are grown in a microfluidic chip with a height of 40 μ m instead of 10 μ m, “spicular” growth is not observed due to a tendency of the crystals to orient

themselves with the basal plane parallel to the coverslip (Movie S3). Additionally, the crystal in Movie S3 grows and stabilizes in less than 0.3 s, showing a typical growth step (note that this is not a full burst).

During cooling, ice crystals of the B face mutant T178Y and C face mutants S188Y and T209Y, similar to wt, grow in a stepwise manner. Differently, B face mutants T67Y and T223Y and C face mutant T247Y demonstrate gradual crystal growth. Such differences can be correlated to the low TH observed (T223Y 15% of wt activity, T67Y 10%, and T247Y 5%).⁸ Nevertheless, during the burst, wt and all mutants grow as thin circular discs in the *a*-axis direction (Figure S6).

Ice Crystal Behavior in 2D Confinement within Mutant Solutions. GFP-*EfcIBP* mutants T67Y, T223Y, and T247Y were placed between coverslips in an attempt to investigate their binding kinetics to ice. Of the six mutants studied, these three mutants show the lowest TH activity.⁸ For all three mutants, ice shaping was observed; however, there was no complete block of ice growth, and we did not see the accumulation of fluorescent signal on the ice surface (Figure S7). Consistent with previous work,⁸ we see ice recrystallization in a solution of GFP-T247Y, the weakest ice recrystallization inhibitor of the mutants (Figure S7C).

CONCLUSION

This study reveals new shaping and plane binding dynamics of the *EfcIBP* that were not described in other IBPs before. Through docking simulations, *EfcIBP* is shown to bind to the basal and pyramidal planes of ice with a higher surface complementarity than to the prism plane. Surprisingly, all three (A, B, and C) faces of the protein show surface complementarity to the pyramidal plane, while only the B and C faces are thought to be used when binding to the basal plane. These docking simulations provide insight into the possible mechanism of *EfcIBP* action.

EfcIBP has TH activity, and by that, it can prevent the ice growth and keep crystals stable at a constant temperature within the TH gap but is less effective in preventing ice from growth compared to other IBPs. Lowering the temperature within the TH gap but not below the hysteresis freezing point revealed a stepwise planar growth of the ice crystal. This observed behavior of *EfcIBP* suggests that freezing point depression is not likely the natural role of this protein. As was discussed by Mangiagalli et al.,⁹ the *EfcIBP* possesses an N-terminal sequence that is a potential transport signal for excretion. We suggest that the protein is secreted into the local environment around the bacteria and acts to shape and control ice growth. In particular, the fast basal binding by this protein may contribute to the high ability to inhibit ice recrystallization. The experiments show that *EfcIBP* has low TH⁹ and fast adsorption dynamics like moderate proteins, but it has a clear basal and near-basal plane affinity with unique fast basal accumulation that was not observed in other known basal binders. While hyperactivity has previously been attributed to basal binding, we stress that this takes the prismatic adsorption into account as well. Here, we define a new moderate AFP class, which we term “moderate basal binders”, that binds to the basal plane but is a weak prismatic binder. The basal affinity and fast kinetics explain the unique Saturn-like ice burst shape of *EfcIBP*.

It remains to be investigated how fast basal binding by IBPs is important for IRI. This paper provides insight into the

properties of *Efc*IBP binding to ice, which may shed light on IBP recrystallization inhibition characteristics.

■ ASSOCIATED CONTENT

📄 Supporting Information

The Supporting Information is available free of charge on the ACS Publications website at DOI: 10.1021/acs.langmuir.8b01914.

Figure S1. Ice crystal growth and burst in 10 μ M *Efc*IBP (A–H) and in 25 μ M GFP-*Efc*IBP (I–P). Letters indicate the sequence of frames (PDF)

Figure S2. Models of ice crystal shapes formed in *Efc*IBP solutions. (A) Hexagonal bifrustum, ice crystal shape formed by the T67Y mutant. (B) A simplified model of Saturn-shaped burst perpendicular to the *c*-axis. For simplicity, the example is given for the T67Y mutant (PDF)

Figure S3. Thermal hysteresis activity of *Efc*IBP compared to GFP-*Efc*IBP. Each point presents the average of three independent measurements, with 95% confidence intervals (PDF)

Figure S4. GFP-tagged *Efc*IBP accumulation on ice crystals. Colored rectangles show areas of fluorescence intensity measurements: red, basal plane (truncated sheet); yellow, pyramidal plane (crystal side); cyan, background (PDF)

Figure S5. *Efc*IBP mutation sites. Mutated residues on the B (yellow) and C (green) faces of the *Efc*IBP structure are shown as sticks and indicated by arrows and labels (PDF)

Figure S6. Ice crystal shapes and their growth pattern during cooling in solutions of *Efc*IBP mutants. The letters in parentheses indicate the protein face that was mutated. T67Y, T178Y, T223Y, and T209Y are 10 μ M; S188Y is 3.3 μ M; and T247Y is 50 μ M. The circled dot indicates *c*-axis normal to the image plane (PDF)

Figure S7. GFP-*Efc*IBP mutants growth and burst after cooling below the TH freezing point, as seen between two coverslips. After the burst, the temperature is held constant. (A) GFP-T67Y mutant at 20 μ M. (B) GFP-T223Y mutant at 17 μ M. (C) GFP-T247Y mutant at 17 μ M (PDF)

Movie S1. Ice crystal growth and burst in the wt *Efc*IBP 5 μ M solution during cooling. The first 30 s are accelerated four times while the rest of the movie is in real time (AVI)

Movie S2. Ice crystals burst in 7.6 μ M GFP-*Efc*IBP solution. A growing parallel ice sheet is blocked by a perpendicular ice sheet (tilted *a*-axis) (AVI)

Movie S3. Single ice crystal in 10 μ M GFP-*Efc*IBP grown in a microfluidic chip with a height of 40 μ m. Photos were taken with a time interval of 0.3 s. The edge of the microfluidic chip can be seen in the frame as curved lines around the ice crystal (AVI)

■ AUTHOR INFORMATION

Corresponding Author

*E-mail: Ido.braslavsky@mail.huji.ac.il. Tel: +972-54-8820955.

ORCID

Aleksei Kaleda: 0000-0001-9003-130X

Guy Sarusi: 0000-0001-7643-0267

Tova Pinsky: 0000-0001-9165-092X

Marco Mangiagalli: 0000-0001-8211-165X

Marina Lotti: 0000-0001-5419-7572

Marco Nardini: 0000-0002-3718-2165

Ido Braslavsky: 0000-0001-8985-8211

Author Contributions

#These authors contributed equally.

Author Contributions

The manuscript was written through contributions of all authors. All authors have given approval to the final version of the manuscript.

Notes

The authors declare no competing financial interest.

■ ACKNOWLEDGMENTS

This work was partly supported by a grant Progetto Nazionale di Ricerche in Antartide PEA 2014–2016 and the RISE-MSCA Project “Metable” to M.L. I.B. acknowledges support by European Research Council (grant No. 281595) and by Israel Science Foundation (grant No. 930/16). A.K. acknowledges support by European Regional Development Fund. We thank Sivan Ben Bassat for TH measurements.

■ ABBREVIATIONS

AFP, antifreeze protein; BSA, bovine serum albumin; FIPA, fluorescence-based ice-plane affinity; IBP, ice-binding protein; IRI, ice recrystallization inhibition; MCF, microfluidic cold-finger; SC, shape complementarity; TH, thermal hysteresis; wt, wild type;

■ REFERENCES

- (1) Bar Dolev, M.; Braslavsky, I.; Davies, P. L. Ice-Binding Proteins and Their Function. *Annu. Rev. Biochem.* **2016**, *85*, 515–542.
- (2) Scotter, A. J.; Marshall, C. B.; Graham, L. A.; Gilbert, J. A.; Garnham, C. P.; Davies, P. L. The Basis for Hyperactivity of Antifreeze Proteins. *Cryobiology* **2006**, *53*, 229–239.
- (3) Celik, Y.; Graham, L. A.; Mok, Y.-F.; Bar, M.; Davies, P. L.; Braslavsky, I. Superheating of Ice Crystals in Antifreeze Protein Solutions. *Proc. Natl. Acad. Sci. U. S. A.* **2010**, *107*, 5423–5428.
- (4) Knight, C. A.; Duman, J. G. Inhibition of Recrystallization of Ice by Insect Thermal Hysteresis Proteins: A Possible Cryoprotective Role. *Cryobiology* **1986**, *23*, 256–262.
- (5) Davies, P. L. Antarctic Moss Is Home to Many Epiphytic Bacteria That Secrete Antifreeze Proteins. *Environ. Microbiol. Rep.* **2016**, *8*, 1–2.
- (6) Raymond, J. A. Dependence on Epiphytic Bacteria for Freezing Protection in an Antarctic Moss, *Bryum Argenteum*. *Environ. Microbiol. Rep.* **2016**, *8*, 14–19.
- (7) Pucciarelli, S.; Chiappori, F.; Devaraj, R. R.; Yang, G.; Yu, T.; Ballarini, P.; Miceli, C. Identification and Analysis of Two Sequences Encoding Ice-Binding Proteins Obtained from a Putative Bacterial Symbiont of the Psychrophilic Antarctic Ciliate *Euplotes Focardii*. *Antarctic Science* **2014**, *26*, 491–501.
- (8) Mangiagalli, M.; Sarusi, G.; Kaleda, A.; Bar Dolev, M.; Nardone, V.; Vena, V. F.; Braslavsky, I.; Lotti, M.; Nardini, M. Structure of a Bacterial Ice Binding Protein with Two Faces of Interaction with Ice. *FEBS J.* **2018**, *285*, 1653–1666.
- (9) Mangiagalli, M.; Bar-Dolev, M.; Tedesco, P.; Natalello, A.; Kaleda, A.; Brocca, S.; de Pascale, D.; Pucciarelli, S.; Miceli, C.; Braslavsky, I.; Lotti, M. Cryo-Protective Effect of an Ice-Binding Protein Derived from Antarctic Bacteria. *FEBS J.* **2017**, *284*, 163–177.
- (10) Drori, R.; Davies, P. L.; Braslavsky, I. When Are Antifreeze Proteins in Solution Essential for Ice Growth Inhibition? *Langmuir* **2015**, *31*, 5805–5811.

- (11) Park, K. S.; Do, H.; Lee, J. H.; Park, S. I.; Kim, E. jung; Kim, S.-J.; Kang, S.-H.; Kim, H. J. Characterization of the Ice-Binding Protein from Arctic Yeast *Leucosporium* Sp. AY30. *Cryobiology* **2012**, *64*, 286–296.
- (12) Middleton, A. J.; Marshall, C. B.; Faucher, F.; Bar-Dolev, M.; Braslavsky, I.; Campbell, R. L.; Walker, V. K.; Davies, P. L. Antifreeze Protein from Freeze-Tolerant Grass Has a Beta-Roll Fold with an Irregularly Structured Ice-Binding Site. *J. Mol. Biol.* **2012**, *416*, 713–724.
- (13) Bayer-Giraldi, M.; Sazaki, G.; Nagashima, K.; Kipfstuhl, S.; Vorontsov, D. A.; Furukawa, Y. Growth Suppression of Ice Crystal Basal Face in the Presence of a Moderate Ice-Binding Protein Does Not Confer Hyperactivity. *Proc. Natl. Acad. Sci. U. S. A.* **2018**, *115*, 7479–7484.
- (14) Hanada, Y.; Nishimiya, Y.; Miura, A.; Tsuda, S.; Kondo, H. Hyperactive Antifreeze Protein from an Antarctic Sea Ice Bacterium *Colwellia* Sp. Has a Compound Ice-Binding Site without Repetitive Sequences. *FEBS J.* **2014**, *281*, 3576–3590.
- (15) Davies, P. L.; Baardsnes, J.; Kuiper, M. J.; Walker, V. K. Structure and Function of Antifreeze Proteins. *Philos. Trans. R. Soc., B* **2002**, *357*, 927–935.
- (16) Pertaya, N.; Marshall, C. B.; Celik, Y.; Davies, P. L.; Braslavsky, I. Direct Visualization of Spruce Budworm Antifreeze Protein Interacting with Ice Crystals: Basal Plane Affinity Confers Hyperactivity. *Biophys. J.* **2008**, *95*, 333–341.
- (17) Drori, R.; Celik, Y.; Davies, P. L.; Braslavsky, I. Ice-Binding Proteins That Accumulate on Different Ice Crystal Planes Produce Distinct Thermal Hysteresis Dynamics. *J. R. Soc., Interface* **2014**, *11*, 20140526.
- (18) Wilson, P. W.; Beaglehole, D.; Devries, A. L. Antifreeze Glycopeptide Adsorption on Single Crystal Ice Surfaces Using Ellipsometry. *Biophys. J.* **1993**, *64*, 1878–1884.
- (19) Chapsky, L.; Rubinsky, B. Kinetics of Antifreeze Protein-Induced Ice Growth Inhibition. *FEBS Lett.* **1997**, *412*, 241–244.
- (20) Knight, C. A.; DeVries, A. L. Ice Growth in Supercooled Solutions of a Biological “Antifreeze”, AFGP 1–5: An Explanation in Terms of Adsorption Rate for the Concentration Dependence of the Freezing Point. *Phys. Chem. Chem. Phys.* **2009**, *11*, 5749–5761.
- (21) Takamichi, M.; Nishimiya, Y.; Miura, A.; Tsuda, S. Effect of Annealing Time of an Ice Crystal on the Activity of Type III Antifreeze Protein. *FEBS J.* **2007**, *274*, 6469–6476.
- (22) Bredow, M.; Tomalty, H. E.; Smith, L.; Walker, V. K. Ice and Anti-Nucleating Activities of an Ice-Binding Protein from the Annual Grass, *Brachypodium distachyon*. *Plant, Cell Environ.* **2018**, *41*, 983–992.
- (23) Bar-Dolev, M.; Celik, Y.; Wettlaufer, J. S.; Davies, P. L.; Braslavsky, I. New Insights into Ice Growth and Melting Modifications by Antifreeze Proteins. *J. R. Soc., Interface* **2012**, *9*, 3249–3259.
- (24) Tedeschi, G.; Mangiagalli, M.; Chmielewska, S.; Lotti, M.; Natalello, A.; Brocca, S. Aggregation Properties of a Disordered Protein Are Tunable by pH and Depend on Its Net Charge per Residue. *Biochim. Biophys. Acta, Gen. Subj.* **2017**, *1861*, 2543–2550.
- (25) Studier, F. W. Protein Production by Auto-Induction in High Density Shaking Cultures. *Protein Expression Purif.* **2005**, *41*, 207–234.
- (26) Braslavsky, I.; Drori, R. LabVIEW-Operated Novel Nanoliter Osmometer for Ice Binding Protein Investigations. *J. Visualized Exp.* **2013**, e4189.
- (27) Basu, K.; Garnham, C. P.; Nishimiya, Y.; Tsuda, S.; Braslavsky, I.; Davies, P. Determining the Ice-Binding Planes of Antifreeze Proteins by Fluorescence-Based Ice Plane Affinity. *J. Visualized Exp.* **2014**, e51185.
- (28) Knight, C. A.; Cheng, C. C.; DeVries, A. L. Adsorption of Alpha-Helical Antifreeze Peptides on Specific Ice Crystal Surface Planes. *Biophys. J.* **1991**, *59*, 409–418.
- (29) Petrenko, V. F.; Whitworth, R. W. *Physics of Ice*; Oxford University Press: New York, 2002.
- (30) Brumberg, A.; Hammonds, K.; Baker, I.; Backus, E. H. G.; Bisson, P. J.; Bonn, M.; Daghlian, C. P.; Mezger, M.; Shultz, M. J. Single-Crystal Ice Surfaces Unveil Connection between Macroscopic and Molecular Structure. *Proc. Natl. Acad. Sci. U. S. A.* **2017**, *114*, 5349–5354.
- (31) Haleva, L.; Celik, Y.; Bar-Dolev, M.; Pertaya-Braun, N.; Kaner, A.; Davies, P. L.; Braslavsky, I. Microfluidic Cold-Finger Device for the Investigation of Ice-Binding Proteins. *Biophys. J.* **2016**, *111*, 1143–1150.
- (32) Pertaya, N.; Marshall, C. B.; DiPrinzio, C. L.; Wilen, L.; Thomson, E. S.; Wettlaufer, J. S.; Davies, P. L.; Braslavsky, I. Fluorescence Microscopy Evidence for Quasi-Permanent Attachment of Antifreeze Proteins to Ice Surfaces. *Biophys. J.* **2007**, *92*, 3663–3673.
- (33) Celik, Y.; Drori, R.; Pertaya-Braun, N.; Altan, A.; Barton, T.; Bar-Dolev, M.; Groisman, A.; Davies, P. L.; Braslavsky, I. Microfluidic Experiments Reveal That Antifreeze Proteins Bound to Ice Crystals Suffice to Prevent Their Growth. *Proc. Natl. Acad. Sci. U. S. A.* **2013**, *110*, 1309–1314.
- (34) Ritchie, D. W.; Venkatraman, V. Ultra-Fast FFT Protein Docking on Graphics Processors. *Bioinformatics* **2010**, *26*, 2398–2405.
- (35) Lawrence, M. C.; Colman, P. M. Shape Complementarity at Protein/Protein Interfaces. *J. Mol. Biol.* **1993**, *234*, 946–950.
- (36) Winn, M. D.; Ballard, C. C.; Cowtan, K. D.; Dodson, E. J.; Emsley, P.; Evans, P. R.; Keegan, R. M.; Krissinel, E. B.; Leslie, A. G. W.; McCoy, A.; McNicholas, S. J.; Murshudov, G. N.; Pannu, N. S.; Potterton, E. A.; Powell, H. R.; Read, R. J.; Vagin, A.; Wilson, K. S. Overview of the CCP4 Suite and Current Developments. *Acta Crystallogr., Sect. D: Biol. Crystallogr.* **2011**, *67*, 235–242.
- (37) Do, H.; Kim, S.-J.; Kim, H. J.; Lee, J. H. Structure-Based Characterization and Antifreeze Properties of a Hyperactive Ice-Binding Protein from the Antarctic Bacterium *Flavobacterium frigidum* PS1. *Acta Crystallogr., Sect. D: Biol. Crystallogr.* **2014**, *70*, 1061–1073.
- (38) Vance, T. D. R.; Graham, L. A.; Davies, P. L. An Ice-Binding and Tandem Beta-Sandwich Domain-Containing Protein in *Shewanella frigidimarina* Is a Potential New Type of Ice Adhesin. *FEBS J.* **2018**, *285*, 1511–1527.
- (39) Lee, J. K.; Park, K. S.; Park, S.; Park, H.; Song, Y. H.; Kang, S.-H.; Kim, H. J. An Extracellular Ice-Binding Glycoprotein from an Arctic Psychrophilic Yeast. *Cryobiology* **2010**, *60*, 222–228.
- (40) Hoshino, T.; Kiriaki, M.; Ohgiya, S.; Fujiwara, M.; Kondo, H.; Nishimiya, Y.; Yumoto, I.; Tsuda, S. Antifreeze Proteins from Snow Mold Fungi. *Can. J. Bot.* **2003**, *81*, 1175–1181.
- (41) Kondo, H.; Hanada, Y.; Sugimoto, H.; Hoshino, T.; Garnham, C. P.; Davies, P. L.; Tsuda, S. Ice-Binding Site of Snow Mold Fungus Antifreeze Protein Deviates from Structural Regularity and High Conservation. *Proc. Natl. Acad. Sci. U. S. A.* **2012**, *109*, 9360–9365.
- (42) Garnham, C. P.; Nishimiya, Y.; Tsuda, S.; Davies, P. L. Engineering a Naturally Inactive Isoform of Type III Antifreeze Protein into One That Can Stop the Growth of Ice. *FEBS Lett.* **2012**, *586*, 3876–3881.
- (43) Mahatabuddin, S.; Hanada, Y.; Nishimiya, Y.; Miura, A.; Kondo, H.; Davies, P. L.; Tsuda, S. Concentration-Dependent Oligomerization of an Alpha-Helical Antifreeze Polypeptide Makes It Hyperactive. *Sci. Rep.* **2017**, *7*, 42501.
- (44) Meyer, K.; Keil, M.; Naldrett, M. J. A Leucine-Rich Repeat Protein of Carrot That Exhibits Antifreeze Activity. *FEBS Lett.* **1999**, *447*, 171–178.
- (45) Mahatabuddin, S.; Fukami, D.; Arai, T.; Nishimiya, Y.; Shimizu, R.; Shibazaki, C.; Kondo, H.; Adachi, M.; Tsuda, S. Polypentagonal Ice-like Water Networks Emerge Solely in an Activity-Improved Variant of Ice-Binding Protein. *Proc. Natl. Acad. Sci. U. S. A.* **2018**, *115*, 5456–5461.

SUPPORTING INFORMATION

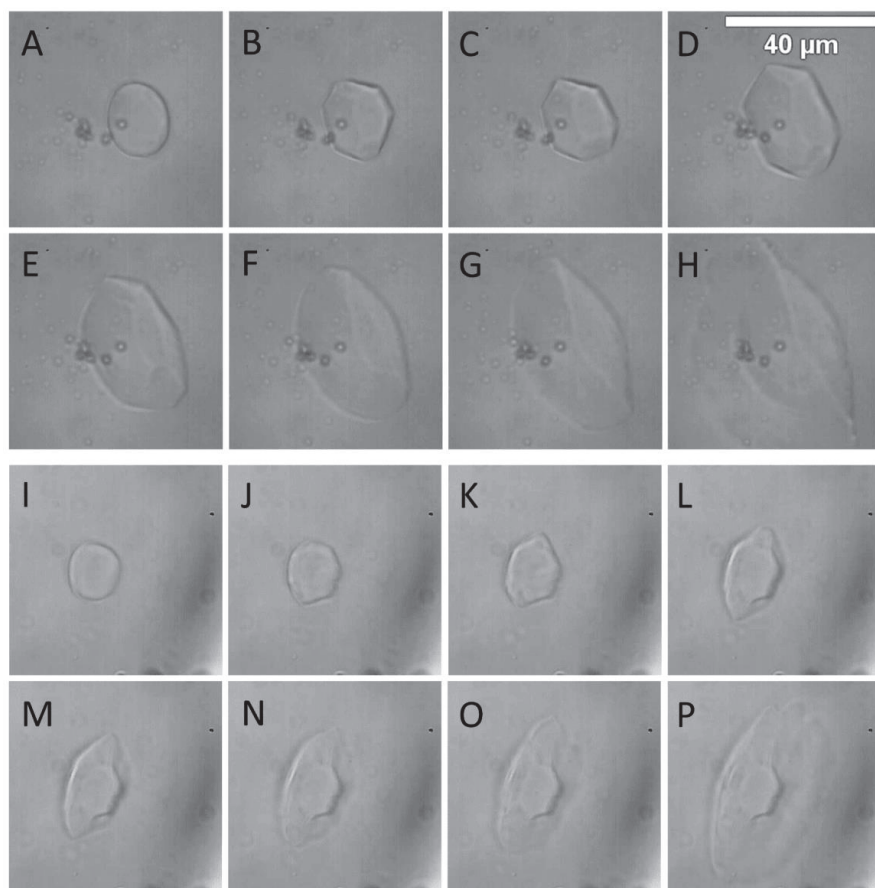


Figure S1. Ice crystal growth and burst in A-H) 10 μM *EfcIBP* and I-P) in 25 μM GFP-*EfcIBP*.

Letters indicate the sequence of frames.

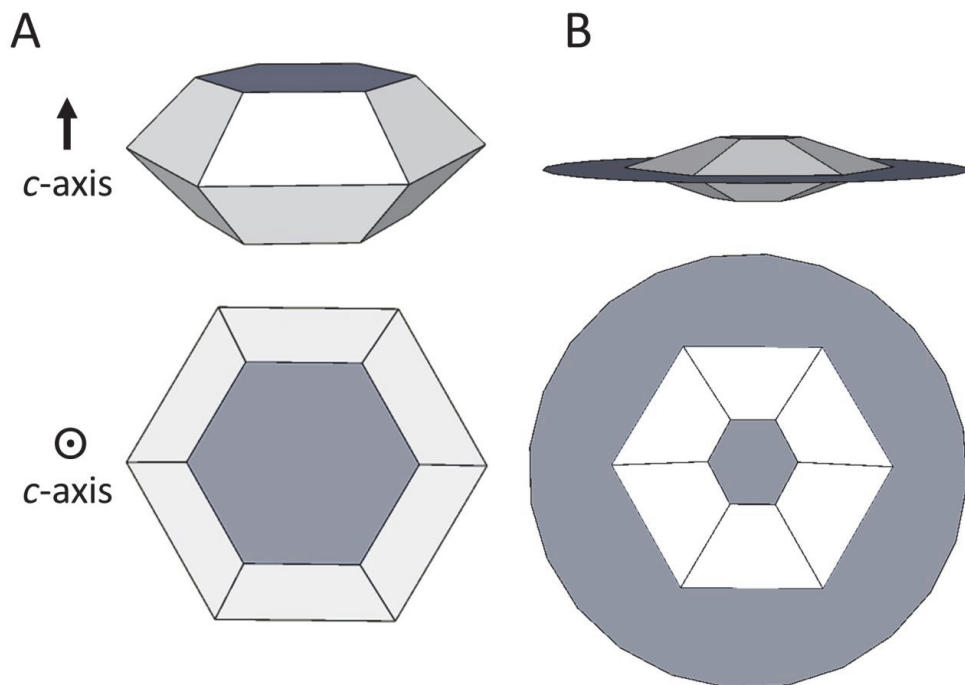


Figure S2. Models of ice crystal shapes formed in *Efc*IBP solutions. A) Hexagonal bistrustum, ice crystal shape formed by the T67Y mutant. B) A simplified model of Saturn-shaped burst perpendicular to the *c*-axis. For simplicity, the example is given for the T67Y mutant.

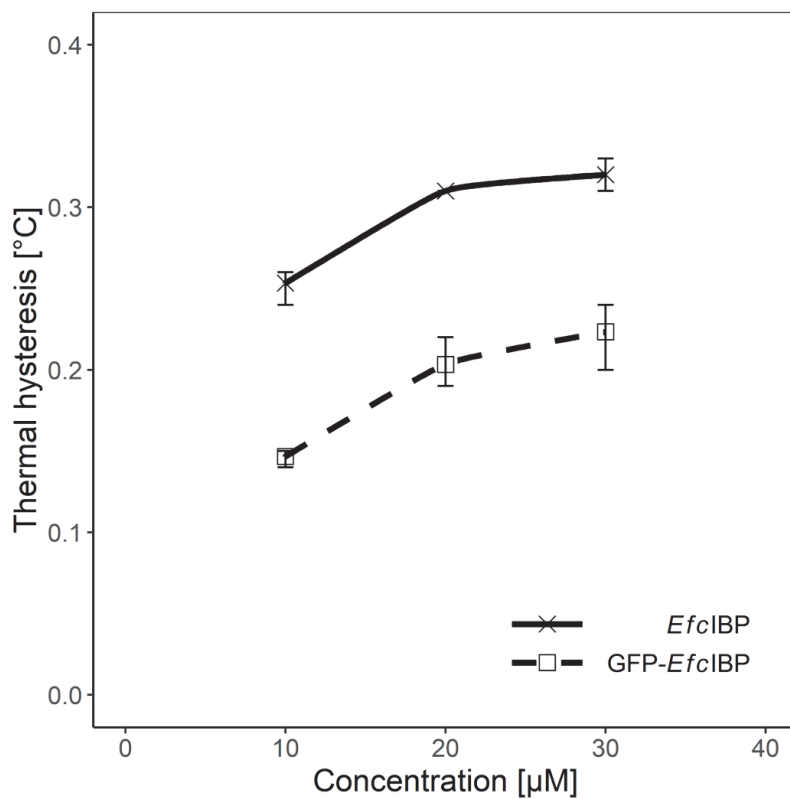


Figure S3. Thermal hysteresis activity of *EfcIBP* compared to GFP-*EfcIBP*. Each point presents the average of three independent measurements, with 95% confidence intervals.

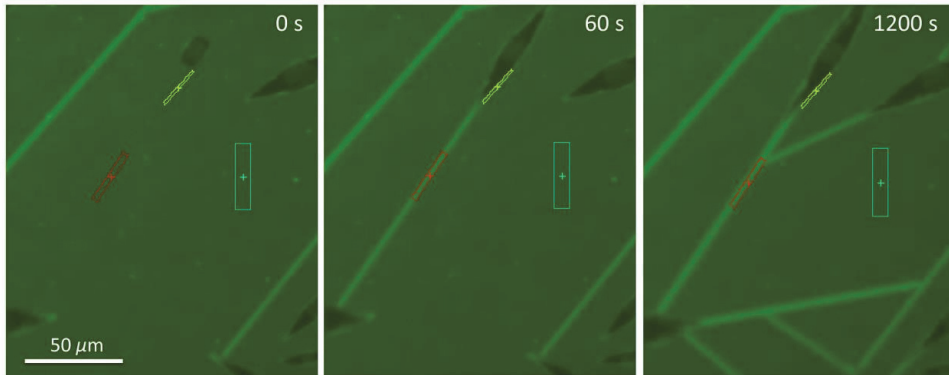


Figure S4. Wild type *EfcIBP* accumulation on ice crystals. Colored rectangles show areas of fluorescence intensity measurements: red - basal plane (truncated sheet), yellow - pyramidal plane (crystal side), cyan - background.

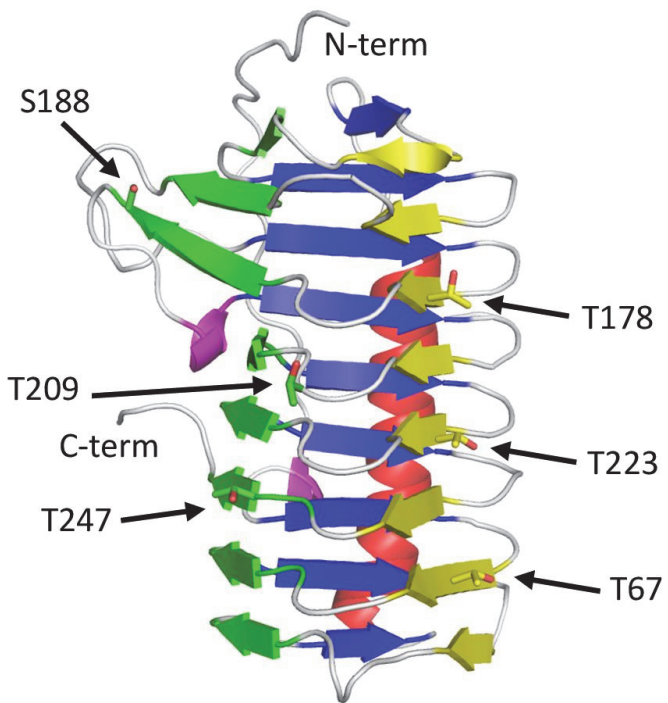


Figure S5. *EfcIBP* mutation sites. Mutated residues on the B (yellow) and C (green) faces of the *EfcIBP* structure are shown as sticks and indicated by arrows and labels.

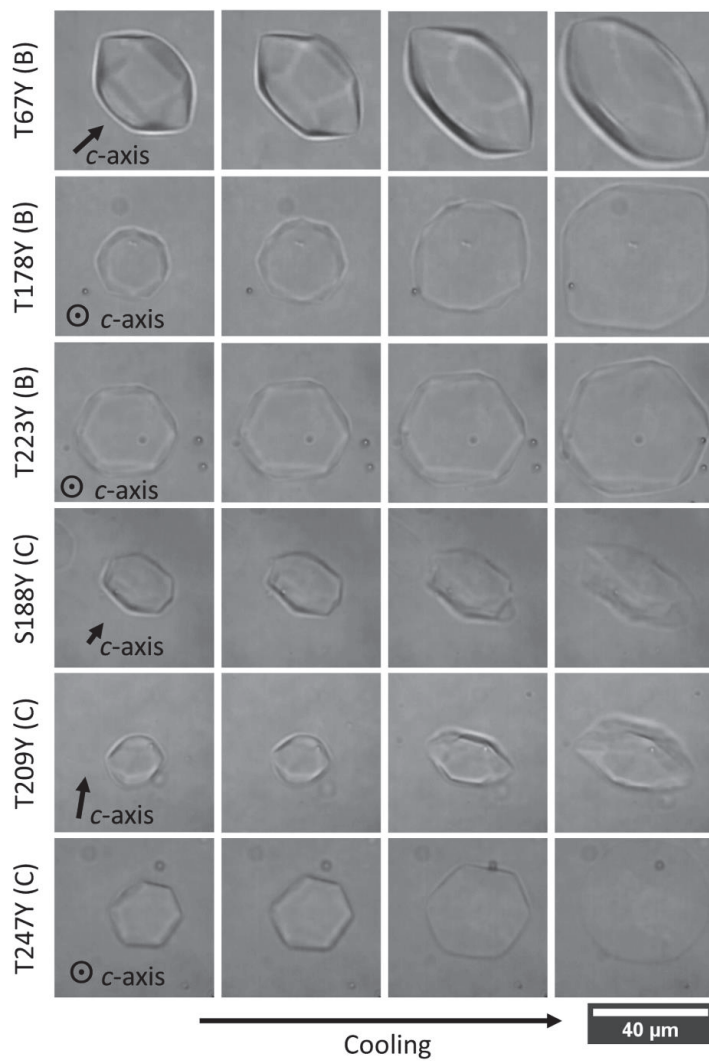


Figure S6. Ice crystal shapes and their growth pattern during cooling in solutions of *EfcIBP* mutants. The letter in parenthesis indicates the protein face that was mutated. T67Y, T178Y, T223Y, and T209Y are 10 μM; S188Y 3.3 μM; T247Y 50 μM. The circled dot indicates *c*-axis normal to the image plane.

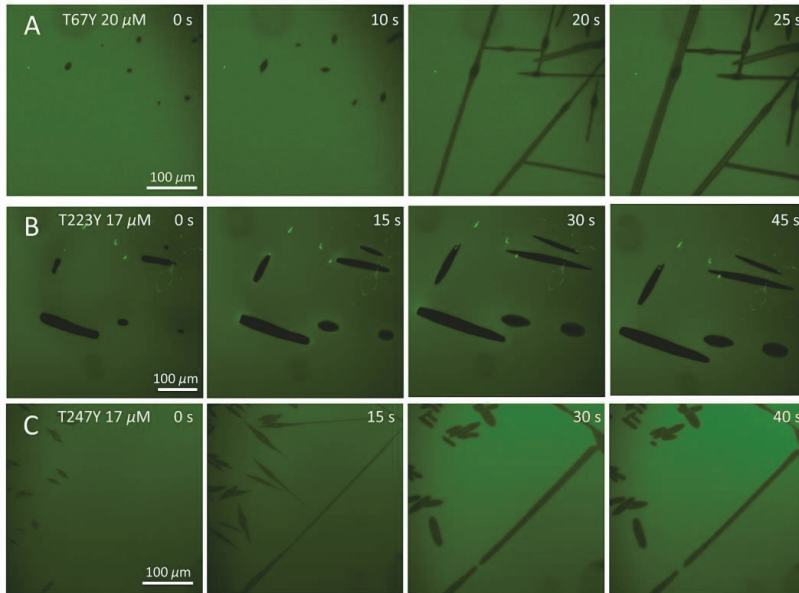


Figure S7. GFP-*EfcIBP* mutants growth and burst after cooling below the TH freezing point, as seen between two coverslips. After the burst, the temperature is held constant. A) GFP-T67Y mutant at 20 μM . B) GFP-T223Y mutant at 17 μM . C) GFP-T247Y mutant at 17 μM .

Movie S1. Ice crystal growth and burst in the wt *EfcIBP* 5 μM solution during cooling.

Movie S2. Ice crystals burst in 7.6 μM GFP-*EfcIBP* solution. A growing parallel ice sheet is blocked by a perpendicular ice sheet (tilted *a*-axis).

Movie S3. Single ice crystal in 10 μM GFP-*EfcIBP* grown in a microfluidic chip with a height of 40 μm . Photos were taken with a time interval of 0.3 seconds. The edge of the PDMS chip can be seen in the frame as curved lines around the ice crystal.

Appendix 4

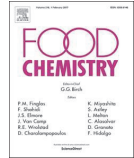
Publication IV

Kaleda, A., Tsanev, R., Klesment, T., Vilu, R., Laos, K. (2018). Ice cream structure modification by ice-binding proteins. *Food Chemistry*, 246, 164–171. doi:10.1016/j.foodchem.2017.10.152



Contents lists available at ScienceDirect

Food Chemistry

journal homepage: www.elsevier.com/locate/foodchem

Ice cream structure modification by ice-binding proteins



Aleksi Kaleda*, Robert Tsanev*, Tiina Klesment, Raivo Vilu, Katrin Laos

Department of Chemistry and Biotechnology, School of Science, Tallinn University of Technology, Ehitajate tee 5, 19086 Tallinn, Estonia
 Center of Food and Fermentation Technologies, Akadeemia tee 15A, 12618 Tallinn, Estonia

ARTICLE INFO

Keywords:

Ice-binding protein (antifreeze protein)
 Ice recrystallization inhibition
 Ice cream microstructure

ABSTRACT

Ice-binding proteins (IBPs), also known as antifreeze proteins, were added to ice cream to investigate their effect on structure and texture. Ice recrystallization inhibition was assessed in the ice cream mixes using a novel accelerated microscope assay and the ice cream microstructure was studied using an ice crystal dispersion method. It was found that adding recombinantly produced fish type III IBPs at a concentration 3 mg L^{-1} made ice cream hard and crystalline with improved shape preservation during melting. Ice creams made with IBPs (both from winter rye, and type III IBP) had aggregates of ice crystals that entrapped pockets of the ice cream mixture in a rigid network. Larger individual ice crystals and no entrapment in control ice creams was observed. Based on these results a model of ice crystals aggregates formation in the presence of IBPs was proposed.

1. Introduction

Ice cream is a complex frozen food system that contains proteins, crystallized fat and water, air, minerals, additives, and sweeteners. Concerning the ice phase, the ice crystal texture is strongly affected by the recrystallization phenomena, which depend principally on formulation factors, on freezing process and on storage temperature conditions (Donhowe & Hartel, 1996). Ice recrystallization is evidenced by an increase in mean size and width of the crystal size distribution. Large ice crystals are perceived as rough particles on the palate (Goff & Hartel, 2013) causing coarse mouthfeel.

One of the solutions to reduce ice crystal size and improve ice cream temperature stability is addition of ice-binding proteins (IBP), also known as antifreeze proteins (Griffith & Ewart, 1995; Regand & Goff, 2006). IBPs belong to a class of proteins capable of protecting organisms such as fish, insects, plants, terrestrial arthropods, fungi, and bacteria from damage in subzero environments (Buckley & Lillford, 2009; Duman, 2001). IBPs have a remarkable property of binding to ice crystals significantly reducing their size while simultaneously inhibiting recrystallization (Clarke, Buckley, & Lindner, 2002). Conventional stabilizers used in ice cream production are able to decrease recrystallization by lowering water mobility (Regand & Goff, 2003; Smith & Schwartzberg, 1985), however IBPs are more potent by orders of magnitude requiring very small amounts to inhibit recrystallization (Mangiagalli et al., 2017; Regand & Goff, 2003).

IBP type III acts as recrystallization inhibitor (Antson et al., 2001; Chao, Sönnichsen, DeLuca, Sykes, & Davies, 1994; Graether et al., 1999) and is approved by U. S. Food & Drug Administration (2013) and

European Food Safety Authority (2008) for human consumption in ice cream products as being a non-toxic, non allergenic ingredient. The protein was originally described in the arctic fish ocean pout functioning as an antifreeze that prevents ice crystals growth and freezing of the fish blood at subzero temperatures (Hew et al., 1988). It is a small globular peptide with molecular mass of 7.5 kDa. The protein exhibits a compact fold with a relatively large hydrophobic core, several short and irregular β sheets and one helical turn. The ice-binding site, which encompasses parts of the C-terminal sheet and a loop, is planar and relatively nonpolar. The specific spatial arrangement of the polar side-chain atoms of the putative ice-binding residues are Gln9, Asn14, Thr15, Thr18 and Gln44 (Sönnichsen, DeLuca, Davies, & Sykes, 1996).

IBPs from winter rye (*Secale cereale* L) have also been proposed for use in ice cream production as being more acceptable for consumers than the fish protein (Griffith, 2004). During cold acclimation of winter rye six pathogenesis-related IBPs accumulate together with ice nucleating proteins to protect the plant from cellular damages. Two of these IBPs are similar to endo- β -1,3-glucanases, two are similar to endochitinases and two are thaumatin-like proteins with size from 16 to 35 kDa (Hon, Griffith, Mlynarz, Kwok, & Yang, 1995).

The influence of IBPs on the ice cream structure is not clear with different results being reported. Some authors speculate that IBPs might be the key for higher quality ice cream (Feeney & Yeh, 1998; Regand & Goff, 2006; Wille, Vieira, De Kruijff, Floris, & Slangen, 2012), however others have reported that IBP ice cream has higher hardness and stiffness (Byass et al., 2004; Daniel, Hoddle, Jones, Oldroyd, & Singleton, 2007). Crilly (2007) and Goff, Regand, and Tharp (2002) hypothesize that ice recrystallization inhibition activity can be achieved at

* Corresponding authors at: Department of Chemistry and Biotechnology, School of Science, Tallinn University of Technology, Ehitajate tee 5, 19086 Tallinn, Estonia.
 E-mail address: robert.tsanev@ttu.ee (R. Tsanev).

concentrations below those that lead to ice crystal habit modification. Another critical point for smooth texture, as these authors emphasize, is ice cream formulation – the suitability between type and concentration of both stabilizer and IBP.

To the best of authors' knowledge, no reports have shown how the IBPs influence the microstructure of the ice cream. So the aim of the current study was to more thoroughly investigate the effect of IBPs on texture and microstructure of low-fat ice cream.

2. Materials and methods

2.1. Materials

Winter rye leaves (*Secale cereale*) of cultivar "Visello" were collected from a field in Estonia in November 2012, when average daily air temperature was +3 °C. Leaves were dried and stored at room temperature until extraction.

Ice cream mix was produced from fresh butter (Tere, Estonia), skimmed milk powder (E-Piim, Estonia), sucrose (Nordzucker Polska, Poland), polydextrose (Danisco, Denmark), maltodextrin (Tate & Lyle, Slovakia), glycerol monostearate (Danisco), locust bean gum (Danisco) and guar gum (Danisco). Alternatively locust bean gum and guar gum were replaced by commercial ice cream stabilizer Luxice 1005 (Cargill, France), containing carrageenan and guar gum mix.

Tryptone, yeast extract and acid hydrolysed casein were obtained from LabM (United Kingdom).

All other chemicals used in the investigation were of analytical grade and were purchased from Sigma-Aldrich Co. LLC.

2.2. Extraction of winter rye IBPs

Rye IBPs were extracted using a modified Hon, Griffith, Chong, and Yang (1994) method. Briefly, cold acclimated leaves were cut into 10 cm pieces, rinsed with distilled water, and then vacuum-infiltrated (Heidolph Laborota 4010, Germany) at 70 mbar with 20 mM CaCl₂ solution for 30 min to allow the extraction solution penetrate into apoplast, where rye IBPs are located. After that leaves were placed into sieves with liquid collectors and centrifuged (Hettich Zentrifugen Rotanta 420R, Germany) at 2000 × g at 4 °C for 20 min. Extracted liquid containing IBPs was collected, held for 20 min at 75 °C and centrifuged at 21,000 × g for 10 min at 4 °C to precipitate unrelated proteins. The supernatant was then lyophilized (Heto PowerDry PL3000, Czech Republic) and stored at –20 °C. Total protein content in extract was determined in two replicates by Kjeldahl method (DK 8 Heating Digester and UDK 142 Automatic Distillation Unit, Velp Scientifica) according to manufacturer instruction guide. Lyophilized extract yield was 2.8% (w/w). The extract contained 16.4% (w/w) proteins, with other components being soluble polysaccharides and salts from extraction procedure.

2.3. Expression of recombinant type III IBP in *E. coli*

The gene encoding for type III IBP, also named antifreeze protein HPLC12 or QAE, was constructed based on the native protein sequence (PIR A30839) with two exceptions. An initiating methionine was added to express the protein and the C-terminal sequence was replaced from YPPA to YAAKDEL to improve the protein solubility (Sönnichsen et al., 1996). The most frequently used codons for *E. coli* were used to maximize the protein yield. The constructed gene was ordered from GeneArt (Thermo Fisher Scientific) and transferred into pET11C protein expression vector (Invitrogen, Carlsbad, CA, US). The prepared construct was transformed into a protein producing strain *E. coli* (BL 21). Bacteria cultivations were performed in 1.25 L Biobundle bioreactor (Applikon, Schiedam, the Netherlands) controlled by Applikon EZ-control bioreactor together with BioXpert XP software (Applikon). The fermentations were carried out at 37 °C, pH 7 at an agitation speed

of stirrer 700 rpm in a fed-batch mode. During the batch phase the bacteria grew in LB medium, supplemented with ampicillin. A chemically defined media, modified from Nahku et al. (2010), containing glucose 10 g·L⁻¹, MgSO₄ 1 g·L⁻¹, (NH₄)₂SO₄ 8.6 g·L⁻¹, K₂HPO₄ 4 g·L⁻¹, acid hydrolysed casein 5 g·L⁻¹, minerals (FeSO₄ 5 mg·L⁻¹, MnSO₄ 2 mg·L⁻¹, CaCl₂ 5 mg·L⁻¹, ZnSO₄ 2 mg·L⁻¹, CoSO₄ 0.4 mg·L⁻¹, CuSO₄ 0.5 mg·L⁻¹, (NH₄)₆Mo₇O₂₄ mg·L⁻¹ dissolved in 5 M HCl), ampicillin and antifoam was used during the fed-batch phase of cultivation. The growth rate during fed-batch was maintained at 0.3 h⁻¹, the growth rate decreased after the induction of protein synthesis. IBP expression was induced at OD₆₀₀ 6 for four hours. The biomass was collected by centrifugation (Hettich Zentrifugen Rotanta 420R, Germany) at 2000 × g for ten minutes at 4 °C. Biomass was stored at –80 °C until use. After thawing the bacterial cells were dissolved in five mass volumes of milliQ water. For obtaining the IBP, cells were disrupted by incubating with lysozyme at 0.1 mg·mL⁻¹ final concentration, at room temperature for one hour. After that the cell lysate was sonicated on a ice water bath for two minutes at maximum power with cycles of five seconds on and fifteen seconds off (Sonics Vibra cell, VCX130, Sonics & Materials, CT, US). After sonication the solution was frozen again at –20 °C overnight. On the following morning the frozen solution was thawed and sonicated with the same indicated parameters. The solution was clarified by centrifugation at 11,000 × g for fifteen minutes at 4 °C (Hettich Zentrifugen Rotanta 460R, Germany). The supernatant containing soluble IBP was stored at –20 °C until used. The concentration of IBP in the sample was determined on tricine-SDS gels (Schägger, 2006) by comparing the dilution series of probe to that of lysozyme. The gels were analyzed with ImageQuant software (Amersham Bioscience, United Kingdom). The total production yield was 40 mg of IBP per g of wet biomass. This amount was distributed equally as to 20 mg in the soluble fraction and 20 mg as inclusion bodies.

2.4. Preparation of ice cream

A low-fat dairy ice cream was used in the experiments. The recipe was adapted from Bramley, Gray, Turan, Spors, and Frisch (2011). The ice cream consisted of 0.5% milk fat, 11.5% milk solids non fat, 29.4% carbohydrates, 0.15% emulsifier and 0.2% stabilizer. Dry components were measured together and carefully mixed to homogeneity with a small amount of water to avoid clumps. Remaining liquid components were added after that. The ice cream mix was heated to 65 °C and homogenized with a two stage homogenizer (Gea Niro Soavi, Italy) at the homogenization pressure of 12 MPa on the first stage and 28 MPa on the second stage according to a local ice cream manufacturer instruction. After that the mix was pasteurised at 85 °C and left to cool and ripen overnight at 4 °C. IBPs were added into the mix before freezing: *E. coli* extract containing type III IBP up to concentration 35 mg·L⁻¹ of IBP, and 65 mg·L⁻¹ of winter rye extract total protein (400 mg·L⁻¹ lyophilized extract dry weight). The ice cream mixes were frozen using a freezer (Armfield FT-25-BA, UK) at a set draw temperature –5 °C and packed into 300 mL containers. The ice cream was hardened at –40 °C for 24 h and afterwards stored at –18 °C. Ice cream without IBP was marked as control ice cream.

2.5. Measurement of ice recrystallization inhibition in ice cream mixes

Ice recrystallization inhibition (IRI) was determined by a modified sucrose sandwich assay described by Regand and Goff (2005). A 3 µL drop of ice cream mix (35% dry solids) containing different concentrations of IBPs was placed between microscope slide and 18 mm square cover slip and sealed with silicone oil to prevent evaporation. Sample was flash frozen in liquid nitrogen and placed onto a cold stage (Linkam PE120, UK) mounted on a microscope (Nikon Eclipse E200-LED, Japan). A drop of cold ethanol was placed on top of the sample to prevent condensation. Cold stage temperature at the beginning of experiment was ~1 °C and it was programmed to change temperature in 6

Table 1
Temperature fluctuation program of the microscope cold stage used to assess the ice recrystallization inhibition.

Step	Hold temperature, °C	Hold time, s	Temperature change speed, °Cmin ⁻¹
1	-10.0	30	20
2	-6.4	15	10
3	-9.0	15	10
4	-6.8	60	10
5	-8.0	5	10
6	-6.8	180	10

steps (Table 1). The temperatures were experimentally selected to be close to melting temperature of the sucrose solution to maintain a large population of small separate ice crystals and to increase recrystallization speed. Two photos of crystals were made at the end of steps 4 and 6, with 200 s total time in between the photos. Photos were automatically analyzed with a macro written for Fiji program (public domain software) and mean radius of ice crystals was calculated. The strategy for crystal detection was segmentation of crystal apparent edges by color threshold, removal of air bubbles using filtering by local thickness (air bubbles have wider visual edges) and detection of circular objects. An example of typical microscope image and its segmented counterpart is presented in Supplementary materials (Fig. S1). At least 8000 crystals were measured in each photo. The IRI was calculated as described by Budke, Heggemann, Koch, Sewald, and Koop (2009). Mean cubic radius of ice crystals was plotted against time and the slope of the line was taken as recrystallization rate constant (k_d). Average recrystallization rates of at least two replicates per point were plotted against concentration and a sigmoidal curve given by Budke et al. (2009) was fitted. The inflection point of the curve (C_i) represents IBP concentration that inhibits ice recrystallization by 50%.

2.6. Visualization of ice crystal aggregates from ice cream

Ice crystals aggregates were visualized using polarized light microscopy (Nikon Eclipse E200-LED, Japan). The method was elaborated from the one used by Ndoye and Alvarez (2015). Sample preparation and microscopy were performed entirely in a cold chamber at temperature $-18\text{ }^{\circ}\text{C}$ to avoid temperature fluctuations and crystal melting. Tiny ice cream piece was resuspended in 100 μL of silicone oil ($-18\text{ }^{\circ}\text{C}$) in a test tube and vortexed for 10 s. A drop of suspension was pressed between microscope slide and cover slip. The sample was then placed on a microscope cold stage holding the temperature at $-18\text{ }^{\circ}\text{C}$ and a drop of ethanol was placed on top of cover slip to prevent condensation. Photos were analyzed with Fiji software, aggregate area, aggregate mean RGB color and image background mean RGB color were recorded. Background color was subtracted from aggregate color and result converted to Lab color space to calculate Euclidean distance to color brown (RGB 150, 75, 0).

2.7. Analysis of ice cream hardness

Type III IBP ice cream hardness was determined by a penetration test with a TA.XT2i texture analyser (Stable Micro Systems, United Kingdom). The procedure was elaborated from Varela, Pintor, and Fiszman (2014). Each sample container ($4 \times 6 \times 10\text{ cm}$) was taken out of the freezer ($-18\text{ }^{\circ}\text{C}$) and tested at room temperature ($+21\text{ }^{\circ}\text{C}$) exactly after 10 min. The samples were penetrated to a depth of 15 mm with a 3-mm diameter cylindrical probe at a speed of 2 mm s^{-1} . The maximum applied force (N) was used as a measure of hardness.

2.8. Sensory analysis

A trained panel of seven ice cream assessors evaluated ice cream

samples containing extract from winter rye (65 mg L^{-1} of total protein) comparing it to the same ice cream without rye extract. Ice cream stabilizers were locust bean gum and guar gum. The trained panelists had at least 2 years of experience and attended several times the ice cream sensory test done periodically by the department.

Sensory analysis was based on the Bodyfelt, Tobias, and Trout (1988) and Guinard et al. (1997) methods. Samples were divided as separate portions in 30 mL plastic cups and were assessed in duplicate. The samples were coded and their order randomized. Ice cream samples were prepared and stored at $-18\text{ }^{\circ}\text{C}$, before evaluation the samples were let at room temperature for 5 min. The experts were asked to assess the ice cream sweetness, roughness and friability in a scale from 0 to 15, with score fifteen for very sweet, friable or rough ice cream.

2.9. Ice cream melting

Control and type III IBP (3 mg L^{-1}) ice creams were cut into blocks of equal weight and immediately transferred onto metal sieves with 1 mm opening. Generic webcams were placed in front of the samples and photos were made at regular intervals. Experiment was performed at room temperature $+21\text{ }^{\circ}\text{C}$ and samples were held for 2.5 h to ensure complete melting. Two replicates were made. Photos were processed in Fiji software and relative sample height was calculated.

2.10. Statistical analysis

All statistical analysis was performed in R 3.4.0 Statistical Software (Foundation for Statistical Computing, Vienna, Austria).

Curve fitting for ice recrystallization inhibition assessment was performed by non-linear regression with brute force in R “nlstools” 0.2 package and 95% profile likelihood confidence interval for the C_i point was calculated using “nlstools” 1.0–2 R package. Mean k_d value of 5 replicates of ice cream mix without IBP was used in curve fitting as a growth limiting rate constant for vanishing protein concentration.

Crystal aggregate size measurement was performed in 4 replicates. For each ice cream sample 40 pictures were made, from which at least 450 crystal aggregates were analyzed to determine aggregate median Feret (maximum caliper) diameter.

Hardness test was performed 8 times in different areas of the same ice cream sample and mean hardness was calculated.

Sensory analysis mean values and 95% confidence intervals were calculated by nonparametric bootstrapping method from R package “Hmisc” 4.0-2 using 1000 resamples.

3. Results and discussion

3.1. Ice recrystallization inhibition activity

Ice recrystallization inhibition (IRI) activity in ice cream mixes was measured to confirm that winter rye extract and *E. coli* extract contain active IBPs. Recrystallization rate constants were plotted against concentration and sigmoid curves proposed by Budke et al. (2009) were fitted for both samples (Fig. 1). Given that winter rye extract contains several IBPs (Yu, Griffith, & Wiseman, 2001) total protein concentration (16.4% (w/w) in extract) was used for fitting. Both samples exhibit ice recrystallization inhibition activity. The curve inflection points (C_i) that represent 50% IRI were $0.17 \pm 0.06\text{ mg mL}^{-1}$ for winter rye extract and $0.10 \pm 0.06\text{ }\mu\text{g mL}^{-1}$ ($0.013 \pm 0.008\text{ }\mu\text{M}$) for recombinant type III fish IBP. No previous measurements of winter rye extract IRI activity, reported in the literature are available. However, C_i for type III protein in sucrose solution has been measured as $4 \pm 2\text{ }\mu\text{M}$ (Olijve, Oude Vrielink, & Voets, 2016), $5.9\text{ }\mu\text{M}$ (Olijve, Meister et al., 2016) and $0.05 \pm 0.02\text{ }\mu\text{M}$ (Mangiagalli et al., 2017). In this work IRI was measured in ice cream mix that can explain higher activity of type III IBP compared to other works. IBP molecules migrate from the ice cream mix to the crystal interface and then diffuse around the ice crystal

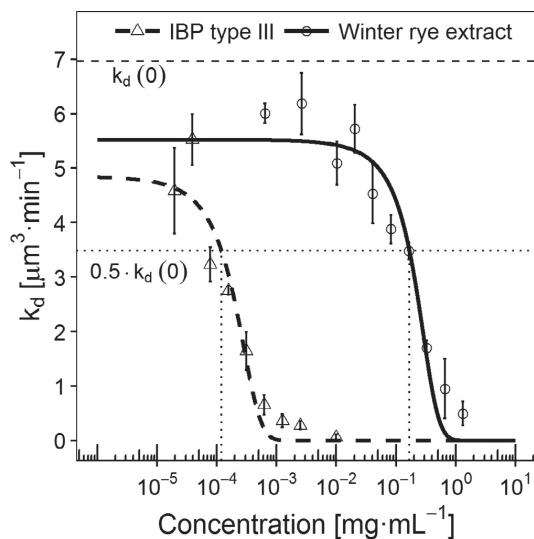


Fig. 1. Ice recrystallization rate in ice cream mixtures as a function of the content of winter rye extract or type III IBP. Standard deviations are shown ($n = 2$). The horizontal dashed line $k_d(0)$ represents the recrystallization rate of an ice cream mix without IBP. Dotted lines point to protein concentrations that inhibit ice recrystallization rate by 50%.

surface to find an appropriate binding location. Simultaneously, other molecules in the ice cream mix (sugars, other proteins, polysaccharides, salts, etc.) must diffuse to allow IBP adsorption. During ice recrystallization IBPs remain localized in the surroundings of the ice-water interface due to the reduction of molecular mobility because of the addition of the stabilizer (Regand & Goff, 2006).

The accelerated IRI method used in this work does not follow the constraints imposed by the Budke's method (Budke et al., 2009), such as low total ice fraction, ice crystals far from each other, constant recrystallization temperature and 2 h experimental time to observe the inhibitor limited recrystallization. However, in-lab experiments with winter rye and winter wheat extracts, fish IBPs type I, II, III and glycoproteins suggest that accelerated method is suitable not only for simple detection of IRI, but also for quantitative evaluation of activity. The main advantage of this method is that it is significantly faster compared to Budke's method, providing final result in a matter of couple of hours rather than few days. Easy sample preparation, simple equipment, automated image analysis and report generation reduce workload even more, thus making the accelerated IRI method a better tool for IBP routine analysis.

The sigmoid curve of IRI activity (Fig. 1) contains the three classical elements of concentration dependent activity profile. Namely, an initial straight line of non detectable activity with IBP concentration up to 10^{-5} mg·mL⁻¹ and 10^{-2} mg·mL⁻¹, for type III and winter rye, respectively. This straight line is followed by an exponential growth of IRI activity with the rise of IBP concentration. The increase of inhibition activity means a decrease of recrystallization speed and hence the sigmoid curve decline seen in Fig. 1. For type III this range is within concentrations from $5 \cdot 10^{-5}$ to 10^{-3} mg·mL⁻¹. For winter rye, 10^{-2} to 10^0 mg·mL⁻¹. And the last, third element of the sigmoid curve is a saturation region, again a straight line where the rise in IBP concentration does not result in any additional increase of IRI activity.

The experimental ice creams made in this study contained a range of IBP type III concentrations starting from $3 \cdot 10^{-3}$ mg·mL⁻¹ up to $3.5 \cdot 10^{-2}$ mg·mL⁻¹. This concentration range was based on Unilever patents, which claim to use $5\text{--}50 \cdot 10^{-3}$ mg·mL⁻¹ (Daniel et al., 2007; Darling & Hoddle, 2001). With the tested concentrations a maximum

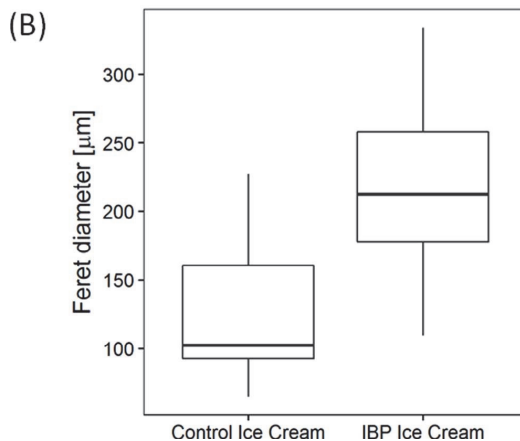
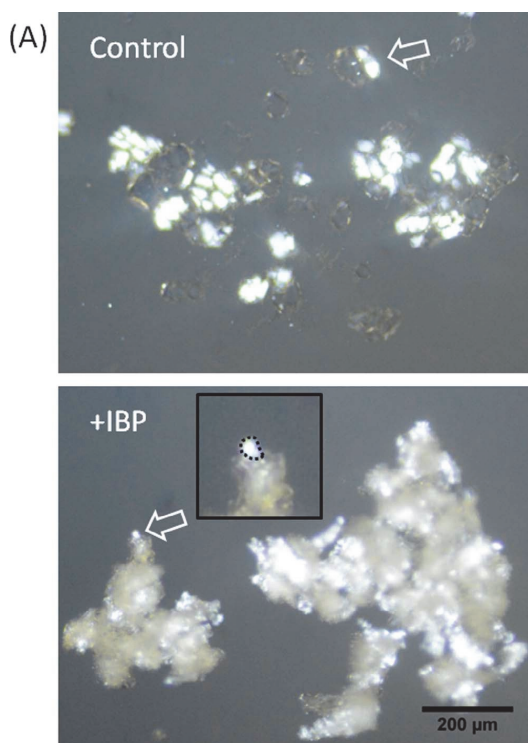


Fig. 2. (A) Representative polarized light images of ice crystal aggregates from control ice cream and ice cream containing type III IBP ($35 \text{ mg} \cdot \text{L}^{-1}$). The arrows indicate singular ice crystals. (B) The crystal aggregate size distribution as measured from polarized light images. Distribution of the central 50% of the data is outlined in a box. The horizontal line within the box represents the median aggregate size. Whiskers extend to the minimum and maximum size of ice aggregates. At least 450 aggregates were measured for each ice cream.

IRI activity was achieved. The concentration points possess in the region of saturated IRI activity (Fig. 1). The ice cream made with winter rye extract contained IBPs with concentration of $6.5 \cdot 10^{-2}$ mg·mL⁻¹ of total protein. This concentration is just at the beginning of measurable

IRI functionality, below 50% ice recrystallization inhibition activity point, in a region of transition from non detectable to exponentially growing activity (Fig. 1). This point was chosen based on speculations by Goff et al. (2002), that lower IBP concentrations could inhibit recrystallization while not affecting crystal morphology.

3.2. Ice cream microstructure

Microstructure of the ice creams was investigated to reveal the impact of IBP addition on the size of ice crystals. Representative pictures of the obtained ice crystals are shown in Fig. 2A (high resolution pictures are provided in Supplementary materials, Fig. S5, S6). The IBP ice cream contained 35 mg·L⁻¹ type III protein. Under polarized light the ice crystals are seen in white or black color depending on their polarization angle. On the picture of the control ice cream black ice crystals are detectable owing to their lighter edges. However, the ice crystals from IBP ice cream are much different. They differ in their size and organization. The individual ice crystals of the IBP ice cream are, as expected, smaller relative to the control because the IBP inhibited crystal growth rate. More interestingly, these smaller crystals are gathered up in a markedly bigger conglomerates observed in all tested IBP ice creams. Differently, the ice crystals from the control ice cream are presented as separate crystals or gathered in small groups (Fig. 2A). The dimensions of ice crystal aggregates from all measurements are summarized in Fig. 2B. The median Feret (maximum caliper) diameter of IBP crystal aggregates is 210 μm, being two times that of the control, 100 μm. These aggregates are fragments of the ice phase within the ice cream. The fact that addition of IBP to ice cream increases the agglomerate sizes suggests that IBP force ice crystals to connect tightly to one another forming a network-type structure. This has been noted also by Regand and Goff (2006) with IBPs from winter wheat. The study was performed on ice cream solutions observing crystals accretion in presence of IBP and formation of a network-type structures. However, little is known about ice organization within the ice cream in the presence of IBP. Clarke (2012) showed on a microtome slices of ice cream that the ice is organized as continuous phase within an IBP ice cream and as discontinuous within the control ice cream. These observations together with the present data strongly suggest that IBP induces aggregation of ice crystals into a network-type organized ice phase in ice cream.

Study of images of IBP-induced ice aggregates shows that these aggregates have more than one plane of focus. On the contrary, control ice crystals are observed within a single plane of focus without extending out of it (Fig. 2A). On polarized light microscope images, the ice cream matrix produces a different color as compared to ice crystals, therefore, entrapment of ice cream matrix within aggregates results in change of aggregate color relative to control crystals. For images of IBP ice aggregates an increase of 17% of mean signal in the red channel and 7% in green channel was detected together with 5% decrease in blue channel relative to images of control crystals. The color of IBP ice aggregates is detectably different appearing more brownish compared to control ice crystals that are more bluer. This indicates that ice cream matrix is present within IBP ice aggregates favoring the model of matrix phase being fragmented and ice phase probably being continuous as shown also by Clarke (2012). On the other hand, it is also possible that the shift of aggregates color is caused by different light refraction from the much smaller IBP ice crystals compared to refraction of the bigger ice crystals from the control ice cream. But in this case the color would be scattered throughout the whole spectrum and not be summed up as a distinct color change. As an apparent color difference was detected for the IBP ice crystals relative to control crystals, the latter possibility is not likely. The color change is a microscopy method phenomenon, not resulting in color difference of the ice cream. If the IBP ice crystal aggregates are filled with ice cream matrix then the bigger aggregates should enclose more matrix and respectively be more brownish. Indeed, such a size to color correlation was found (Fig. S2). The bigger aggregates were browner than the smaller ones indicating more matrix

containment within the bigger aggregates. Correlation of color to size was weak for the control crystals, supporting the conclusion made.

Different stabilizers were tested in altering the IBP effect on ice crystal aggregation. Stabilizers are polysaccharides capable of sequestering water into their big molecules. In this way the stabilizers unify the water distribution within the ice cream. A commercial stabilizer (Luxice 1005) was selected. Using this in the presence of IBP (35 mg·L⁻¹) reduced the size of ice aggregates to 140 μm median diameter (Fig. S3). This is substantial decrease in size, compared to 210 μm median diameter (Fig. 2B), when locust bean gum together with guar gum is used as a stabilizer. However, despite the size decrease, the aggregation process is still present. The amelioration effect Luxice 1005 had on the structure of IBP ice cream was at IBP concentration where a maximum IRI activity is observed, the region of saturated IRI functionality (Fig. 1). For production of ice cream with smooth texture without crystal aggregation, potentially most interesting are the concentrations of IBP lying at the beginning of detectable IRI functionality (Fig. 1). In combination with an appropriate stabilizer, it remains to be seen whether the stabilizer can have an additive effect on IBP to achieve optimal IRI activity where ice crystals are small but not connected to each other.

Altogether, these results favor a model for ice cream organization where addition of IBP leads to the formation of smaller ice crystals that aggregate and encapsulate ice cream matrix in small pockets.

3.3. A model of IBP binding in ice cream

Based on the images of IBP ice aggregates a potential model for formation of network-type ice phase within IBP ice cream is proposed. The geometry of IBP ice aggregates is spheric-like. This geometry indicates that the contacts between individual ice crystals are likely to be established from many plane faces of the crystals. In opposite to contact formation by crystal tip-to-tip connections in which case an elongated aggregates are to be expected.

On a crystal surface the bound IBP molecule prevents further ice growth at that place (Knight, Cheng, & DeVries, 1991). However, between the IBP molecules the ice is still growing, leading to formation of a tiny bud, illustrated in Fig. 3. The bud's width is fixed by IBPs that are located on its sides. With ice development the surface will become increasingly curvy, this renders the bud thermodynamically unstable being the first place where melting starts. When two buds from adjacent crystals happened to be in a close proximity to one another, a possible stabilization by fusion is likely to take place. This process results in

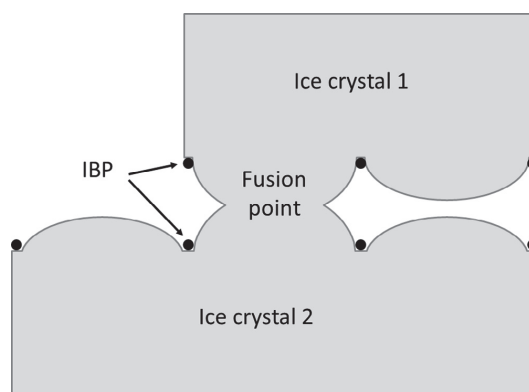


Fig. 3. Schematic representation of the proposed mechanism of how ice crystals fuse in the presence of IBPs. The outline is a fragment of the interface between two ice crystals. Ice crystals are depicted in gray. The black dots represent ice bound IBPs. Curved areas feature the sites of ice accretion and the place of connection between two curvatures is where the crystals fuse.

formation of a bridge between the two crystals and can be thought as accretion recrystallization. However its advancement is limited by bound IBPs and does not progress to complete crystal joining and rounding. In this way adjacent crystals are connected to one another eventually forming a randomly organized network-type ice phase within the IBP ice cream. Such network-organized ice phase might serve as an internal stabilizer of the ice cream shape. In the case of control ice cream, ice phase is not organized as an internal skeleton, ice crystals are separated from each other so that the ice phase is not a support for the matrix phase.

3.4. Hardness of ice cream

If the observed ice aggregates are organized in a continuous network-type ice phase this network would serve as an internal skeleton within the ice cream altering the structure to become harder. Hardness analysis was performed to evaluate the effect of IBP addition on the texture of the ice cream. Unilever patents declare use of type III IBP in ice cream products at concentrations 5–50 mg·L⁻¹ (Daniel et al., 2007; Darling & Hoddle, 2001). Considering this, ice creams containing 3–25 mg·L⁻¹ of fish type III IBP were tested in this work. Locust bean gum and guar gum were used as stabilizers. The results of the test shown in Fig. 4 reveal a remarkable relationship between IBP concentration and ice cream hardness. The maximum force required to penetrate the probe into control ice cream is about 5 N, but addition of IBP as little as 3 mg·L⁻¹ makes ice cream five times harder (24 N), at 25 mg·L⁻¹ ice cream hardness reaches 64 N. The hardness plot shows saturation dynamic at concentrations higher than 10 mg·L⁻¹. Other tested sources of IBPs (winter wheat, winter rye, fish types I, II, III, fish glycoprotein) also resulted in a hard ice cream (data not shown). This uncovers that the ice phase organizing property is not limited only to the type III IBP but is a wider phenomenon concerning more if not all IBPs. These results are consistent with Daniel, Hoddle, Jones, Oldroyd, and Singleton (2003) work where addition of 5 mg·L⁻¹ type III fish IBP into un-aerated water ice confectionary resulted in increased hardness. Here, the softest IBP ice cream contained the least amount of protein (3 mg·L⁻¹). But already that concentration has a saturated IRI activity (Fig. 1). It has been speculated that recrystallization inhibition can occur at lower concentrations than those leading to crystal aggregation

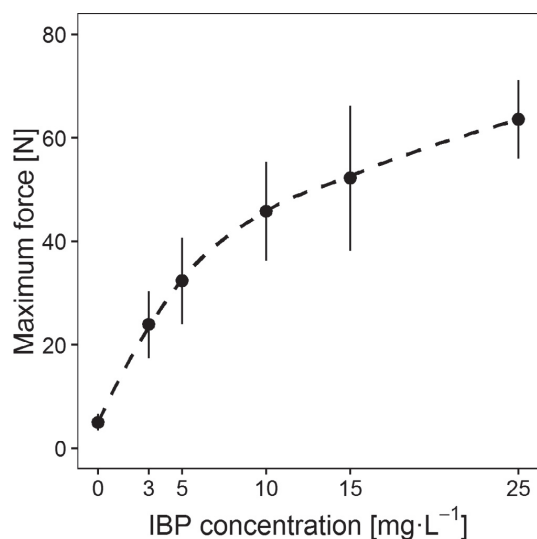


Fig. 4. Hardness of ice cream containing type III IBP. Control ice cream has 0 mg·L⁻¹ IBP. Standard deviations are shown (n = 8).

(Crilly, 2007; Goff et al., 2002). Extrapolating the results presented in Fig. 4, predicts that the ice cream would have been softer by using lower amounts of IBP. This remains to be explored in further investigations.

Each ice cream was tested in 8 different places of the same sample. All IBP ice creams showed higher variability compared to control ice cream, which is probably caused by non-uniform consistency of the samples and uneven distribution of ice aggregates within the ice cream. The difference of IBP ice cream texture from control ice cream was already noticed during freezing process. Fresh ice cream that comes out of the freezer is a continuous extruded cylinder that is packed into a container. The IBP ice cream retains its cylinder structure in the sample container with harder areas inside the cylinders and softer disconnected areas in between. In other words, IBP ice cream did not form continuous uniform mass during ice cream collection into the container. This also confirms that the unique IBP ice cream texture forms immediately inside the freezer and not later during storage.

3.5. Ice cream melting

IBP ice cream was tested for whether it is better in preserving its pregiven shape. To this end, a melting test was performed. Since the IBP alters significantly the ice cream texture, the lowest concentration of IBP was explored for any benefit to the ice cream shape. At the beginning, the samples melted at equal rate. After thirty minutes, the difference between the samples become apparent. After ninety minutes, the control sample was melted to a 47% of its initial height contrary to the IBP ice cream that has preserved 72% of its initial height. Thus, the hypothesis is that within the IBP ice cream the continuously organized ice phase provides an inner support for the ice cream. After two hours both samples melted equally to 30% and 33% of initial height for control and IBP ice cream respectively (Fig. S4). The equal end point of melting was to be expected because the difference in ice phase organization was the only cause for the melting discrepancy between the two ice cream types and that ice phase eventually melted irrespectively of its arrangement.

3.6. Sensory analysis

Instrumental texture analysis of IBP ice cream had revealed that this ice cream is harder than the control ice cream. To investigate whether the altered texture results also in a different mouthfeel, a sensory analysis was performed. For this an ice cream containing IBPs derived from winter rye was used. The recombinant type III IBP was not applied because of the protein expression host. European Food Safety Authority does not regard *E. coli* as a safe organism for production of food additives (EFSA Panel on Biological Hazards, 2015). As seen from the instrumental texture analysis of IBP ice cream, the concentration of IBP is what influences ice cream texture. That is why a low amount of IBPs was used here (6.5·10⁻² mg·mL⁻¹ of total protein).

The assessors panel evaluated ice cream samples based on three parameters – sweetness, friability and roughness. The IBP-containing and the control ice cream were made from the same initial ice cream mixture. The sweetness was not affected by IBPs as both ice cream types were scored similarly by the evaluators (Fig. 5) (95% confidence interval for control ice cream 8.0–11.1; IBP ice cream 8.9–11.0). Differently, the panel felt IBP-containing ice cream to be more friable than the control ice cream (95% confidence interval for control ice cream 2.0–4.6; IBP ice cream 5.6–10.3). This feeling being caused probably by disruption of the continuous ice phase when biting the ice cream. Likewise, IBP-ice cream was scored higher for being rougher than the control ice cream (95% confidence interval for control ice cream 0.3–1.4; IBP ice cream 2.0–6.7). Probably owing to the fact that the IBP-aggregates are big enough to be felt in mouth. Similar results of crystalline texture of ice cream containing low concentrations of winter wheat extract were presented by Regand and Goff (2006).

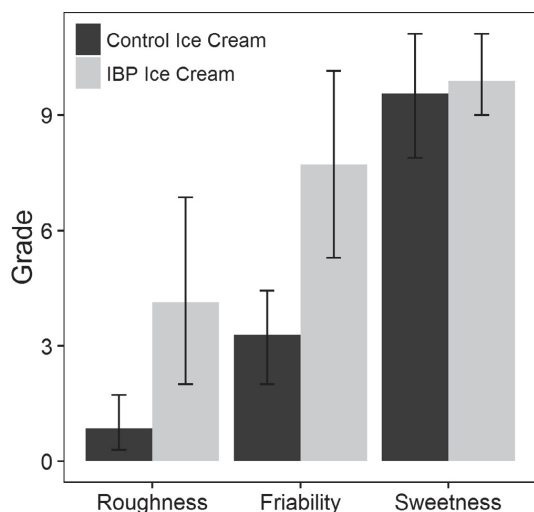


Fig. 5. Sensory analysis of the roughness, friability and sweetness of control ice cream and ice cream containing winter rye IBPs ($65 \text{ mg} \cdot \text{L}^{-1}$ of total protein). The y-axis provides the mean grades given by the seven assessors. Vertical bars indicate 95% confidence intervals.

Together, the sensory analysis results are in line with the instrumental texture analysis data showing that the IBP alters the texture making the ice cream harder.

4. Conclusions

The current study was undertaken by a desire to create an ice cream with smooth texture and improved resistance to recrystallization. To achieve this, established inhibitors of ice crystal growth, ice-binding proteins were employed. Two novel methods to study the effect of IBPs were developed. An accelerated ice recrystallization inhibition assessment method demonstrated that IBPs are active in ice cream mixes. Additionally, a microscopy method for visualizing ice crystals was created to study ice cream microstructure. In the presence of IBPs ice crystals within ice cream are substantially smaller and recrystallization is inhibited. This was expected to result in an ice cream with smoother texture and improved tolerance to temperature fluctuations. However, in addition to creating smaller ice crystals, it was discovered that IBPs brings about an additional effect namely the aggregation of the crystals into a rigid three dimensional network. This effect is associated with both tested IBP types (winter rye extract, fish type III). In IBP ice cream, the ice phase is organized continuously with the matrix phase being distributed discontinuously, shielded in a portions within the ice aggregates. The network-type arrangement of ice phase results in ice cream texture that is significantly harder, more brittle, feels crystalline and rough on the palate.

It has been speculated that the concentration of IBP is the key factor influencing ice cream structure. It might be possible to achieve smoother structure with concentrations of IBP below 50% ice recrystallization inhibition point ($0.17 \text{ mg} \cdot \text{mL}^{-1}$ for winter rye extract and $0.10 \text{ } \mu\text{g} \cdot \text{mL}^{-1}$ for type III IBP). These low concentrations of IBP have to be combined with an appropriate stabilizer and it remains to be seen whether the IBP and stabilizer couple will have an additive effect to each other in respect to IRI activity. In this work, regardless of stabilizer selection high concentrations of type III IBP had no positive contribution to ice cream smoothness, nor such an effect was seen with winter rye IBPs at concentration below 50% inhibition point. It is to be expected that even at low concentrations as long as IBP modifies ice

crystal surface, it renders the convex crystal area between IBP molecules thermodynamically unstable, resulting in fusion of adjacent crystals.

On the other hand, the organization of ice phase within the IBP ice cream provides it with endorsed shape-preserving capability enabling longer consumption time, production of more elaborately shaped products or even production of novel frozen desserts where harder texture is desirable.

Conflicts of interest

No conflict of interest to declare.

Acknowledgments

Authors thank Sten Erm for excellent technical assistance and Maya Bar-Dolev and David W Schryer for critical review of the manuscript.

This work was supported by the European Regional Development Fund (project EU48667) and Estonian Ministry of Education (project IUT19-27).

Appendix A. Supplementary data

Supplementary data associated with this article can be found, in the online version, at <http://dx.doi.org/10.1016/j.foodchem.2017.10.152>.

References

- Antton, A. A., Smith, D. J., Roper, D. I., Lewis, S., Caves, L. S. D., Verma, C. S., ... Hubbard, R. E., et al. (2001). Understanding the mechanism of ice binding by type III antifreeze proteins. *Journal of Molecular Biology*, *305*(4), 875–889.
- Bodyfelt, F. W., Tobias, J., & Trout, G. M. (1988). *The sensory evaluation of dairy products*. New York: Van Nostrand Reinhold.
- Bramley, A. S., Gray, S. J., Turan, S. M., Spors, D. D., Frisch, S. M. (2011). Low fat frozen confectionery product. US Patent 8,003,151.
- Buckley, S. L., & Lillford, P. J. (2009). Antifreeze proteins: Their structure, binding and use. In S. Kasapis, I. T. Norton, & J. B. Ubbink (Eds.). *Modern biopolymer science* (pp. 93–128). San Diego: Academic Press.
- Budke, C., Heggemann, C., Koch, M., Sewald, N., & Koop, T. (2009). Ice recrystallization kinetics in the presence of synthetic antifreeze glycoprotein analogues using the framework of LSW theory. *The Journal of Physical Chemistry B*, *113*(9), 2865–2873.
- Byass, L. J., Doucet, C. J., Fenn, R. A., McArthur, A. J., Sidebottom, C. M., Smallwood, M. F. (2004). Carrot antifreeze polypeptides. US Patent 6,797,690.
- Chao, H., Sännichsen, F. D., DeLuca, C. I., Sykes, B. D., & Davies, P. L. (1994). Structure-function relationship in the globular type III antifreeze protein: Identification of a cluster of surface residues required for binding to ice. *Protein Science*, *3*(10), 1760–1769.
- Clarke, C. (2012). *The science of ice cream* (2nd ed.). Cambridge: RSC Publishing (Chapter 7).
- Clarke, C. J., Buckley, S. L., & Lindner, N. (2002). Ice structuring proteins – A new name for antifreeze proteins. *CryoLetters*, *23*(2), 89–92.
- Crilly, J. (2007). ISP: A breakthrough for better ice cream. *New Food*, *3*, 40–44.
- Daniel, A., Hoddle, A., Jones, A., Oldroyd, J. R., Singleton, S. (2003). Ice confection. US Patent 6,565,908.
- Daniel, A., Hoddle, A., Jones, A., Oldroyd, J. R., Singleton, S. (2007). Ice cream confection containing an antifreeze protein. European Patent EP1417892.
- Darling, D.F., Hoddle, A. (2001). Frozen food product. US Patent 6,200,622.
- Donhowe, D., & Hartel, R. W. (1996). Recrystallization of ice in ice cream during controlled accelerated storage. *International Dairy Journal*, *6*(11–12), 1191–1208.
- Duman, J. G. (2001). Antifreeze and ice nucleator proteins in terrestrial arthropods. *Annual Review of Physiology*, *63*(1), 327–357.
- EFSA Panel on Biological Hazards (2015). Statement on the update of the list of QPS-recommended biological agents intentionally added to food or feed as notified to EFSA. 2: Suitability of taxonomic units notified to EFSA until March 2015. *EFSA Journal*, *13*(6), 4138–4167.
- European Food Safety Authority (2008). Safety of ‘Ice Structuring Protein (ISP)’ – Scientific opinion of the panel on dietetic products, nutrition and allergies and of the panel on genetically modified organisms. *EFSA Journal*. doi: 10.2903/j.efsa.2008.768.
- Feeley, R. E., & Yeh, Y. (1998). Antifreeze proteins: Current status and possible food uses. *Trends in Food Science & Technology*, *9*(3), 102–106.
- Goff, H. D., & Hartel, R. W. (2013). *Ice cream* (7th ed.). New York: Springer (Chapter 12).
- Goff, H. D., Regand, A., & Tharp, B. W. (2002). The potential for natural ice-structuring proteins in ice cream. *Dairy Industries International*, *67*(10), 30–32.
- Graether, S. P., DeLuca, C. I., Baardsnes, J., Hill, G. A., Davies, P. L., & Jia, Z. (1999). Quantitative and qualitative analysis of type III antifreeze protein structure and function. *Journal of Biological Chemistry*, *274*(17), 11842–11847.

- Griffith, M. (2004). Cold tolerances in plants. European Patent EP0589928.
- Griffith, M., & Ewart, K. V. (1995). Antifreeze proteins and their potential use in frozen foods. *Biotechnology Advances*, 13(3), 375–402.
- Guinard, J. X., Zoumas-Morse, C., Mori, L., Uatoni, B., Panyam, D., & Kilara, A. (1997). Sugar and fat effects on sensory properties of ice cream. *Journal of Food Science*, 62, 1087–1094.
- Hew, C. L., Wang, N. C., Joshi, S., Fletcher, G. L., Scott, G. K., Hayes, P. H., et al. (1988). Multiple genes provide the basis for antifreeze protein diversity and dosage in the ocean pout, *Macrozoarces americanus*. *The Journal of Biological Chemistry*, 263(24), 12049–12055.
- Hon, W.-C., Griffith, M., Chong, P., & Yang, D. S. C. (1994). Extraction and isolation of antifreeze proteins from winter rye (*Secale cereale* L.) leaves. *Plant Physiology*, 104(3), 971–980.
- Hon, W.-C., Griffith, M., Mlynarz, A., Kwok, Y. C., & Yang, D. S. C. (1995). Antifreeze proteins in winter rye are similar to pathogenesis-related proteins. *Plant Physiology*, 109, 879–889.
- Knight, C., Cheng, C., & DeVries, A. (1991). Adsorption of alpha-helical antifreeze peptides on specific ice crystal surface planes. *Biophysical Journal*, 59(2), 409–418.
- Mangiagalli, M., Bar-Dolev, M., Tedesco, P., Natalello, A., Kaleda, A., Brocca, S., et al. (2017). Cryo-protective effect of an ice-binding protein derived from Antarctic bacteria. *The FEBS Journal*, 284(1), 163–177.
- Nahku, R., Valgepea, K., Lahtvee, P. J., Erm, S., Abner, K., Adamberg, K., et al. (2010). Specific growth rate dependent transcriptome profiling of *Escherichia coli* K12 MG1655 in accelerostat cultures. *Journal of Biotechnology*, 145, 60–65.
- Ndoye, F. T., & Alvarez, G. (2015). Characterization of ice recrystallization in ice cream during storage using the focused beam reflectance measurement. *Journal of Food Engineering*, 148, 24–34.
- Olijve, L. L., Meister, K., DeVries, A. L., Duman, J. G., Guo, S., Bakker, H. J., et al. (2016b). Blocking rapid ice crystal growth through nonbasal plane adsorption of antifreeze proteins. *Proceedings of the National Academy of Sciences*, 113(14), 3740–3745.
- Olijve, L. L., Oude Vrielink, A. S., & Voets, I. K. (2016a). A simple and quantitative method to evaluate ice recrystallization kinetics using the circle Hough transform algorithm. *Crystal Growth & Design*, 16(8), 4190–4195.
- Regand, A., & Goff, H. D. (2003). Structure and ice recrystallization in frozen stabilized ice cream model systems. *Food Hydrocolloids*, 17(1), 95–102.
- Regand, A., & Goff, H. D. (2005). Freezing and ice recrystallization properties of sucrose solutions containing ice structuring proteins from cold-acclimated winter wheat grass extract. *Journal of Food Science*, 70(9), E552–E556.
- Regand, A., & Goff, H. D. (2006). Ice recrystallization inhibition in ice cream as affected by ice structuring proteins from winter wheat grass. *Journal of Dairy Science*, 89(1), 49–57.
- Schägger, H. (2006). Tricine-SDS-PAGE. *Nature Protocols*, 1(1), 16–22.
- Smith, C. E., & Schwartzberg, H. G. (1985). Ice crystal size changes during ripening in freeze concentration. *Biotechnology Progress*, 1(2), 111–120.
- Sönnichsen, F. D., DeLuca, C. I., Davies, P. L., & Sykes, B. D. (1996). Refined solution structure of type III antifreeze protein: hydrophobic groups may be involved in the energetics of the protein-ice interaction. *Structure*, 4(11), 1325–1337.
- U. S. Food and Drug Administration (2003). Agency Response Letter GRAS Notice No. GRN 000117.
- Varela, P., Pintor, A., & Fiszman, S. (2014). How hydrocolloids affect the temporal oral perception of ice cream. *Food Hydrocolloids*, 36, 220–228.
- Wille, H. J. E., Vieira, J. B., De Kruif, C. G., Floris, T. A. G., & Slangen, K. J. (2012). Ice-structuring peptides of lactic origin. European Patent EP1917865.
- Yu, X. M., Griffith, M., & Wiseman, S. B. (2001). Ethylene induces antifreeze activity in winter rye leaves. *Plant Physiology*, 126(3), 1232–1240.

Curriculum vitae

Personal data

Name: Aleksei Kaleda
Date of birth: 19.05.1988
Place of birth: Kohtla-Järve, Estonia
Citizenship: Estonian

Contact data

E-mail: alex_kaleda2000@hotmail.com

Education

2016, 2017–2018 The Hebrew University of Jerusalem, Faculty of Agriculture, Food, and Environment. Visiting researcher
2013–2018 Tallinn University of Technology, School of Engineering. PhD
2010–2012 Tallinn University of Technology, Faculty of Chemical and Materials Technology, Department of Food Processing. MSc
2010 University of Helsinki, Faculty of Agriculture and Forestry. Student exchange
2006–2010 Tallinn University of Technology, Faculty of Chemical and Materials Technology, Department of Food Processing. BSc

Language competence

Russian Native
English Fluent
Estonian Good

Professional employment

2013–current Center of Food and Fermentation Technologies, Tallinn, Estonia. Research & Development

Supervising

2016 Siiri Saarma, MSc. Extraction of ice structuring proteins from fish and assessment of activity in baltic herring, baltic sprat, northern pike, pike-perch and european perch
2016 Maxim Bilovitskiy, MSc. Effects of oligosaccharides and antifreeze proteins on ice recrystallization in ice cream
2015 Kerstin Metsla, BSc. Ice structuring protein activity in winter wheat depending on cultivar and leaf storage time
2015 Jekaterina Kovalskaja, MSc. Isolation of ice structuring proteins by adsorption to ice
2014 Siiri Saarma, BSc. Growing and cold acclimation of winter wheat and extraction of ice structuring proteins
2014 Mariya Krupina, MSc. Hydrolysis on casein and fish gelatin and measurement of recrystallisation inhibition activity of hydrolysates
2013 Laura Taal, MSc. Extraction and determination of activity of ice structuring proteins from winter rye and winter wheat
2013 Evelyn Rumma, MSc. Activity determination of fish ice structuring proteins in frozen sucrose solutions and ice cream mix, using fast method

Elulookirjeldus

Isikuandmed

Nimi: Aleksei Kaleda
Sünniaeg: 19.05.1988
Sünnikoht: Kohtla-Järve, Eesti
Kodakondsus: Eesti

Kontaktandmed

E-post: alex_kaleda2000@hotmail.com

Hariduskäik

2016, 2017–2018 Heebrea Ülikool, Iisrael. Külalisteadur
2013–2018 Tallinna Tehnikaülikool, Inseneriteaduskond. PhD
2010–2012 Tallinna Tehnikaülikool, Keemia ja materjalitehnoloogia, Toidutehnika ja tootearendus. MSc
2010 Helsinki Ülikool. Välisõppe
2006–2010 Tallinna Tehnikaülikool, Keemia ja materjalitehnoloogia, Toidutehnika ja tootearendus. BSc

Keelteoskus

Vene keel Emakeel
Inglise keel Kõrgtase
Eesti keel Kõrgtase

Teenistuskäik

2013–... Toidu- ja fermentatsioonitehnoloogia arenduskeskus, Tallinn, Eesti. Teadur

Juhendamine

2016 Siiri Saarma, MSc. Jääd struktureerivate valkude ekstraheerimine kalast ja nende aktiivsuse määramine räimes, kilus, haugis, kohas ja ahvenas
2016 Maxim Bilovitskiy, MSc. Antifriisvalkude ja oligosahhariidide mõju jää rekristallisatsioonile jäätises
2015 Kerstin Metsla, BSc. Jääd struktureerivate valkude aktiivsuse sõltuvus talinisu sordist ning lehtede säilitamise ajast
2015 Jekaterina Kovalskaja, MSc. Jääd struktureerivate valkude isoleerimine adsorptsiooni teel jää pinnale
2014 Siiri Saarma, BSc. Talinisu kasvatamine, külmaklimatiseerimine ja jääd struktureerivate valkude ekstraheerimine
2014 Mariya Krupina, MSc. Kaseiini ja kala želatiini hüdroolüüs ning hüdroolüsaatide rekristallisatsiooni inhibeerimise aktiivsuse määramine
2013 Laura Taal, MSc. Talirukki ja talinisu jääd struktureerivate valkude ekstraheerimine ja aktiivsuse määramine
2013 Evelyn Rumma, MSc. Kala jääd struktureerivate valkude aktiivsuse määramine külmutatud sahharoosilahustes ja jäätisesegus, kasutades kiirendatud meetodit